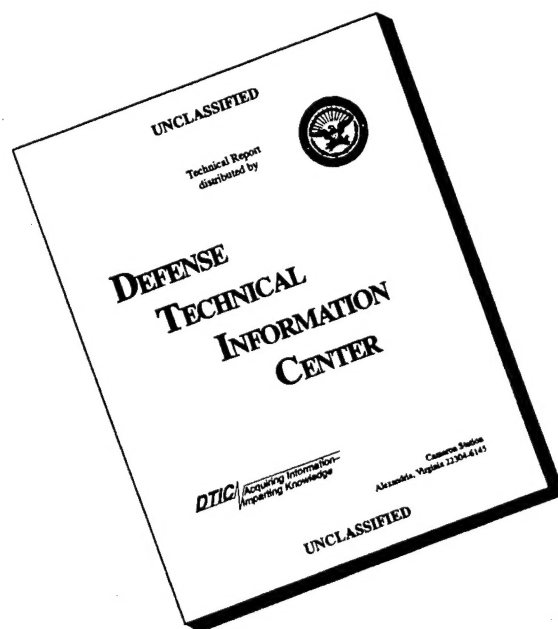


REPORT DOCUMENTATION PAGE			Form Approved OMB No. 0704-0188	
Public reporting burden for this collection of information is estimated to average 1 hour per response, including the time for reviewing instructions, searching existing data sources, gathering and maintaining the data needed, and completing and reviewing the collection of information. Send comments regarding this burden estimate or any other aspect of this collection of information, including suggestions for reducing this burden, to Washington Headquarters Services, Directorate for Information Operations and Reports, 1215 Jefferson Davis Highway, Suite 1204, Arlington, VA 22202-4302, and to the Office of Management and Budget, Paperwork Reduction Project (0704-0188), Washington, DC 20503.				
1. AGENCY USE ONLY (Leave blank)		2. REPORT DATE		3. REPORT TYPE AND DATES COVERED
				Final, 12-14 December 1993
4. TITLE AND SUBTITLE			5. FUNDING NUMBERS	
Workshop on Nonlinear Interactions in Magnetic and Magneto-optic Materials			DAAH04-94-G-0013	
6. AUTHOR(S)			DTIC SELECTED JUL 11/13/1995 B	
R. F. Wallis				
7. PERFORMING ORGANIZATION NAME(S) AND ADDRESS(ES)			8. PERFORMING ORGANIZATION REPORT NUMBER	
University of California, Irvine Irvine CA 92717-4575				
9. SPONSORING/MONITORING AGENCY NAME(S) AND ADDRESS(ES)			10. SPONSORING/MONITORING AGENCY REPORT NUMBER	
U.S. Army Research Office P.O. Box 12211 Research Triangle Park, NC 27709-2211			ARO 32522.1-PH-CF	
11. SUPPLEMENTARY NOTES				
The views, opinions and/or findings contained in this report are those of the author(s) and should not be construed as an official Department of the Army position, policy, or decision, unless so designated by other documentation.				
12a. DISTRIBUTION/AVAILABILITY STATEMENT			12b. DISTRIBUTION CODE	
Approved for public release; distribution unlimited.				
13. ABSTRACT (Maximum 200 words)				
<p>The Workshop consisted of six sessions. The first session included talks on magnetic phase transitions in both bulk materials and in magnetic superlattices and on certain types of magnetic excitations. The second session concerned magneto-optic materials and their applications in practical devices. The third session was devoted to magnetic resonance and the control of chaos arising from spin wave instabilities. The fourth session featured the experimental and theoretical aspects of soliton propagation in magnetic systems. The fifth session was devoted to the phenomenon of giant magnetoresistance and its applications. The sixth session involved additional talks on magnetic solitons and other nonlinear magnetic excitations. The Workshop closed with a panel discussion on important issues and future prospects.</p> <p>All comments indicate that the Workshop was a great success in providing a stimulating atmosphere for the exchange of the latest information and enabling graduate students and postdoctoral fellows to interact with the leading figures in the field.</p> <p style="text-align: center;">DTIC QUALITY INSPECTED 3</p>				
14. SUBJECT TERMS			15. NUMBER OF PAGES	
magnetic phase transitions, magnetic superlattices, magnetic excitations, magneto-optic materials, magnetic resonance, chaos, spin wave instabilities, giant magnetoresistance, solitons				
16. PRICE CODE				
17. SECURITY CLASSIFICATION OF REPORT			18. SECURITY CLASSIFICATION OF THIS PAGE	
UNCLASSIFIED			UNCLASSIFIED	
19. SECURITY CLASSIFICATION OF ABSTRACT			20. LIMITATION OF ABSTRACT	
UNCLASSIFIED			UL	

DISCLAIMER NOTICE



THIS DOCUMENT IS BEST QUALITY AVAILABLE. THE COPY FURNISHED TO DTIC CONTAINED A SIGNIFICANT NUMBER OF PAGES WHICH DO NOT REPRODUCE LEGIBLY.

FINAL REPORT

Workshop on Nonlinear Interactions in
Magnetic and Magneto optic Materials

12-14 December 1993

Countryside Inn, Costa Mesa, CA

U. S. Army Research Office Contract No. DAAH04-94-G-0013

19950705 008

Accession For	
DTIC GRA&I	<input checked="checked" type="checkbox"/>
DTIC TAB	<input type="checkbox"/>
Unannounced	<input type="checkbox"/>
Justification	
By	
Distribution/	
Availability Codes	
Dist	Avail and/or Special

The Workshop on Nonlinear Interactions in Magnetic and Magneto-optic Materials was held December 12-14, 1993, at the Countryside Inn in Costa Mesa, California. It was sponsored by:

California Coordinating Committee for Nonlinear Studies
Institute for Surface and Interface Science, University of California,
Irvine
Physics Department, University of California, Irvine
U.S. Army Research Office.

The organizing committee was:

R. F. Wallis (Chair), D. L. Mills, C. S. Tsai; U. C. Irvine
R. F. Soohoo; U. C. Davis
A. D. Boardman; University of Salford.

The Workshop was attended by 42 participants representing the United States, United Kingdom, Russia, China, Italy, Japan, Germany, Israel and Brazil. The program consisted of 21 invited talks and 6 contributed talks. Topics covered were critical behavior and phase transitions in magnetic systems, nonlinear spin waves and magnetic solitons, properties and device applications of magnetooptic materials, magnetic resonance and chaos in nonlinear magnetic materials, and giant magnetoresistance. The detailed program follows:

Saturday 12/11/93

6:00 - 7:30 PM Registration

Sunday 12/12/93

8:00 - 8:45 AM Registration

8:45 - 9:00 Welcome address and administrative information

Session 1 Chair: P. E. Wigen

9:00 - 9:40 H. Suhl, UC San Diego
"Critical Behavior of Magnetic Domains"

9:40 - 10:20 D. L. Mills, UC Irvine
"Field Induced Phase Transitions in Magnetic Superlattices"

10:20 - 10:50 Coffee

10:50 - 11:30 S. Nikitov, Institute of Radioeng. & Elect., Moscow
"Nonlinear CW Magnetostatic Spin Waves in Ferromagnetic Films: Modulation Instability, Decay Processes, Multistability, and New Effects"

11:30 - 12:10 A. D. Boardman, U. of Salford
"Fundamental Theory of Bright and Dark Solitons in Magnetic Media"

- 12:10 - 2:00 Lunch**
- Session 2 Chair: W. J. Miceli**
- 2:00 - 2:40 C. S. Tsai, UC Irvine**
 "Magnetostatic Waves-Based Guided Wave Magneto-optic Interactions, Devices and Applications"
- 2:40 - 3:20 F. Hellman, UC San Diego**
 "Anisotropy in Amorphous Materials for Magneto-optics"
- 3:20 - 3:50 Coffee**
- 3:50 - 4:30 H. H. He, Huazong Univ. of Science and Tech., China**
 "Magneto-optic Thin Films and Waveguide Isolators"
- 4:30 - 5:10 Y. Miyazaki, Toyohashi Univ. of Technology, Japan**
 "Switching and Filtering Characteristics of Optical Devices Using MSSW in Multilayered Magneto-optic Waveguides"
- 5:10 - 5:50 Y. Fetisov, Inst. of Radioeng., Electr. and Autom., Moscow**
 "Anomalous Optical Waveguide Modes Conversion in YIG Film under Microwave Pumping"

Monday 12/13/93

- Session 3 Chair: C. E. Patton**
- 9:00 - 9:40 P. E. Wigen, Ohio State U.**
 "Controlling Chaos in Nonlinear Magnetic Thin Films"
- 9:40 - 10:20 S. M. Rezende and F. M. de Aguiar, Fed. U. of Pernambuco, Brazil**
 "Crises and Control of Chaos in Spin Wave Instabilities"
- 10:20 - 10:50 Coffee**
- 10:50 - 11:30 R. F. Soohoo, UC Davis**
 "Internal Fields in the Ferromagnetic Resonance of Soft Ferromagnetic Materials"
- 11:30 - 12:10 A. Slavin, Oakland University**
 "Sample-Size Effect in Spin Wave Auto-oscillations"
- 12:10 - 2:00 Lunch**
- Session 4 Chair: M. Ciftan**
- 2:00 - 2:40 P. Kabos, Colorado State U.**
 "Paramagnetic Magnon Wavevector Distribution in Yttrium Iron Garnet Films by Brillouin Light Scattering"

- 2:40 - 3:20** **R. Marcelli & P. De Gasperis, Inst. of Electronics, Rome**
 "Power Thresholds and Frequency Shifts in the Excitation of
 Magnetostatic Volume Wave Solitons in Delay Line
 Configurations"
- 3:20 - 3:50** **Coffee**
- 3:50 - 4:30** **B. A. Kalinikos, St. Petersburg Electrotechnical Univ.**
 "Spin Wave Envelope Solitons in YIG Films: Formation,
 Propagation, Reflection and Collision Effects"
- 4:30 - 5:10** **D. Young, Rockwell Intl. and C. S. Tsai, UC Irvine**
 "Some Observations of Nonlinear Phenomena in Magneto-
 static Waves and Guided-Wave Magneto-optic Experiments"
- 5:10 - 5:30** **K. Booth, U. of Salford**
 "Observation of Spatial Solitons in Magnetic Thin Films"
- 5:30 - 5:50** **M. Chen, Colorado State U.**
 Backward Volume Wave Microwave Magnetic Envelope Solitons
 in Yttrium Iron Garnet Films"
- 7:00** **Banquet**

Tuesday 12/14/93

Session 5 Chair: R. Marcelli

- 9:00 - 9:40** **A. Berkowitz, UC San Diego**
 "Giant Magnetoresistance and Intercluster Exchange
 Interactions in Heterogeneous Alloys"
- 9:40 - 10:20** **R. E. Camley, U. of Colorado, Colorado Springs**
 "Giant Magnetoresistance in Magnetic Multilayers"
- 10:20 - 10:50** **Coffee**
- 10:50 - 11:30** **I. Schuller, UC San Diego**
 "Connection Between Structure and Giant Magnetoresistance"
- 11:30 - 12:10** **A. C. Ehrlich, Naval Research Laboratory**
 "Quantum-Well States and Giant Magnetoresistance in
 Magnetic Multilayers"
- 12:10 - 2:00** **Lunch**

Session 6 Chair: A. Slavin

- 2:00 - 2:20** **M. Tsankov, Colorado State U.**
 "Forward Volume Wave Microwave Magnetic Envelope Solitons
 in Yttrium Iron Garnet Films"

2:20 - 2:40	A. Pomyalov, Bar Ilan University, Israel "The Fine Structure of Subsidiary Absorption at Parametric Excitations of SW in YIG Films"
2:40 - 3:00	M. M. Shabat, Islamic University of Gaza "Nonlinear Electromagnetic Surface Waves Guided by a Grounded Gyromagnetic Film"
3:00 - 3:20	N. Waby, U. of Salford "On the Existence of Envelope Solitons in Antiferromagnetic Thin Films"
3:20 - 3:50	Coffee
3:50 - 4:50	Panel Discussion on Important Issues and Future Prospects Moderator: D. L. Mills Panelists: A. Berkowitz, A. D. Boardman, C. E. Patton, C. S. Tsai, P. E. Wigen
4:50 - 5:00	Closing Remarks

The Workshop served a very worthwhile function in bringing together experts from all over the world in a setting conducive to intense one-on-one interactions. Particularly significant was the interaction between experimentalists and theorists which led to a clarification of important issues concerning magnetic solitons. Also of great interest was the overview of present and prospective applications of giant magnetoresistance and magneto optic materials to useful devices.

LECTURE NOTES

WORKSHOP ON NONLINEAR INTERACTIONS IN MAGNETIC AND MAGNETOOPTIC MATERIALS

12-14 December 1993
Countryside Inn, Costa Mesa, California

Sponsors:

Department of Physics, University of California, Irvine
California Coordinating Committee for Nonlinear Studies
Institute for Surface and Interface Science, U.C. Irvine
U.S. Army Research Office

Organizing Committee:

R. F. Wallis (Chair), D. L. Mills, C. S. Tsai, U.C. Irvine
R. F. Soohoo, U.C. Davis
A. D. Boardman, U. of Salford

LECTURE NOTES

WORKSHOP ON NONLINEAR INTERACTIONS IN MAGNETIC AND MAGNETOOPTIC MATERIALS

12-14 December, 1993

	Page
1. A. D. Boardman*, S. A. Nikitov*, H. M. Mehta*, J. M. McNiff†, K. Xie*, A. K. Sangarpaul*, and R. C. J. Putnam *University of Salford, †Defense Research Agency, U.K. <i>Bright / Dark Temporal / Spatial Soliton Propagation in Magnetic Media</i>	3
2. A. C. Ehrlich Naval Research Laboratory <i>Quantum-Well States and Giant Magnetoresistance in Magnetic Multilayers</i>	64
3. R. Marcelli and P. DeGasperis Institute of Electronics, Rome <i>Power Thresholds and Frequency Shifts in the Excitation of Magnetostatic Volume Wave Solitons in Delay Line Configurations</i>	93
4. D. L. Mills University of California, Irvine <i>Magnetic Superlattices</i>	137
5. F. M. de Aguiar, S. M. Rezende and F.C.S. da Silva Federal University of Pernambuco <i>Spin Wave Chaotic Transitions</i>	157
6. S. M. Rezende, F. M. de Aguiar and A. Azevedo Federal University of Pernambuco <i>Controlling Spin-Wave Chaos</i>	168
7. A. N. Slavin Oakland University <i>Sample-Size Effect in Spin Wave Auto-Oscillations</i>	182
8. R. F. Soohoo University of California, Davis <i>Internal Fields in the Ferromagnetic Resonance of Soft Ferromagnetic Materials</i>	199
9. H. Suhl University of California, San Diego <i>Critical Behavior of Magnetic Domains</i>	221

10. **M. A. Tsankov, M. Chen and C. E. Patton** 240
Colorado State University
*Forward Volume Wave Envelope Solitons in a Thin
Unpinned YIG Film*
11. **A. D. Boardman*, S. A. Nikitov[†], and N. A. Waby*** 256
*University of Salford, [†]Institute of Radioengineering
and Electronics, Moscow
Existence of Spin Wave Solitons in an Antiferromagnetic Film
12. **P. E. Wigen** 278
Ohio State University
Controlling Chaos in Nonlinear Magnetic Thin Films

BRIGHT/DARK TEMPORAL/SPATIAL SOLITON PROPAGATION IN MAGNETIC MEDIA

A.D. Boardman^{*}, S.A. Nikitov^{*}, H.M. Mehta^{*},
J.M. McNiff[†], K. Xie^{*}, A.K. Sangarpaul^{*} and
R.C.J. Putman^{*}


^{*} Joule Laboratory,
Department of Physics,
University of Salford,
Salford
M5 4WT

[†] Defence Research Agency
Funtington
Hambrook
Near Chichester
Sussex
England

S.A. Nikitov held a Royal society fellowship from Dec 92 to July 93

- **Nonlinear effects are important in science and engineering**
- **They can be used to transmit and control pulses in various waveguides**
- **Frequency sweep across pulse envelopes**
- **Phase, amplitude, frequencies are changed**

HISTORICAL NOTES

- first observation by John Scott Russell
- August 1834 : Edinburgh-Glasgow canal
- bigger disturbances travelled faster
 -Korteweg-de Vries (KDV)
- break up of larger disturbance into
SOLITARY WAVES
- believed solitary waves to universal
- 1965 : soliton
 -every part of physics
- **SOLITON** 

stable solitary-solitary wave collisions
- nonlinear Schrodinger equation
 - potential proportional to amplitude squared
 - looks like quantum cousin
- gravity waves in DEEP water
 - $\text{sech}(\tau)$ ENVELOPE modulating carrier wave
 - fisherman's warning
 - seventh wave will sink you

- Russell 1834
- prow of barge
- Edinburgh-Glasgow canal
- "great solitary wave"

● $iU_t = -U_{xx} - 2U |U|$

U is complex

LOOKS  LIKE

● $i\psi_t = -\psi_{xx} + V(x)\psi$

$V(x) = -2 |\psi|^2$

Schrödinger
Equation

- 12 harmonic oscillations in a

● SECH
ENVELOPE

● 7th WAVE WILL SINK YOU

■ RAYLEIGH

■ KORTEWEG-DE VRIES (KdV)

■ GRAVITY WAVES IN SHALLOW WATER

■ GRAVITY WAVES IN DEEP WATER



NONLINEAR SCHRÖDINGER EQUATION



SOLITARY WAVES OR SOLITONS

Derivation of Nonlinear Schrodinger Equation

Basic Assumptions

- Transverse field solution is the linear CW guided wave solution
- Transverse waveguiding effects included through the use of the nonlinear (CW) dispersion equation
- Permits use of one-dimensional analysis
- Smooth, slowly varying envelope approximation
- Nonlinearity is weak
- Pulses are long in space (time) compared to the wavelength (carrier period)
- Pulse shape evolves over distances and times that are long compared to the pulse

The Nonlinear Schrödinger Equation

- Maxwell + Landau-Lifshitz equations



equations for amplitudes of magnetic potentials ψ



$$H = -\nabla^2 \psi$$



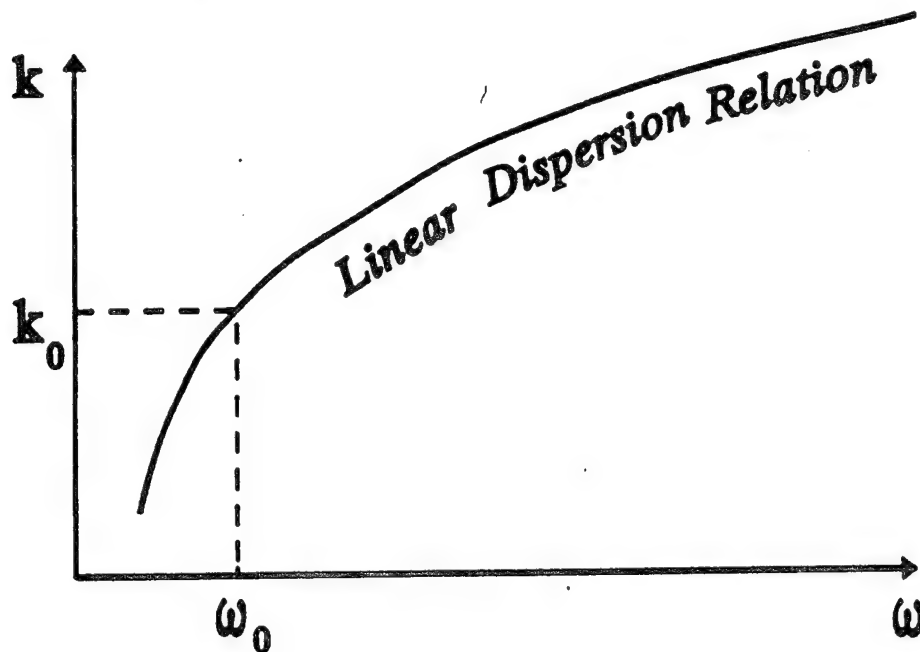
application of boundary conditions



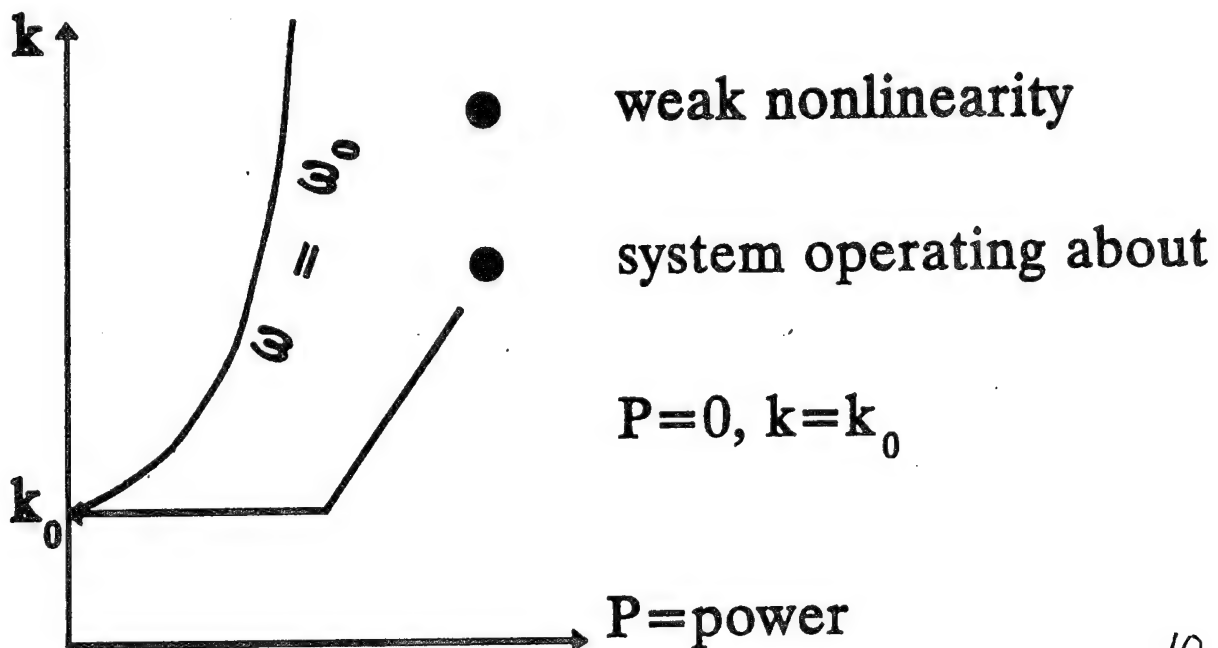
$$D(\omega, k, |A|^2) \cdot A = 0$$

Nonlinear Waves: expansion about (k_0, ω_0)

■ Linear Dispersion Relation



■ For Fixed ω_0 , a Curve of k Against Power



The Nonlinear Schrödinger Equation

- A is the complex amplitude of the magnetic potential

- Angular frequency (ω), wave vector (k)

- Choose a working point

$$(\omega_0, k_0)$$

- weakly nonlinear weakly dispersive

expand $D(\omega, k, |A|^2) \cdot A = 0$ about $(\omega_0, k_0, 0)$

- Define small deviation K from k_0

$$K = k - k_0$$

$$k_0 = (0, 0, k_0)$$

$$K = (K_p, 0, K_z)$$

The Nonlinear Schrödinger Equation

$$\omega(\underline{k}) \approx \omega(k_o) + \left(\frac{\partial \omega}{\partial k} \right)_{k_o} \left[\sqrt{K_p^2 + (k_o + K_z)^2} - k_o \right]$$

$$+ \frac{1}{2} \left(\frac{\partial^2 \omega}{\partial k^2} \right)_{k_o} K_p^2 + \frac{\partial \omega}{\partial |A|^2} |A|^2$$

$$\approx \omega(k_o) + \left(\frac{\partial \omega}{\partial k} \right)_{k_o} \left(K_z + \frac{K_p^2}{2k_o} \right) + \frac{1}{2} \left(\frac{\partial^2 \omega}{\partial k^2} \right)_{k_o} K_p^2 + \frac{\partial \omega}{\partial |A|^2} |A|^2$$

■ hence

$$\omega - \omega(k_o) - v_g \left(K_z + \frac{K_p^2}{2k_o} \right) - \frac{1}{2} v'_g K_z + \frac{\partial \omega}{\partial |A|^2} |A|^2 = 0$$

The Nonlinear Schrödinger Equation

■ identifications

$$\omega - \omega_o = i \frac{\partial}{\partial t}, \quad K = -i \nabla, \quad \frac{\partial}{\partial t} = -v_g \frac{\partial}{\partial z}$$



$$i \left(\frac{\partial A}{\partial t} + v_g \frac{\partial A}{\partial z} \right) + \frac{1}{2} v_g \frac{\partial^2 A}{\partial z^2} + \frac{1}{2} \frac{v_g}{k_o} \frac{\partial^2 A}{\partial x^2} - \gamma |A|^2 A = 0$$

**PARABOLIC NONLINEAR
SCHRÖDINGER EQUATION**

- z: longitudinal coordinate
- x: transverse coordinate

The Nonlinear Schrödinger Equation

- temporal solitons

Frequency

$$i \frac{\partial A}{\partial s} + \frac{1}{2} v_g \frac{\partial^2 A}{\partial w^2} - \gamma_\omega |A|^2 A = 0$$

- transformation $s = t$ $w = z - v_g t$

$$\frac{\partial}{\partial t} = -v_g \frac{\partial}{\partial w} + \frac{\partial}{\partial s} \qquad \frac{\partial}{\partial z} = \frac{\partial}{\partial w}$$

- w is measured in the frame of reference moving with the pulse

The Nonlinear Schrödinger Equation

Wavenumber

$$i \frac{\partial A}{\partial \xi} - \frac{\beta_2}{2} \frac{\partial^2 A}{\partial t^2} + \gamma_k |A|^2 A = 0$$

$$\xi = z \quad T = t - z\beta_1 \quad \beta_1 = \left(\frac{1}{v_g} \right)$$

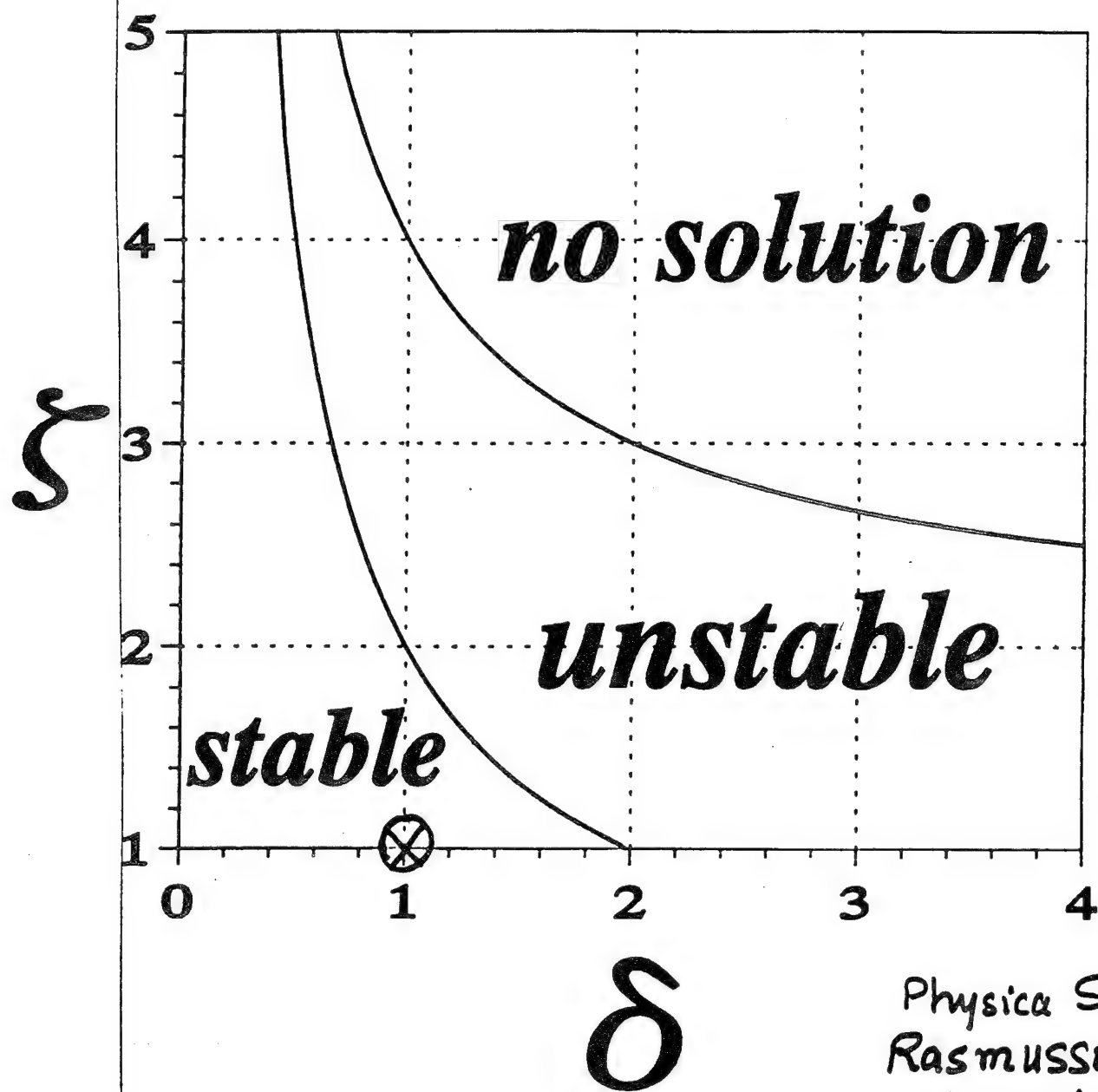
- T measured in frame of reference moving with pulse

$$\beta_2 = \frac{\partial^2 k}{\partial \omega^2} = - \frac{1}{v_g^3} \frac{\partial^2 \omega}{\partial k^2}$$

$$\gamma_k = \frac{\partial k}{\partial |A|^2} = - \frac{1}{v_g} \frac{\partial \omega}{\partial |A|^2}$$

$$\text{■ } L_D = \frac{T_o^2}{|\beta_2|} \quad : \text{dispersion length}$$

$$\text{■ } L_{NL} = \frac{1}{\gamma_k P_o} \quad : \text{nonlinear length}$$



Physica Scripta
Rasmussen &
Rypdal (1986)

$$i \frac{\partial \psi}{\partial z} + \nabla^2 \psi + 2|\psi|^2 \psi = 0$$

$$\nabla^2 = \frac{\partial^2}{\partial x_1^2} + \frac{\partial^2}{\partial x_2^2} + \dots + \frac{\partial^2}{\partial x_r^2}$$

DIMENSIONLESS FORM : TEMPORAL

$$i \frac{\partial A}{\partial t} + \frac{\omega_2}{2} \frac{\partial^2 A}{\partial \omega^2} - \gamma_\omega |A|^2 A = 0$$

$$\omega_2 = \frac{\partial^2 \omega}{\partial \kappa^2}$$

■ Define $w = \frac{D_o}{\sqrt{2}} \eta$ $s = \frac{|\omega_2|}{D_o^2} \xi$

■ Hence $[s' \equiv \xi, w' \equiv \eta]$

$$i \frac{\partial A}{\partial s'} + \frac{\text{sgn}(\omega_2)}{2} \frac{\partial^2 A}{\partial w'^2} - \text{sgn}(\gamma_\omega) \frac{|\gamma_\omega|}{|\omega_2|} D_o^2 |A|^2 A = 0$$

■ define $A = \sqrt{\frac{P_o}{g}} u$; P_o is incident power

■ Lighthill criterion $\Rightarrow \text{sgn}(\omega_2) \cdot \text{sgn}(\gamma_\omega) < 1$

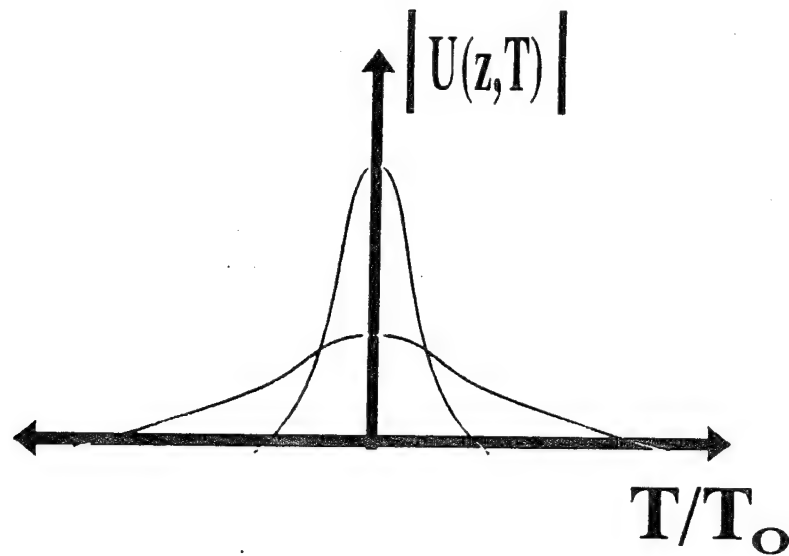
■ drop the primes + use (ξ, η)

$$i \frac{\partial U}{\partial \xi} + \frac{1}{2} \frac{\partial^2 U}{\partial \eta^2} + |U|^2 U = 0$$

$$N^2 = \frac{|\gamma_\omega| D_o^2 P_o}{2 |\omega_2| g} \quad U = Nu$$

■ N is the soliton order

GROUP-VELOCITY DISPERSION (GVD)



$$i \frac{\partial U}{\partial z} = \frac{1}{2} \beta_2 \frac{\partial^2 U}{\partial T^2}$$

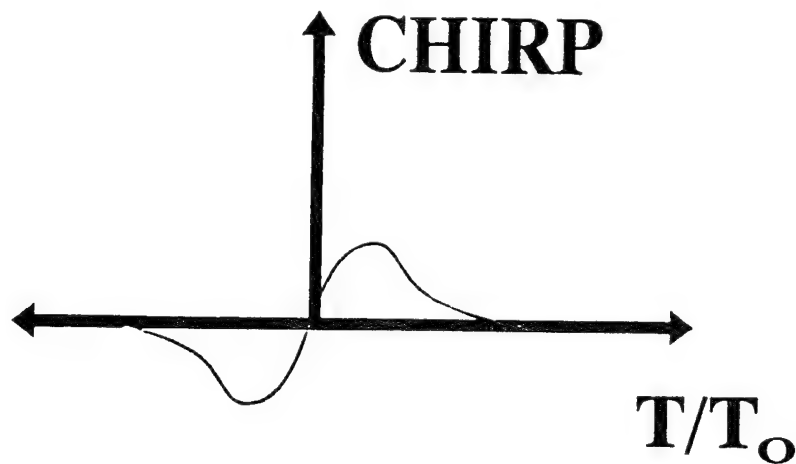
$$U(0,T) = \exp(-T^2/2T_0^2)$$

$$U(z,T) = U(0,T) \exp(i\phi(z,T))$$

Linear frequency CHIRP $\frac{\partial \phi}{\partial T} = -\delta\omega$

$$L_D = \frac{T_0^2}{|\beta_2|} \quad \beta_2 = \frac{\partial^2 K}{\partial \omega^2}$$

SELF-PHASE MODULATION



$$\frac{\partial U}{\partial Z} = i \frac{|U|^2 U}{L_{NL}}$$

$$U(Z,T) = U(0,T) \exp(i\phi(Z,T))$$

$$\phi(Z,T) = |U(0,T)|^2 \frac{Z}{L_{NL}}$$

$$\delta\omega = -\frac{\partial\phi}{\partial T} = \frac{\partial}{\partial T} |U(0,T)|^2 \frac{Z}{L_{NL}}$$

$$L_{NL} = \frac{1}{\gamma P_0}$$

Split-step Fourier method

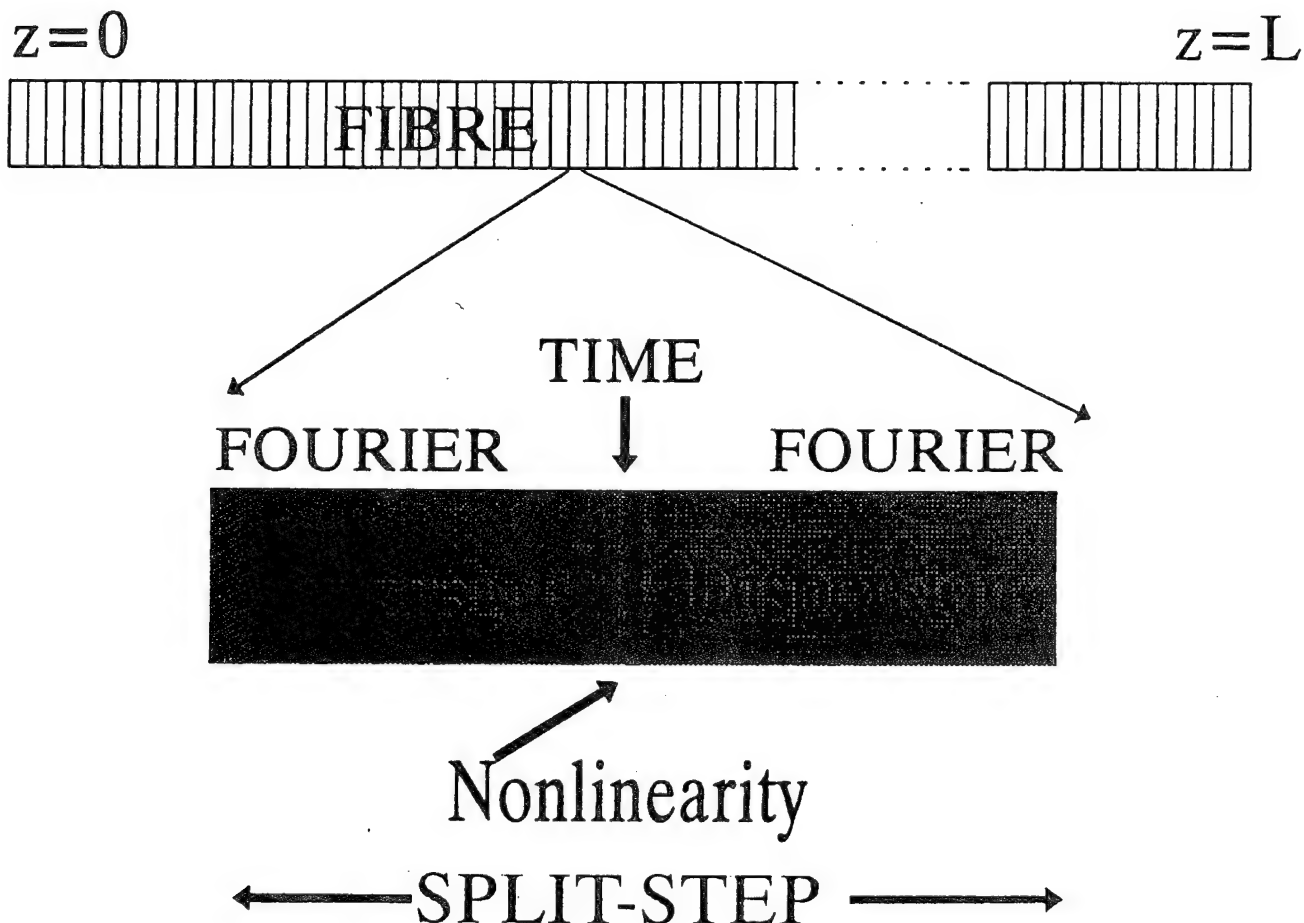
- express the NLS as:

$$\frac{\partial \mathbf{u}}{\partial \xi} = (\mathbf{D} + \mathbf{N}) \mathbf{u}$$

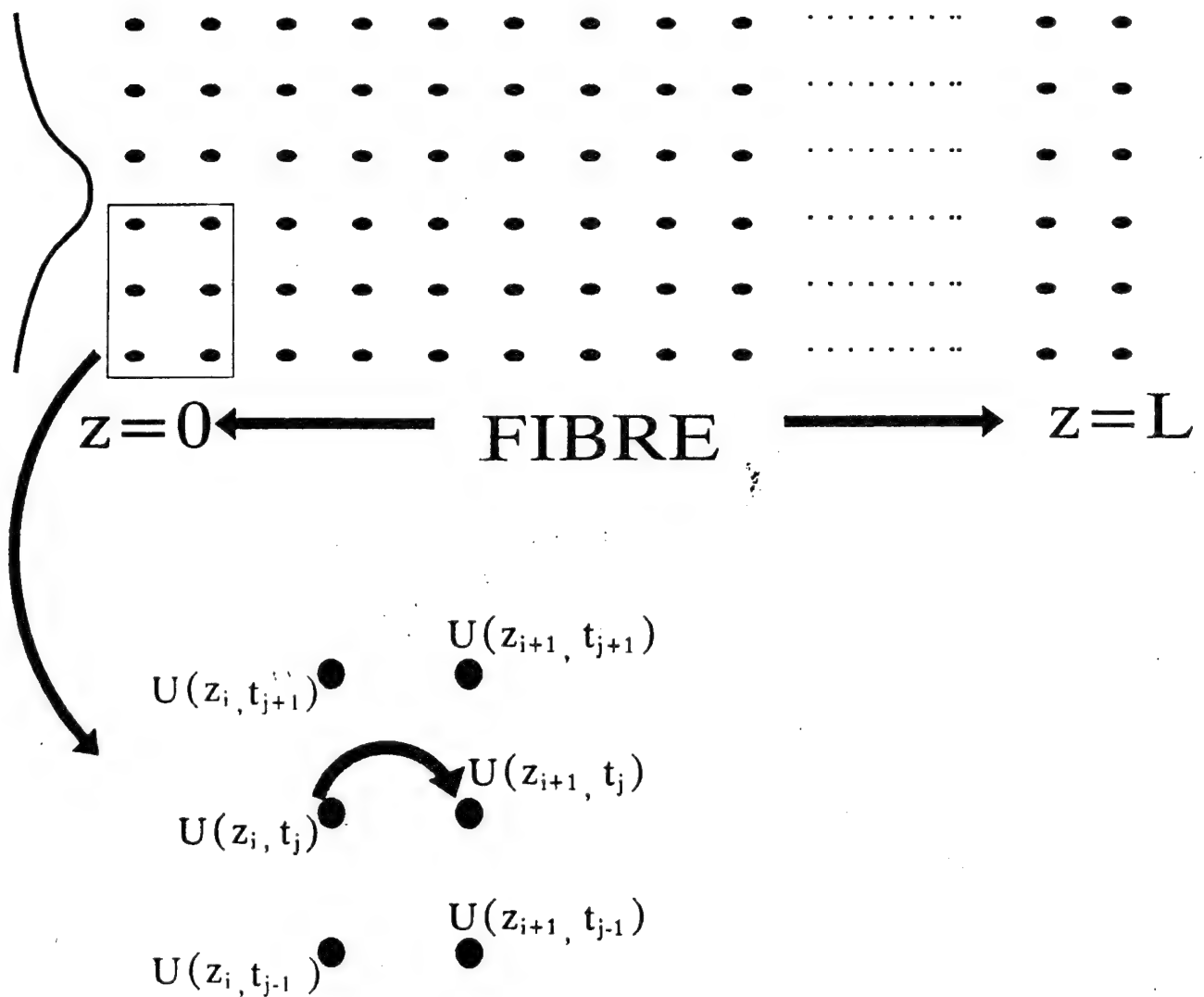
- where:

$$\mathbf{D} = \text{sgn}(\beta_2) \frac{-i}{2} \frac{\partial^2 \mathbf{u}}{\partial \eta^2}$$

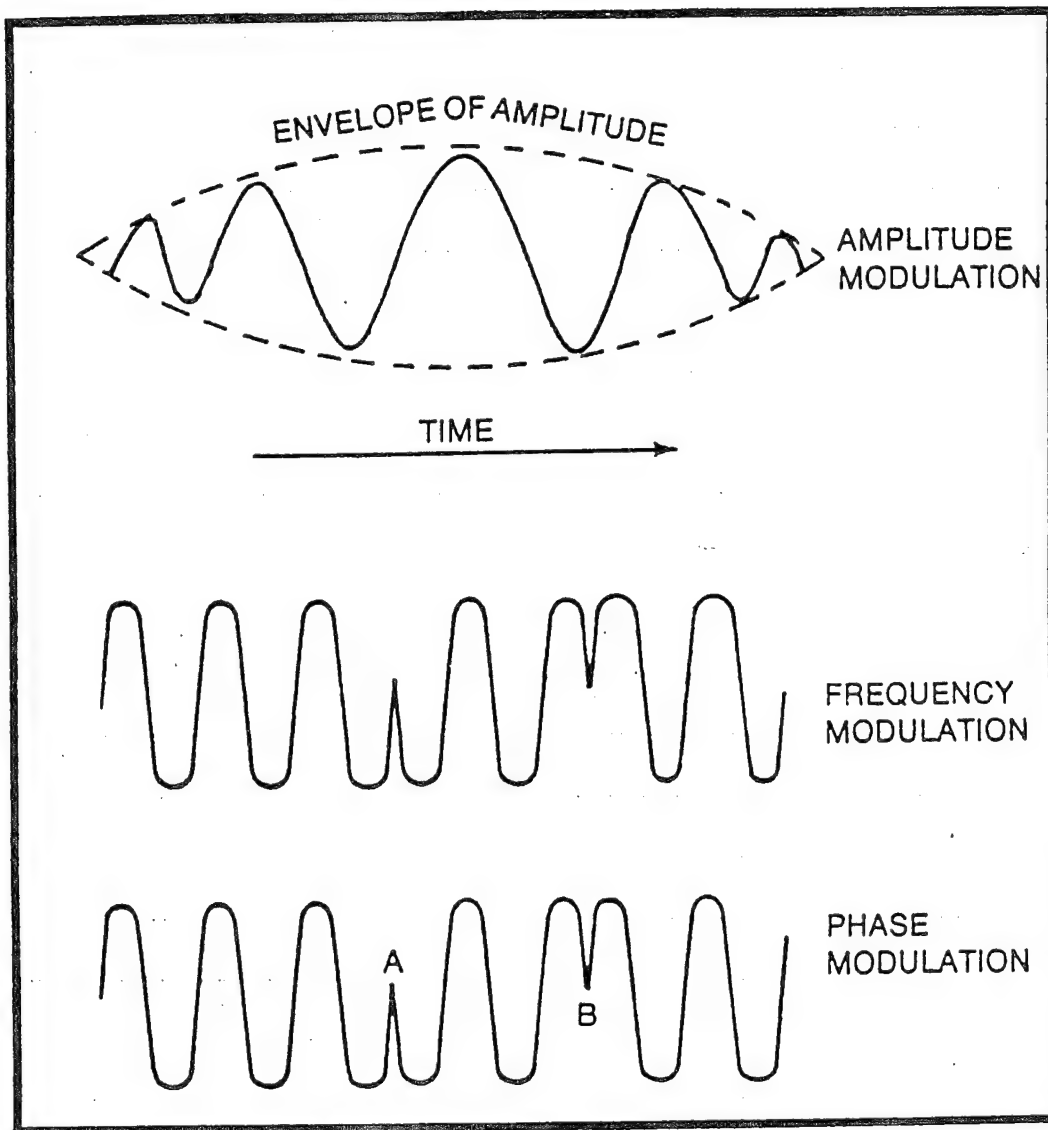
$$\mathbf{N} = i |u|^2 u$$



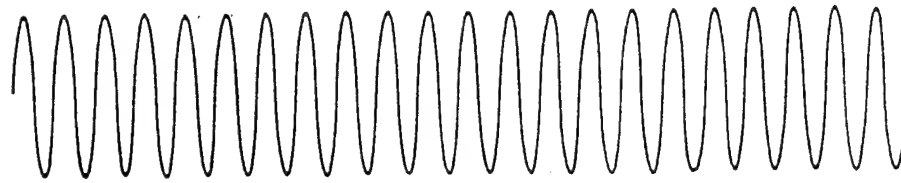
Finite-difference



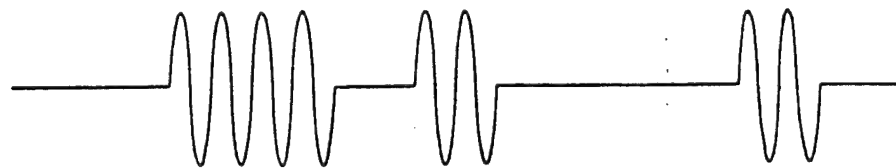
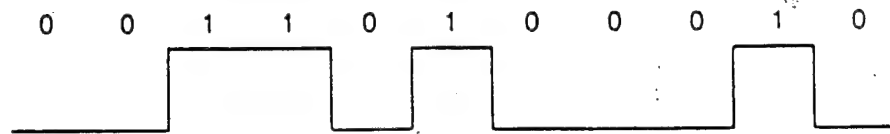
■ we can use $U(z_i, t_{j+1})$, $U(z_i, t_{j-1})$, and $U(z_i, t_j)$ to find the next step along the fibre $U(z_{i+1}, t_j)$



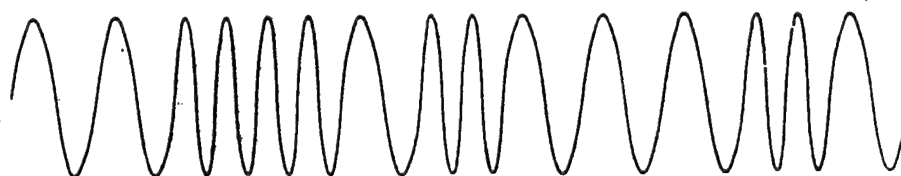
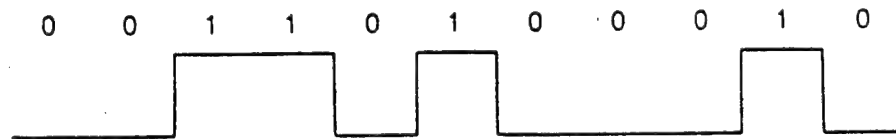
The three fundamental modulation techniques.



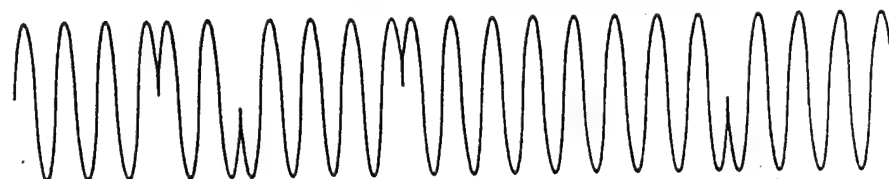
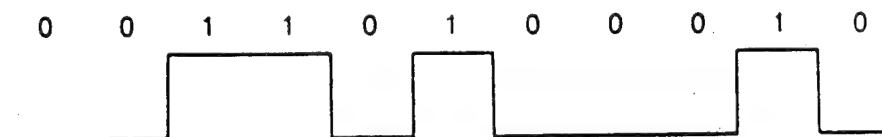
a. Carrier



b. Amplitude Modulation



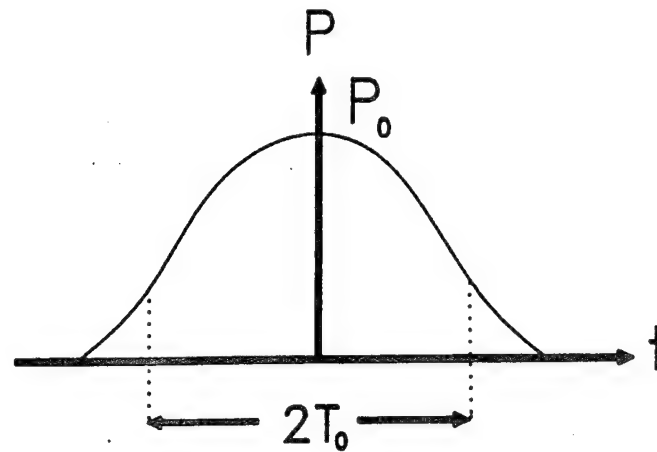
c. Frequency Modulation



d. Phase Modulation

Figure 9.7 Types of Modulation

SOLITON THRESHOLD



Balancing dispersion against nonlinearity
(at $t=0$) for coherent Gaussian pulse

$$P_{th} = \frac{|\beta_2|}{2 T_0^2 \gamma}$$

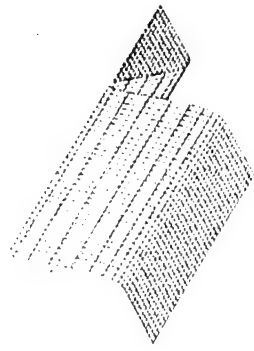
More rigorously for both coherent and
incoherent Gaussian pulses

$$P_{th} \simeq \frac{|\beta_2|}{4 T_0^2 \gamma}$$

$P_0 < P_{th} \longrightarrow$ no solitons

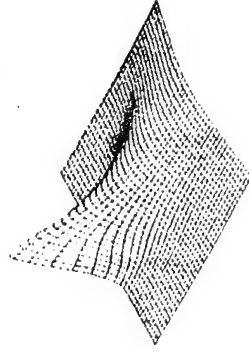
$P_0 \ll P_{th} \longrightarrow$ linear behaviour

Linear Dispersionless



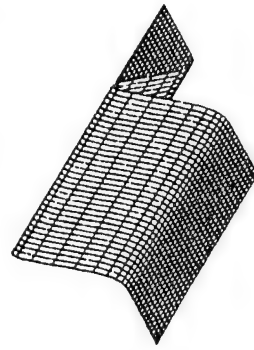
SOLITARY WAVES

Linear with Dispersion



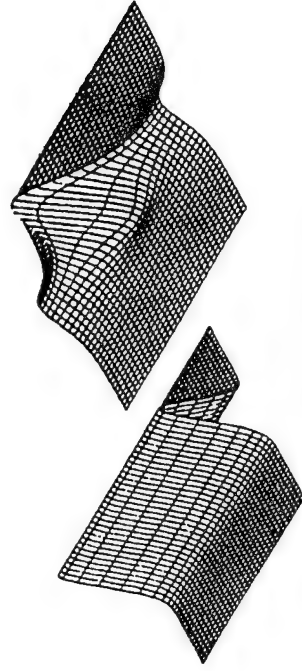
NO SOLITARY WAVES

Nonlinear Dispersionless



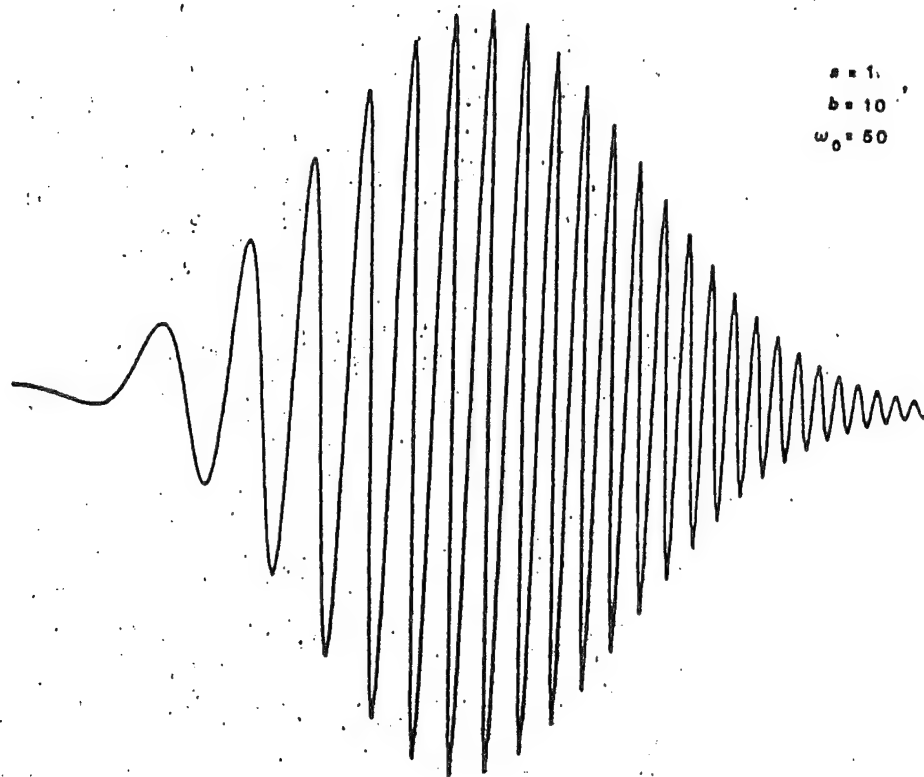
NO SOLITARY WAVES

Nonlinear with Dispersion



SOLITARY WAVES

PHASE AND GROUP VELOCITIES



A chirped gaussian pulse

NONLINEAR COEFFICIENTS AND DERIVATIVES OF DISPERSION CURVES

- dispersion relationship $D=0$
- define a surface $D=\omega-f(k)$

$$\frac{\partial^2 k}{\partial \omega^2} = -\frac{1}{v_g^3} \frac{\partial^2 \omega}{\partial k^2}$$

$$\left[\frac{\partial D}{\partial k} \right]_{\omega} = -v_g$$

$$\left[\frac{\partial D}{\partial \omega} \right]_k = 1$$

$$\frac{\partial k}{\partial |A|^2} = -\frac{1}{v_g} \frac{\partial \omega}{\partial |A|^2}$$

$$\frac{\partial^2 \omega}{\partial k^2} \frac{\partial \omega}{\partial |A|^2} = v_g^4 \frac{\partial^2 k}{\partial \omega^2} \frac{\partial k}{\partial |A|^2}$$

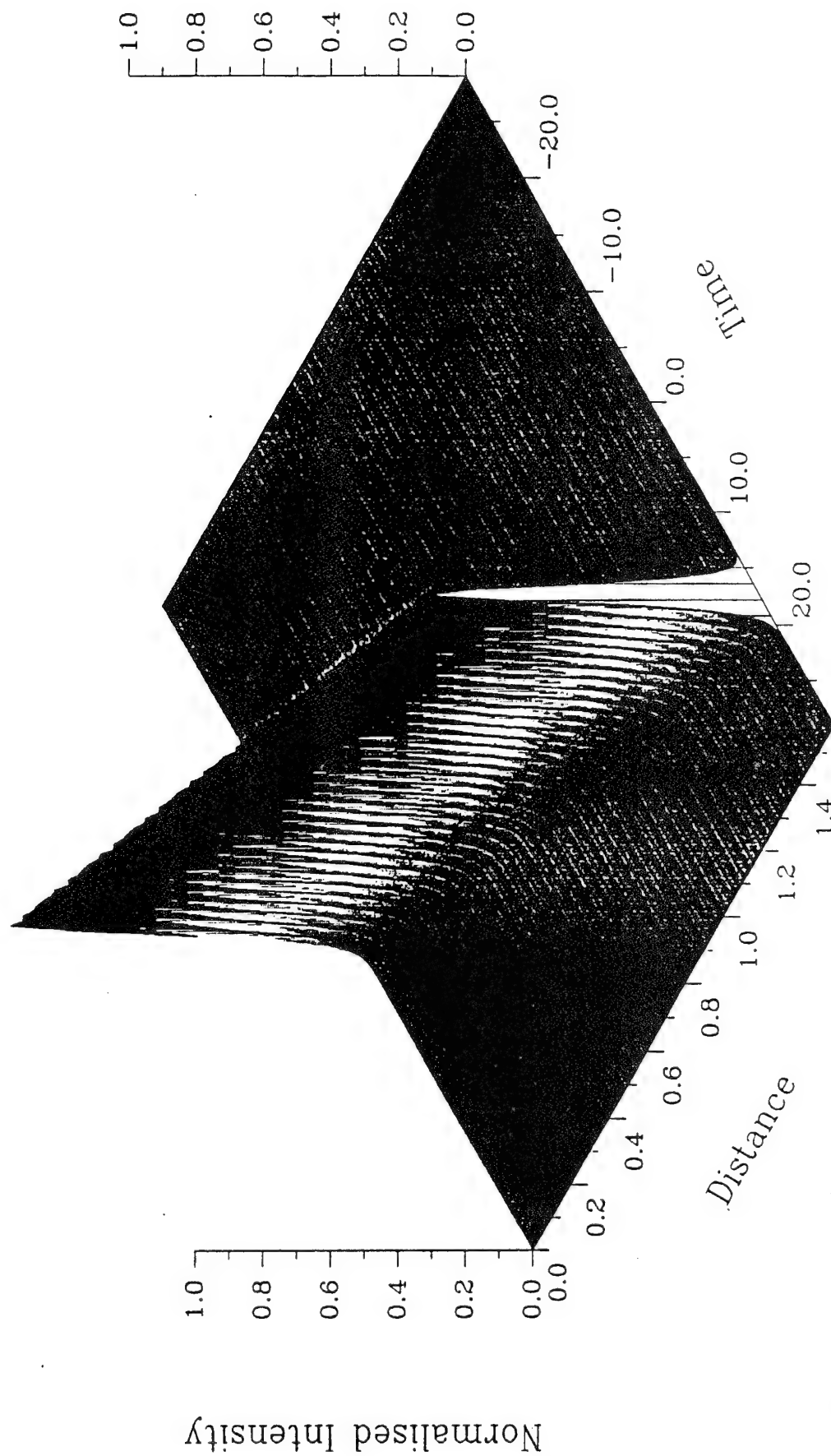
LIGHTHILL CRITERION

**BRIGHT
SOLITONS**

$$\left[\frac{\partial^2 \omega}{\partial k^2} \right]_L \frac{\partial \omega}{\partial |A|^2} < 0$$

$$\left[\frac{\partial^2 k}{\partial \omega^2} \right]_L \frac{\partial k}{\partial |A|^2} < 0$$

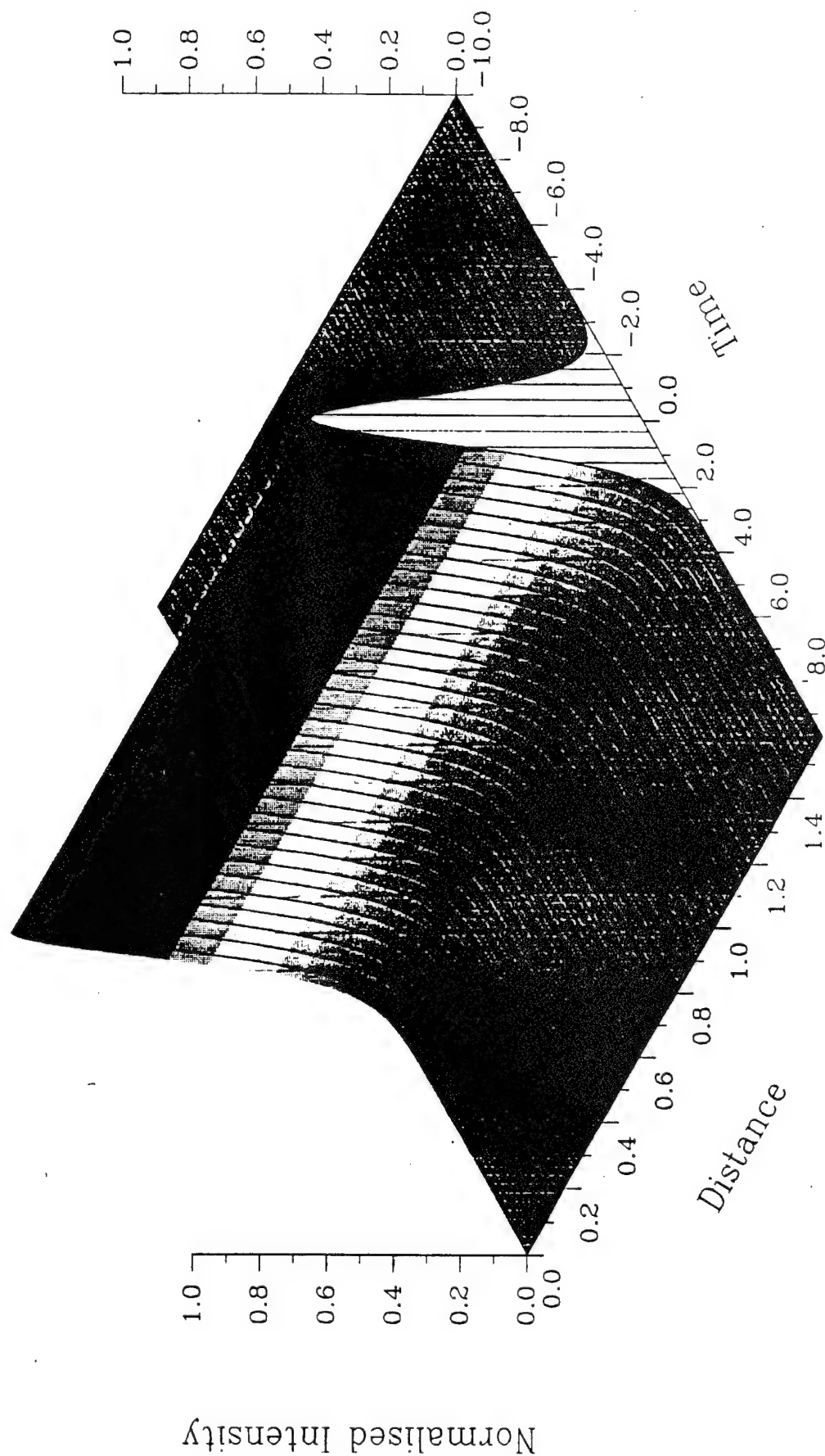
Fundamental Soliton In Stationary Frame



Y axis

X axis

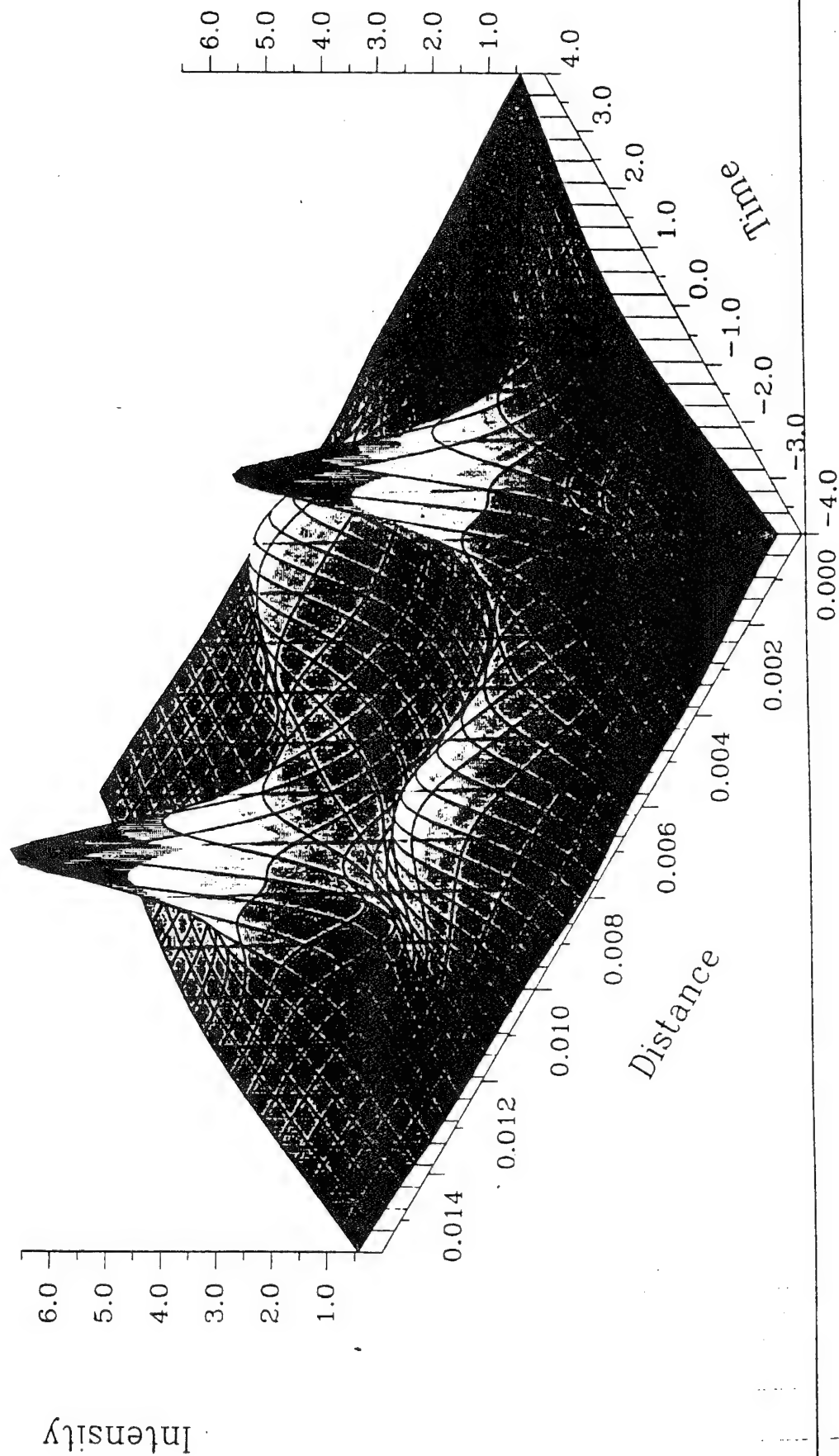
Fundamental Soliton In Retarded Frame



Y axis

X axis

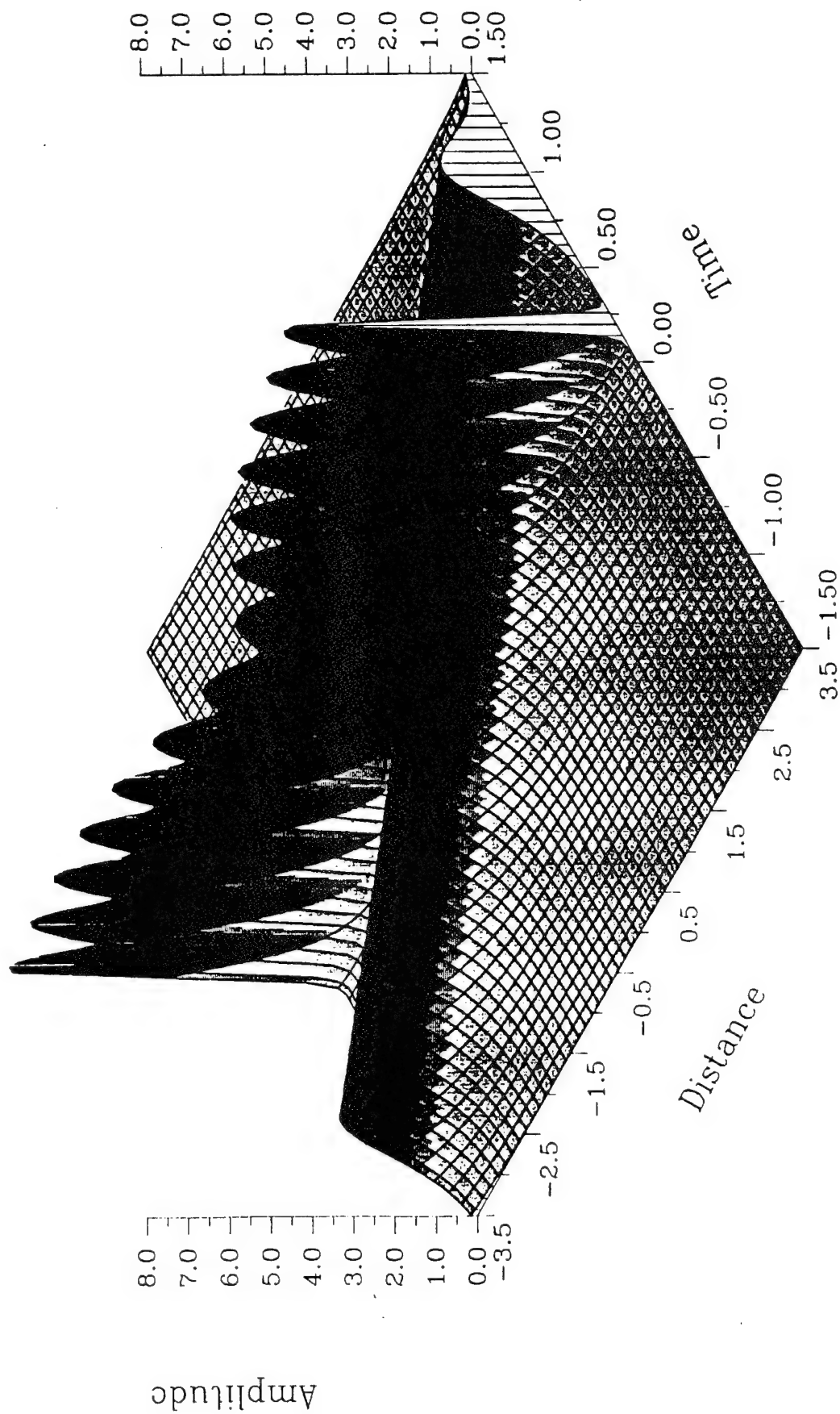
3rd-Order Soliton



Y axis

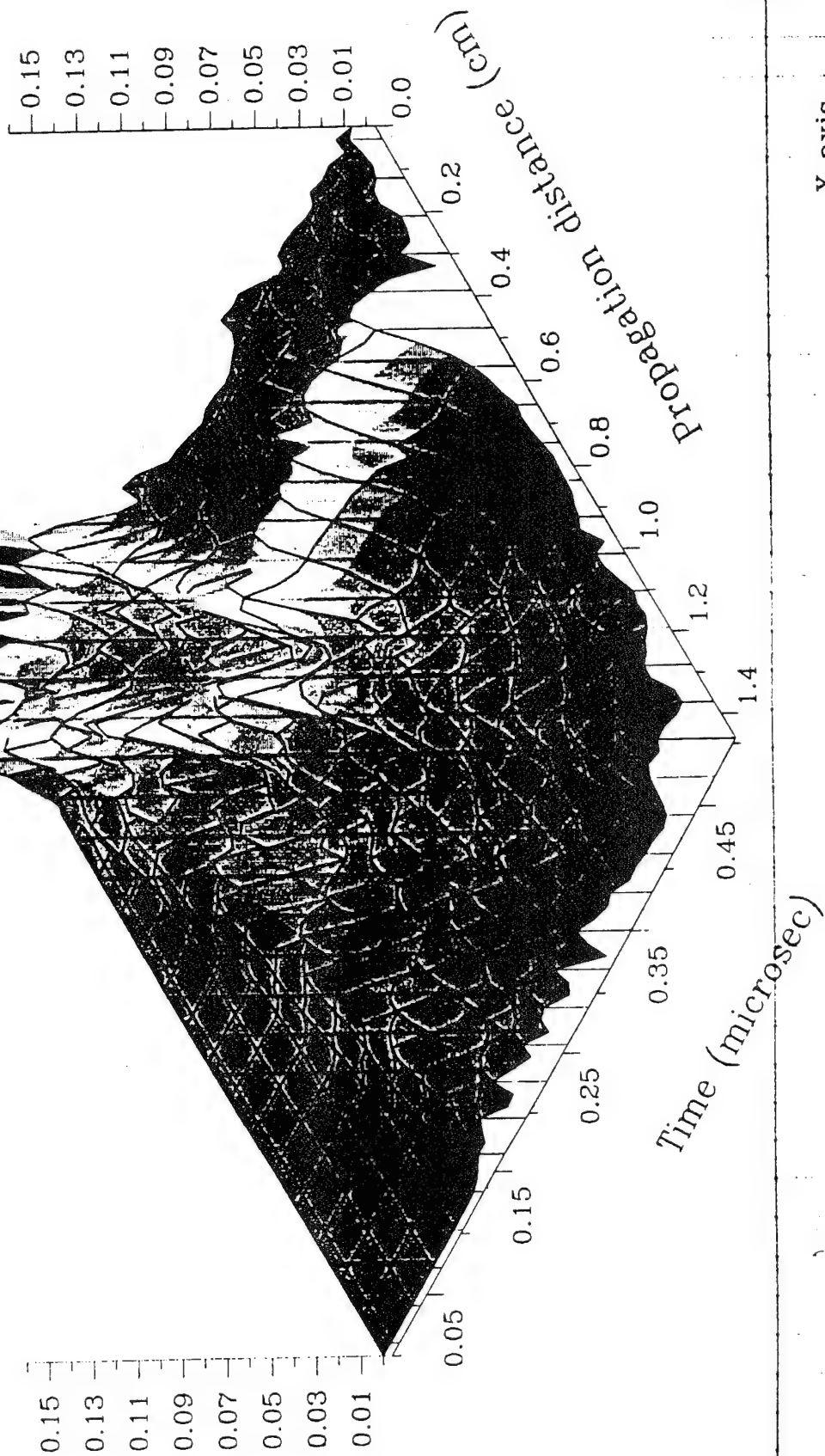
X axis

Soliton Collision



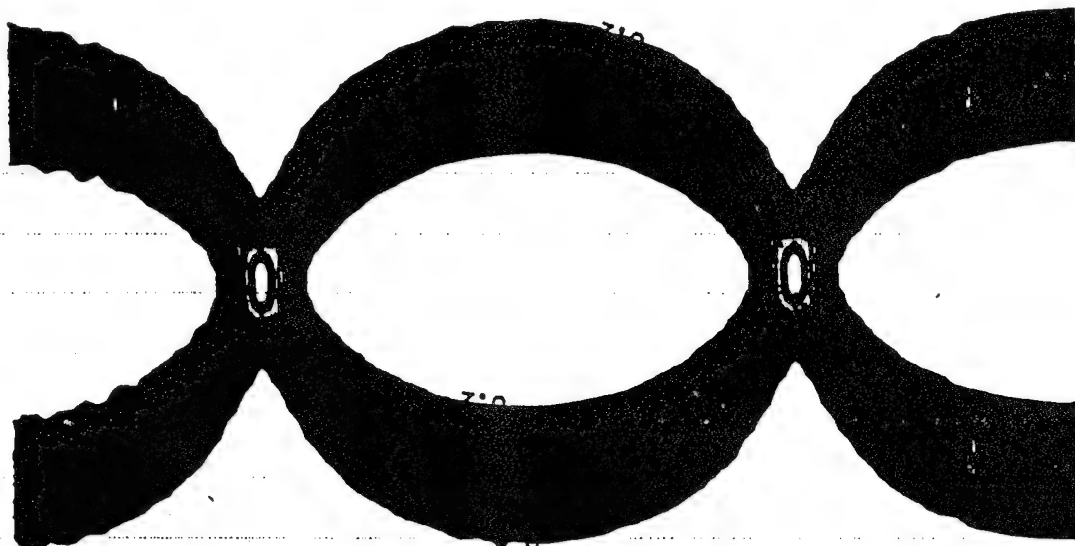
Undamped Pulse On A 5 Micron YIG Film
 Square Pulse: Input Amplitude 0.1

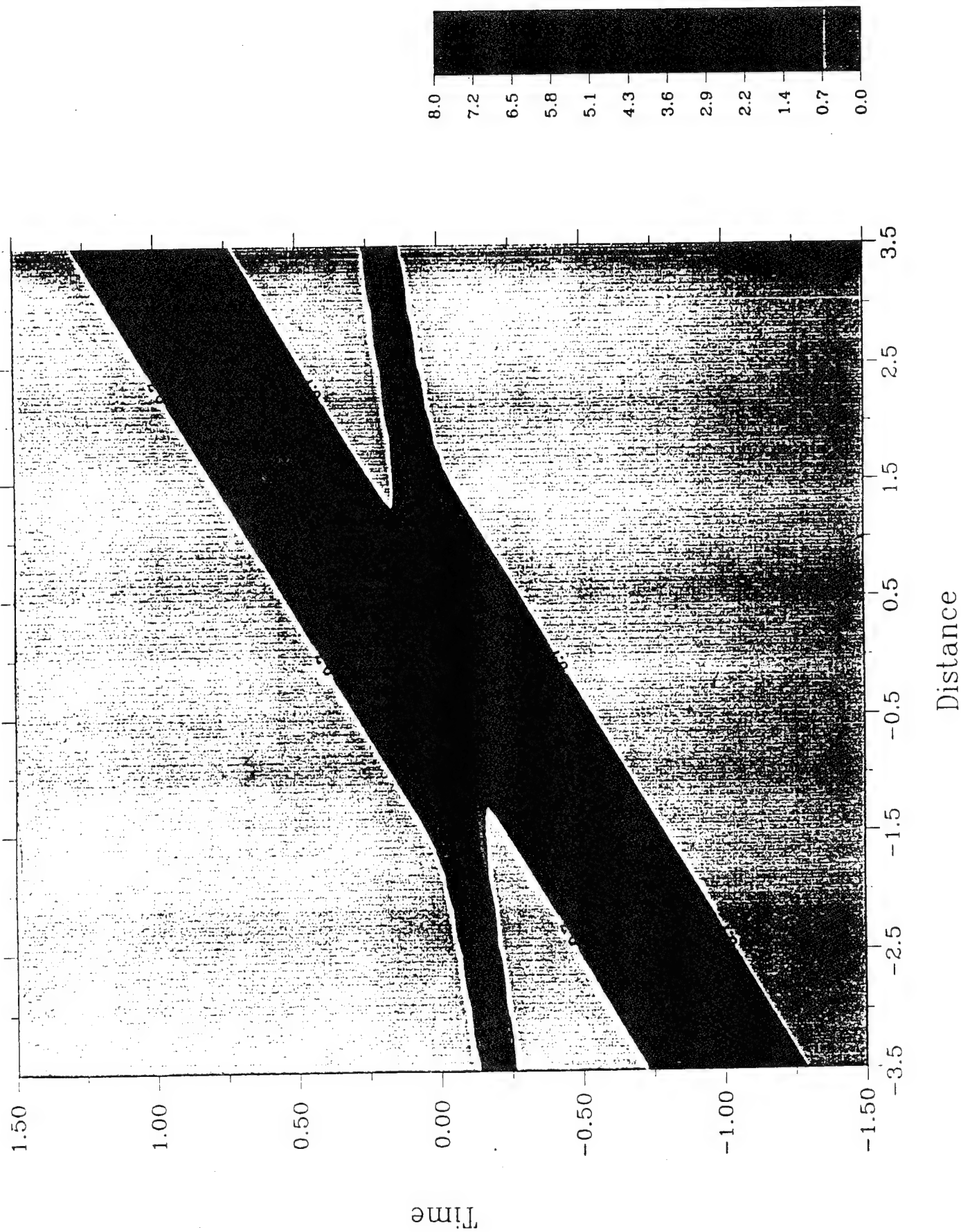
Magnetostatic Potential $|U|$



Y axis

X axis



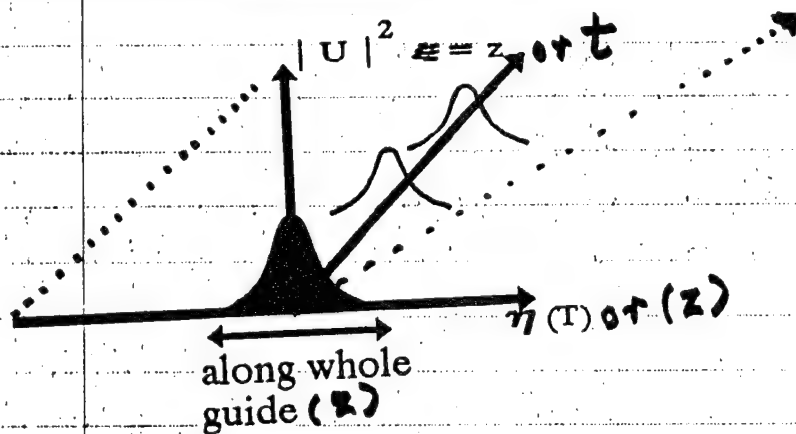


NUMERICAL SOLUTIONS

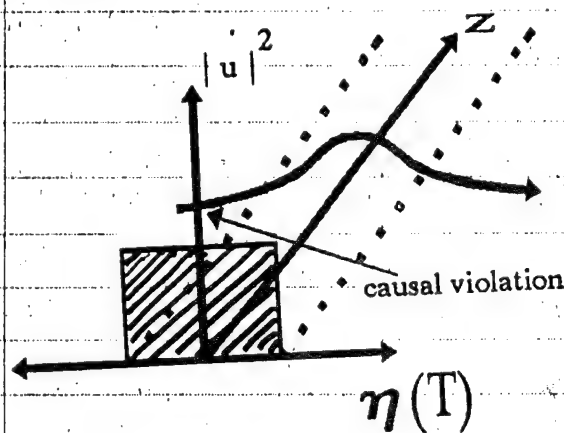
$$i \frac{\partial u}{\partial \xi} + \frac{1}{2} \frac{\partial^2 u}{\partial \eta^2} + |u|^2 u = 0$$

- ξ is 'propagation' distance
- η is transverse variable

Boundary conditions

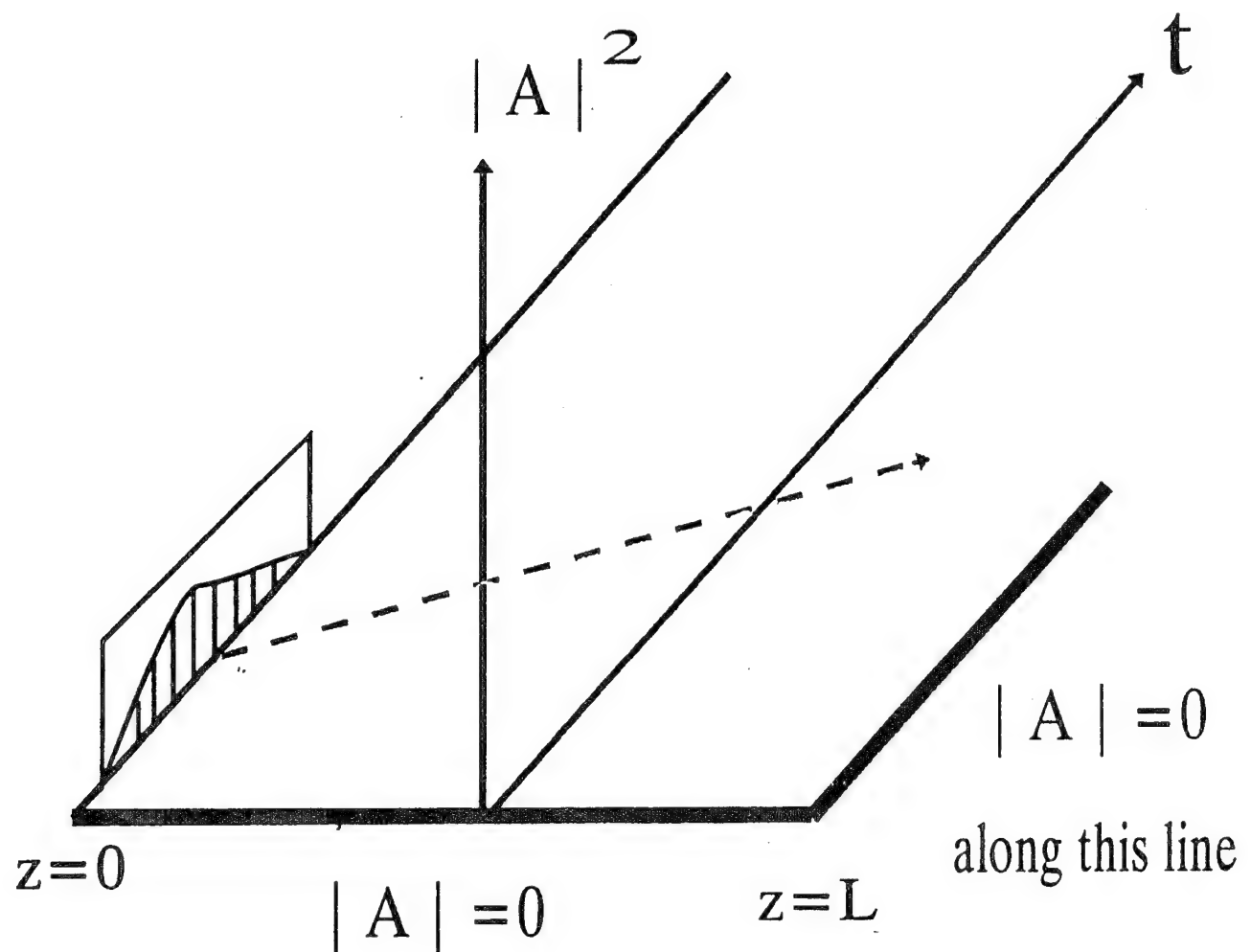


- produces symmetric pulses



- can use beam propagation

Alternative boundary condition

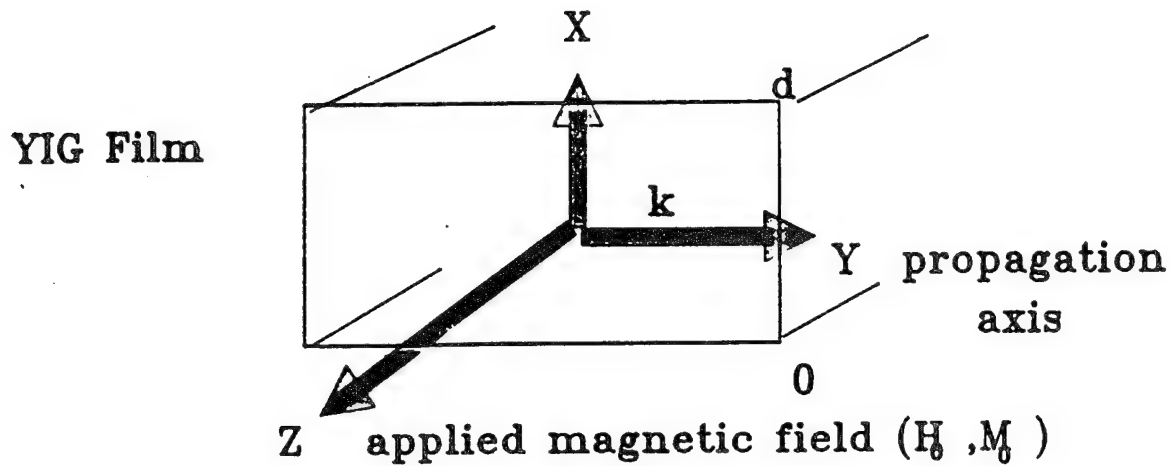


- clamped boundary condition
- needs finite-difference method
- produces asymmetric pulse shapes

SPIN WAVE ELECTRONICS

- **SOLITON FORMATION**
- **DECAY INSTABILITIES**
- **SELF-INTERACTION**
- **MAGNETOELASTIC WAVES**
- **BISTABILITY**
- **CONSTRUCTION OF rf DEVICES**
- **PARAMETRIC INTERACTIONS**

MAGNETOSTATIC WAVES (MSW)



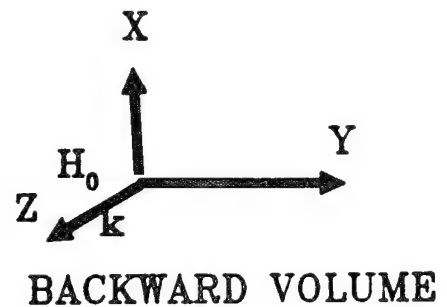
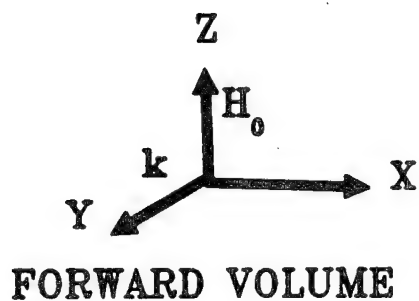
OUT

ferrimagnetic film

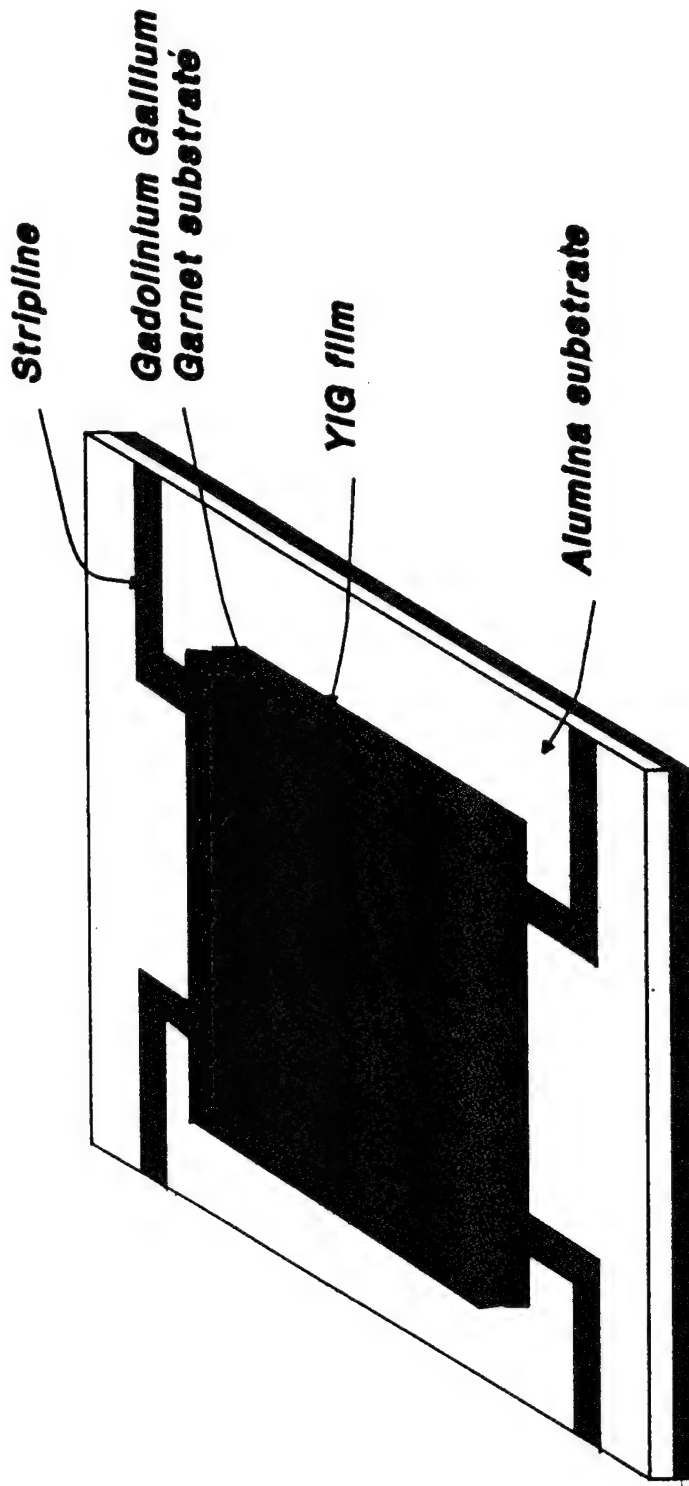
RETURN

A vector diagram showing the magnetization M as the sum of a static component M_0 along the Z -axis and a small precessional component m . The equation $M = M_0 z + m$ is written next to it.

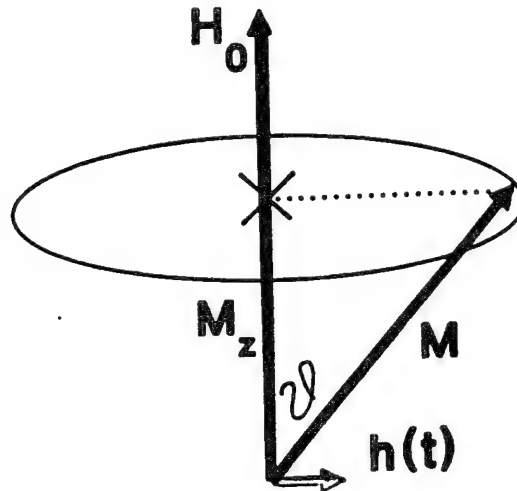
m is small



MSW Delay Line

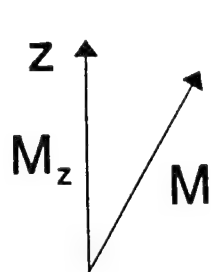
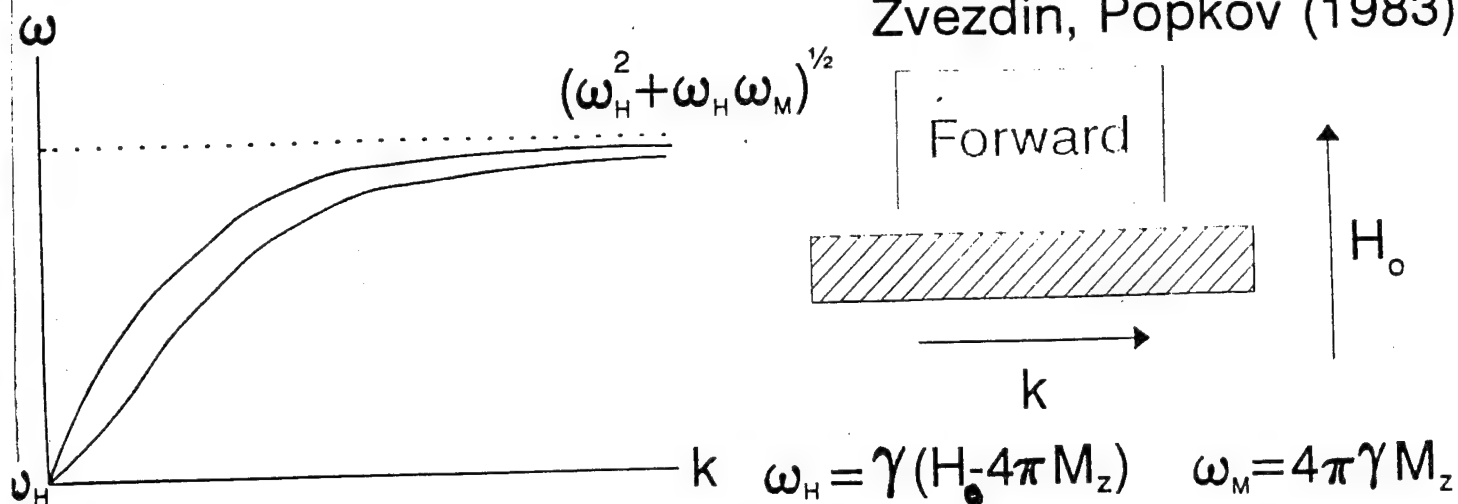


NUTATION OF MAGNETISATION ABOUT DC FIELD



- $\omega_H = \mu \gamma H_1$ = precession frequency
- $\omega_M = \mu \gamma M_z$ = magnetisation frequency
- H_1 is effective field (Intrnal field) = $(H_0 + NM_z)$
- angle ϑ is very small in linear systems
- $M_z \rightarrow M_0$ $N=0$ for surface waves
- power increase means nonlinearity
- M_z will decrease
- band edges will move up or down with power
- solitons can be looked for

Zvezdin, Popkov (1983)

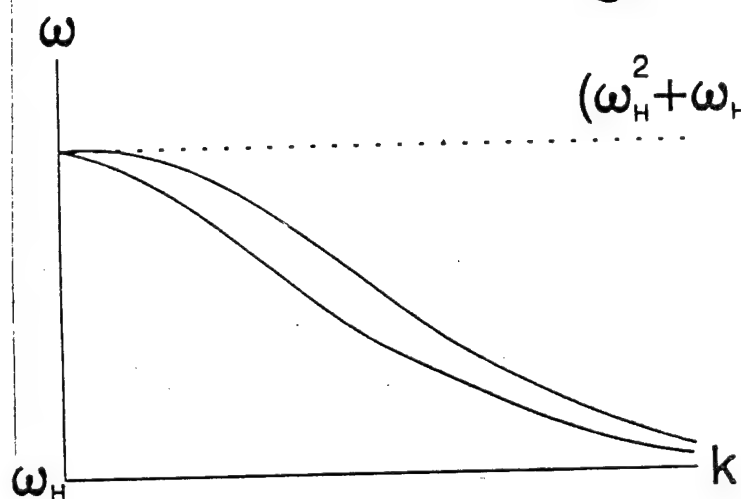


Power Increase $\rightarrow M_z \downarrow \rightarrow \omega_H \uparrow$

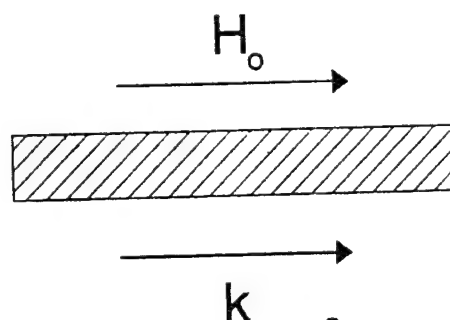
Therefore positive nonlinear change

$$\frac{\partial^2 \omega}{\partial k^2} < 0$$

$$\Delta \omega^{NL} > 0$$



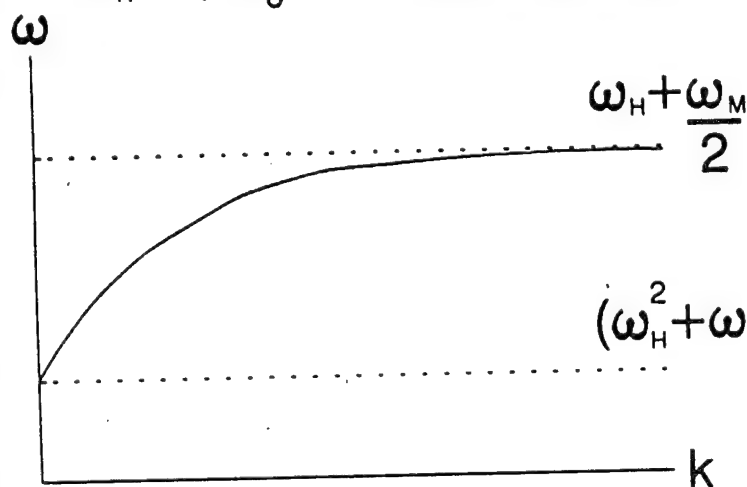
Backward



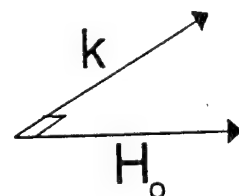
$$\omega_H = \gamma H_0$$

$$\omega_M = 4\pi\gamma M_z$$

$$M_z \downarrow \quad \omega_M \downarrow \quad \frac{\partial^2 \omega}{\partial k^2} > 0 \quad \Delta \omega^{NL} < 0$$

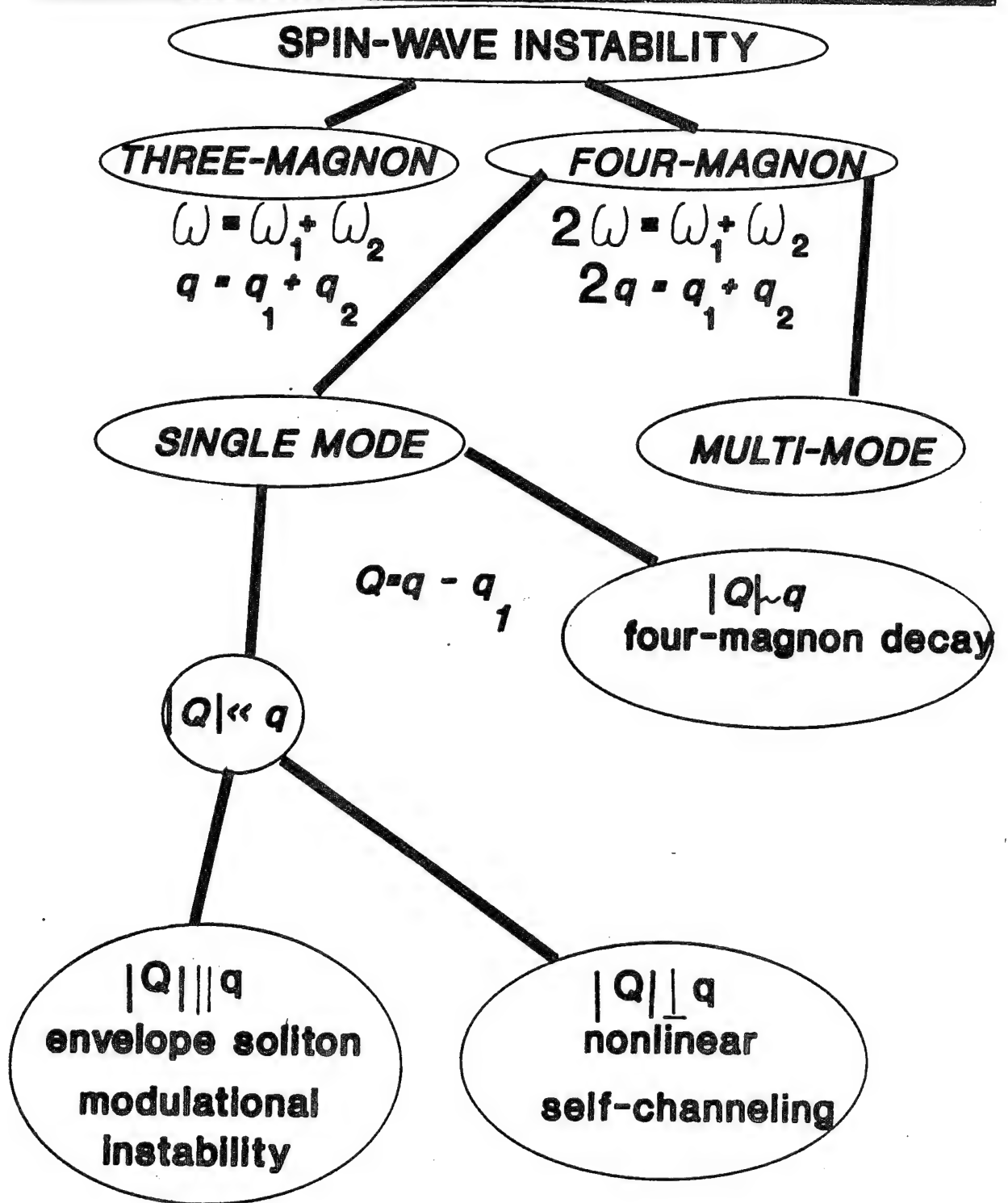


Surface



$$M_z \downarrow \quad \omega_M \downarrow \quad \frac{\partial^2 \omega}{\partial k^2} < 0 \quad \Delta \omega^{NL} < 0$$

NONLINEAR PROCESSES IN MAGNETIC MATERIALS



Data used:

■ width of square input pulse $0.18 \mu s$

■ normalised input intensity $|U_o|^2 = 0.0009$ $\left. \begin{array}{l} 0.0001 \\ 0.01 \end{array} \right\}$

■ group velocity of linear wave packets $\omega'_k = 1.8 \text{ cm} / \mu s$

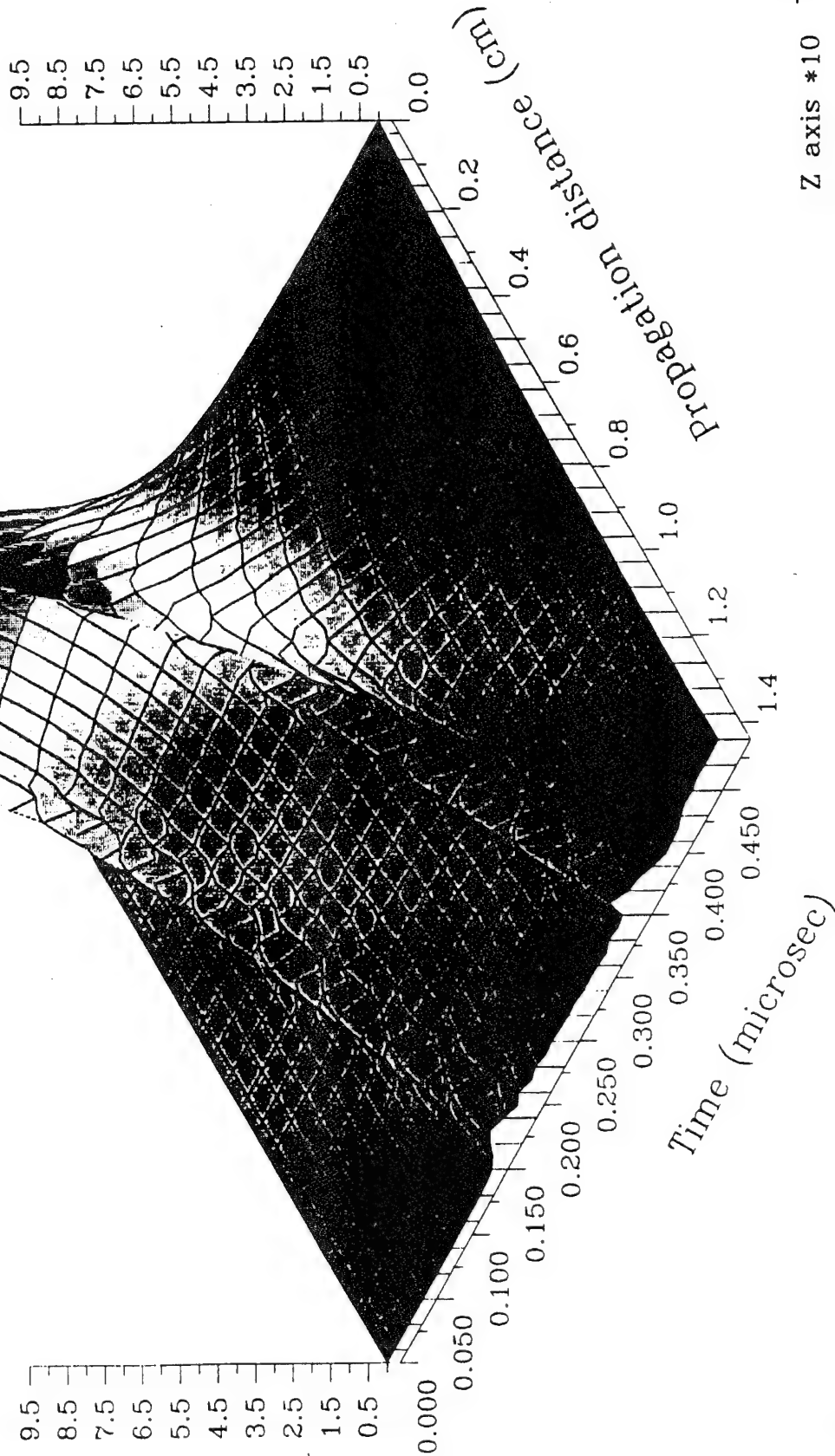
■ dispersion of medium $\omega''_k = -0.3 \text{ cm}^2 / \mu s$

■ derivative of the spin wave frequency with respect
to $|U|^2 = 30,000 / \mu s$

■ damping coefficient $\eta = 6.0 / \mu s$

Damped Pulse On A 5 Micron YIG Film Square Pulse: Input Amplitude 0.01

Magnetostatic Potential $|U|$



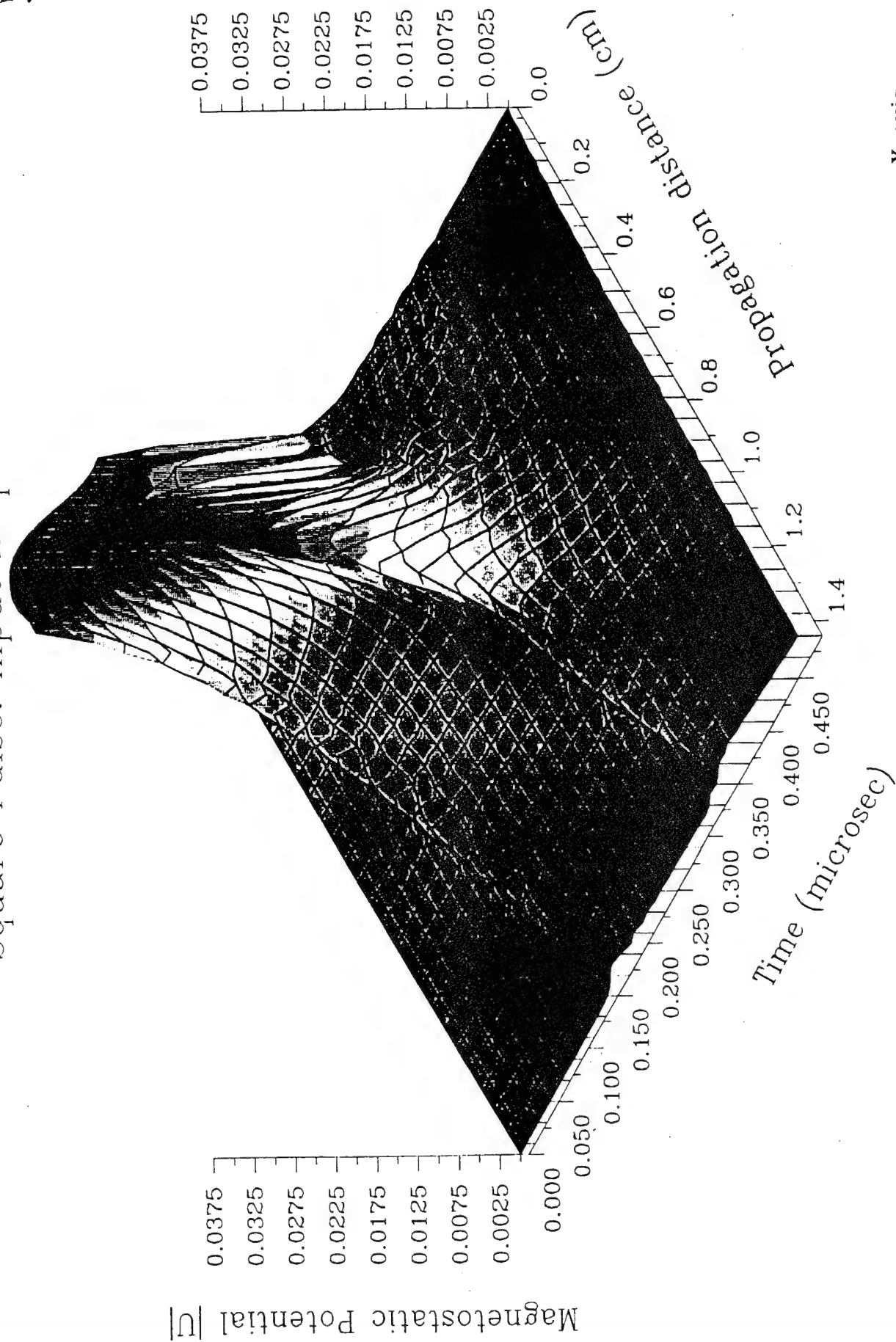
Y axis

Z axis *10
 X axis

-3

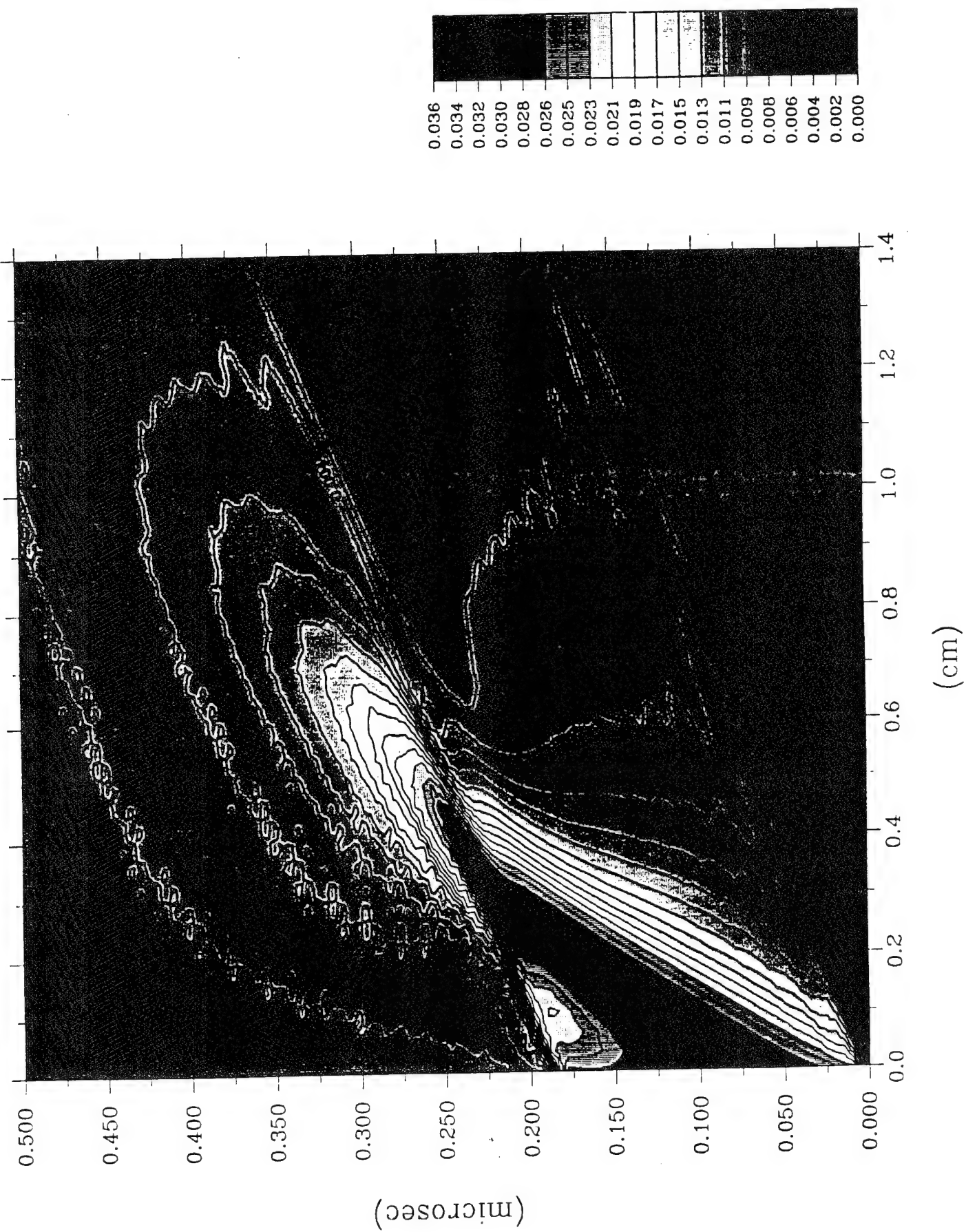
Damped Pulse On A 5 Micron YIG Film Square Pulse: Input Amplitude 0.03

45

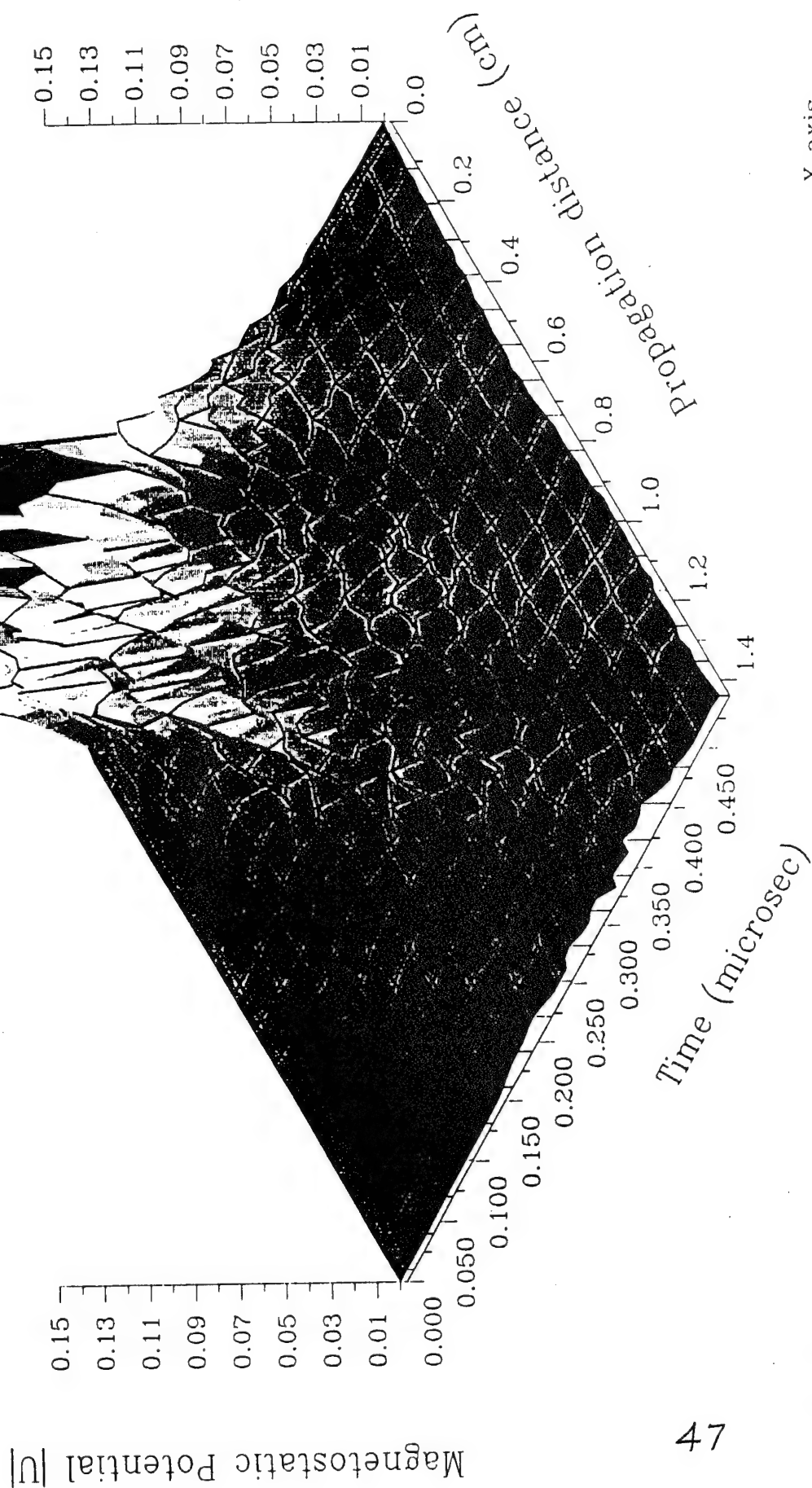


X axis

Y axis



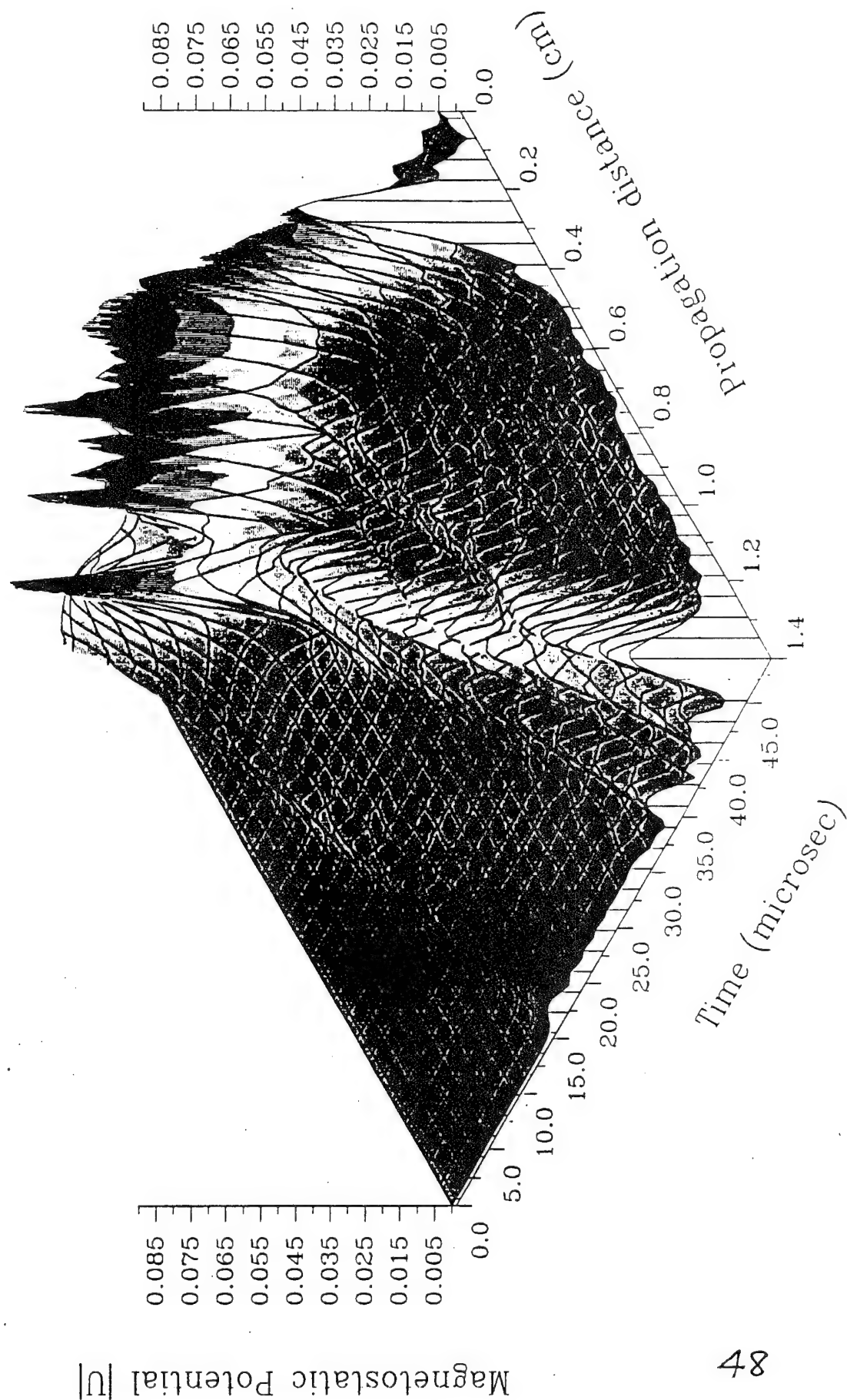
Damped Pulse On A 5 Micron YIG Film Square Pulse: Input Amplitude 0.1



X axis

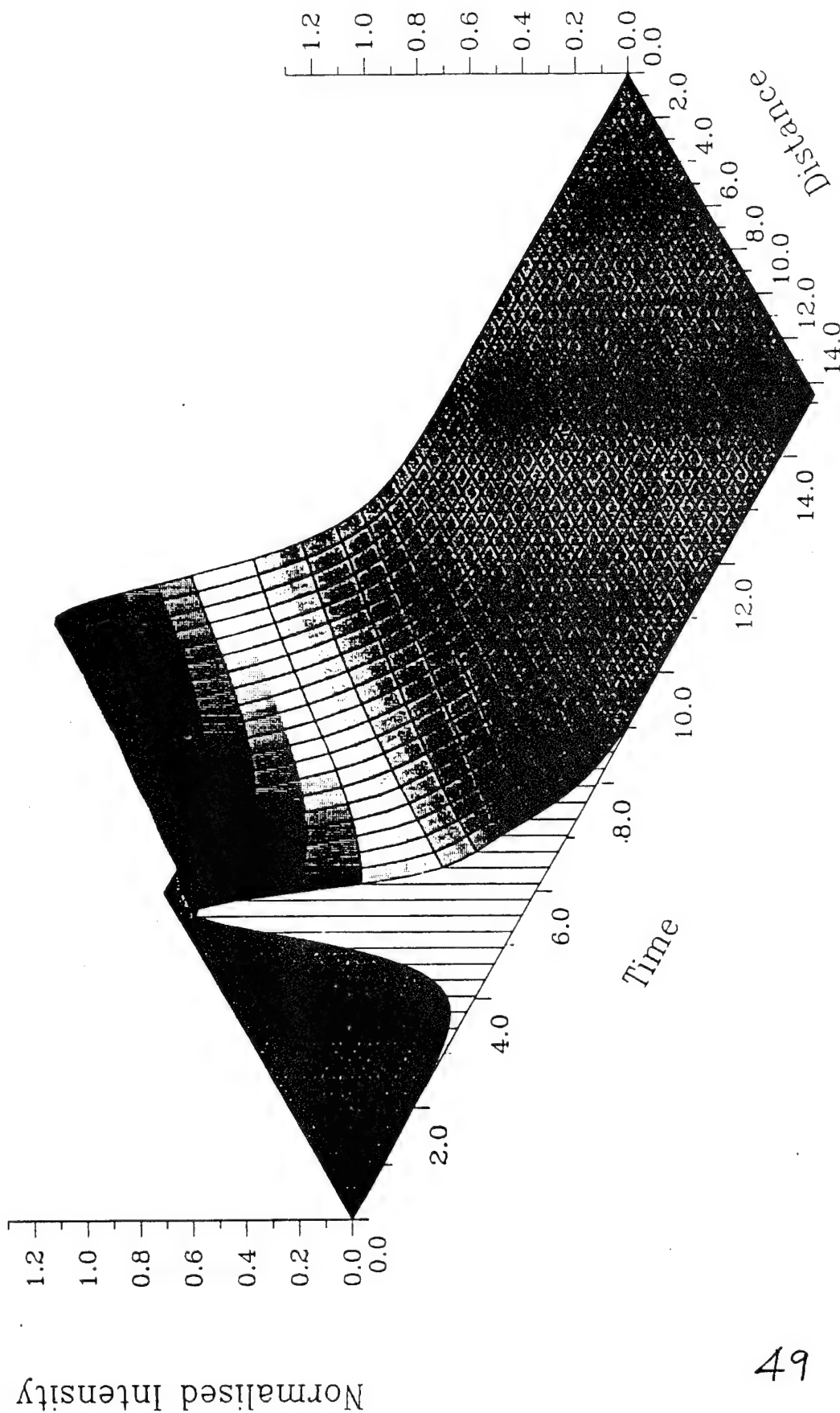
Y axis

Undamped Pulse On A Thin YIG Film



Magnetostatic Potential $|U|$

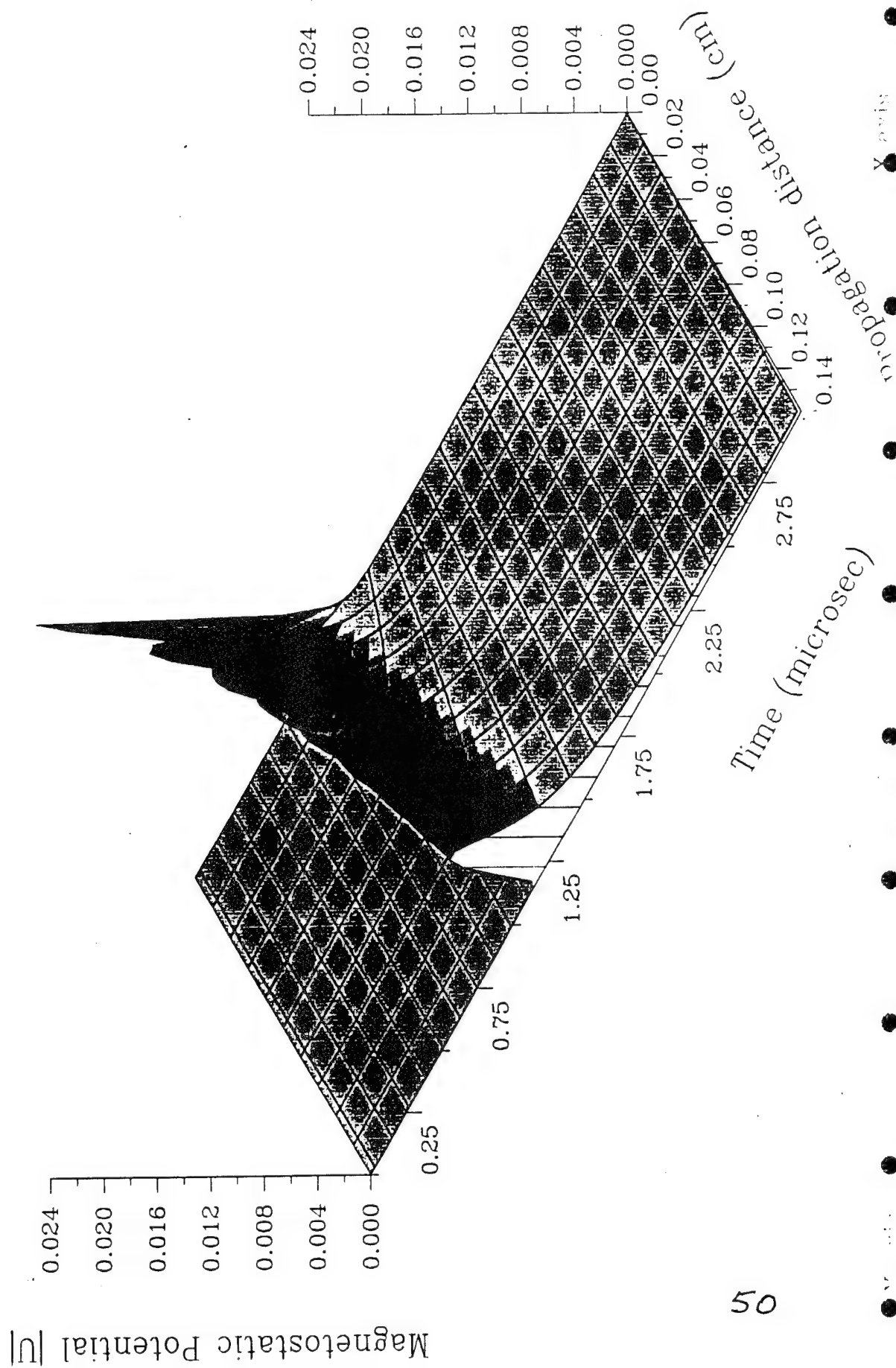
Undamped Fundamental Soliton

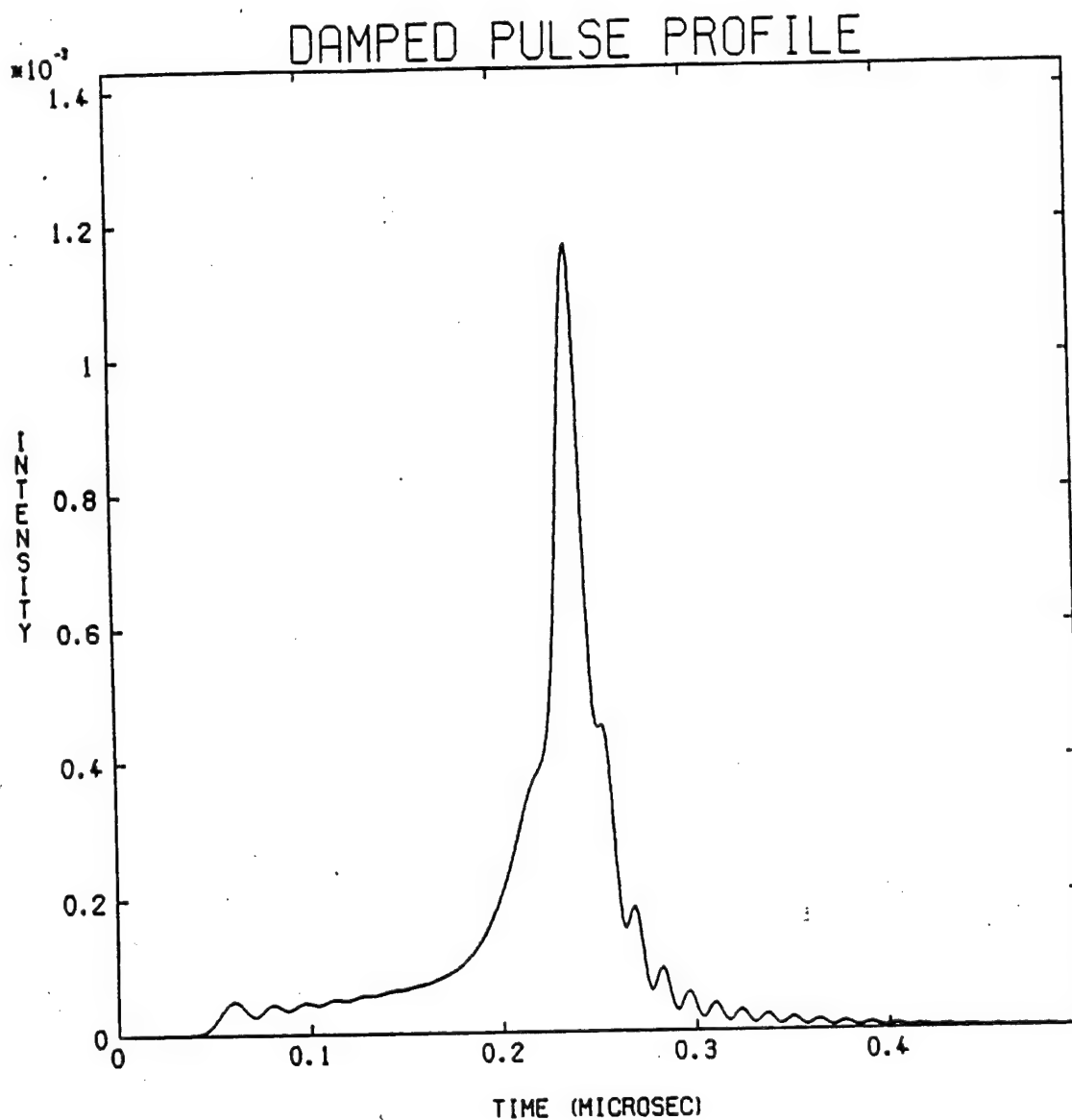


X axis

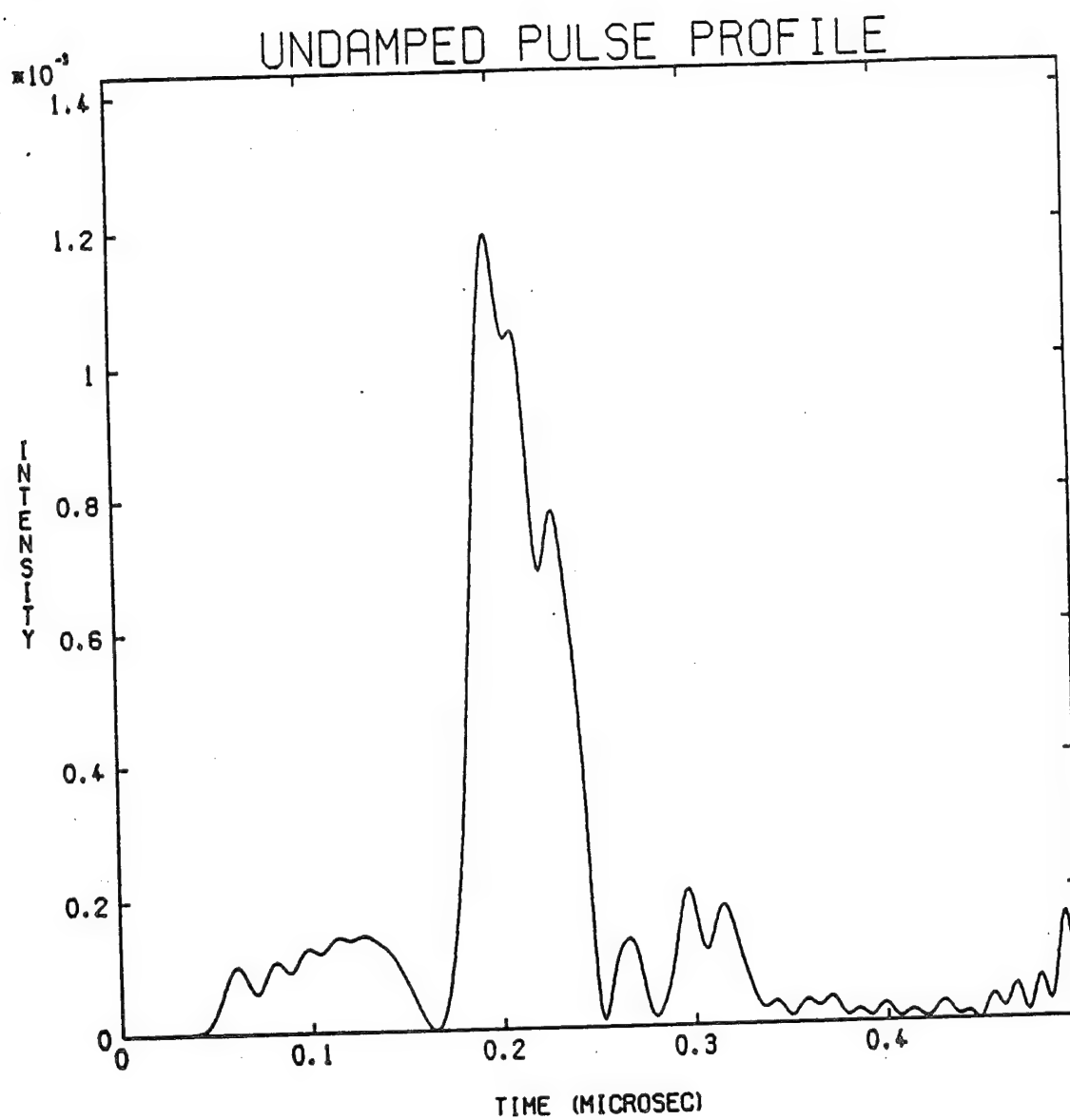
Y axis

Undamped Sech Pulse On Thin YIG Film





Spin wave profile in a YIG thin film at $x=0.4\text{cm}$ with a square 180ns input pulse and normalised intensity of 0.0009 at $x=0.0$ and damping coefficient set at 6.0 per microsec.

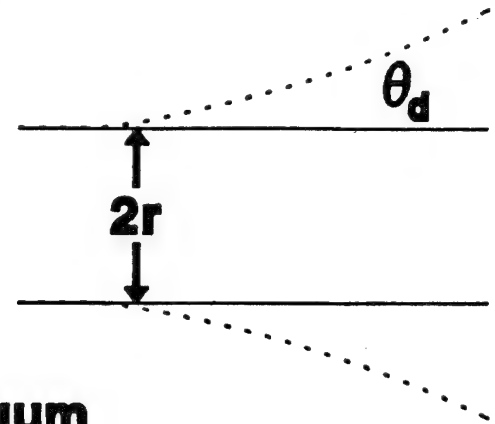


Same as above figure but **WITHOUT** damping.

The Critical Condition of Self-trapping (Self-focusing)

diffraction law :

$$\theta_d = \frac{\lambda}{2\sqrt{\mu_m} r}$$



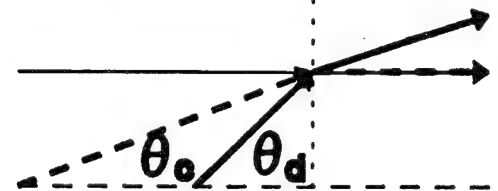
λ : wavelength in vacuum

μ_m : effective magnetic permeability

Snell's law: ($\mu_m^{NL} = \mu_m + \alpha |H|^2$)

$$\sqrt{\mu_m} \sin \pi/2 = (\sqrt{\mu_m} + \frac{\alpha}{2\sqrt{\mu_m}} |H|^2) \cos \theta_o$$

$$\theta_o^2 = \frac{\alpha}{\mu_m} |H|^2$$



● $\theta_o > \theta_d$: rays return to axis

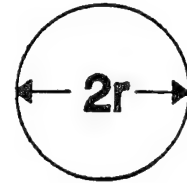
balance obtained : $\theta_o = \theta_d$

$$\alpha |H|^2 = \frac{\lambda^2}{4r^2}$$

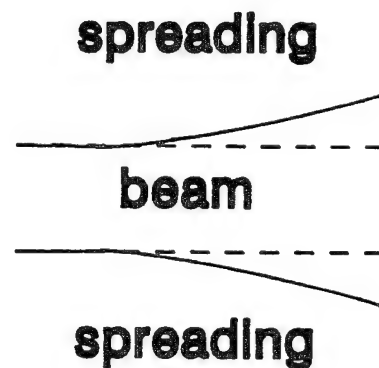
Beam Propagation (Bulk)

■ power at balancing condition:

$$P_0 = \frac{\pi r^2}{2} \frac{\omega \mu_0}{k_0} |H|^2 = \frac{\omega \mu_0 \lambda^3}{8 \alpha}$$



▲ $P < P_0$: diffraction spreading



▲ $P > P_0$: self-focusing



▲ $P = P_0$: diffraction = self-focusing

■ problem: P_0 is fixed, fluctuation in P

runaway to
diffraction

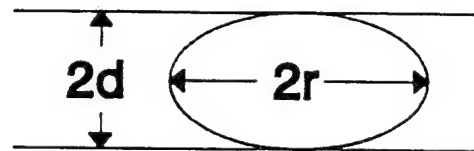
runaway to
self-focusing

Propagation in a Waveguide

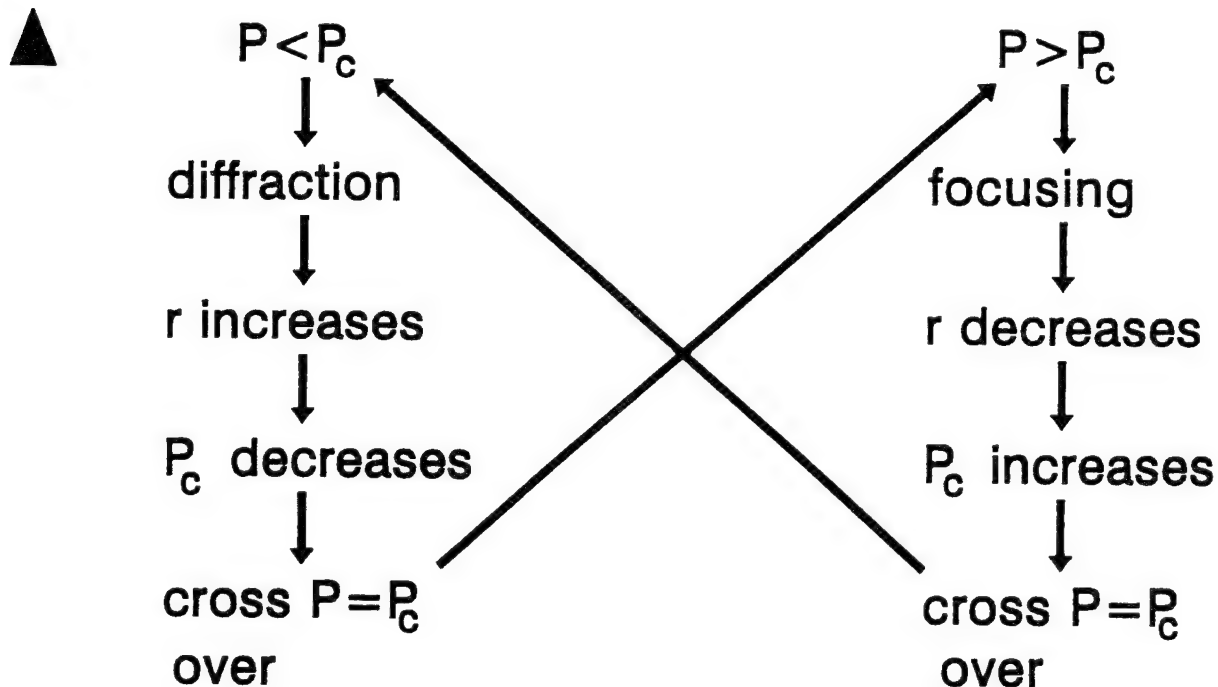
- take advantage of waveguide,
power at balancing condition:

$$P_c = \frac{\pi r d}{2} \frac{\omega \mu_0}{k_0} |H|^2$$

$$= \frac{\omega \mu_0 \lambda^3}{8\alpha} \frac{d}{r}$$



d is guide dimension, focusing changes r but not d

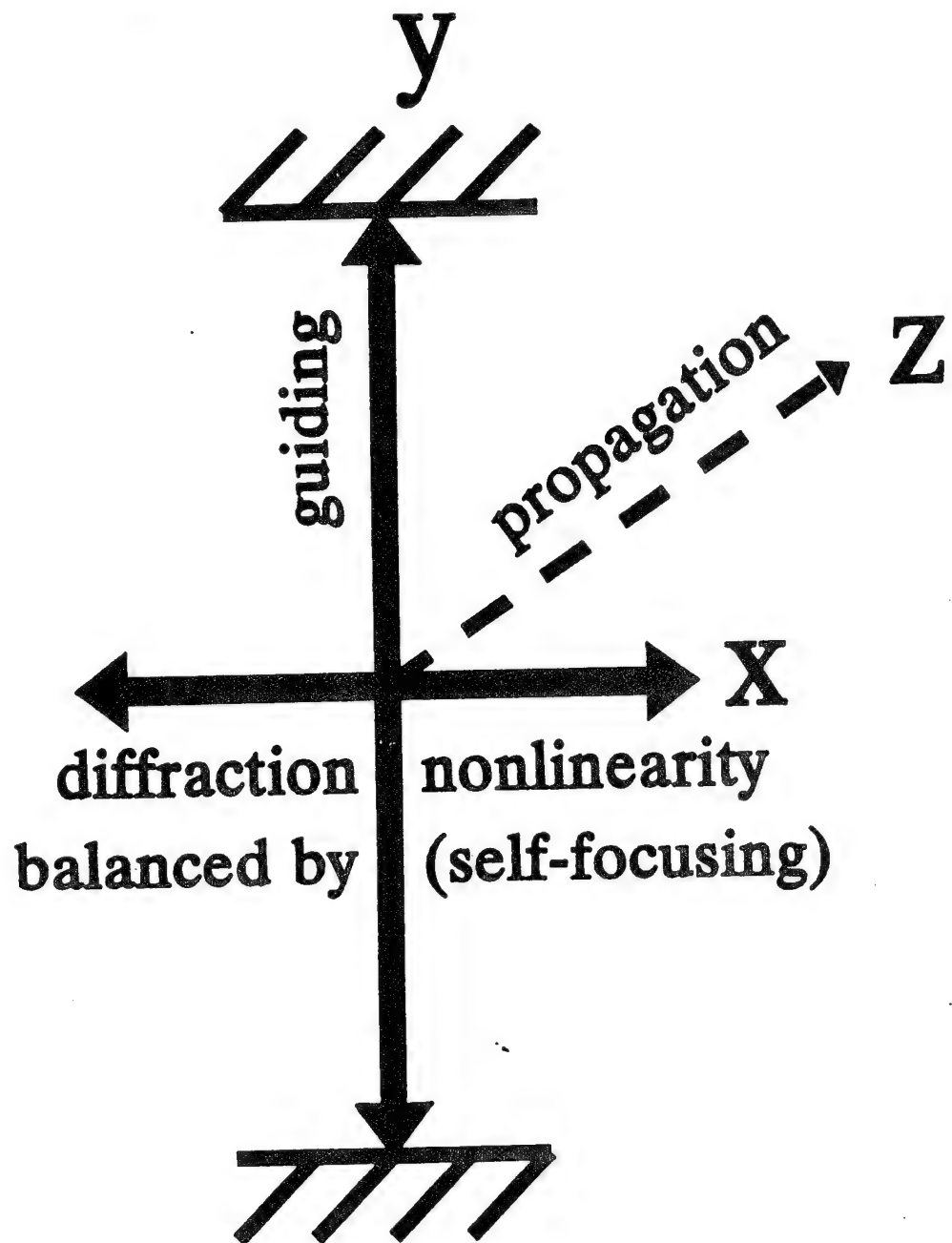


used for the design of the waveguide

▲ $P = P_c$, balance obtained

stable (no runaway)

SPATIAL SOLITONS

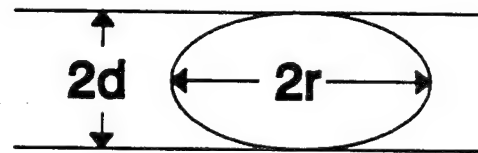


Propagation in a Waveguide

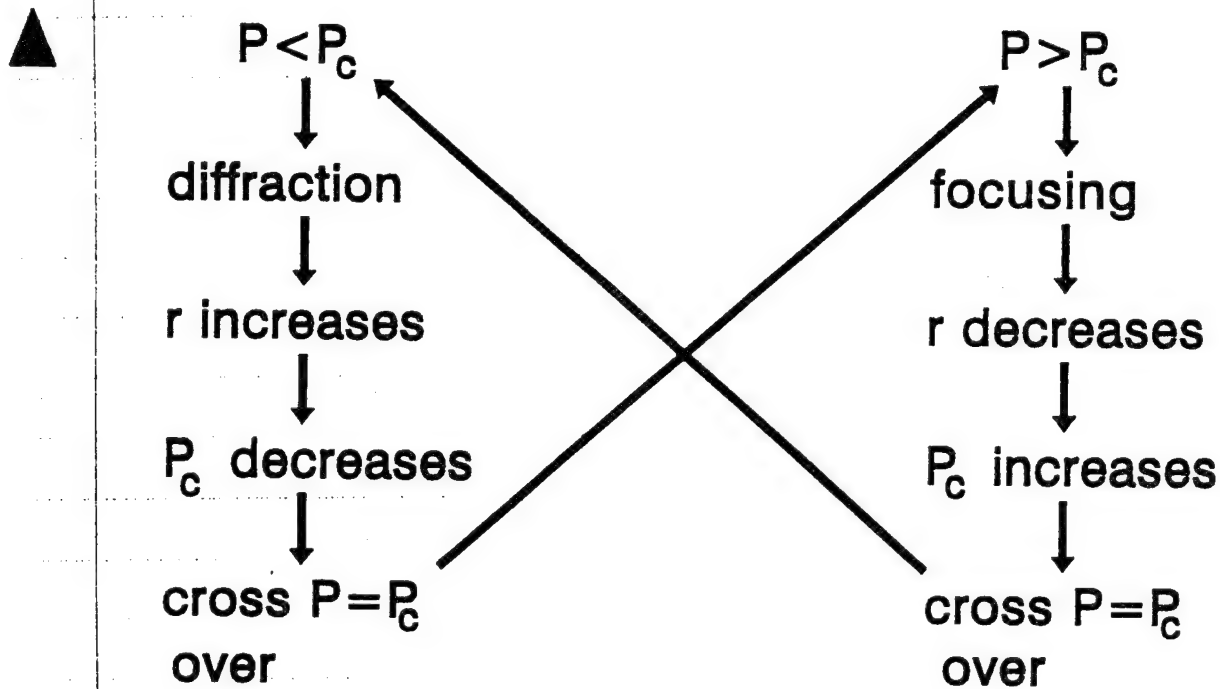
take advantage of waveguide,
power at balancing condition:

$$P_o = \frac{\pi r d}{2} \frac{\omega \mu_0}{k_0} |H|^2$$

$$= \frac{\omega \mu_0 \lambda^3}{8\alpha} \frac{d}{r}$$



d is guide dimension, focusing changes r but not d



oscillate around the point $P = P_c$

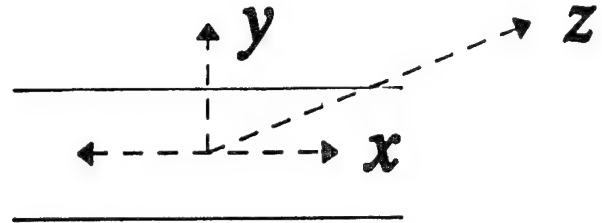
▲ $P = P_c$, balance obtained

stable (no runaway)

Spatial Solitons

$$i \frac{\partial A}{\partial t} + \frac{v_s}{2k_0} \frac{\partial^2 A}{\partial x^2} - \alpha_\omega |A|^2 A = 0$$

$$\frac{\partial}{\partial t} = -v_s \frac{\partial}{\partial z}$$



$$L_D = k_0 D_0^2 \quad z \rightarrow z L_D$$

$$i \frac{\partial A}{\partial z} + \frac{1}{2} \frac{\partial^2 A}{\partial x^2} - \frac{L_D}{v_s} \alpha_\omega |A|^2 A = 0$$

Power flow for $A = A_0 \text{sech}(x/D_0)$:

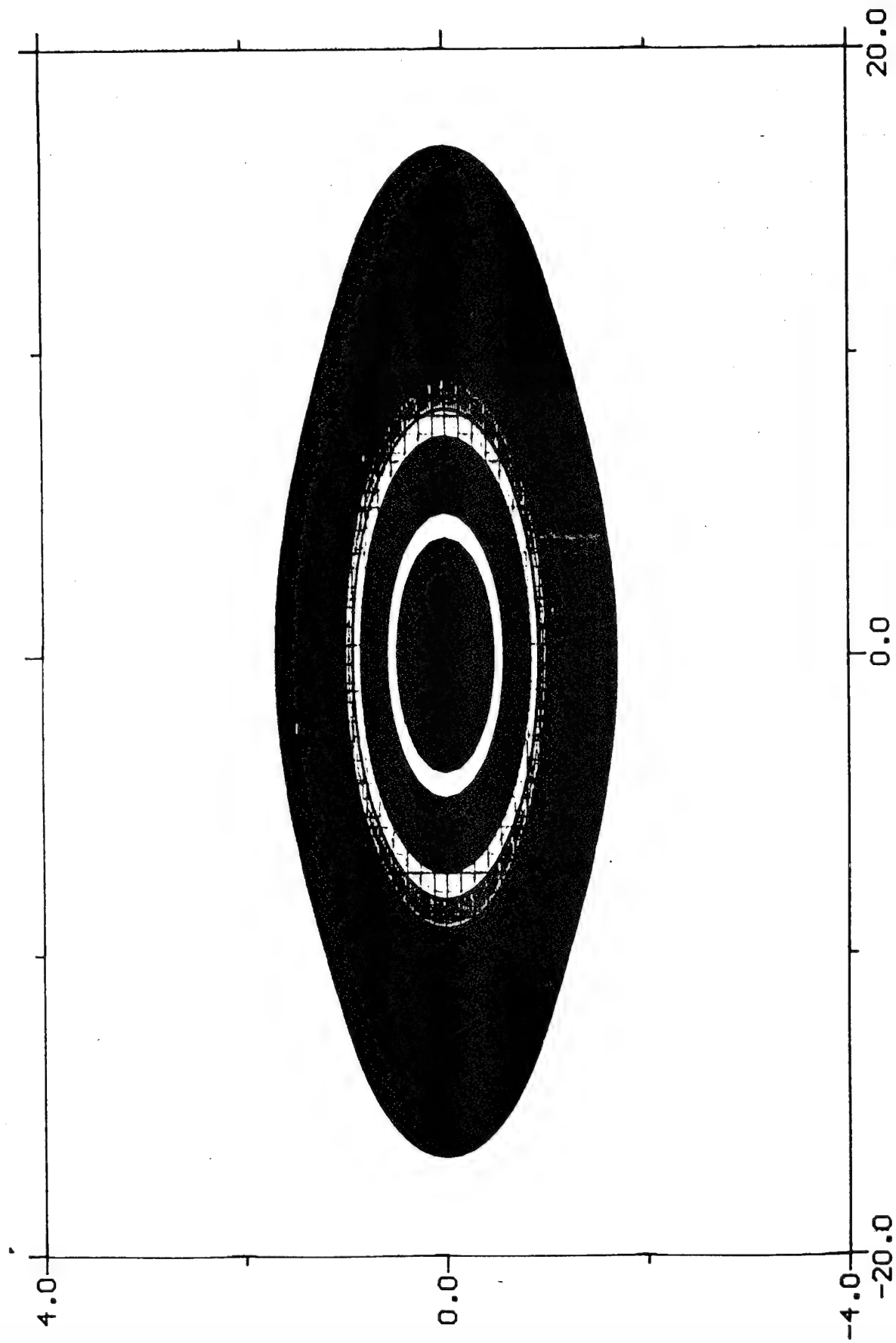
$$P_0 = \mu_0 \omega / 2k_0 \iint H^2 dx dy = \mu_0 \omega D_0 A_0^2 k_0$$

$$A = \sqrt{\frac{P_0}{\mu_0 \omega D_0 k_0}} u \quad L_{NL} = \frac{v_s \mu_0 \omega D_0 k_0}{|\alpha_\omega| P_0}$$

$$i \frac{\partial u}{\partial z} + \frac{1}{2} \frac{\partial^2 u}{\partial x^2} + \frac{L_D}{L_{NL}} |u|^2 u = 0$$

Magnetostatic potential

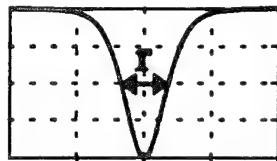
$$\Psi = A(x, z) \frac{B(y)}{\sqrt{1 + \alpha^2 y^2}} \exp(ik_0 z)$$



Contour Height $\times 10^{-4}$

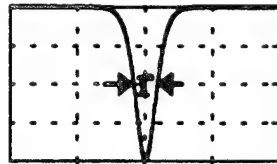
Dark Wave Propagation

Once launched, the amplitude $|H|$ of the background is a constant.

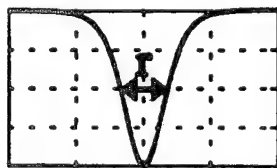


$$|H| > |H_c| \rightarrow \theta_c > \theta_d$$

self-focusing \rightarrow r decreases

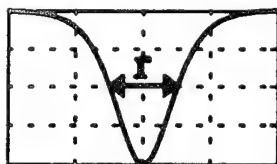


$|H_c|$ increases



$$|H| < |H_c| \rightarrow \theta_c > \theta_d$$

diffraction \rightarrow r increases



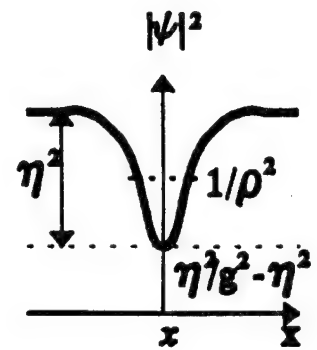
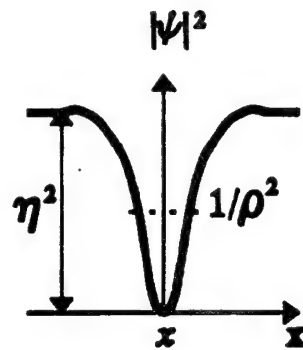
$|H_c|$ decreases

balance obtained at $|H| = |H_c|$

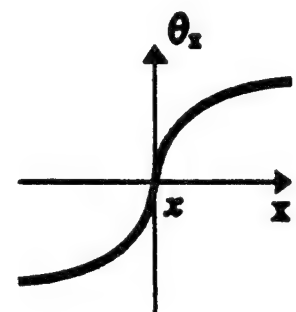
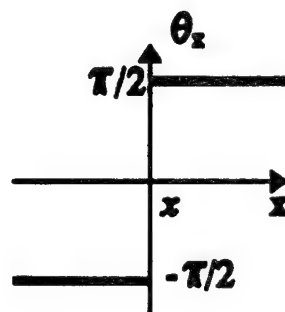
black
($g=1$)

grey

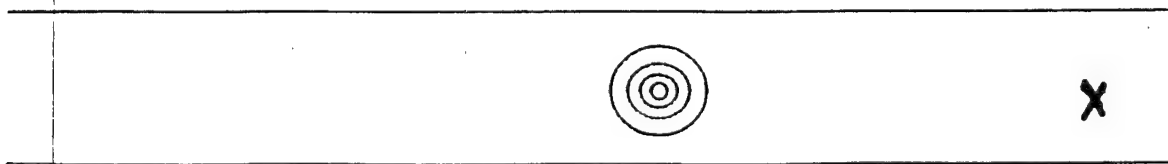
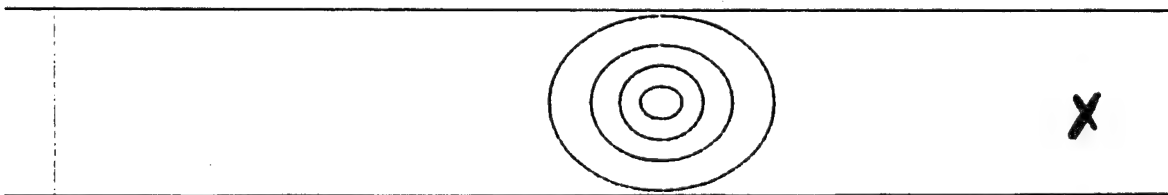
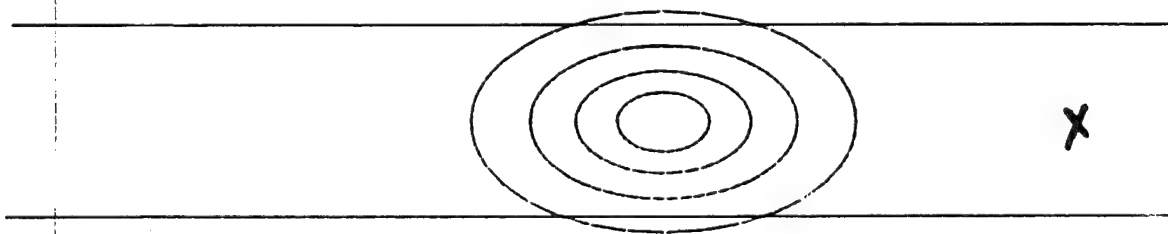
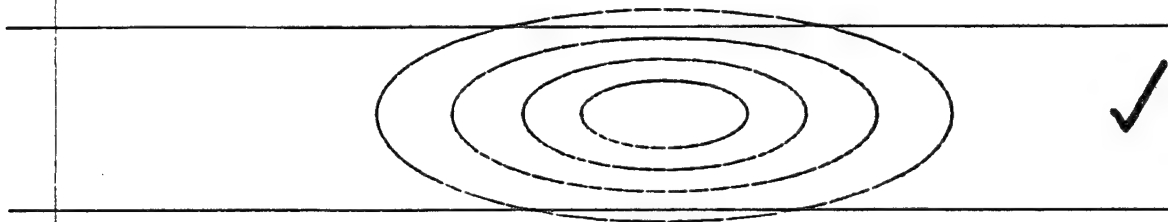
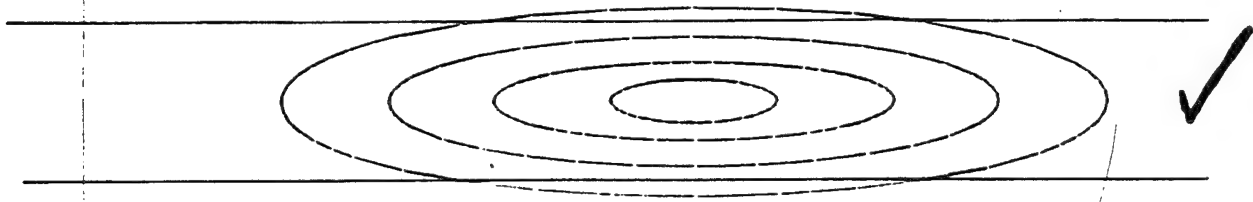
Intensity

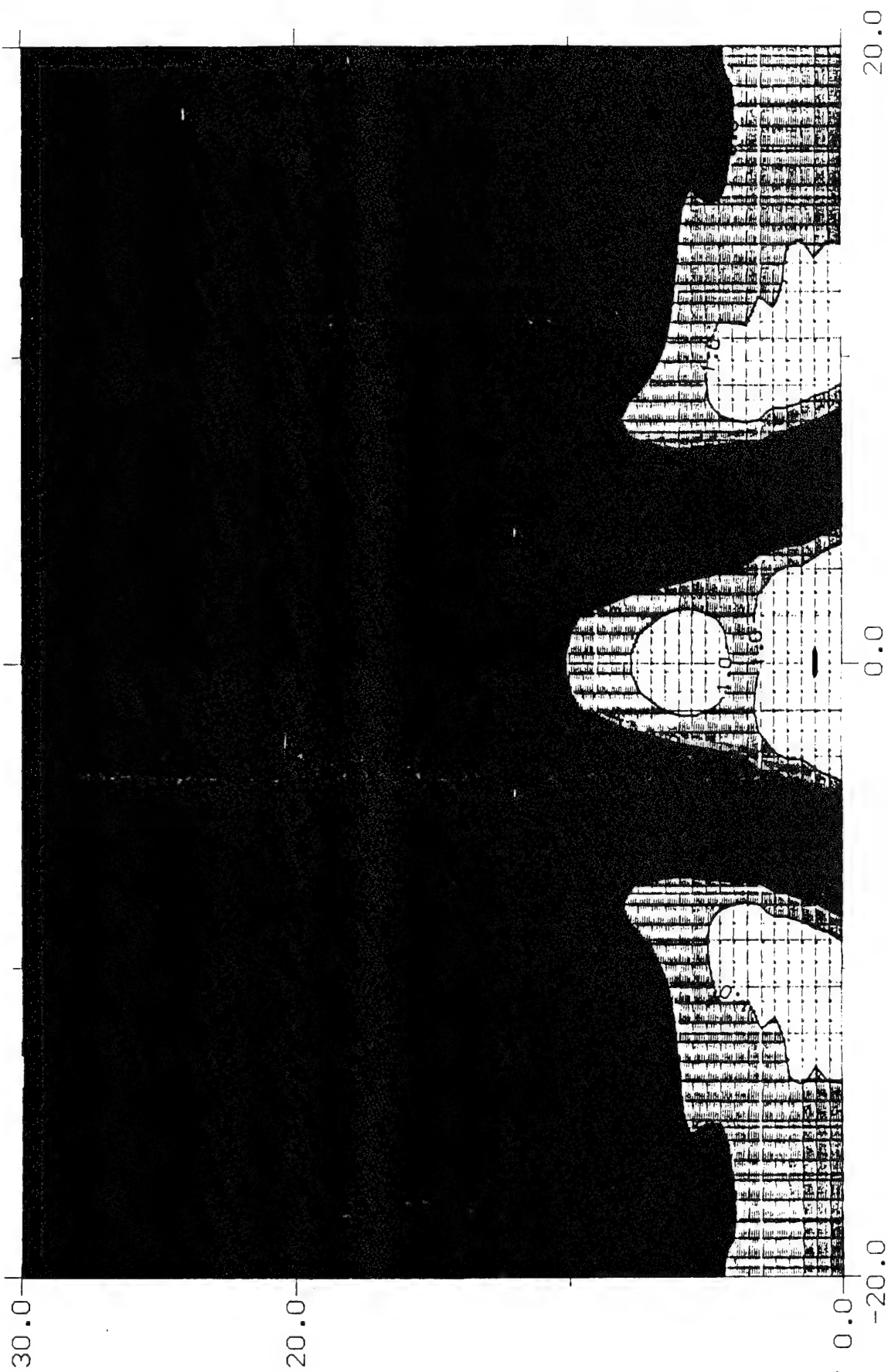


Phase



Intensity and phase of black and grey soliton beams.





QUANTUM-WELL STATES AND
GIANT MAGNETORESISTANCE
IN MAGNETIC MULTILAYERS.

A. C. Ehrlich

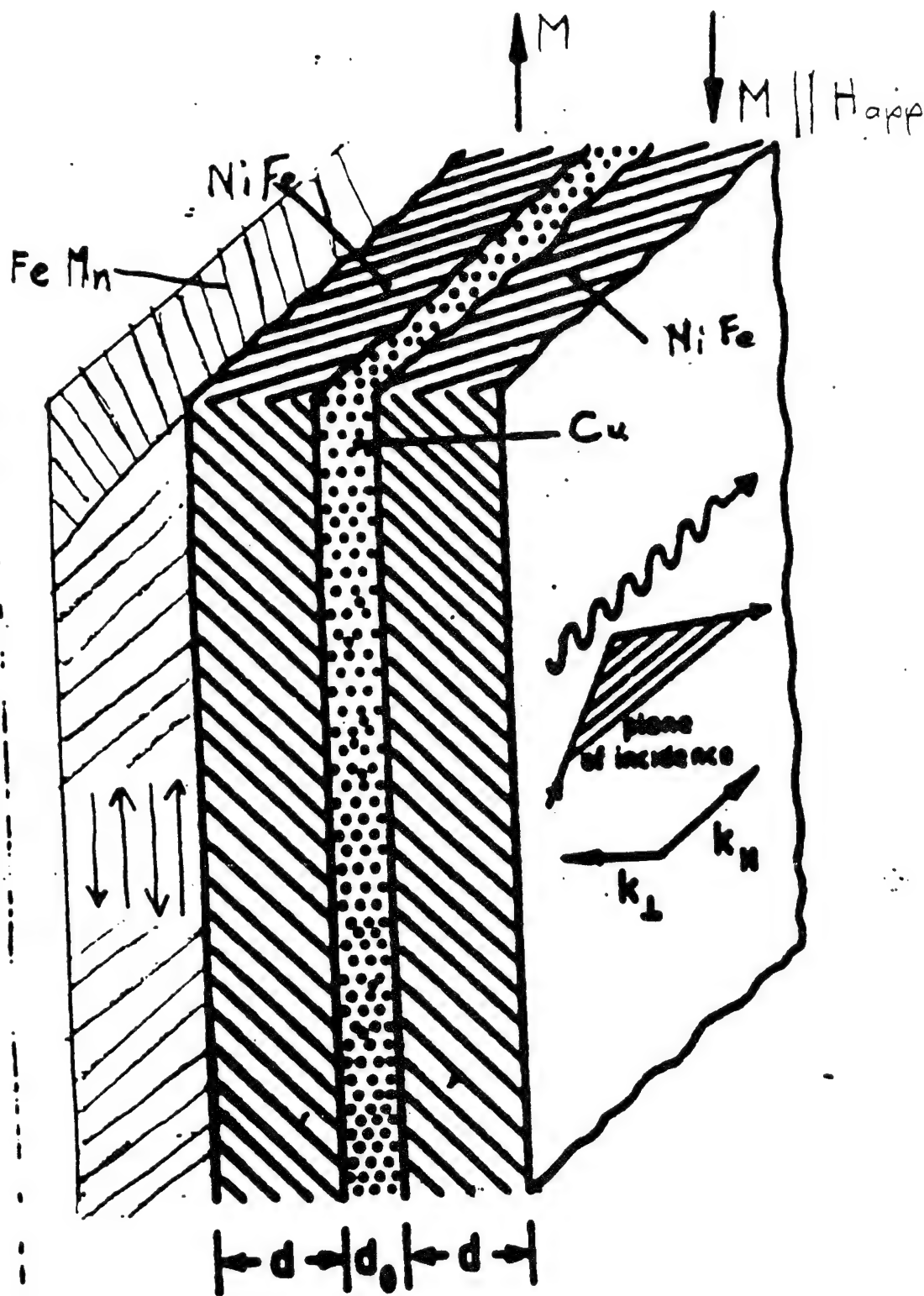


FIG. 1. Ferromagnetic double layer with antiparallel alignment of the magnetizations. Also indicated is the plane of incidence of the laser light for the observation of light scattering

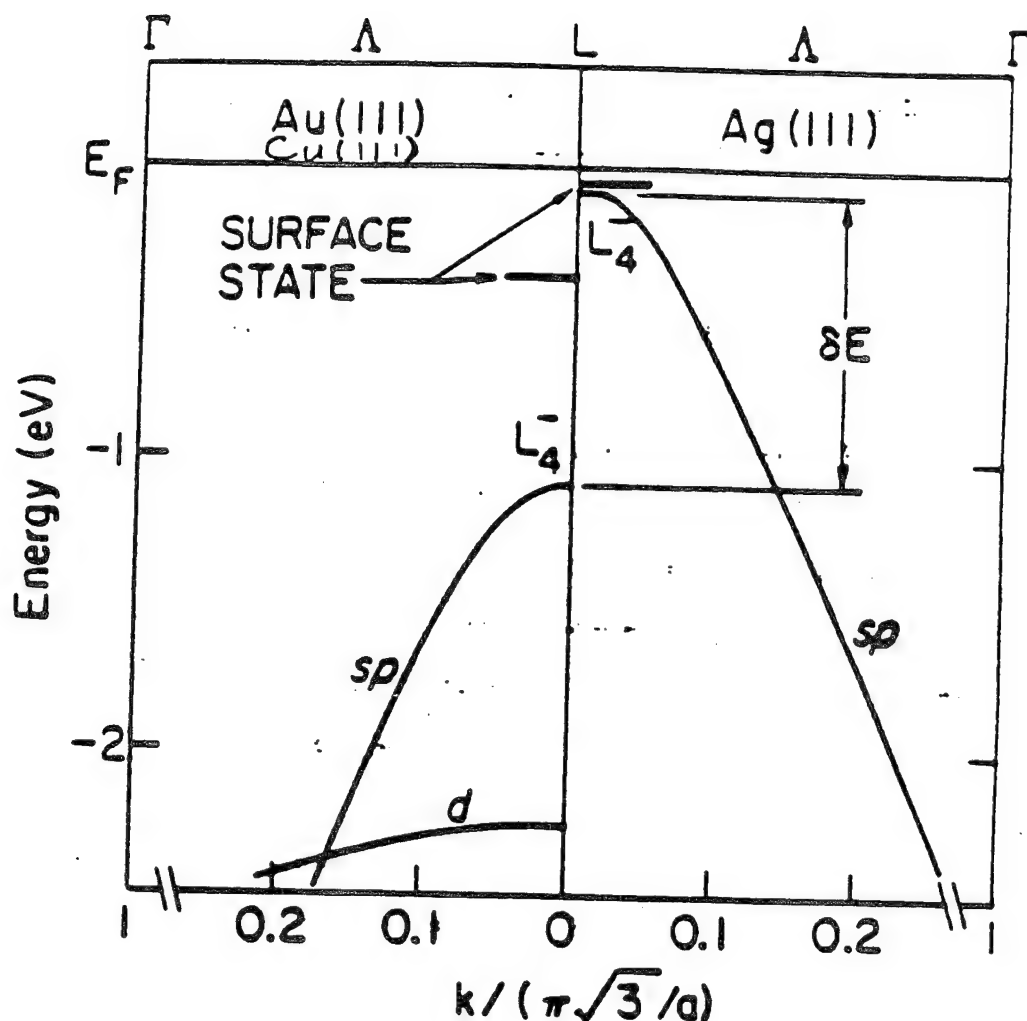


FIG. 2. Valence-band dispersion curves for Ag(111) and Au(111) along the [111] direction. For each system, a surface state is indicated. The wave vector k is measured in terms of $\pi\sqrt{3}/a$, where $a = 4.09 \text{ \AA}$ is the lattice constant for both Ag and Au. The energy window δE for the quantum-well states is indicated.

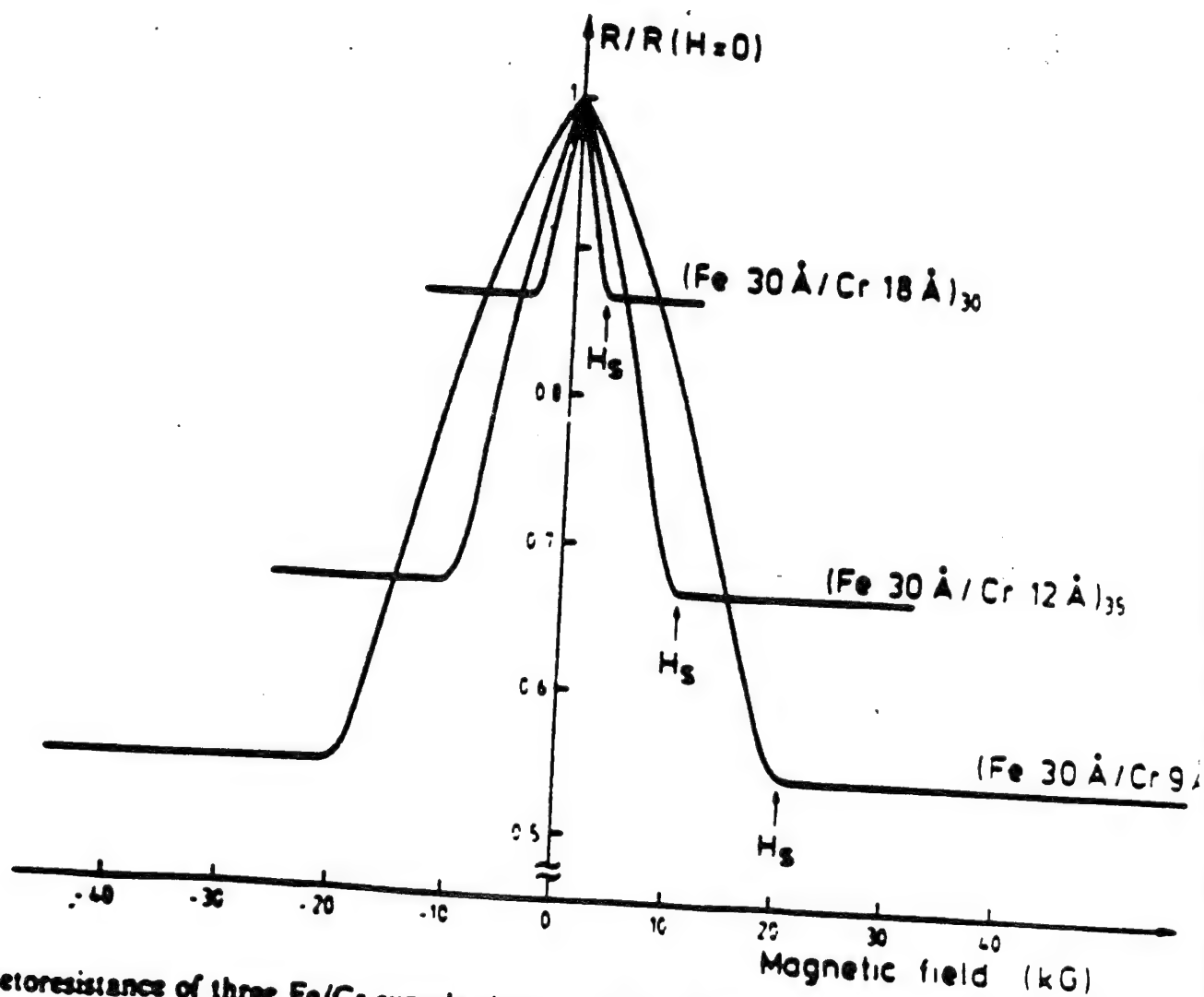


FIG. 3. Magnetoresistance of three Fe/Cr superlattices at 4.2 K. The current and the applied field are along the plane of the layers.

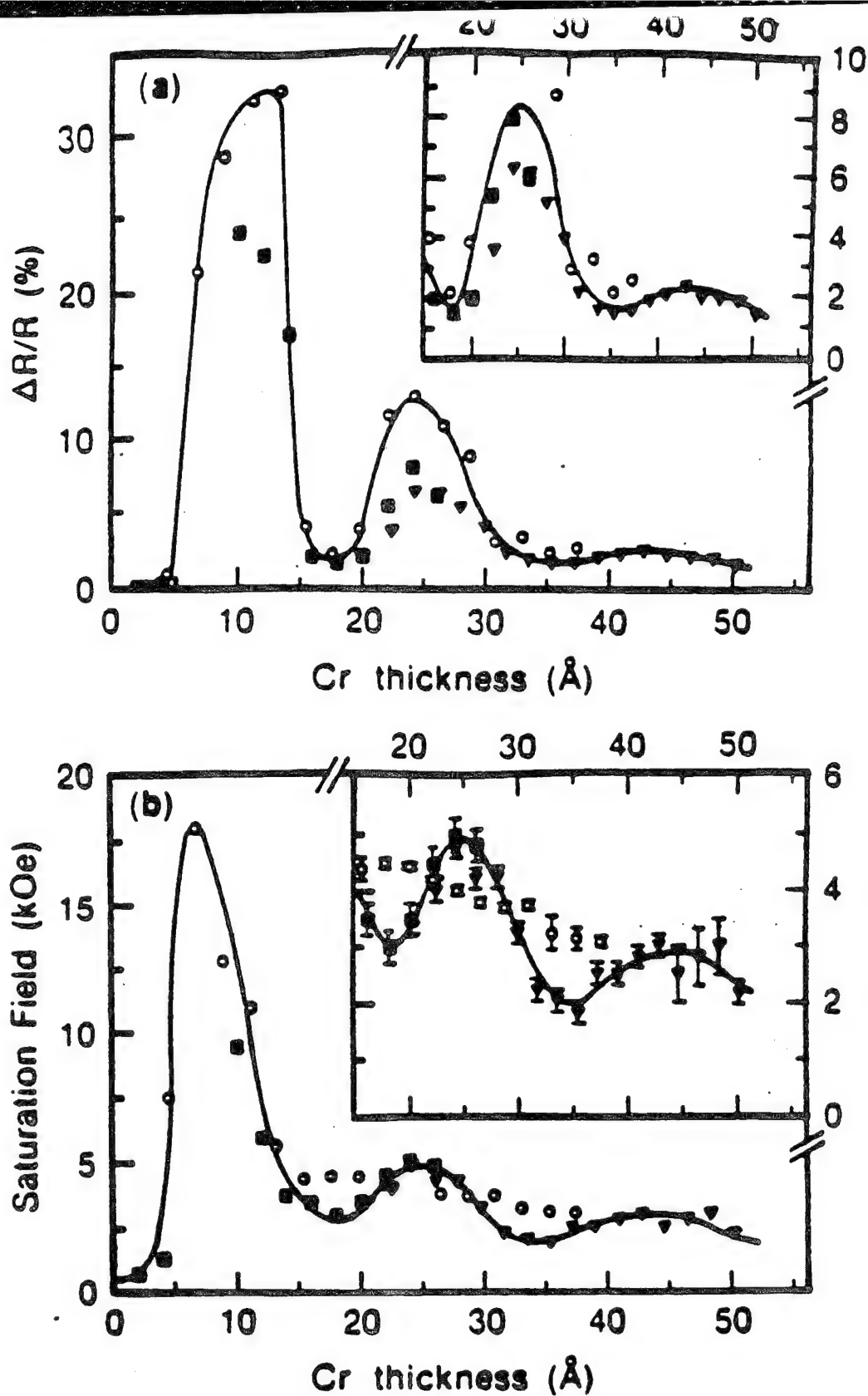


FIG. 4. (a) Transverse saturation magnetoresistance (4.5 K) and (b) saturation field (4.5 K) vs Cr layer thickness for three series of structures of the form Si(111)/(100 Å) Cr/[(20 Å) Fe/ t_{Cr} Cr] $_N$ /(50 Å) Cr, deposited at temperatures of Δ , \blacksquare , \circ 100°C ($N=10$), 125°C ($N=20$), 150°C ($N=30$).

Influence of Intralayer Quantum-Well States on the Giant Magnetoresistance in Magnetic Multilayers

A. C. Ehrlich

Naval Research Laboratory, Washington, D.C. 20375

(Received 17 March 1992; revised manuscript received 28 January 1993)

A model which can account for the experimentally observed variations of the giant magnetoresistance in thin magnetic multilayers with mean free path, interface roughness, magnetic layer, and normal layer thickness has been developed. The model requires the existence of quantum-well states within individual layers or groups of layers, depending on the magnetic state of the film. The calculated results are obtained by the application of quantum size effect transport theory to these individual layers.

PACS numbers: 73.50.Jt, 73.61.Ai, 75.70.-i

The first report by Baibich *et al.* [1] of a very large negative magnetoresistance, the so-called giant magnetoresistance (GMR), in Fe/Cr multilayers has provoked a great deal of experimental work in sandwiches and multilayers of this system [2,3] as well as other magnetic multilayers [4]. This large decrease in resistance with applied magnetic field occurs when an originally antiparallel orientation of the magnetization of adjacent ferromagnetic layers of the film is driven parallel. The origin of the magnetic structure and behavior of these systems is closely related to that of the GMR and like it is also under intense study. Currently, experiments are exploring and finding dependence of the properties of these multilayers on the detailed electronic structure of the constituent materials [5]. In this paper only the behavior of the magnetoresistance arising from the relative orientation of the magnetization will be addressed. We will use "*M*" and "*N*" to mean the magnetic and nonmagnetic layers, respectively, of any of these films.

The goal of this paper is to define a simple and plausible mechanism which can semiquantitatively account for the large number of well-established and still puzzling features associated with these multilayered films. These include the following: a larger effect in a superlattice than in a sandwich structure; a larger effect at low temperatures than at room temperature; a clear enhancement of the GMR with interface roughness [6]; a rapid variation of the effect with *N* thickness [7]; a slower variation with *M* thickness which can have either of two characteristics [4], a monotonic decrease of the GMR with *M* layer thickness above some relatively small thickness (10 Å in Fe/Cr) or an increase of GMR up to large thicknesses of the magnetic layers followed by a broad maximum as the thickness is increased further; and a behavior dependence on the detailed electronic structure of the multilayer materials. The model we present here is a single mechanism which predicts the existence of all of these features in a very natural way.

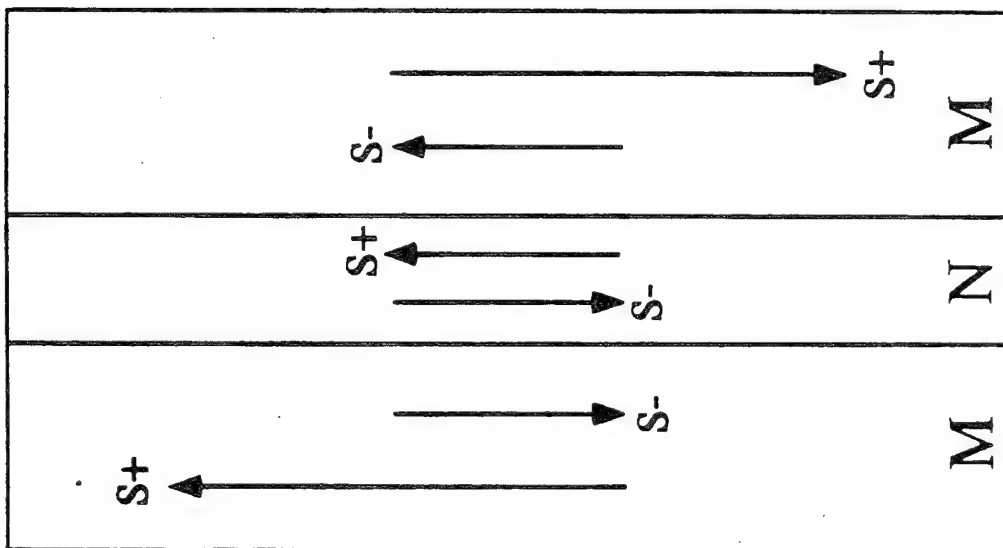
The theoretical modeling has generally emphasized spin dependent scattering [2,4]. More specifically, Inoue, Oguri, and Maekawa [8] addressed the origin of the spin dependent potential responsible for the spin dependent scattering at the *M/N* interface. Camley and Barnas [9]

and, with fewer approximations, Hood and Falicov [10] have extended Fuchs' semiclassical theory [11] of size effect to spin dependent scattering at the Fe/Cr interface. Levy, Zhang, and Fert [12] have followed the quantum mechanical theory of Tesanovic, Jaric, and Maekawa [13] to treat the Fe/Cr interface as a source of spin dependent interfacial roughness scattering. Stearns [14] has treated the spin dependent scattering as arising from the difference in the spin up and spin down density of states.

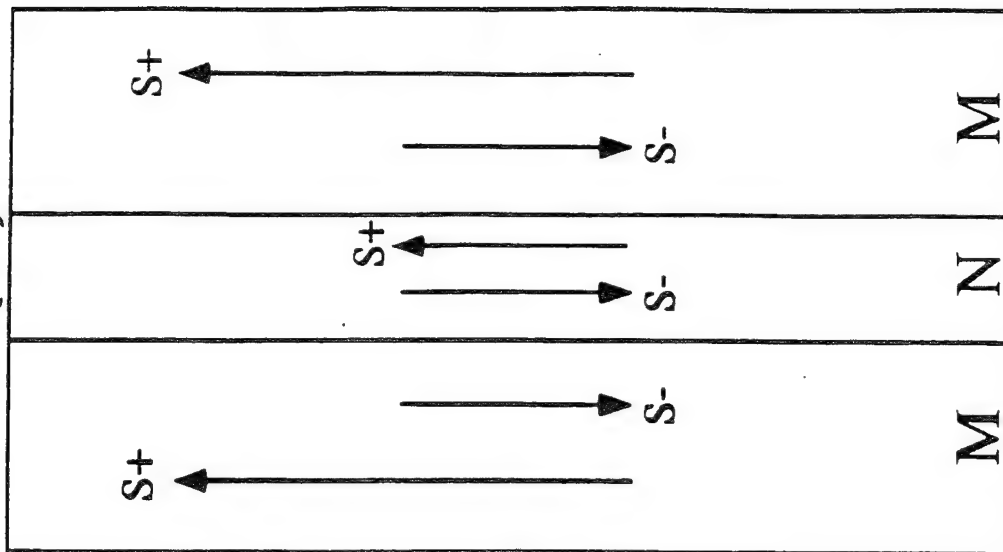
In this paper it is shown that the GMR can be largely understood in terms of (i) the vacuum-metal-like character of the interface between *M* and *N* and the consequent quantum-well-like states established within each layer or groups of layers of certain multilayer films and (ii) the application of already existing quantum mechanical size effect theories of electrical conduction. (i) has already been experimentally established in a number of different overlayers of nonmagnetic metals on other nonmagnetic metal substrates. Furthermore, Edwards and Mathon [15,16] have presented a theory of the exchange coupling of the ferromagnetic layers in magnetic multilayers based on the idea of quantum confinement of the electrons within the individual layers.

Recently, using angle-resolved photoemission Lindgren and Wallden [17] and Chiang and co-workers [18,19] have discovered and explored discrete valence electron states in thin metal overlayers on a metal substrate. These have been identified as arising from electron confinement within the overlayer and thus as quantum well states (QWS) [18]. The degree to which the overlayer states manifest quantum-well behavior revolve around the amount of electron reflection versus electron transmission [18]. This depends on the dissimilarity of the two metals at the interface and the abruptness of the interface. Nevertheless, Ag(111) on Au(111), two very similar metals, displays strong QWS characteristics. For those Ag electrons energetically below the Ag *L* point and above the Au *L* point in the Brillouin zone boundary, this region, called by Chiang and co-workers [18] a "relative" gap, there are no energy gaps in either material, but there are no available states in Au which conserve both energy and the (111) component of the Ag electron

(a)



(b)



Bases of the Model

The interfaces in these films can give rise to quantum well states.

[Chaing et al, Lindgren and Wallden
(photoemission), Himpsel (inverse photoemission)]

The band structure of the non-magnetic material is much more like one of the spin bands of the magnetic material than the other.
(Inoue et al., Papaconstantopoulos (Fe-Cr))

The dimensions of the wells depend on ferro or antiferromagnetic orientation of the magnetic layers.

Thus a magnetoresistance arises from established quantum size effect considerations.

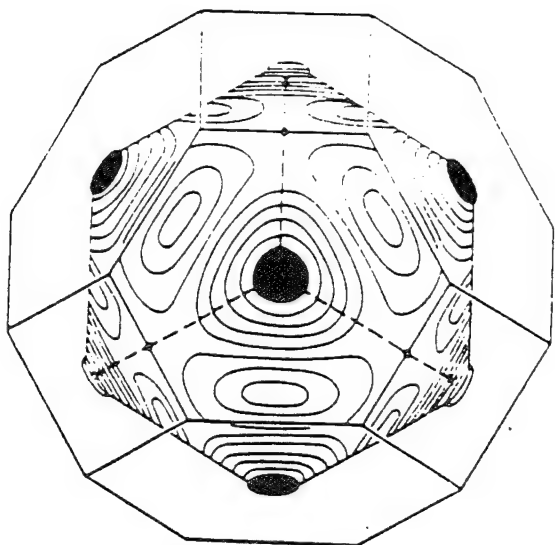


FIG. 5.4. The Fermi surface of Cu (Pippard 1957b).



Fig. 5.2. The Fermi surface of Cu in the periodic zone scheme, from a model by D. Shoenberg.

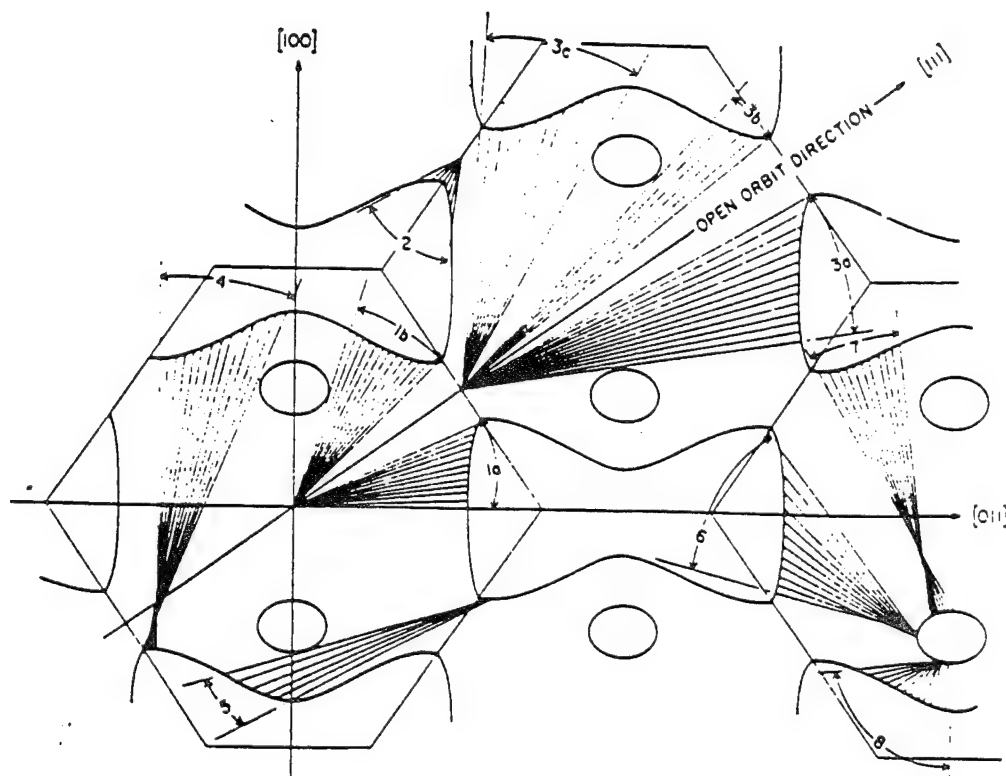


FIG. 5. Fermi surface of copper in an extended-zone space projected onto a (011) plane with the angular ranges of magnetoacoustic orbits indicated, corresponding to the dimensions of Fig. 4. The orbits having a center of symmetry, groups 3a, 3b, and 3c, are indicated radially. The other more complex orbits, groups 4-8 are indicated between their two extremes. The lines shown indicate the location and angular range of the orbits and not the angles of actual measurement.

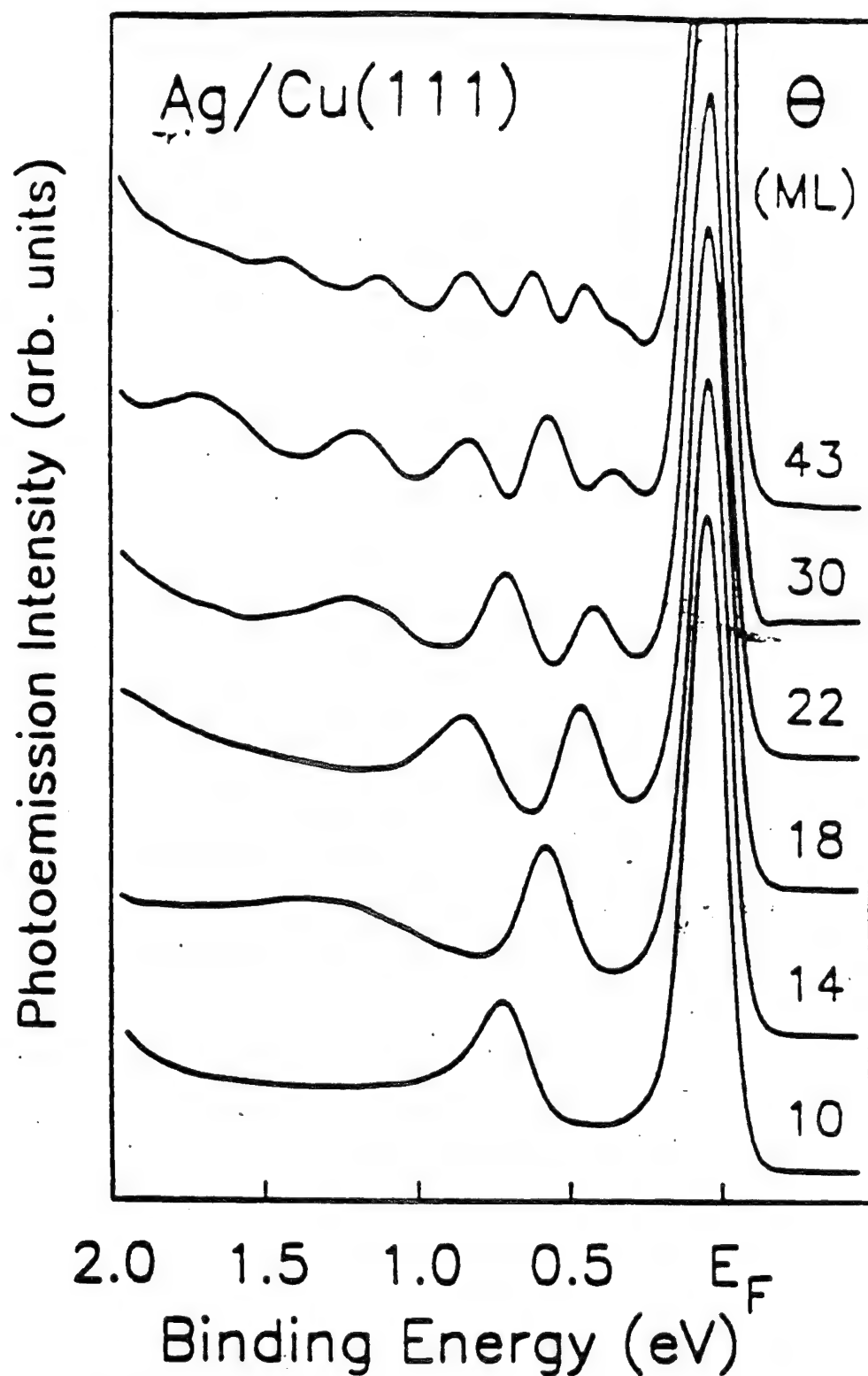


FIG. 1. Normal-emission spectra taken with a photon energy $h\nu = 10$ eV for Cu(111) covered with various amounts of Ag. The coverage Θ is expressed in terms of Ag(111) monolayer (ML). The binding-energy scale is referred to the Fermi level E_F .

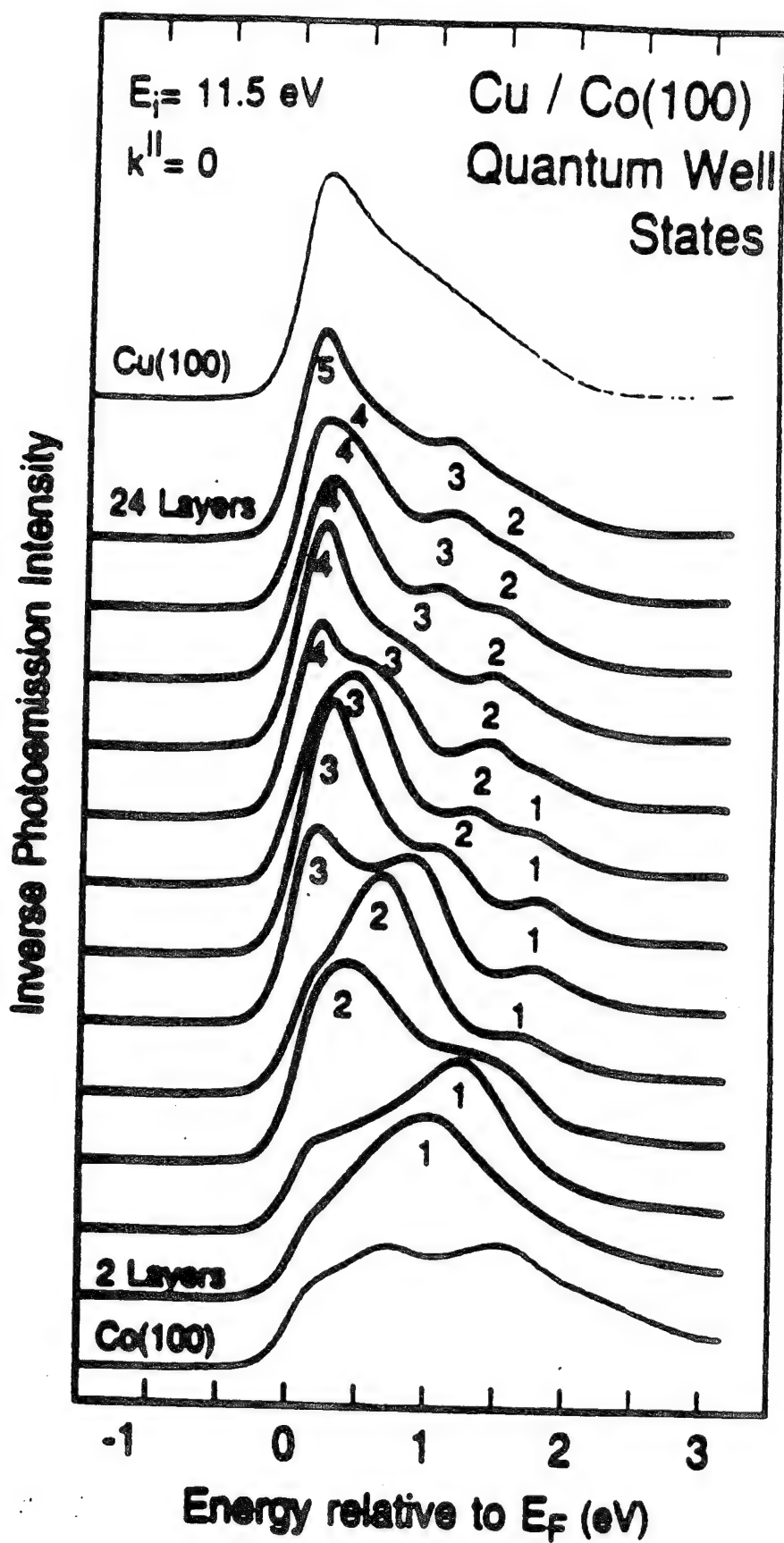
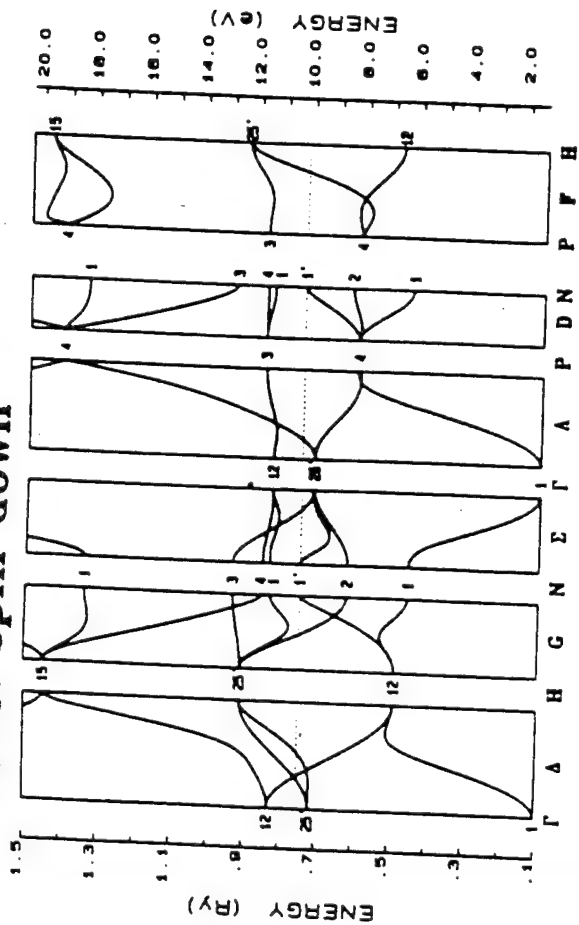
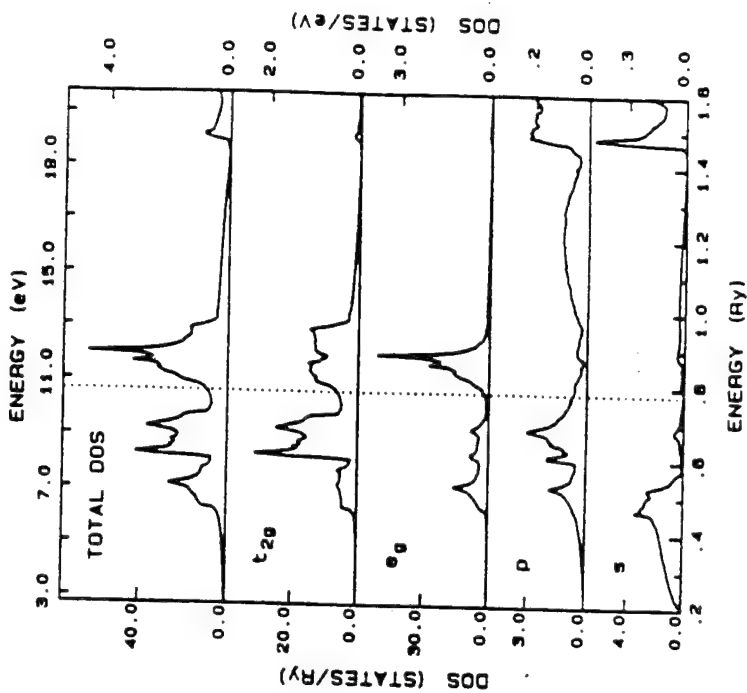
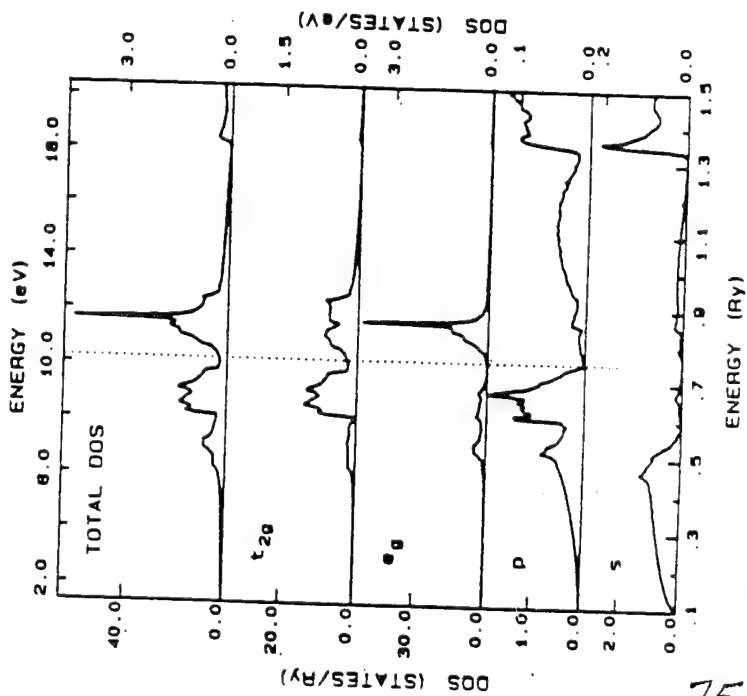
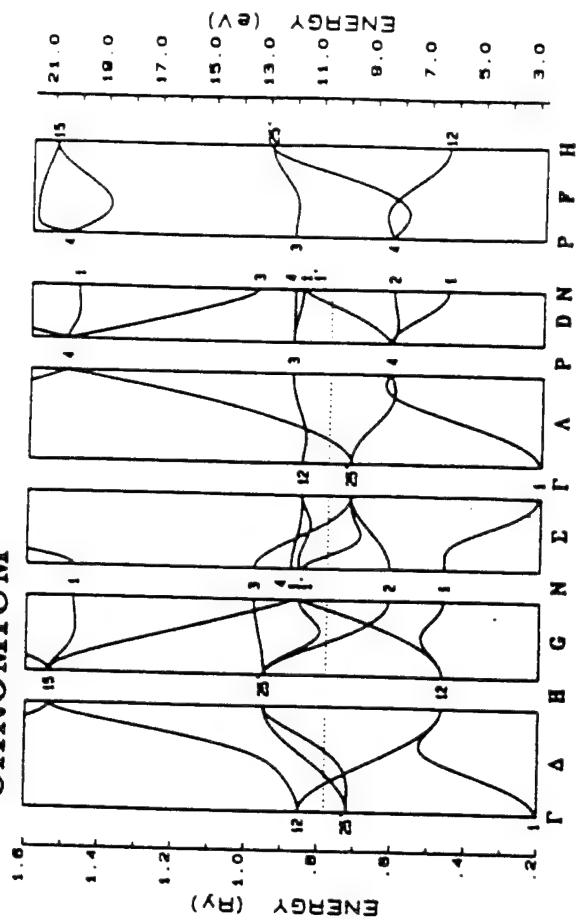


FIG. 1. Inverse photoemission spectra for Cu on Co(100) at normal incidence. The s, p band continuum of bulk Cu(100) (top) is discretized into quantum well states for thin Cu films

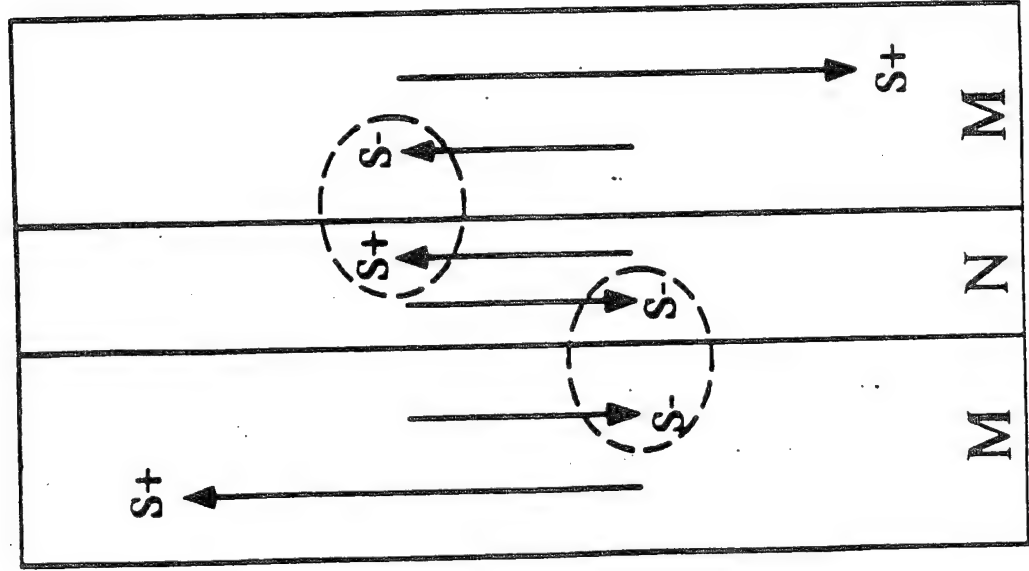
IRON spin down



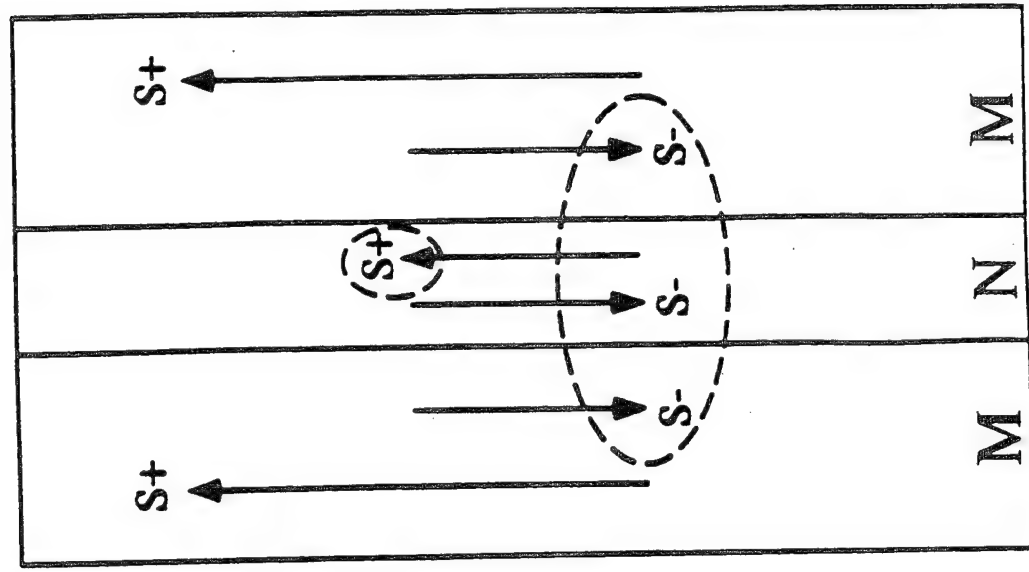
CHROMIUM



(a)



(b)



$$\Psi_{kn}(\mathbf{r}) = \sqrt{2/\Omega} \sin \left[\frac{n\pi z}{d} \right] e^{i\mathbf{k} \cdot \overline{\mathbf{p}}},$$

$$\varepsilon_{kn} = \frac{\hbar^2 k^2}{2m^*} + \varepsilon_0 n^2, \quad n = 1, 2, \dots$$

$$\sigma_{xx}^{I+S} = \frac{e^2 k_F}{\hbar \pi^2} \frac{1}{\kappa} \sum_{n=1}^{n_c} \frac{1 - n^2/\kappa^2}{\left[\frac{2n_c + 1}{k_F l_0 \kappa} + \left[\frac{\delta d}{d_0} \right]^2 \frac{s(n_c) n^2}{3\kappa} \right]},$$

SPIN VALVE MAGNETORESISTANCE CHARACTERISTICS

Rapid variation with thickness of N

**Two characteristic slower variations with
thickness of M:**

- (1) monotonic decrease beyond a
small thickness.**
- (2) a broad maximum at a larger
thickness.**

Increased effect with:

**low temperatures
interface roughness
superlattices vs. sandwiches**

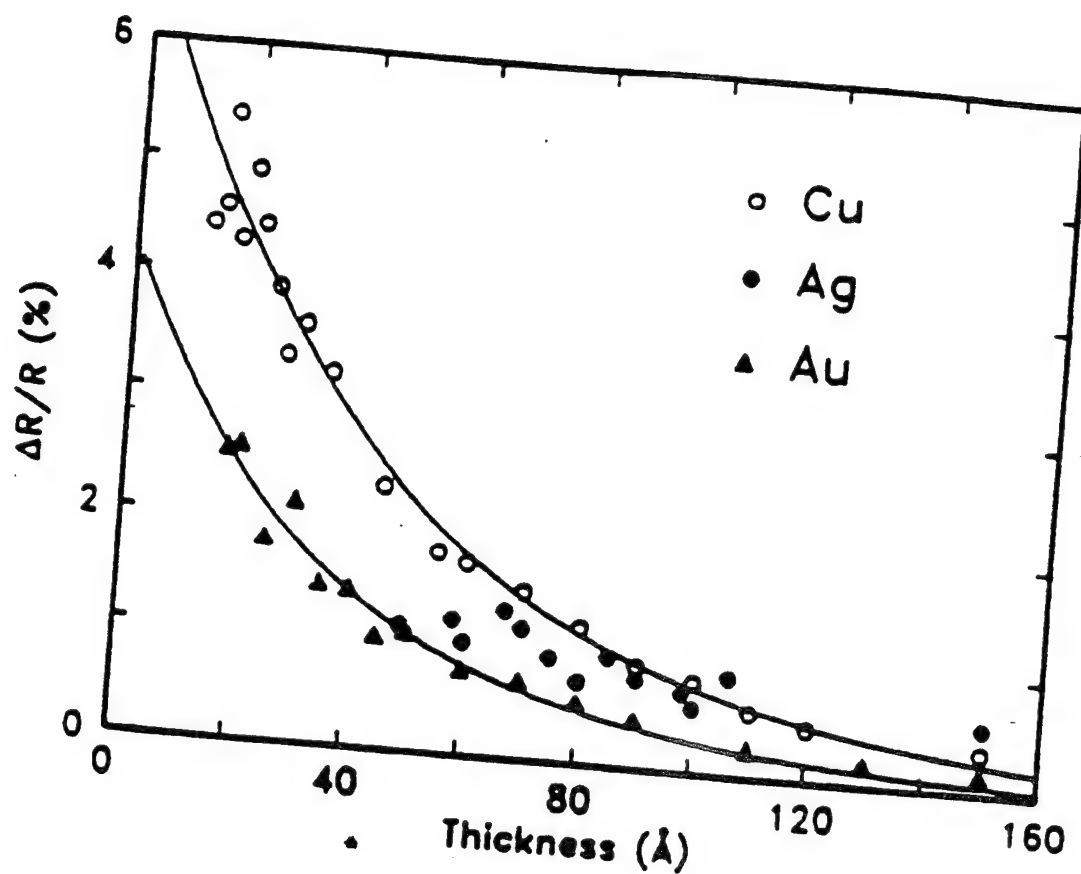


FIG. 8. Amplitude of the magnetoresistance at room temperature vs thickness of the noble-metal layer for the same samples as in Fig. 7.

4778

J. Appl. Phys., Vol. 69, No. 8, 15 April 1991

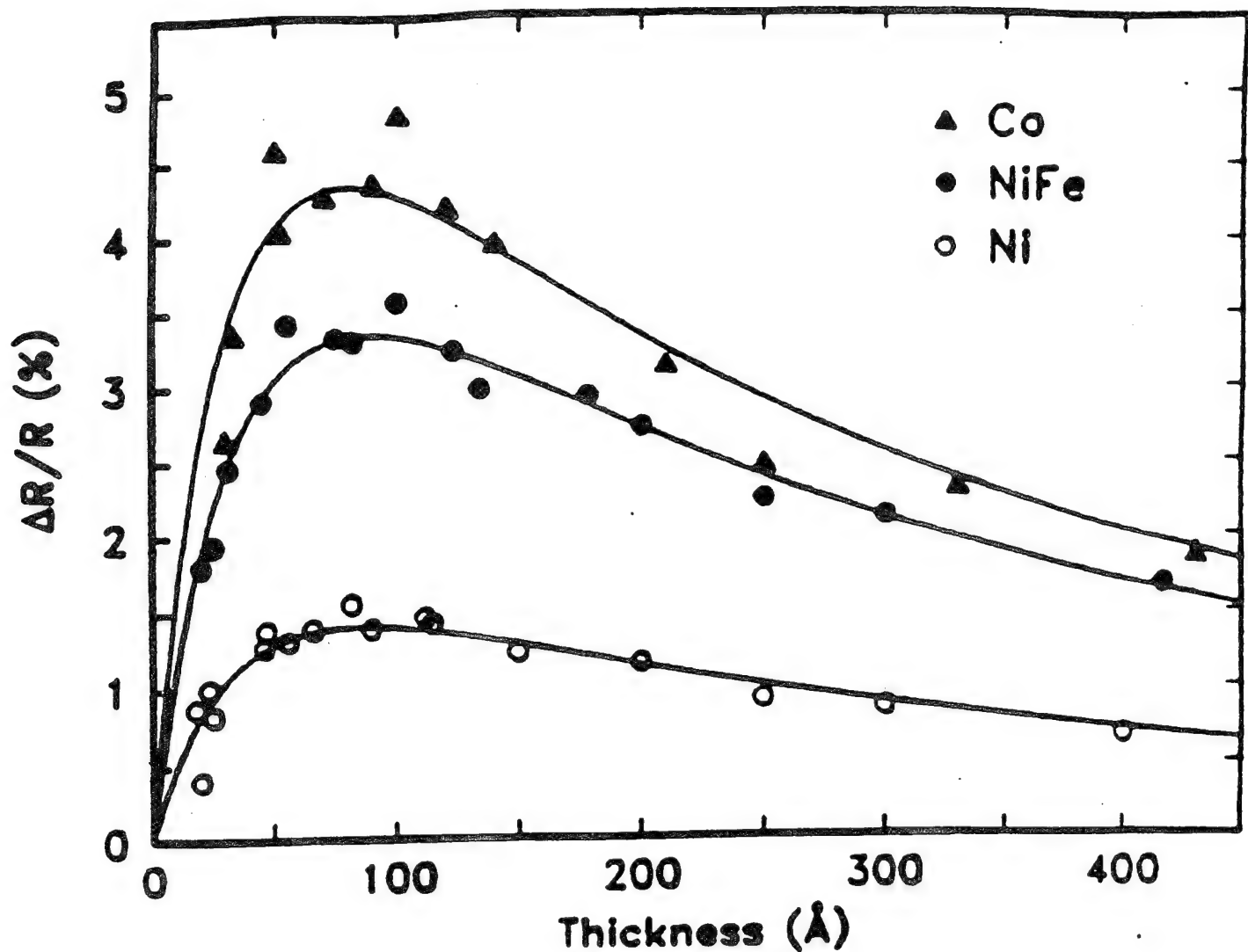


FIG. 9. Variation of the magnetoresistance versus the thickness of the "free" ferromagnetic layer $M(1)$, with $M(1) = \text{Co}$, NiFe , or Ni ; at room temperature. The lines are two-parameter fits according to Eq. (7).

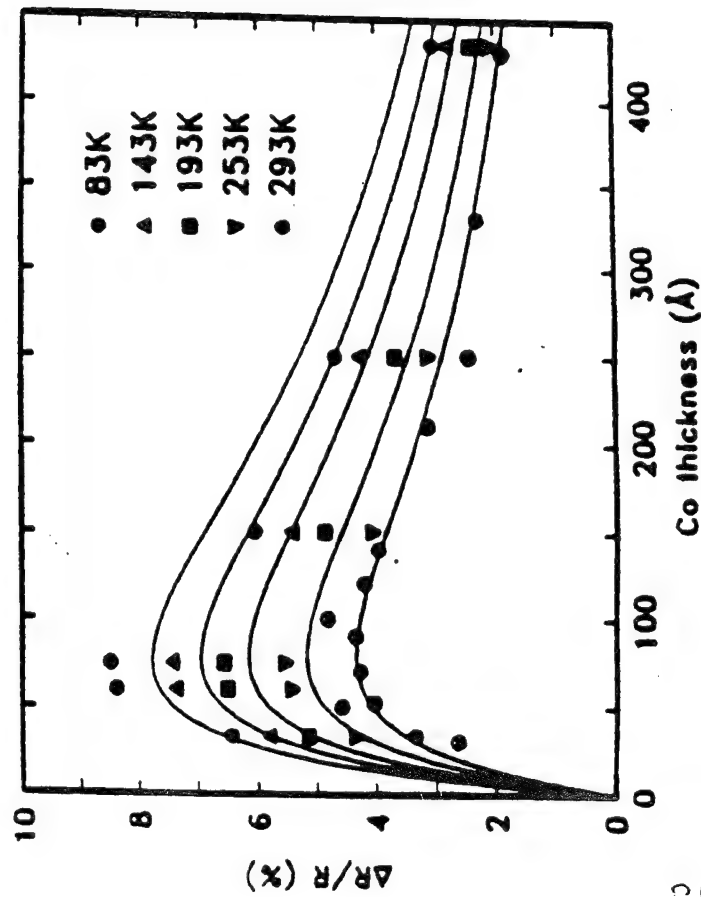


FIG. 11. Variation of the magnetoresistance versus the thickness of the Co layer at different temperatures for the same samples as in Figs. 2 and 6. The lines are two-parameter fits according to the equation $\Delta R/R = A \exp(-Bx) + C \exp(-Dx)$.

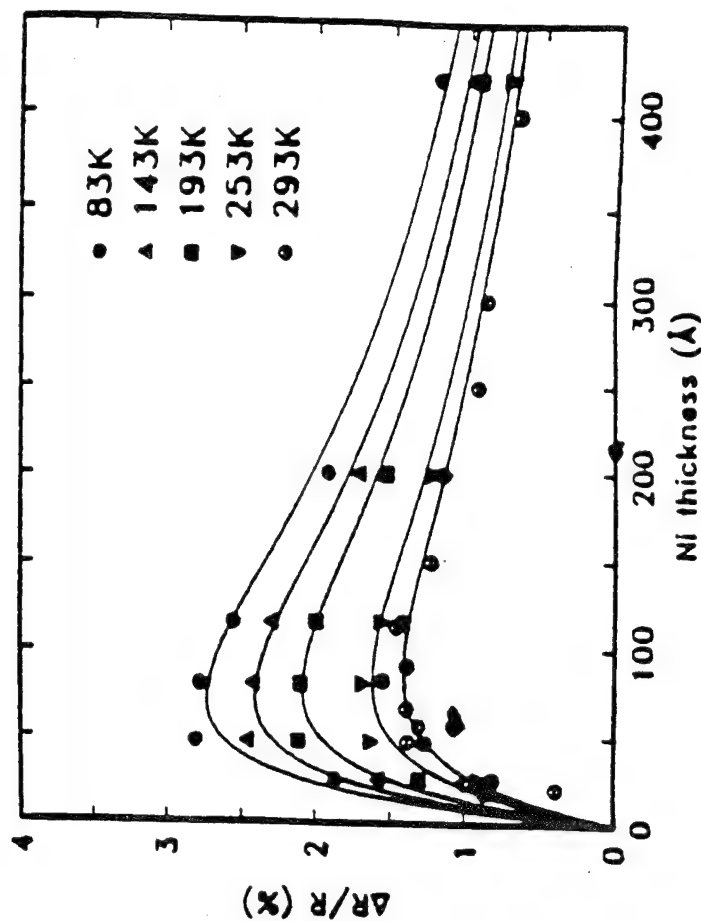
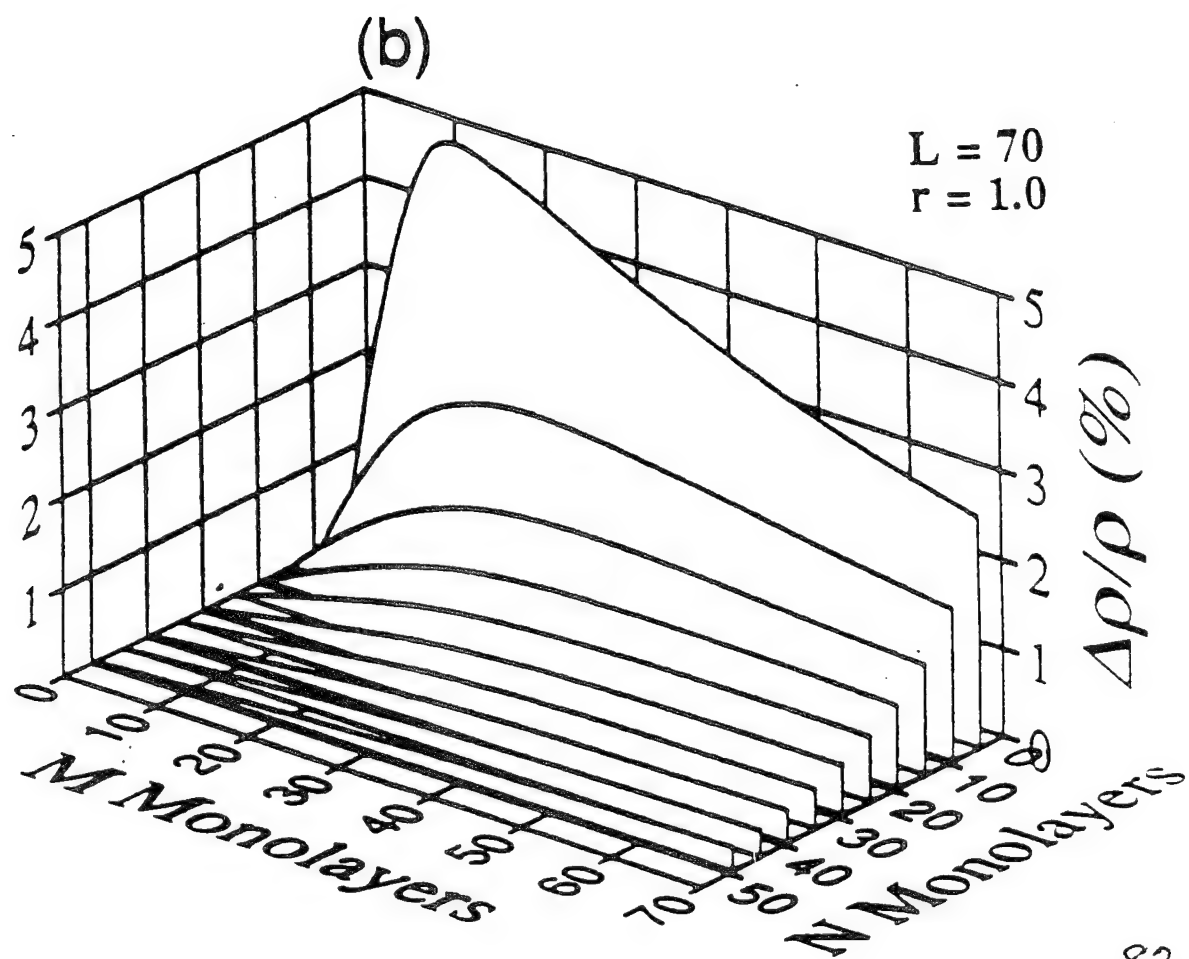
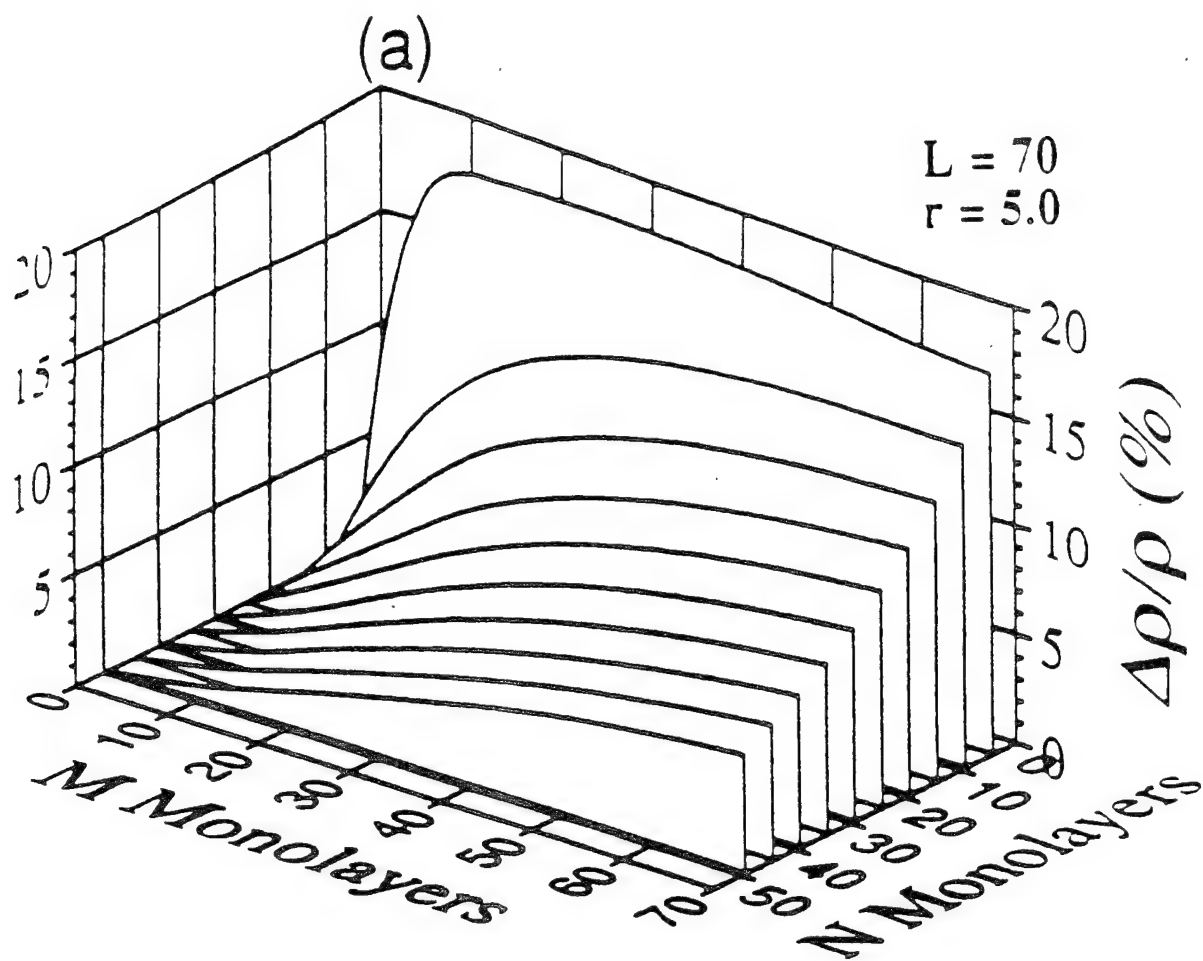
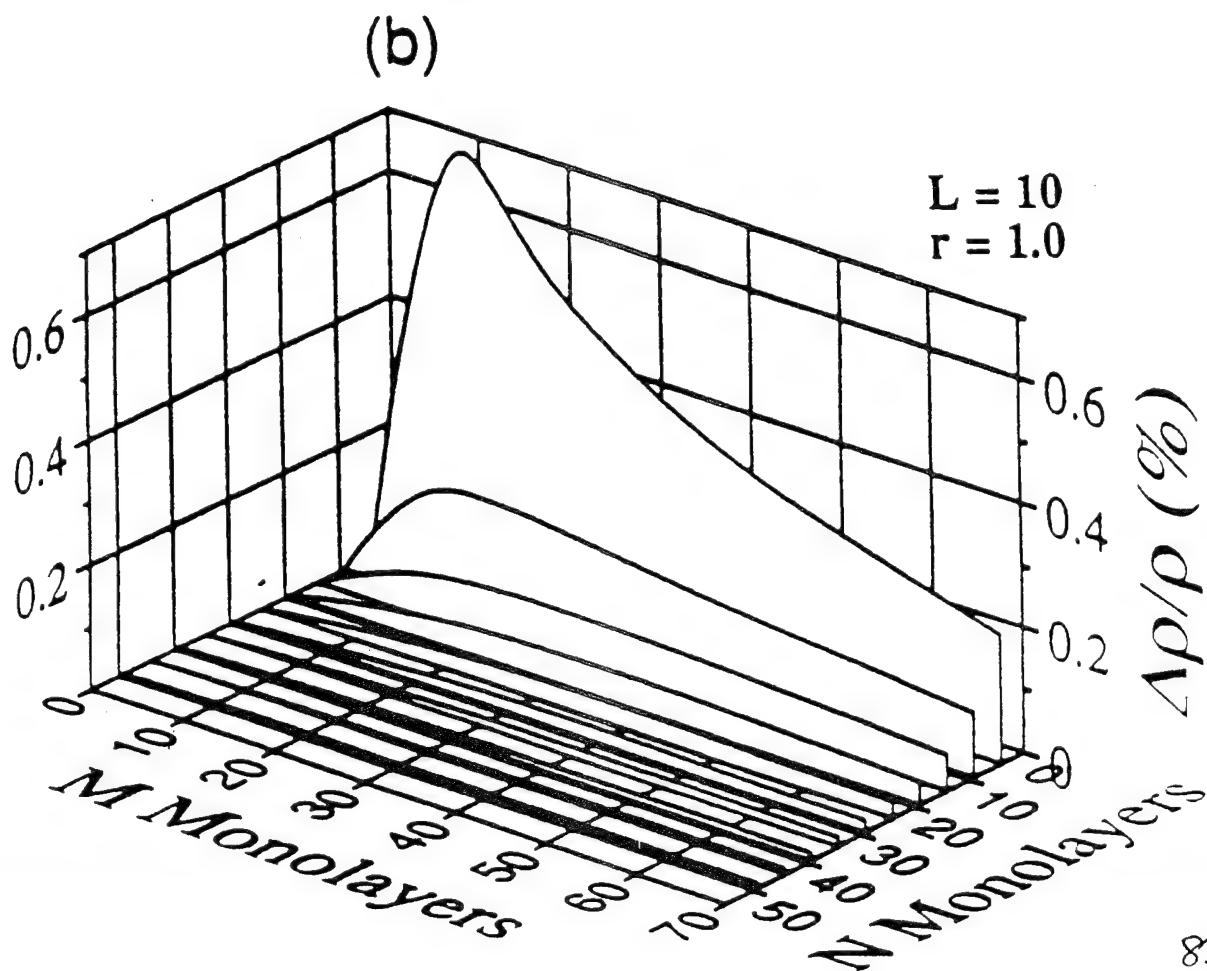
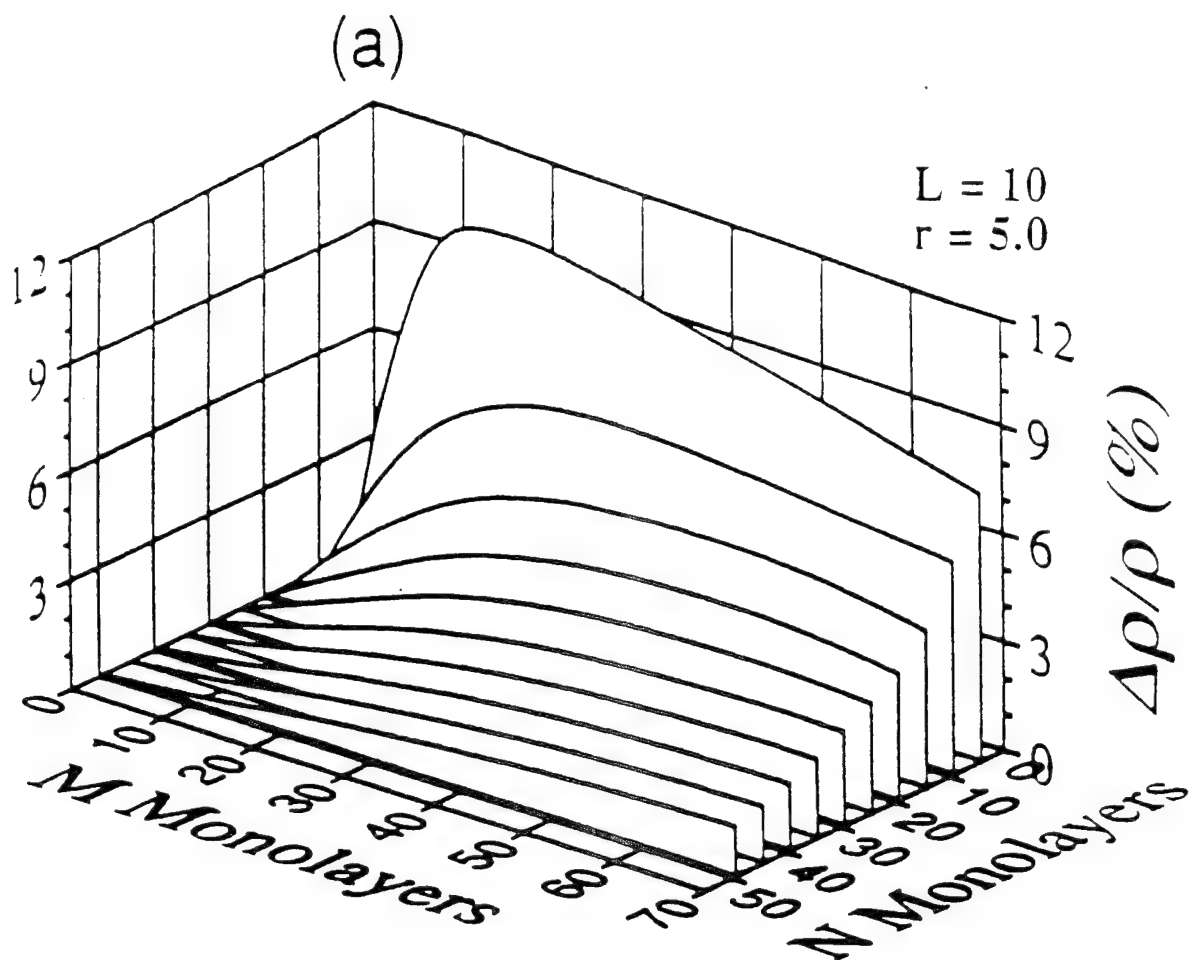


FIG. 13. Variation of the magnetoresistance versus the thickness of the Ni layer at different temperatures for the same samples as in Fig. 4 and 8. The lines are two-parameter fits according to the equation $\Delta R/R = A \exp(-Bx) + C \exp(-Dx)$.





O	O	O	O	O	O	X	X	X	X	X	X
O	O	O	O	O	O	X	X	X	X	X	X
O	O	O	O	O	O	O	X	X	X	X	X
O	O	O	O	O	O	O	X	X	X	X	X
O	O	O	O	O	O	O	X	X	X	X	X
O	O	O	O	O	O	O	X	X	X	X	X
O	O	O	O	O	O	X	X	X	X	X	X
O	O	O	O	O	O	X	X	X	X	X	X
O	O	O	O	O	X	X	X	X	X	X	X
O	O	O	O	O	X	X	X	X	X	X	X
O	O	O	O	O	X	X	X	X	X	X	X

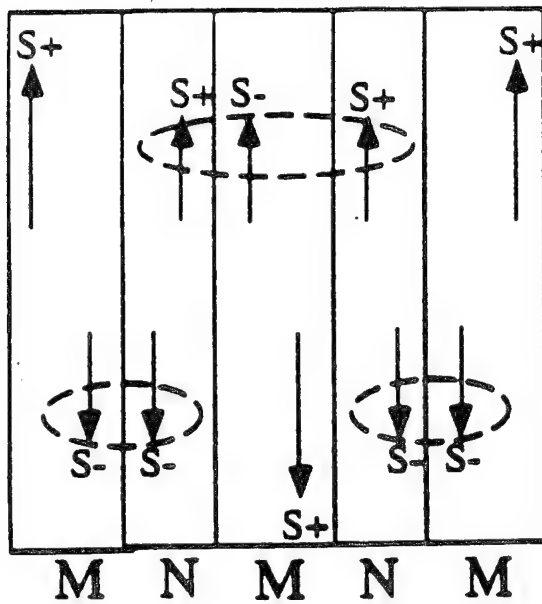
O	O	O	O	O	O	X	X	X	X	X	X
O	O	O	O	O	O	O	X	X	X	X	X
O	O	O	O	O	X	X	X	X	X	X	X
O	O	O	O	O	O	X	X	X	X	X	X
O	O	O	O	O	X	X	X	X	X	X	X
O	O	O	O	O	O	O	X	X	X	X	X
O	O	O	O	O	X	X	O	X	X	X	X
O	O	O	O	O	O	X	O	X	X	X	X
O	O	O	O	O	O	X	X	X	X	X	X

EXTENSION OF MODEL TO:

- i. unequal mean free paths in the different layers.**
- ii. a much smaller electron/atom number (0.131).**
- iii. various numbers of layers (sandwiches to superlattices of 63 pairs +1).**

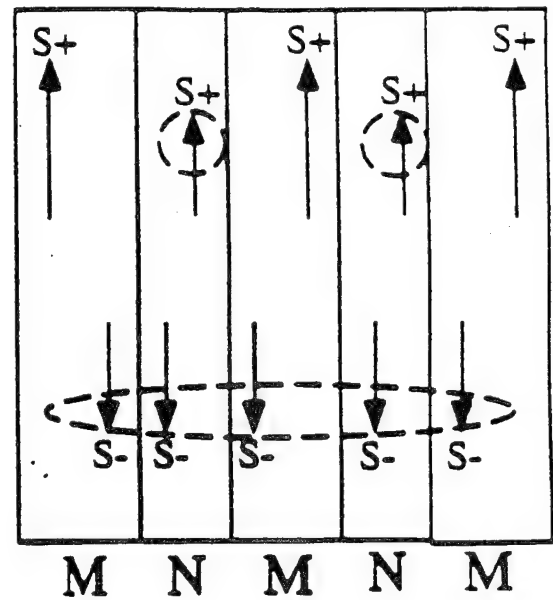
Antiferromagnetic

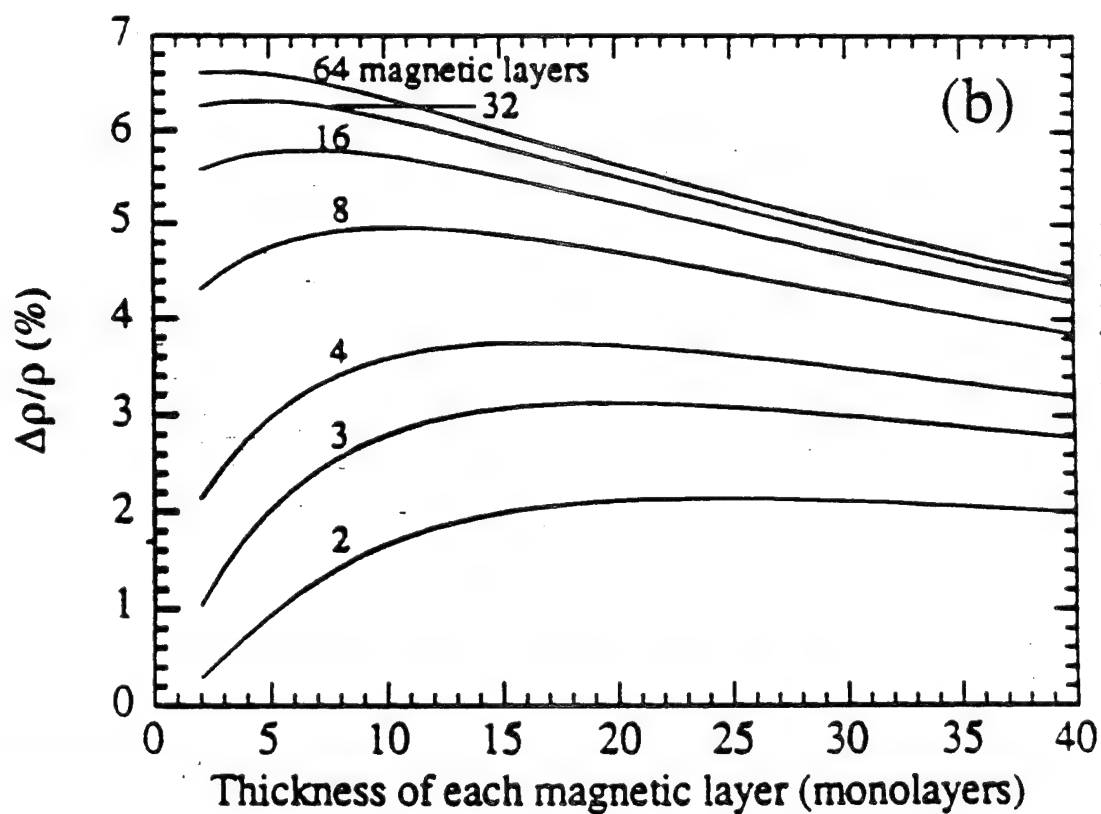
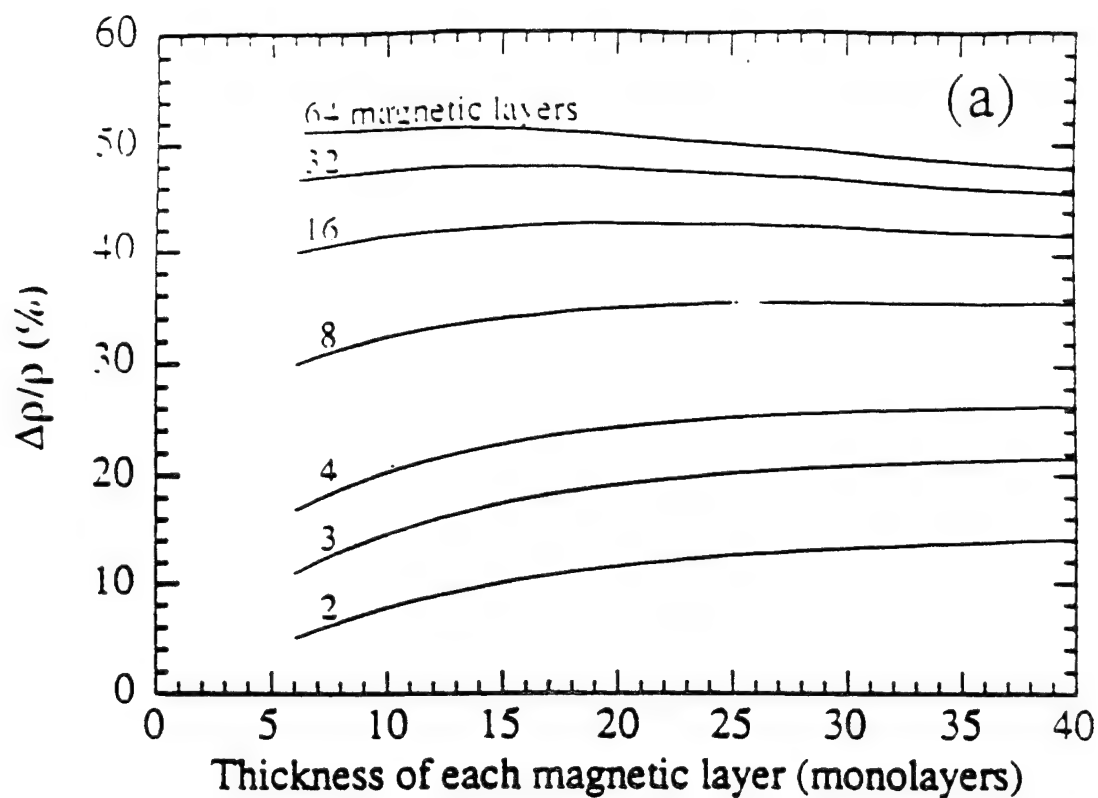
(a)

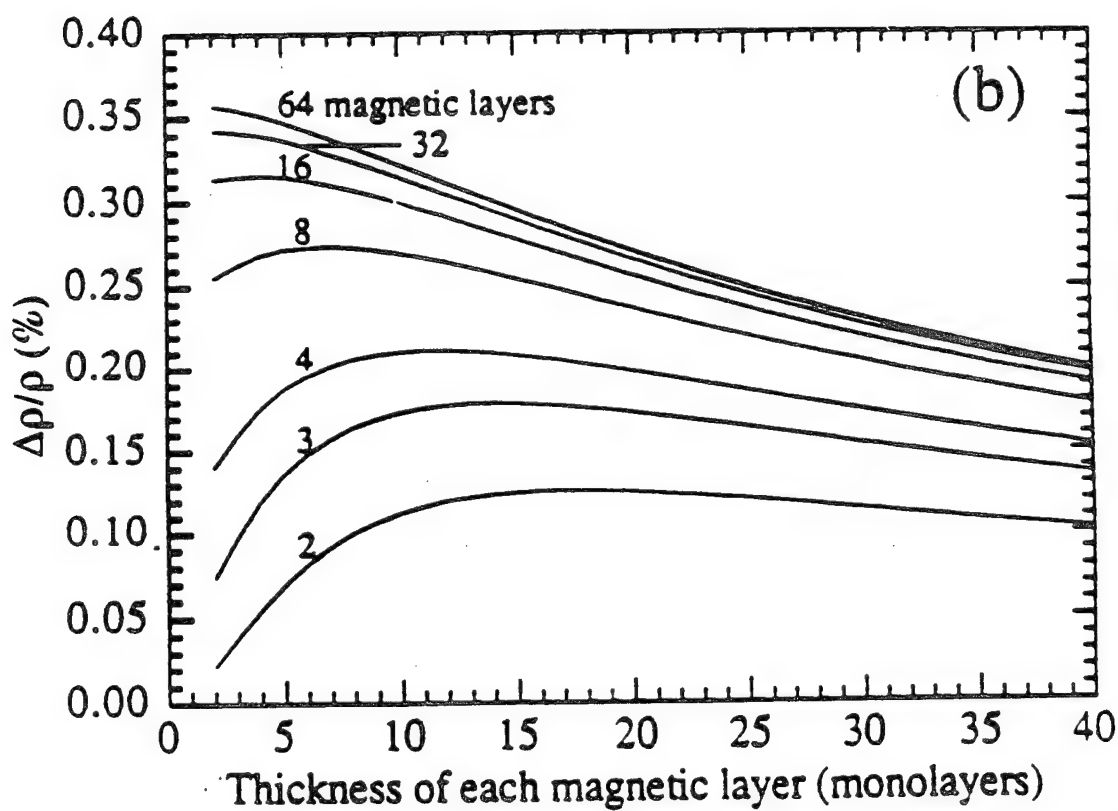
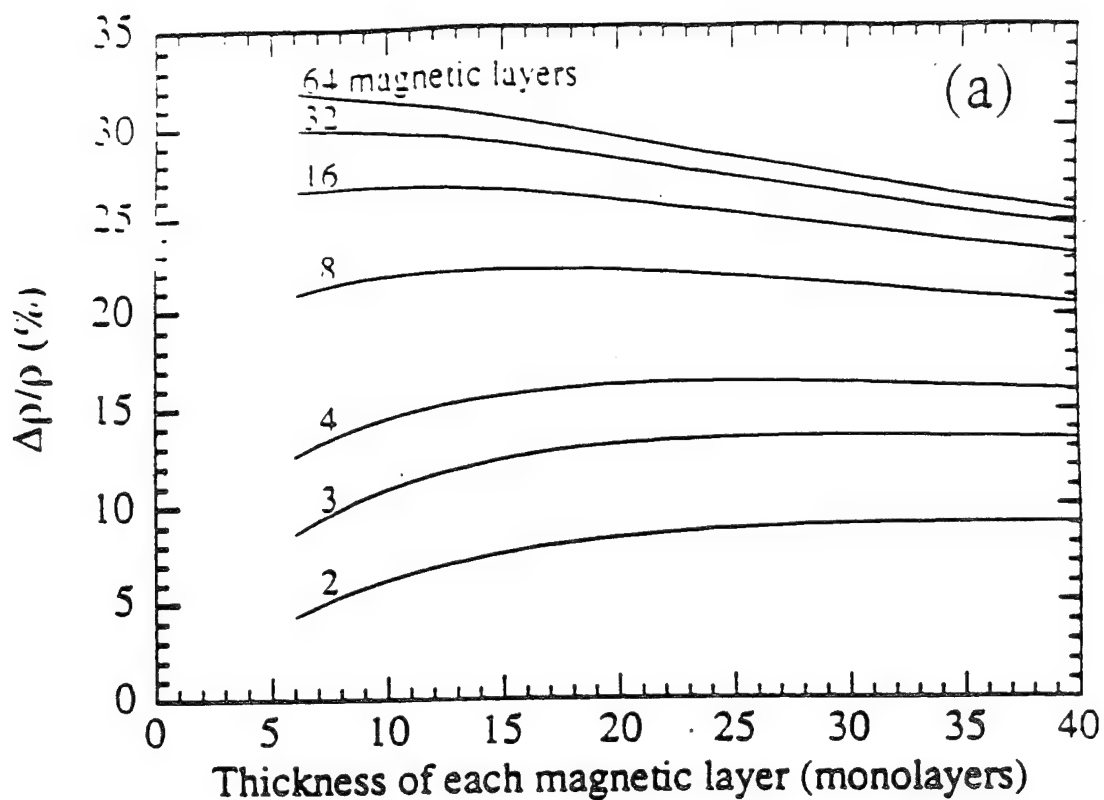


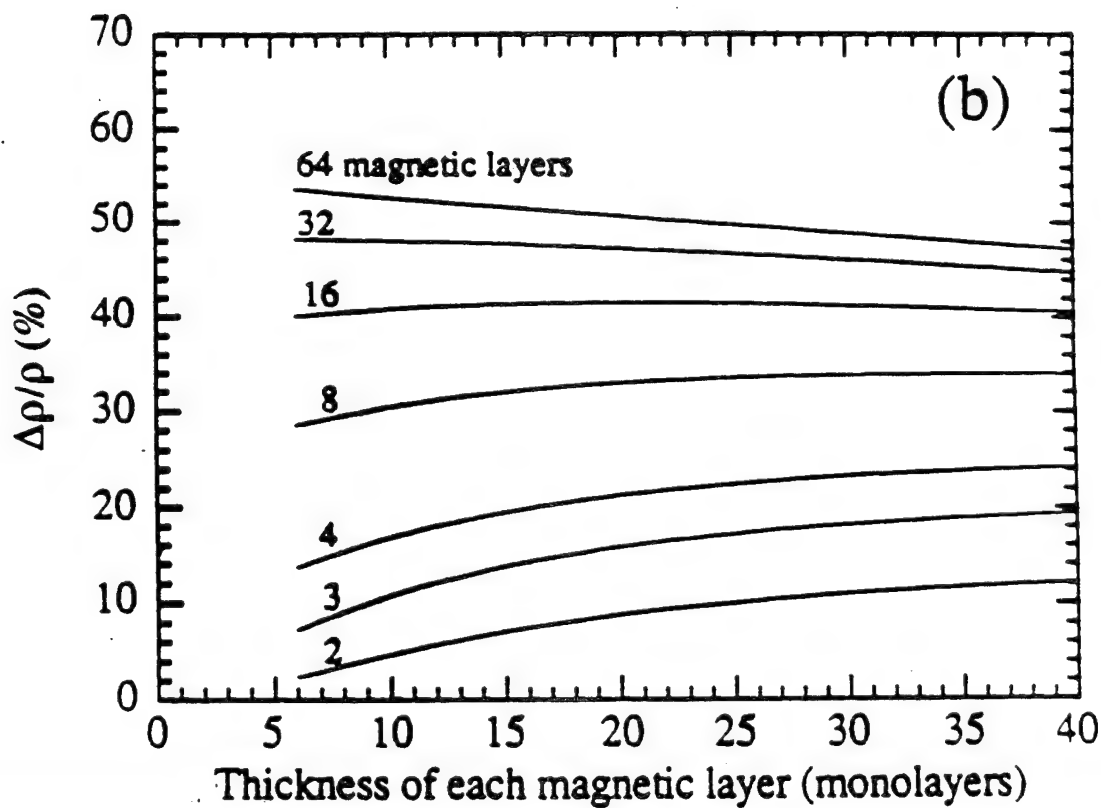
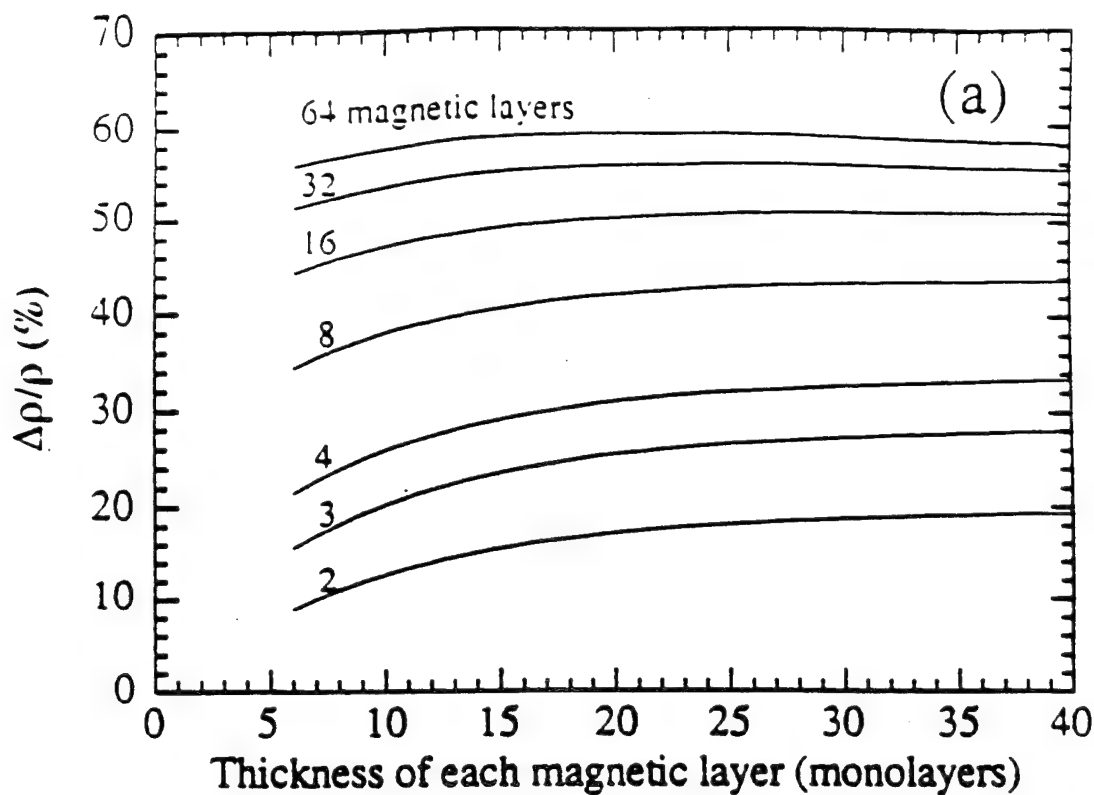
Ferromagnetic

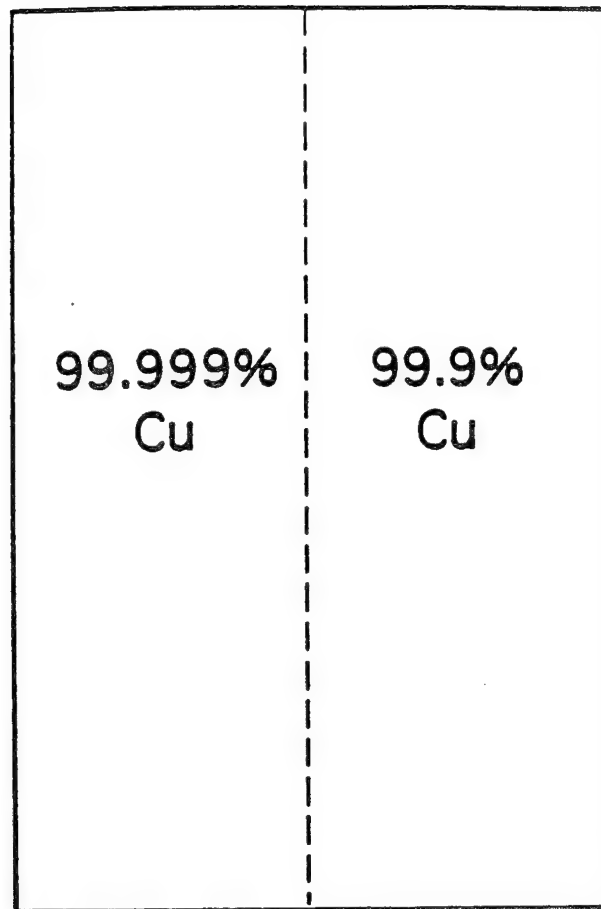
(b)











Bilayer

$$L_{eff} = \frac{L_1 L_2 (t_1 + t_2)}{L_1 t_2 + L_2 t_1}$$

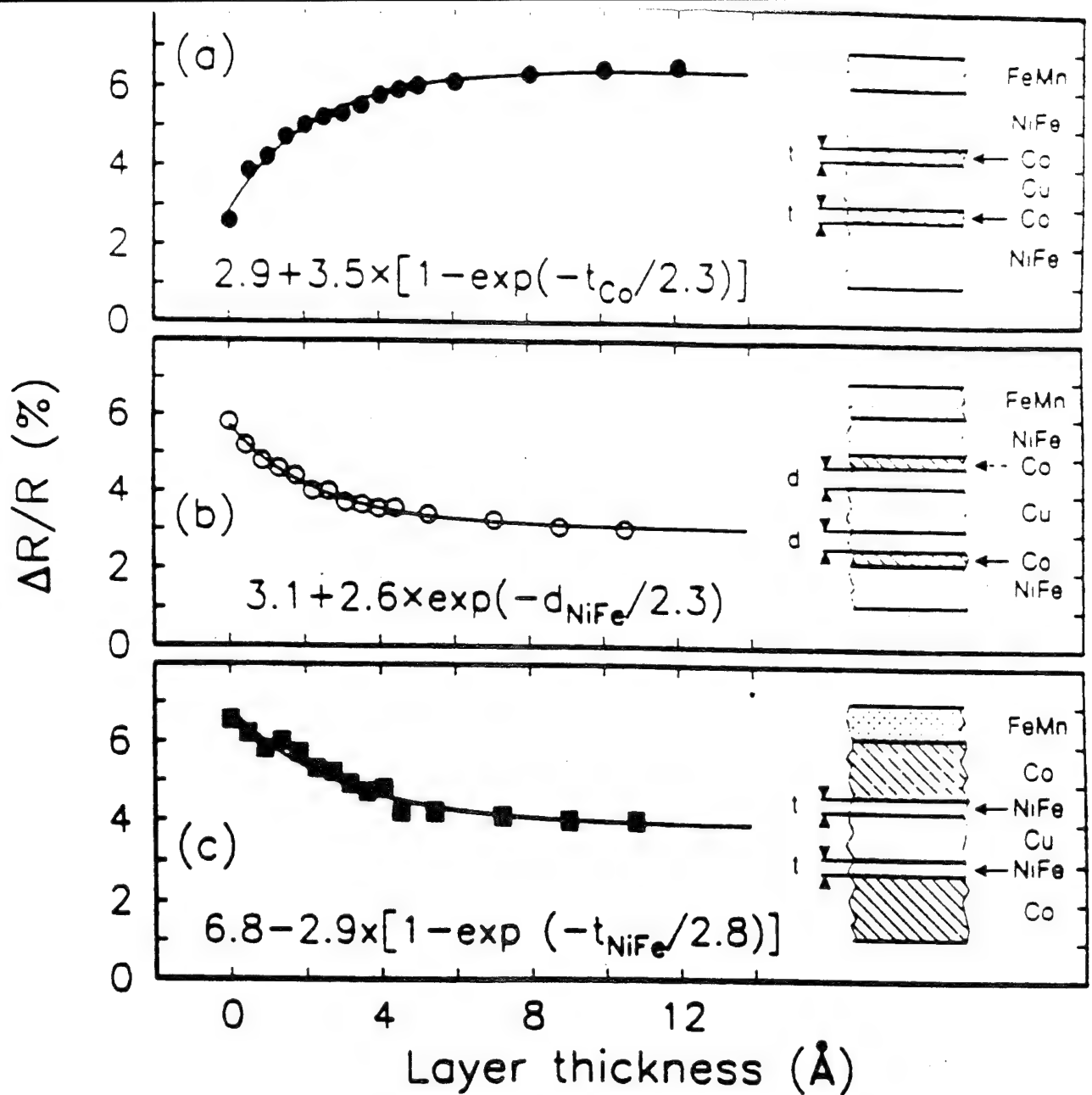
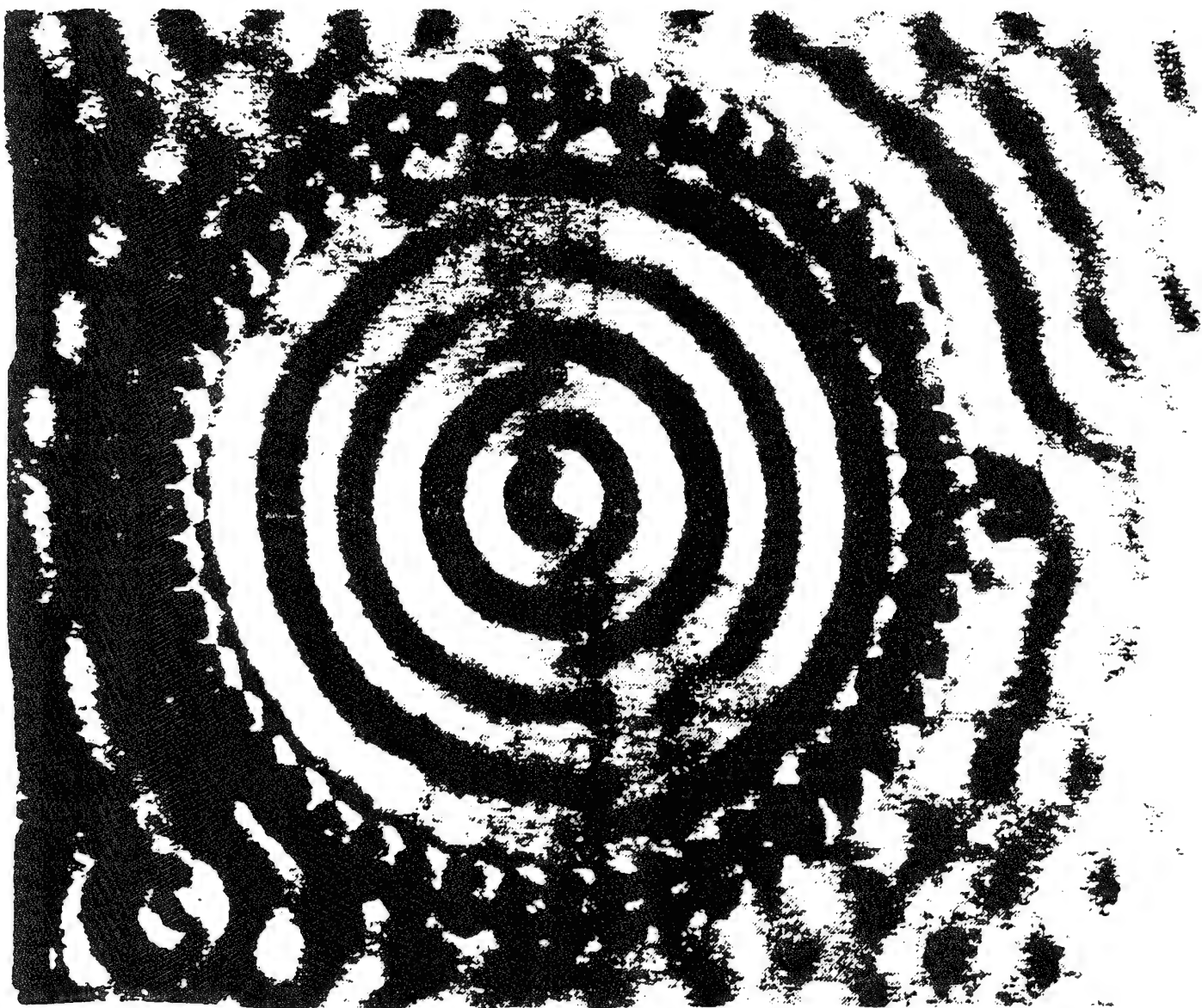


FIG. 2. Dependence of room temperature saturation magnetoresistance on (a) Co interface layer thickness, t_{Co} , sandwiches of the form Si/Py(53- t_i)/Co(t_i)/Cu(32)/Co(t_i)/Py(22- t_i)/FeMn(90)/Cu(10), (b) distance of a 5 Å thick Co layer from the Py/Cu interfaces in sandwiches of the form Si/Py(49- d)/Co(5)/Py(d)/Cu(30)/Py(d)/Co(5)/Py(1- d)/FeMn(90)/Cu(10), and (c) Py interface layer thickness t_i , in sandwiches of the form Si/Co(57- t_i)/Py(t_{Py})/Cu(24)/Py(t_i)/Co(29- t_i)/FeMn(100)/Cu(10). Note layer thicknesses are in angstroms.



i. 2. Spatial image of the eigenstates of a quantum corral. (A)

POWER THRESHOLDS AND FREQUENCY SHIFTS IN THE EXCITATION
OF MAGNETOSTATIC VOLUME WAVE SOLITONS IN DELAY LINE
CONFIGURATIONS

R. MARCELLI AND P. DE GASPERIS
ISTITUTO DI ELETTRONICA DELLO STATO SOLIDO DEL CNR
VIA CINETO ROMANO, 42
00156 ROMA
ITALY

OUTLINE

- THE CONDITIONS FOR THE ONSET OF MODULATIONAL INSTABILITY AND EXCITATION OF SOLITONS IN MAGNETOSTATIC VOLUME WAVE DELAY LINES WILL BE PRESENTED.
- THE FREQUENCY AND WAVEVECTOR SHIFTS INDUCED BY THE NONLINEAR EFFECTS AND THE POWER THRESHOLDS FOR SOLITONS IN REAL DEVICE STRUCTURES WILL BE PREDICTED.

MODULATIONAL INSTABILITY

- INSTABILITY IS A NONLINEAR EFFECT DUE TO BOTH, THREE- AND FOUR-MAGNONS INTERACTIONS.

- MODULATIONAL INSTABILITY IS DUE TO FOUR-MAGNON SELF-INTERACTION PROCESSES ONLY.

- THE ACTIVATION OF THE MULTI-MAGNONS DECAY PROCESSES IN CW REGIME IS A THRESHOLD EFFECT WHICH RESULTS IN A MULTI-STABLE RESPONSE. THAT BEHAVIOUR CAN BE DETECTED BY MEANS OF POWER MEASUREMENTS OR FREQUENCY SPECTRUM MEASUREMENTS, THUS EVIDENTIATING THE CREATION OF SATELLITE FREQUENCIES.

- THE SATELLITES LOCATION DETERMINES THE KIND OF MULTI-MAGNONS INTERACTION, AND THEIR PRESENCE CRITICALLY DEPENDS ON THE FREQUENCY AND ON THE POWER LEVELS.

- A FURTHER PARAMETER TO BE ACCOUNTED IS THE LIGHTHILL CRITERION SATISFACTION. IN FACT, MODULATIONAL INSTABILITY CAN BE DESCRIBED BY THE NONLINEAR SCHROEDINGER EQUATION (NLSE) AND THE RATIO BETWEEN THE NONLINEAR AND THE DISPERSIVE TERM MUST BE NEGATIVE.

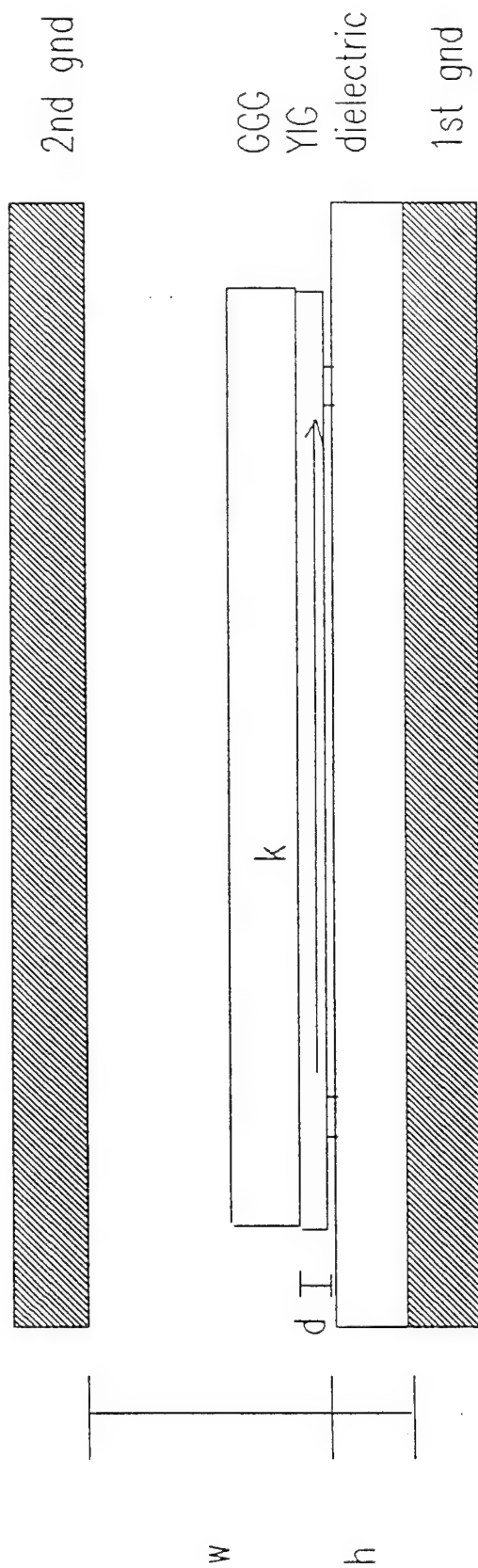
GROUND PLANES CONTRIBUTION TO THE DISPERSION

- THE DISPERSION RELATIONS FOR MSW ARE IMPLICIT, AND FROM THEIR ANALYSIS IT TURNS OUT THAT THE STRONGEST CONTRIBUTION TO THE GROUP VELOCITY TREND IS DUE TO THE GROUND PLANES CONFIGURATION.

- ONE GROUND PLANE IS NECESSARY TO GUARANTEE THE ELECTRICAL MATCHING OF THE MICROSTRIP LINE USED TO LAUNCH THE MICROWAVE SIGNAL INTO THE MAGNETIC FILM, WHILE THE PRESENCE OF A SECOND GROUND PLANE MIGHT BE INTRODUCED IN REAL, CLOSED DEVICE STRUCTURES.

- THE INTRODUCTION OF A SECOND GROUND PLANE CHANGES DRAMATICALLY THE DISPERSION TREND, AND THE EXSISTENCE OF NONLINEAR WAVES FULLFILLING THE LIDTHILL CRITERION IS ALLOWED ONLY IN WELL DEFINED WAVEVECTOR INTERVALS.

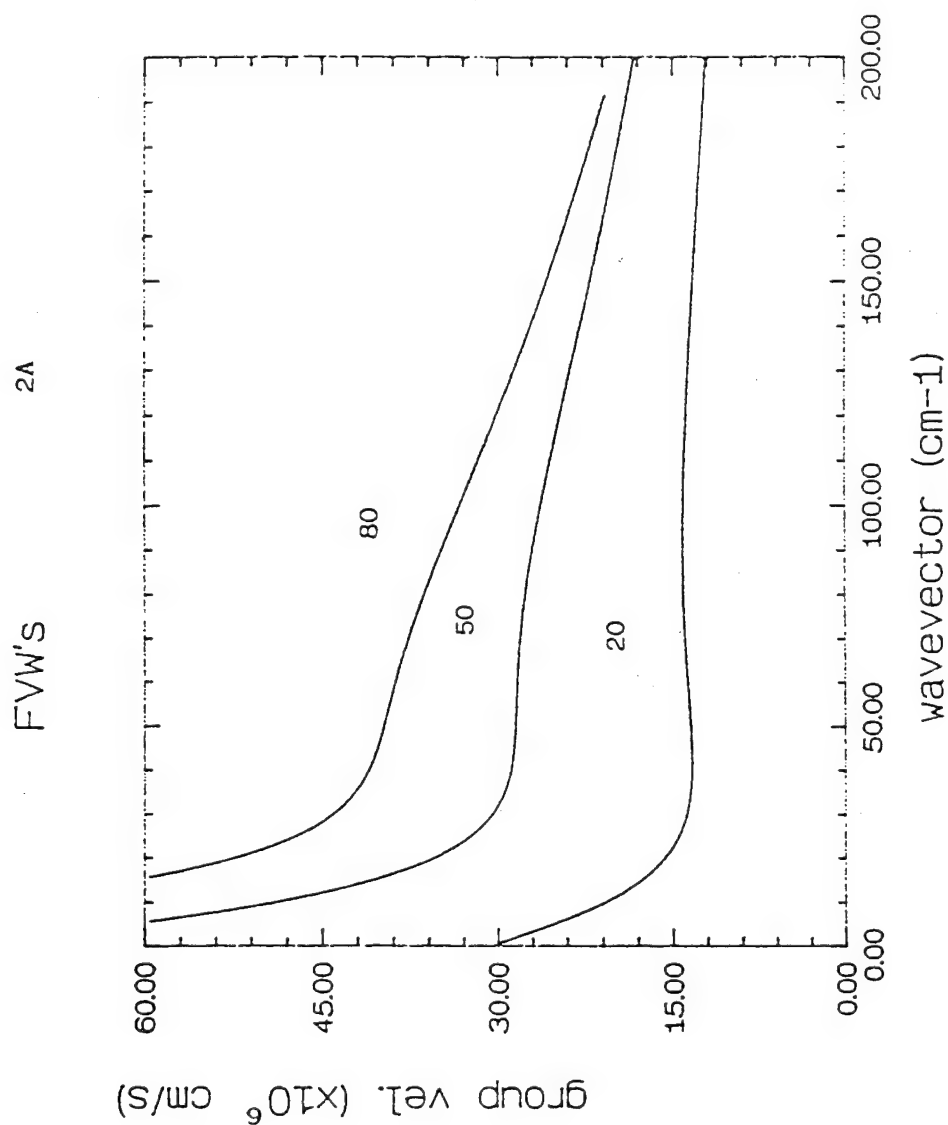
Fig. 1



Ho FW's
Ho BW's

FIG. 2A

1 gnd Configuration
 $h = 254 \mu\text{m}$, $w = \infty$
 $H_0 = 5000 \text{ Oe}$



1 and 2 gnd's
 $h = 254 \mu m$
 $w = \infty, 1 mm$
 $H_0 = 3240 Oe$

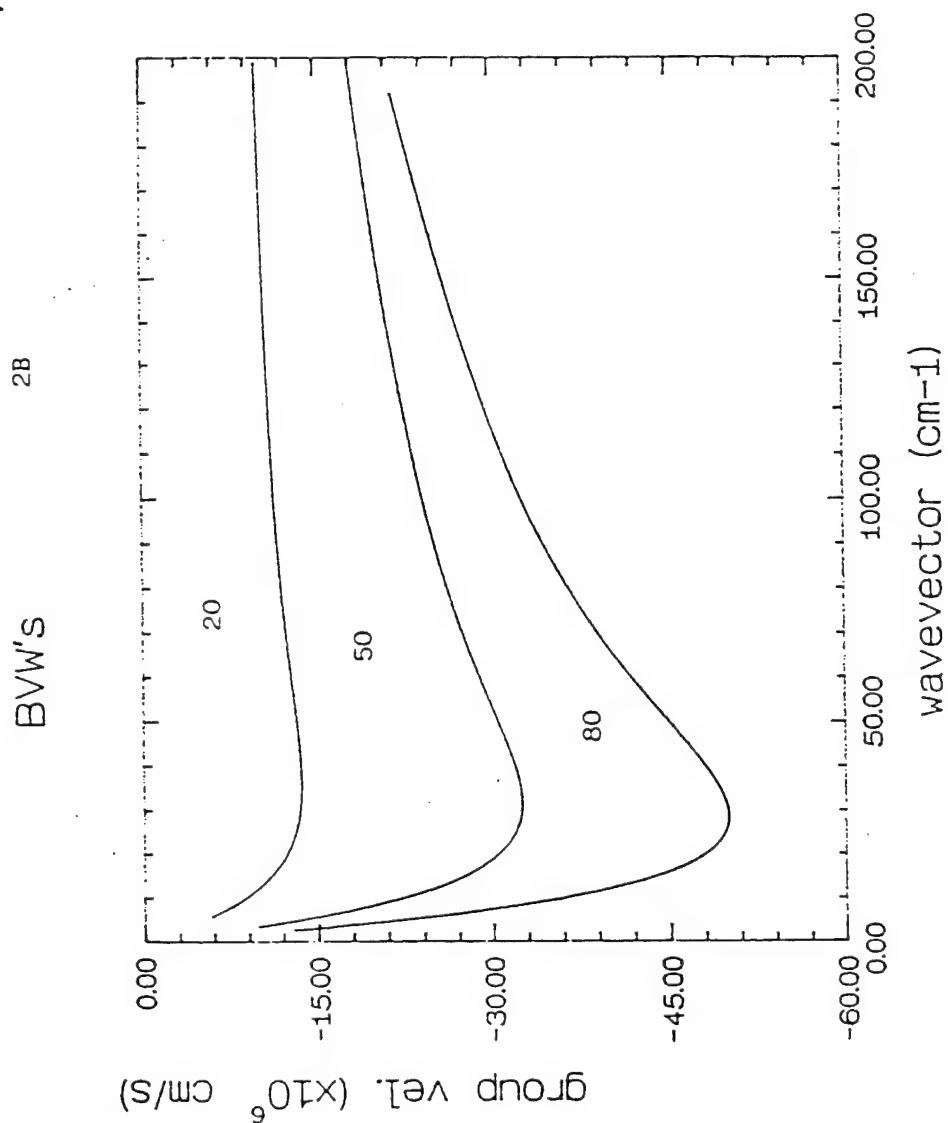


Fig. 2c

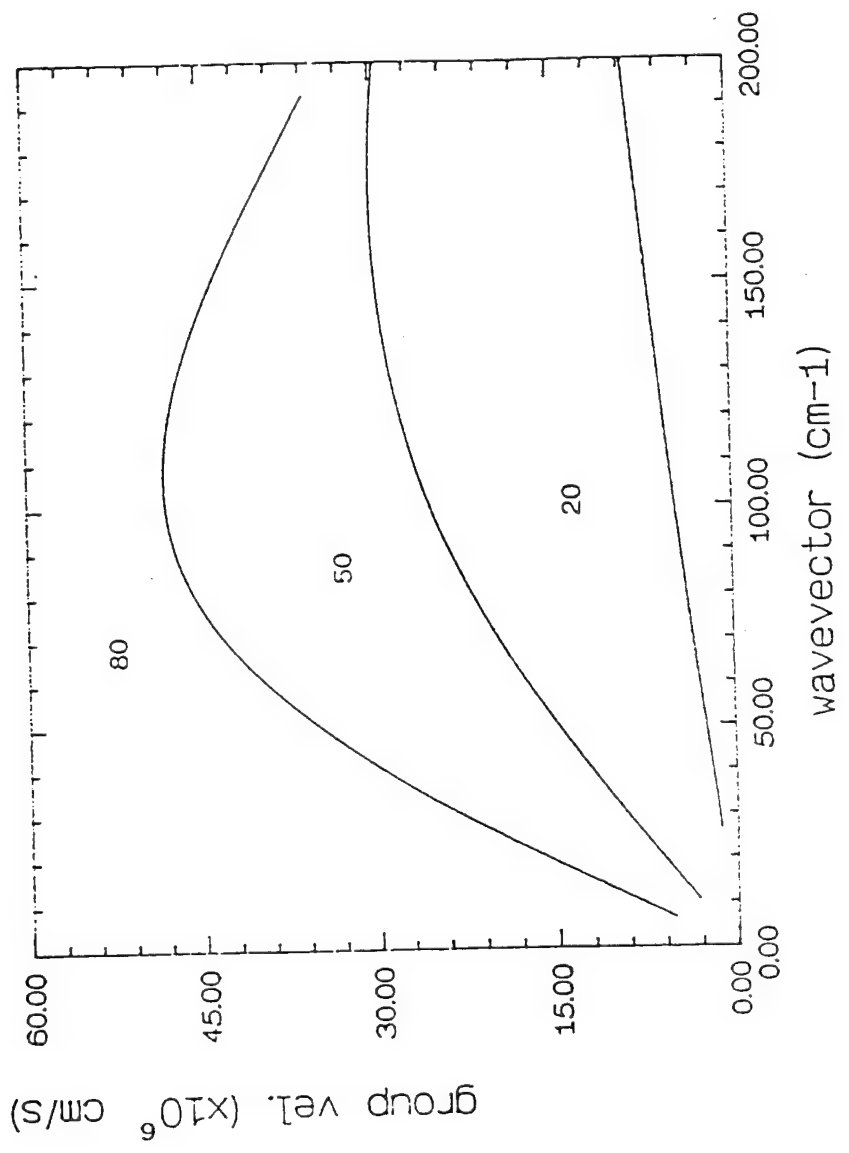
2 gnd's

$h = 254 \mu m$

$w = 1 mm$

$H_0 = 5000 Oe$

FVW's 2c



ENVELOPE SOLITONS

- ENVELOPE SOLITONS OF NLSE ARE EXCITED IN A LOW LOSS MAGNETIC FILM WHEN MICROWAVE PULSES ARE LAUNCHED IN A DELAY LINE DEVICE, WHERE THE MAGNETIC FILM IS THE WAVEGUIDE FOR THE PROPAGATION OF THE ENVELOPE.

- THE SATISFACTION OF THE LIDTHILL CRITERION IS THE BASIC REQUIREMENT TO IDENTIFY THE SOLITONIC NATURE OF THE TRAVELING ENVELOPES.

- IN MAGNETOSTATIC WAVE (MSW) DELAY LINES, THE NONLINEAR TERM MANTAINS THE SAME ORDER OF MAGNITUDE OVER THE ENTIRE EXCITATION BAND DEFINED BY THE DC MAGNETIC BIAS FIELD STRENGTH. ON THE OTHER HAND, THE DISPERSION RELATIONS FOR MSW'S CRITICALLY DEPEND ON THE GEOMETRY OF THE PROBLEM AND NOT ONLY ON THE BIAS FIELD VALUE.

FIG. 3A

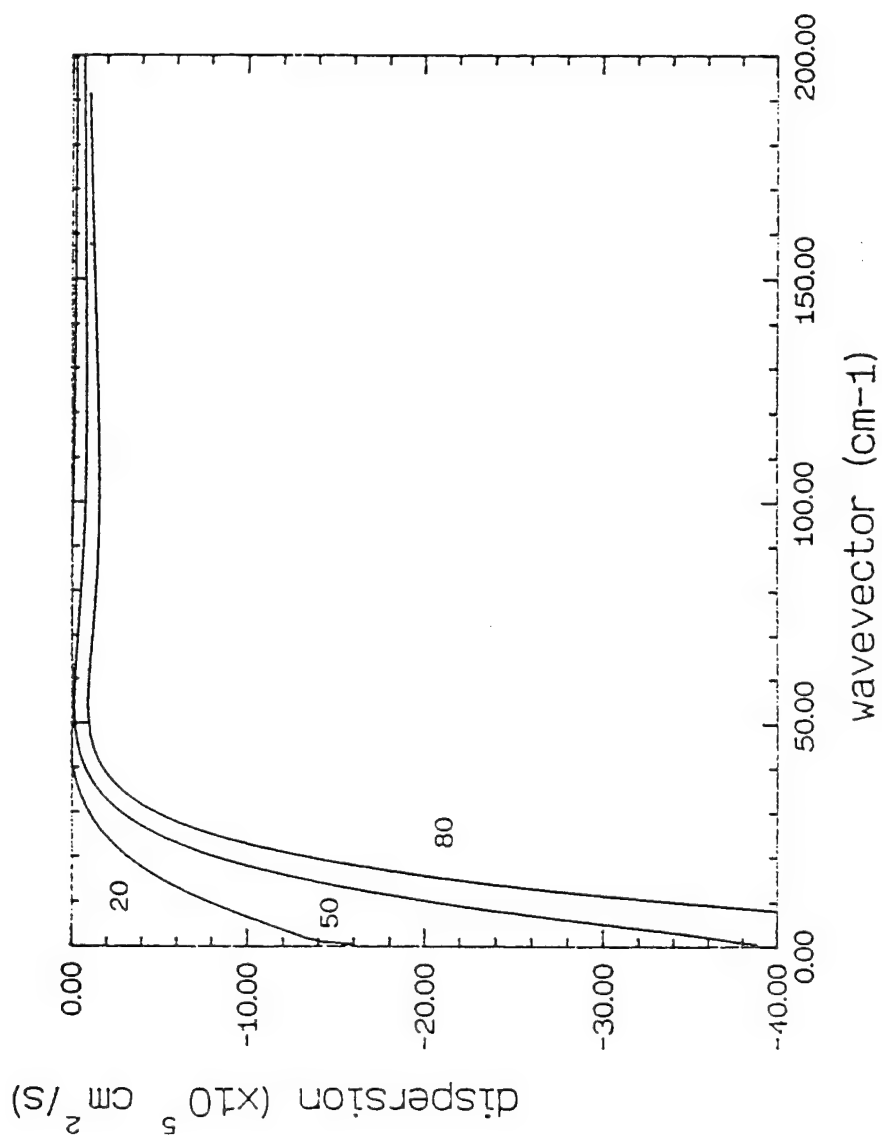
1 gnd

$h = 2.54 \mu m$

$w = \infty$

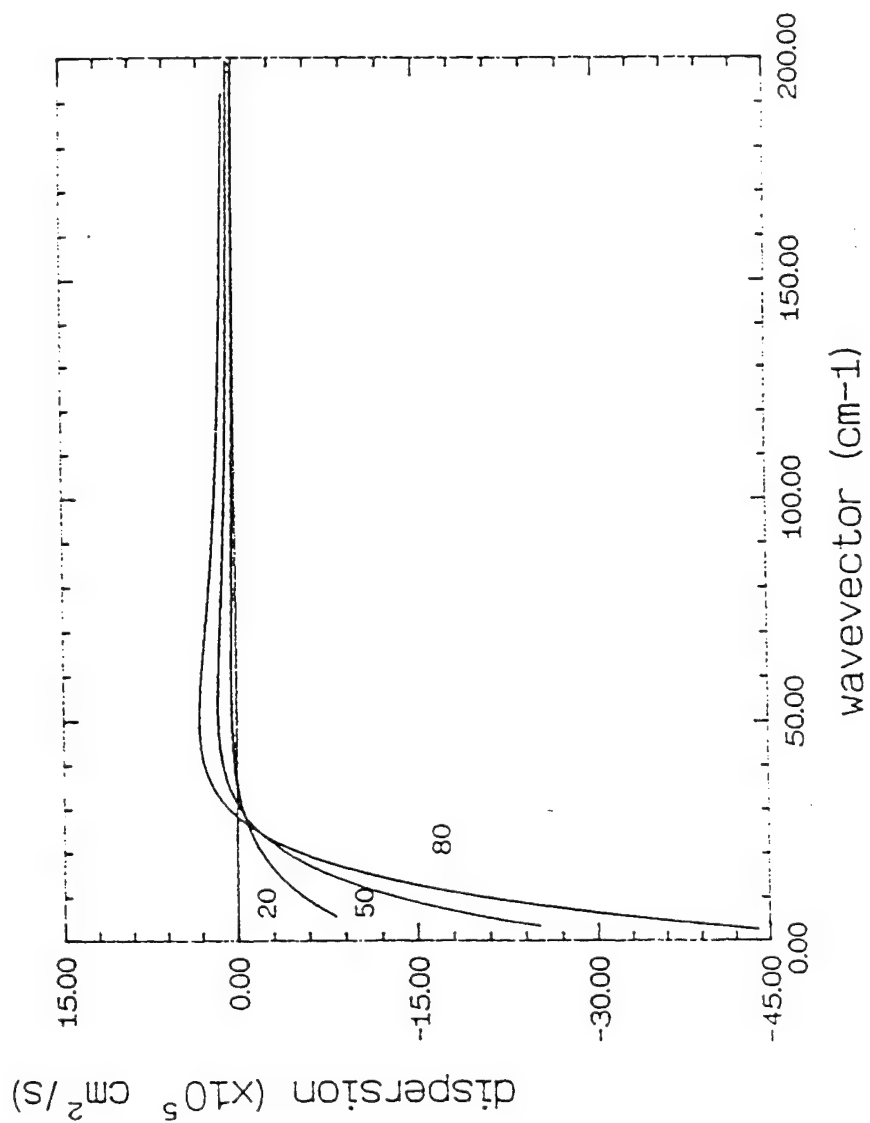
$H_0 = 5000 \text{ Oe}$

FVW's 3A



1 and 2 gnd's
 $h = 254 \mu m$
 $u = \infty, 1 mm$
 $H_0 = 3240 Oe$

BVW's 3B



2 gnd's

$h = 254 \mu m$

$\omega = 1 mm$

$H_0 = 5000 Oe$

FVW's 3C

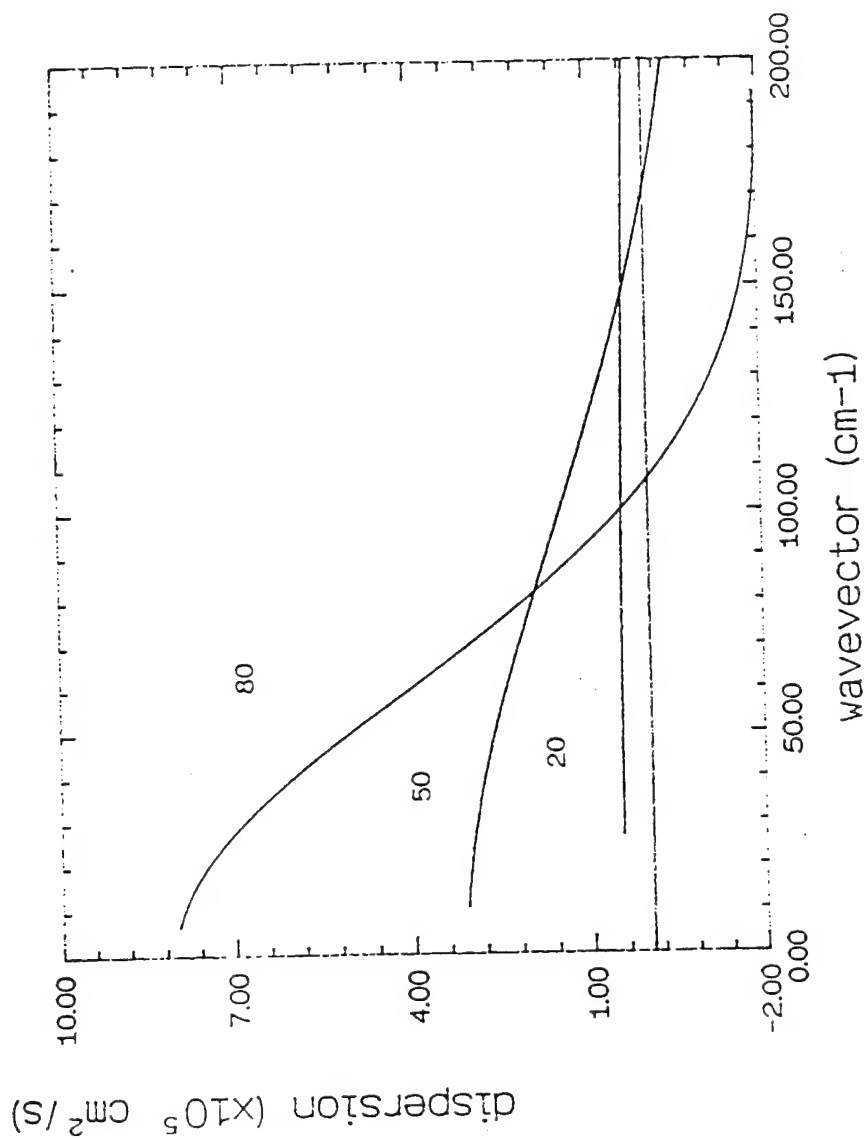


FIG. 4A

1 gnd
 $h = 2.54 \mu m$
 $u = \infty$
 $H_0 = 5000 Oe$

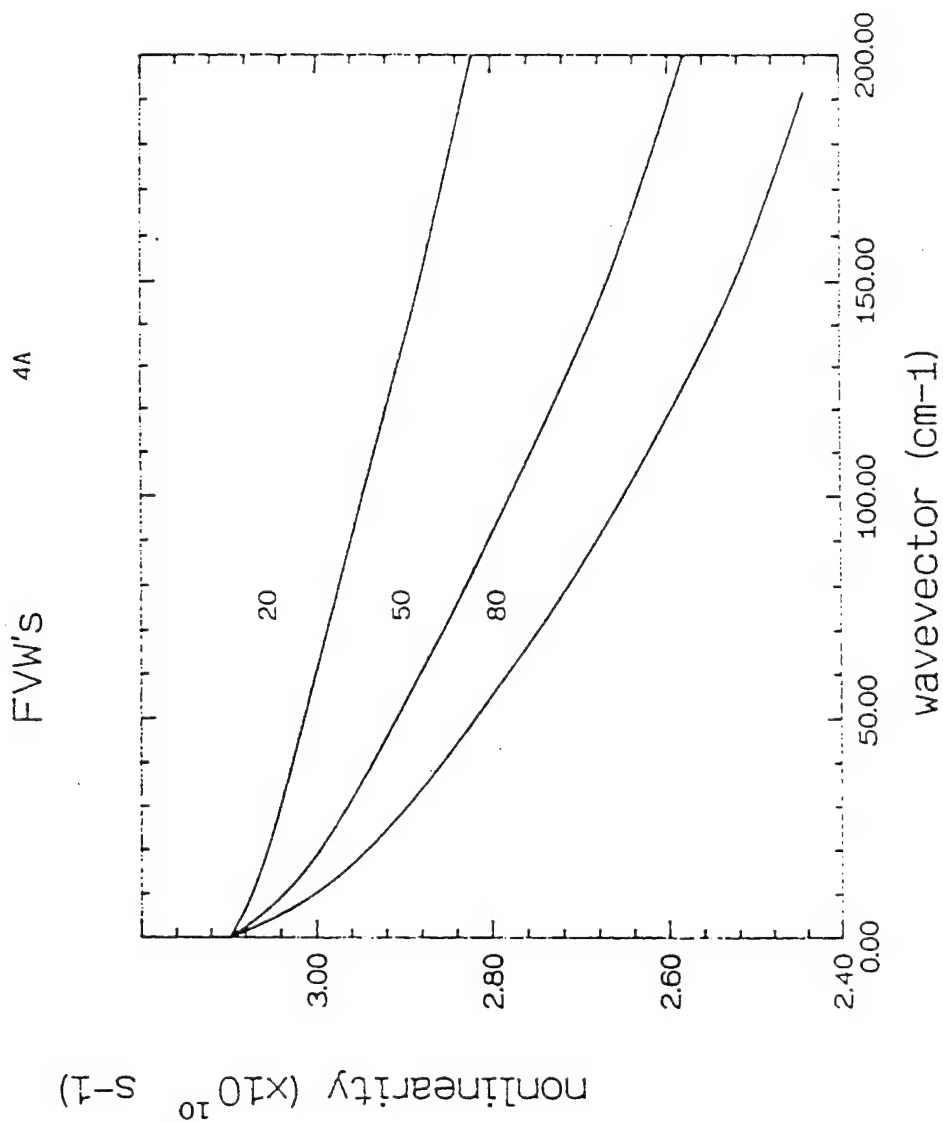


Fig. 4B

1 and 2. grad's
 $h = 2.54 \mu m$
 $\omega = \infty, 1 mm$
 $H_0 = 32.40 Oe$

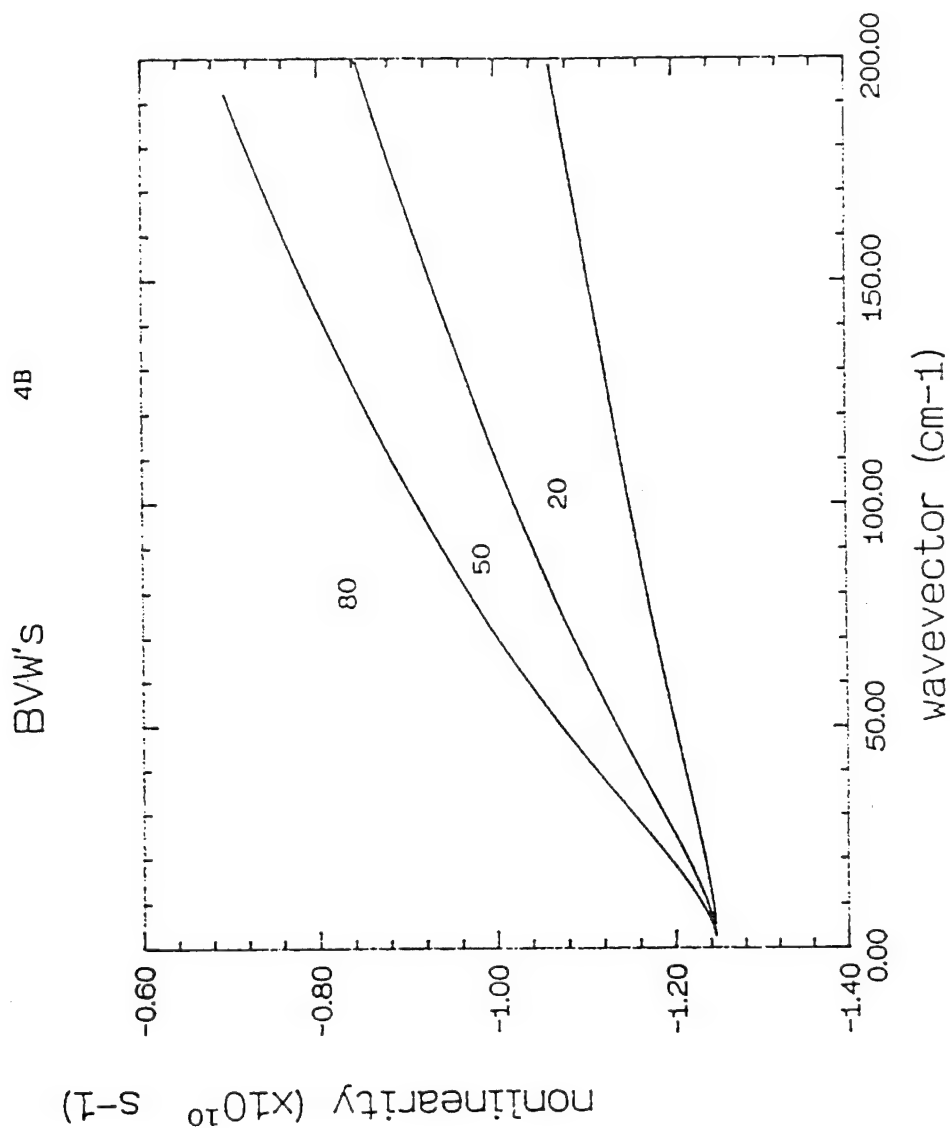
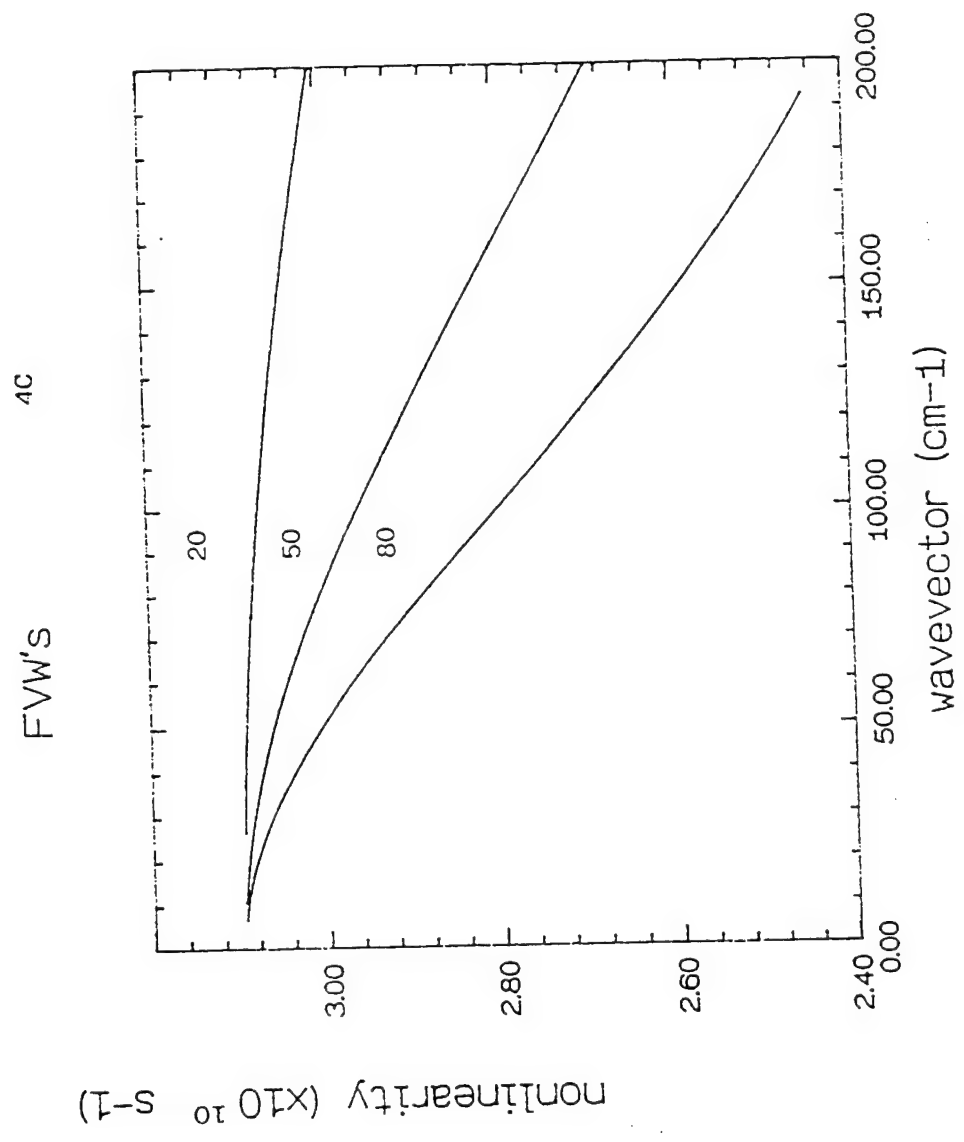


FIG. 4C

2. gnd's
 $h = 254 \mu m$
 $w = 1 mm$
 $H_0 = 5000 De$



FREQUENCY LIMITS FOR THE EXCITATION OF MSW SOLITONS - 1

- A MICROWAVE PULSES TRAIN IS REPRESENTED IN THE FREQUENCY SPECTRUM ACCOUNTING FOR THE CARRIER FREQUENCY f_c , THE PERIOD T AND THE PULSEWIDTH τ (OR THE DUTY CYCLE $D=\tau/T$).

- THE ENVELOPE IN THE FREQUENCY DOMAIN IS CENTERED AT f_c , AND THE MAIN LOBE IS LIMITED BY $f_c \pm 1/\tau$, WITH THE FREQUENCY COMPONENTS WITHIN THE LOBE SEPARATED EACH OTHER BY $1/T$.

- TO AVOID THE CUTTING OF SOME FREQUENCY COMPONENTS OF THE PULSE, AT LEAST THE MAIN LOBE MUST LIE ALL WITHIN THE MSW BAND EXCITATION. IF f_L AND f_H ARE THE LOW AND HIGH FREQUENCY LIMITS FOR THE EXCITATION OF MSW'S, IT WILL BE:

$$f_L < f_c - 1/\tau, \text{ and } f_H > f_c + 1/\tau$$

BY IMPOSING $\tau = 20 \text{ ns}$, f_c MUST BE FAR FROM THE FREQUENCY LIMITS AT LEAST 50 MHz.

FREQUENCY LIMITS FOR THE EXCITATION OF MSW SOLITONS - 2

- GENERALLY SPEAKING, A WIDEBAND RESPONSE IS REQUIRED TO CLEARLY IDENTIFY THE PULSE RESHAPING, BECAUSE A NARROWBAND FILTER INTRODUCES ITSELF A SHAPE MODULATION, THUS MAKING DIFFICULT TO RECOGNIZE THE SOLITONIC BEHAVIOUR IN THE TIME DOMAIN.

- THE IDEAL SITUATION FOR MSW DEVICES IS ASYMPTOTICALLY REACHED WHEN WIDEBAND MICROSTRIP TRANSDUCERS ARE COUPLED TO SUFFICIENTLY THICK MAGNETIC GARNET FILMS CHARACTERIZED BY A SMALL LINEWIDTH.

- BY EXCITING THE FILM AT A FREQUENCY FAR ENOUGH FROM THE MSW BAND LIMITS, THE PULSE WILL SUFFER THE DISPERSION CONTRIBUTION, AND THE RESHAPING OF THE PULSE WILL BE DUE ONLY TO THE SPREAD INDUCED BY THE INTRINSIC DISPERSIVE BEHAVIOUR OF THE MSW DEVICE.

- AT SUFFICIENTLY HIGH POWER LEVELS, THE INTERPLAY BETWEEN NONLINEARITY AND DISPERSION WILL CHANGE AGAIN THE PULSE SHAPE IF A SOLITON IS EXCITED. A PROPER DESIGN OF THE DEVICE EASILY ALLOWS FOR THE NECESSARY WIDEBAND RESPONSE.

ELECTRICAL DESIGN CRITERIA

- BY INTRODUCING THE ELECTRICAL DESIGN OF THE DEVICE, THE FILTER BANDWIDTH IS NARROWER THAN THE MSW LIMITS, WHICH ARE ONLY THE PHYSICAL LIMITS FOR THE EXCITATION OF MSW'S DEFINED BY MEANS OF THE BIAS FIELD STRENGTH.

- THE REAL BANDWIDTH IS OBTAINED BY USING THE CURRENT DENSITY FLOWING IN THE MICROSTRIP TRANSDUCER USED TO EXCITE THE MAGNETIC GARNET FILM. THE CURRENT DENSITY J IS A FUNCTION OF THE MICROSTRIP WIDTH w_m AND OF THE EXCITED WAVEVECTOR k , FOLLOWING THE RELATION:

$$J \approx \sin(w_mk/2)/(w_mk/2).$$

THE MAIN LOBE OF THE FILTERING RESPONSE IS LIMITED BY $w_mk/2=\pi$, THAT IS TO A MAXIMUM ALLOWED k -VALUE OF $2\pi/w_m$.

COMMENT

IT REMAINS THE UNAVOIDABLE LIMITATION INTRODUCED BY THE NARROWBAND FILTERING RESPONSE IN THE PULSE RESHAPING, AND, FROM AN EXPERIMENTAL POINT OF VIEW, THE RISE TIME AND THE FALL TIME OF THE REAL PULSES AT THE INPUT OF THE DEVICE.

FIG. 6

1 gnd

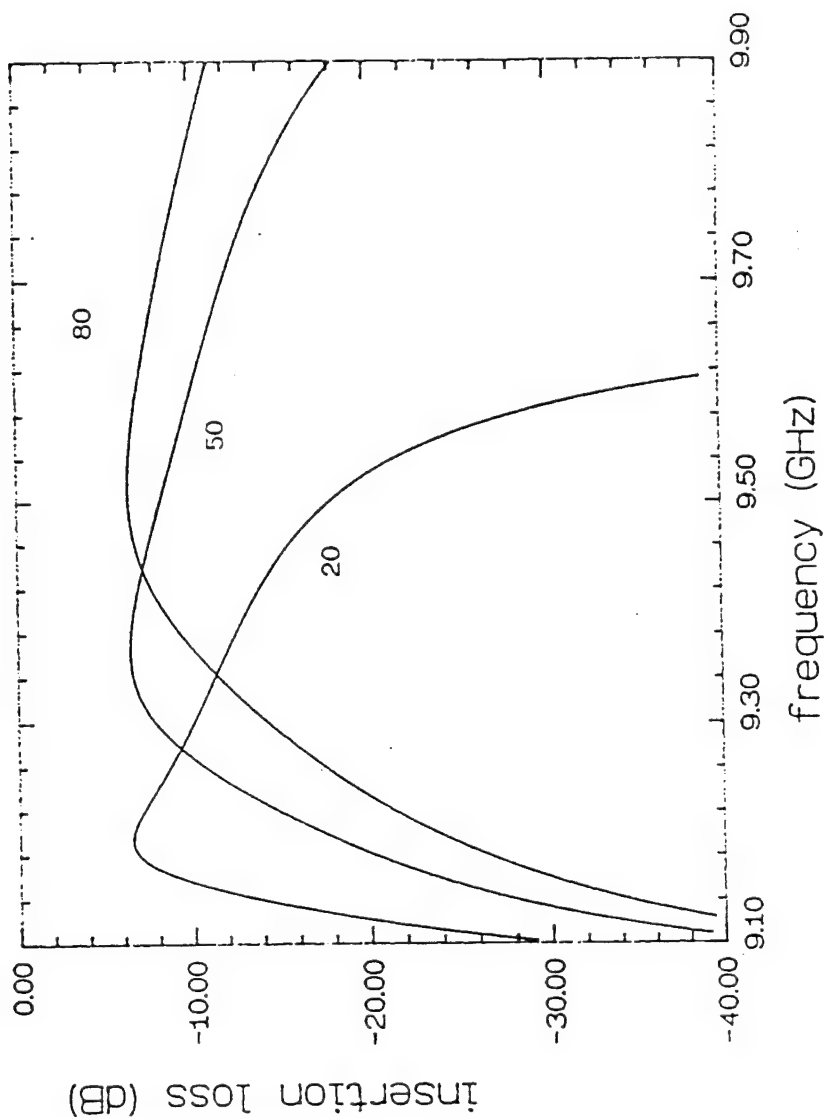
$h = 254 \mu\text{m}$

$\kappa = \infty$

$\omega_m = 240 \mu\text{m}$

$H_0 = 5000 \text{ Oe}$

FVW's



NONLINEAR SCHROEDINGER EQUATION AND FREQUENCY SHIFTS -1

- A POSSIBLE APPROACH IN OBTAINING A NLSE FOR MSW'S IN PURE DIPOLAR REGIME IS THAT OF ZVEZDIN AND POPKOV (1983) BASED ON THE VARIATION OF THE DISPERSION RELATION WITH RESPECT TO THE WAVEVECTOR, THE FREQUENCY AND THE SQUARE MODULUS OF THE MICROWAVE MAGNETIZATION AMPLITUDE NORMALIZED BY THE SATURATION VALUE, IN THE APPROXIMATION OF SMALL SIGNALS.
- AN ALTERNATIVE METHOD IS IN CALCULATING THE VARIATION DIRECTLY ON THE FREQUENCY. FROM BOTH COMPUTATIONS, THE RESULT IS A NLSE WITH THE NONLINEAR AND DISPERSIVE TERMS EASILY OBTAINABLE FROM PARTIAL DERIVATIVES OF THE DISPERSION RELATION.
- A PECULIAR RESULT IS THAT THE TRAVELING WAVE IS AFFECTED BY FREQUENCY AND WAVENUMBER SHIFTS, BOTH RELATED TO THE NONLINEARITY AND THE DISPERSION. THAT CORRESPONDS TO A MODULATION OF THE CARRIER FREQUENCY AND WAVENUMBER, WHOSE VALUES ARE CHANGED WITH RESPECT TO THE ORIGINAL ONES IN THE LINEAR REGIME.

NONLINEAR SCHROEDINGER EQUATION AND FREQUENCY SHIFTS -2

- THE CARRIER WAVENUMBER k_c WILL BE CHANGED IN

$$k_c' = k_c + \kappa$$

AND THE CARRIER FREQUENCY ω_c BECOMES

$$\omega_c' = \omega_c + \Omega,$$

WHERE Ω IS THE FREQUENCY SHIFT AND κ IS THE WAVENUMBER SHIFT, AND THE CONDITIONS $\kappa \ll k_c$ AND $\Omega \ll \omega_c$ ARE SATISFIED.

NONLINEAR SCHROEDINGER EQUATION AND FREQUENCY SHIFTS -3

- BY FOLLOWING THE ANALYSIS PERFORMED BY HASEGAWA AND TAPPERT IN THE CASE OF OPTICAL FIBERS, THE FREQUENCY VARIATION CAN BE WRITTEN AS:

$$\Omega = (\partial\omega/\partial k)\kappa + (1/2)(\partial^2\omega/\partial k^2)\kappa^2 + (\partial\omega/\partial|\varphi|^2)|\varphi|^2$$

WHERE $|\varphi|^2 = (m/M_S)^2$ IS THE QUADRATIC DEVIATION FROM THE EQUILIBRIUM SATURATION MAGNETIZATION M_S . m IS THE AMPLITUDE OF THE MICROWAVE MAGNETIZATION IN THE PLANE NORMAL TO THE EXTERNAL DC BIAS FIELD H_0 , AND THE QUADRATIC TERM ARISES FROM THE TAYLOR EXPANSION OF THE MAGNETIZATION COMPONENT ALONG THE DIRECTION PARALLEL TO H_0 . LET'S ASSUME z THIS COMPONENT, IT WILL BE:

$$M_z = \sqrt{M_S^2 - m^2} = M_S \sqrt{1 - (m/M_S)^2} \approx M_S(1 - (m/M_S)^2) = M_S(1 - |\varphi|^2)$$

NONLINEAR SCHROEDINGER EQUATION AND FREQUENCY SHIFTS -4

- SINCE THE THE SECOND ORDER TERM IS THE LOWEST NOT NEGLIGIBLE TO BE CONSIDERED FOR THE NONLINEAR CONTRIBUTION, THE SAME ORDER HAS TO BE USED FOR THE DISPERSION.

$$\Omega = \delta\omega_{\text{Disp}} + \delta\omega_{\text{NL}}$$

WHERE $\delta\omega_{\text{Disp}}$ AND $\delta\omega_{\text{NL}}$ ARE THE CONTRIBUTIONS TO THE SHIFT DUE TO THE DISPERSION AND THE NONLINEARITY, RESPECTIVELY. BOTH ARE EXPANDED UP TO THE SECOND ORDER AND ARE DEFINED BY:

$$\delta\omega_{\text{Disp}} = (\partial\omega/\partial k)\kappa + (1/2)(\partial^2\omega/\partial k^2)\kappa^2$$

$$\delta\omega_{\text{NL}} = (\partial\omega/\partial |\varphi|^2) |\varphi|^2$$

NONLINEAR SCHROEDINGER EQUATION AND FREQUENCY SHIFTS -5

- AN EXSTIMATION OF THE WAVENUMBER MODULATION IN THE CASE OF MODULATIONAL INSTABILITY CAN BE GIVEN BY ASSUMING THAT THE INSTABILITY GROWTH RATE β GROWS UP TO A MAXIMUM VALUE DEFINED BY:

$$\kappa = \kappa_0 = \sqrt{2} |\beta| / |(\partial^2 \omega / \partial k^2)| \approx \sqrt{2} |\omega_r| / |(\partial^2 \omega / \partial k^2)|$$

WHERE $\omega_r = \gamma \Delta H / 2$ IS THE RELAXATION FREQUENCY, γ IS THE GYROMAGNETIC RATIO AND ΔH IS THE MAGNETIC FULL LINEWIDTH.

- THE LOCATION OF THE SATELLITES WITH RESPECT TO THE INPUT FREQUENCY ω_c CAN BE ROUGHLY EXSTIMATED BY THE QUANTITY $\Omega \approx v_g / \kappa$ IN A FIRST ORDER APPROXIMATION, WHERE v_g IS THE GROUP VELOCITY AND $\Omega \ll \omega_c$.

NONLINEAR SCHROEDINGER EQUATION AND FREQUENCY SHIFTS -6

- WHEN SOLITONS ARE CONSIDERED, IT IS DIFFICULT TO SEPARATE THE CONTRIBUTIONS OF THE DISPERSION AND THE NONLINEARITY, BECAUSE THE COMPONENTS OF THE PERMEABILITY TENSOR ARE THEMSELVES AFFECTED BY THE NONLINEARITY, AND THEY MAKE PART IN THE DEFINITION OF THE PARTIAL DERIVATIVES USED TO CALCULATE THE DISPERSION QUANTITIES.

- THE GROUP VELOCITY IS CHANGED AND, FOR THAT REASON, IT IS ONLY A ROUGH APPROXIMATION TO ASSUME THAT DISPERSION AND NONLINEARITY PLAY INDEPENDENT ROLES IN THE DEFINITION OF Ω .

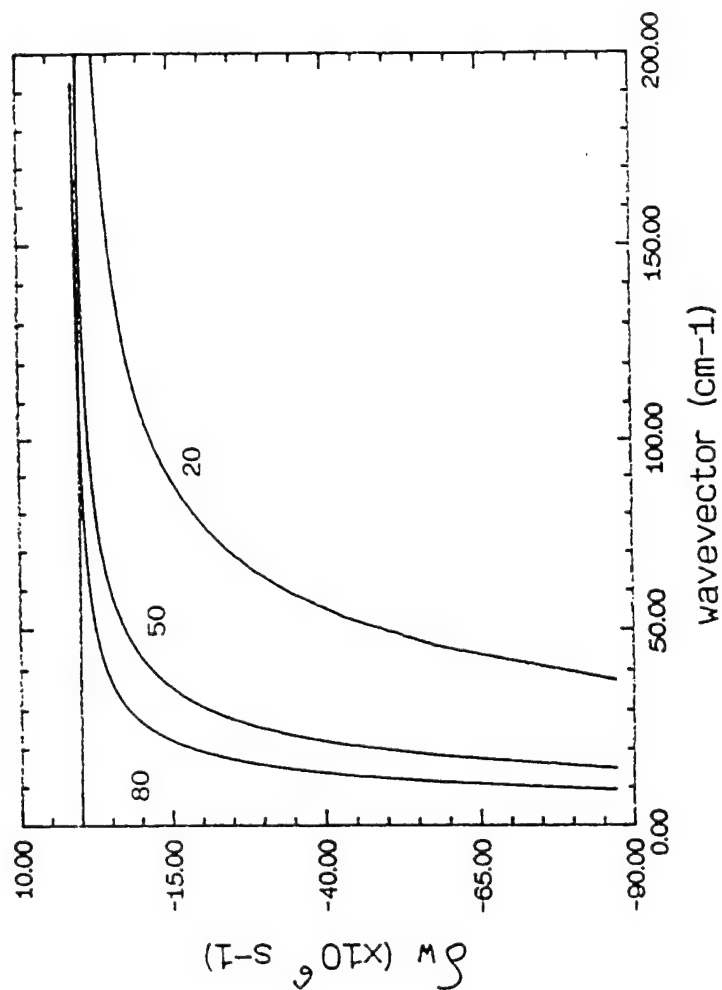
- LET'S ASSUME THE VALIDITY OF THIS APPROXIMATION, WE WILL CALCULATE THE $\delta\omega_{NL}$ VALUE AS A FUNCTION OF THE EXCITED WAVEVECTOR.

DISPERSION, NONLINEARITY AND LIDTHILL CRITERION

- THE FREQUENCY BEHAVIOUR OF ONE- AND TWO-GROUND PLANES CONFIGURATIONS FOR VOLUME MSW DELAY LINES WILL BE SIMULATED, TO ESTABLISH THE FREQUENCY LIMITS ALLOWED FOR THE SOLITONS EXCITATION. BOTH, FORWARD AND BACKWARD VOLUME WAVES WILL BE CONSIDERED.
- FROM THE ANALYSIS OF THOSE PICTURES, IT TURNS OUT THAT THE POSSIBILITY TO FULLFILL THE LIDTHILL CRITERION FOR THE EXCITATION OF ENVELOPE SOLITONS IS STRICTLY RELATED TO THE GEOMETRY OF THE DEVICE, AND MAINLY TO THE PRESENCE OF A SECOND GROUND PLANE AND TO THE FILM THICKNESS VALUE.

2 gnd's
 $h = 254 \mu\text{m}$
 $w = 1 \text{ mm}$
 $H_0 = 5000 \text{ Oe}$

FVW's NL f-shift 2



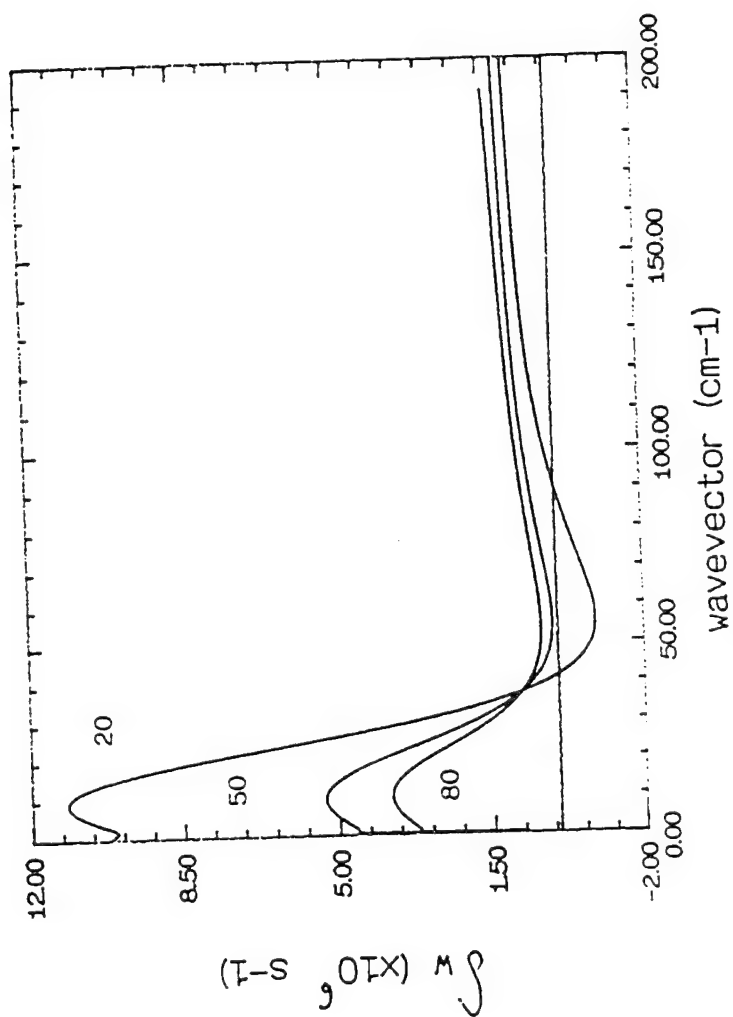
1 gnd

$h = 254 \mu m$

$w_1 = \infty$

$H_0 = 5000 Oe$

FVW's NL f-shift



2. g's unchanged

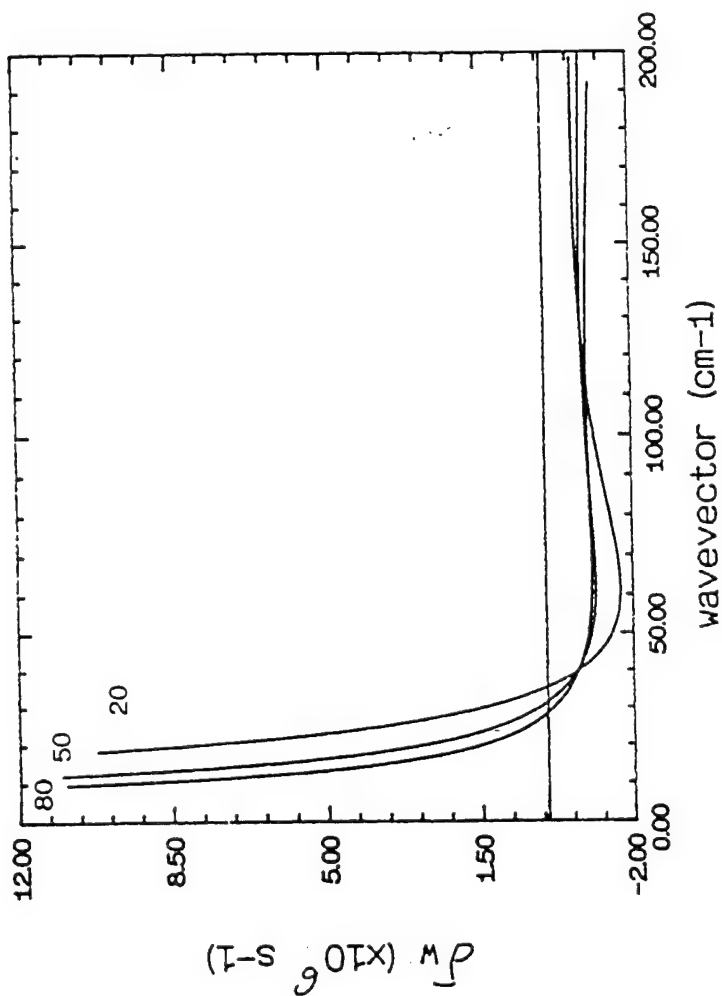
1 and 2. gnd's

$h = 254 \mu m$

$w = \infty, 1 mm$

$H_0 = 3240 Oe$

BVW's NL f-shift



NONLINEAR FREQUENCY SHIFT

- THE SHIFT FOR THE ONE-GROUND PLANE FVW'S IS ALWAYS POSITIVE FOR ALL THE ALLOWED k -VALUES, WHILE POSSIBLE NEGATIVE VALUES DO NOT MAKE SENSE, BECAUSE IN THAT CASE THE LIDTHILL CRITERION IS NOT FULLFILLED.

- TWO-GROUND PLANE FVW'S ARE CHARACTERIZED BY THE SATISFACTION OF THE LIDTHILL CRITERION ONLY FOR HIGH k -VALUES AND THICK FILMS. FOR THOSE REASONS, FVW MSW'S SOLITONS SEEM LESS FAVOURED FOR APPLICATIONS, BECAUSE THEY MEET THE RIGHT SPECIFICATIONS TOO FAR FROM THE FREQUENCIES WHERE THE DEVICE USUALLY EXHIBITS THE LOWEST INSERTION LOSS.

- BVW SOLITONS ARE LESS SENSITIVE TO THE FILM THICKNESS AND TO THE GROUND PLANES. THEY HAVE HAVE ALWAYS NEGATIVE SHIFTS, UNLESS IN THOSE REGIONS WHERE LIDTHILL PROHIBITS THEIR CREATION. ROUGHLY, THE EXPECTED SHIFT FOR WAVEVECTORS $k \geq 40 \text{ cm}^{-1}$ IS $\Omega \approx -10^6 \text{ sec}^{-1}$, CORRESPONDING TO FEW HUNDREDS OF kHz.

- OWING TO THE EXSISTENCE OF ALLOWED AND FORBIDDEN REGIONS, THE FREQUENCY SPECTRUM OF A PULSE PROPAGATING IN THE DELAY LINE MUST LIE WITHIN THE ALLOWED REGIONS.

THRESHOLD POWERS -1

- THE THRESHOLD POWERS FOR THE EXCITATION OF SOLITONS IN A MAGNETIC GARNET FILM CAN BE EASILY DERIVED BY CALCULATING THE POYNTING VECTOR AND BY PERFORMING AN INTEGRATION OVER THE FILM CROSS SECTION.

- THIS APPROACH IS RIGOROUSLY VALID BY ASSUMING AN HOMOGENOUS MAGNETIZATION OVER THE ENTIRE FILM WIDTH, AND IT LOSSES MEANING WHEN NARROW FILMS ARE CONSIDERED.

- IN FACT, THE DEMAGNETIZATION FACTOR IS ALMOST CONSTANT ONLY WHEN THE FILM IS WIDE ENOUGH WITH RESPECT TO ITS THICKNESS. FURTHERMORE, A NARROW FILM IS AFFECTED BY WIDTH MODES, WHICH MAKE WORST THE BAND SHAPE BY INTRODUCING TRANSVERSESE RESONANCES AND THE NOTCHES CORRESPONDING TO THEIR FREQUENCY VALUES.

- FOR ABOVE REASONS, IN MANY PRACTICAL APPLICATIONS A FILM WIDE AT LEAST 4 mm MUST BE CONSIDERED TO ALLOW FOR A RELIABLE PREDICTION BY USING THE POYNTING APPROACH.

THRESHOLD POWERS -2

- THE THRESHOLD POWER P_{thre} HAS BEEN COMPUTED BY USING THE CLASSICAL DEFINITION FOUND ALSO IN THE ZVEZDIN AND POPKOV PAPER (1983).

- WE HAVE NOT LIMITED THE CALCULATION AT $k=0$ (WHICH IS NOT, RIGOROUSLY SPEAKING, WITHIN THE MSW APPROXIMATION), BUT WE HAVE DERIVED THE k -DEPENDENCE OF P_{thre} INSIDE THE BAND OF THE ALLOWED k -VALUES. THE $k=0$ CONDITION HAS BEEN USED ONLY AS A CHECK OF THE COMPARISON BETWEEN OUR RESULTS AND THOSE OBTAINED IN THE $k=0$ LIMIT BY ZVEZDIN AND POPKOV.

- THE CLASSICAL COMPUTATION IS PERFORMED BY USING THE FOLLOWING FORMULA:

$$P_{thre} = \operatorname{Re} \left(\int \mathbf{P} \cdot d\mathbf{S} \right) =$$

$$= (\omega/8\pi) \cdot (-(1+\chi_1)/(\chi_1^2+\chi_2^2)) \cdot (4\pi M_s)^2 \cdot d \cdot w \cdot |\varphi|^2/k$$

WHERE ω IS THE RADIAN FREQUENCY, χ_1 AND χ_2 ARE THE DIAGONAL ELEMENTS OF THE MAGNETIC SUSCEPTIBILITY TENSOR, M_s IS THE SATURATION MAGNETIZATION, d IS THE FILM THICKNESS, w IS THE FILM WIDTH AND k IS THE EXCITED WAVEVECTOR.

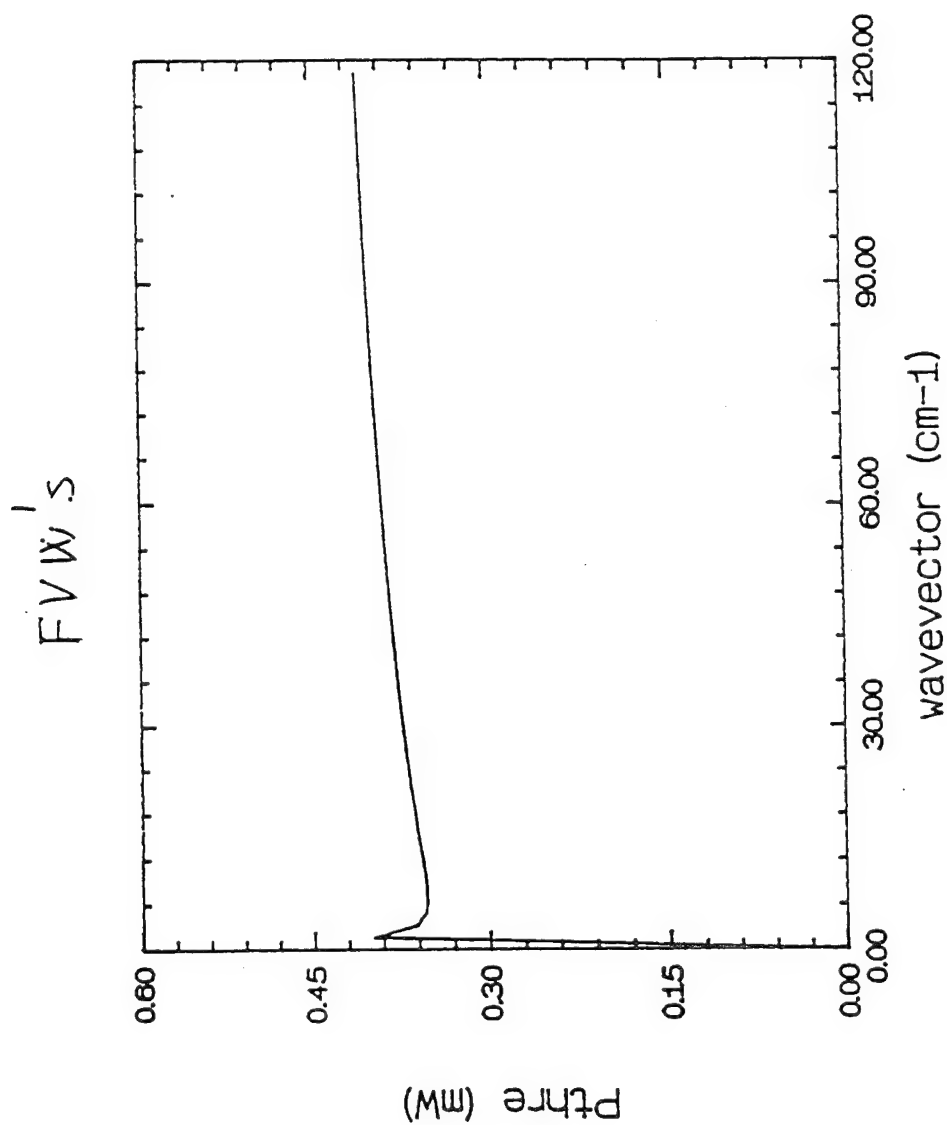
THRESHOLD POWERS -2A

- THE THRESHOLD AMPLITUDE FOR THE NORMALIZED MICROWAVE MAGNETIZATION IS GIVEN BY:

$$|\varphi|^2_{\text{thre}} = (\pi/2) \cdot (1/v_g \tau) \cdot \sqrt{-(\partial^2 \omega / \partial k^2) / (\partial \omega / \partial |\varphi|^2)}$$

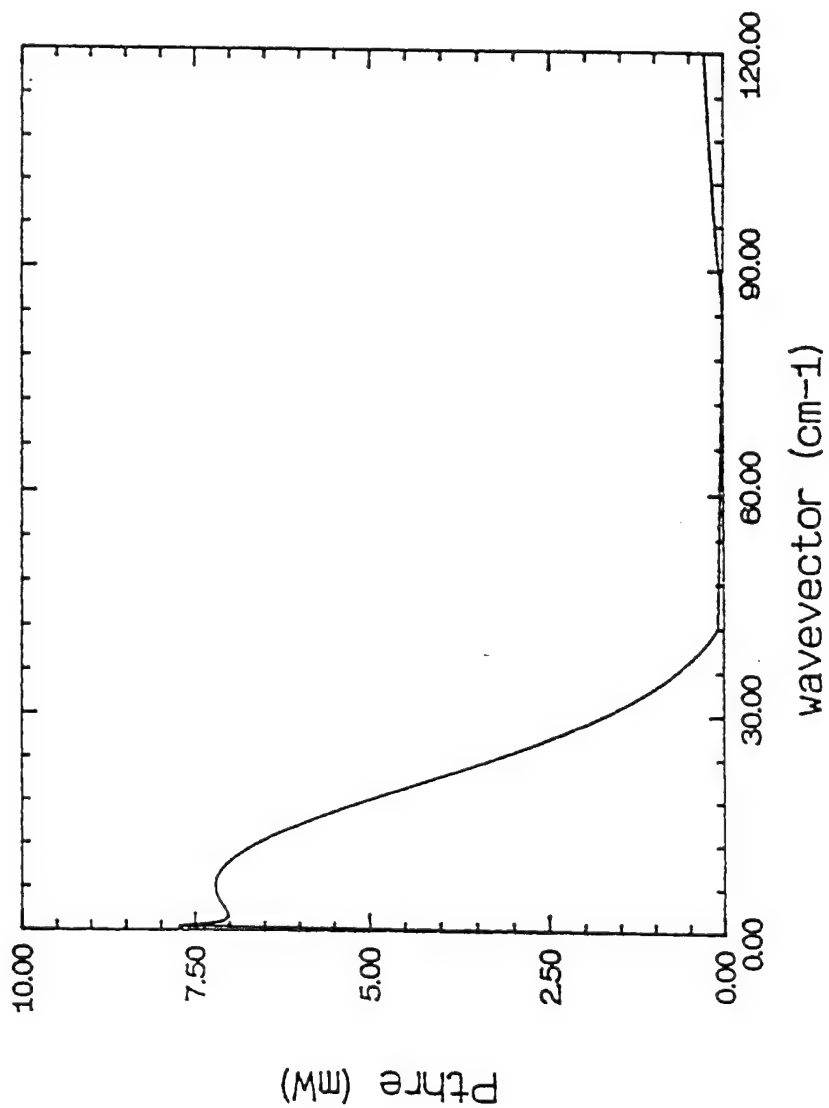
WHERE v_g IS THE GROUP VELOCITY AND τ THE PULSEWIDTH.

no ground
 $d = 10 \mu m$
 $\tau = 20 \text{ nsec}$
 $H_0 = 1955 \text{ Oe}$



1 gnd
 $h = 254 \text{ } \mu\text{m}$
 $k = \infty$
 $J = 10 \text{ } \mu\text{m}$
 $\tau = 20 \text{ nsec}$
 $H_0 = 1955 \text{ Oe}$

FVW's



1 gud

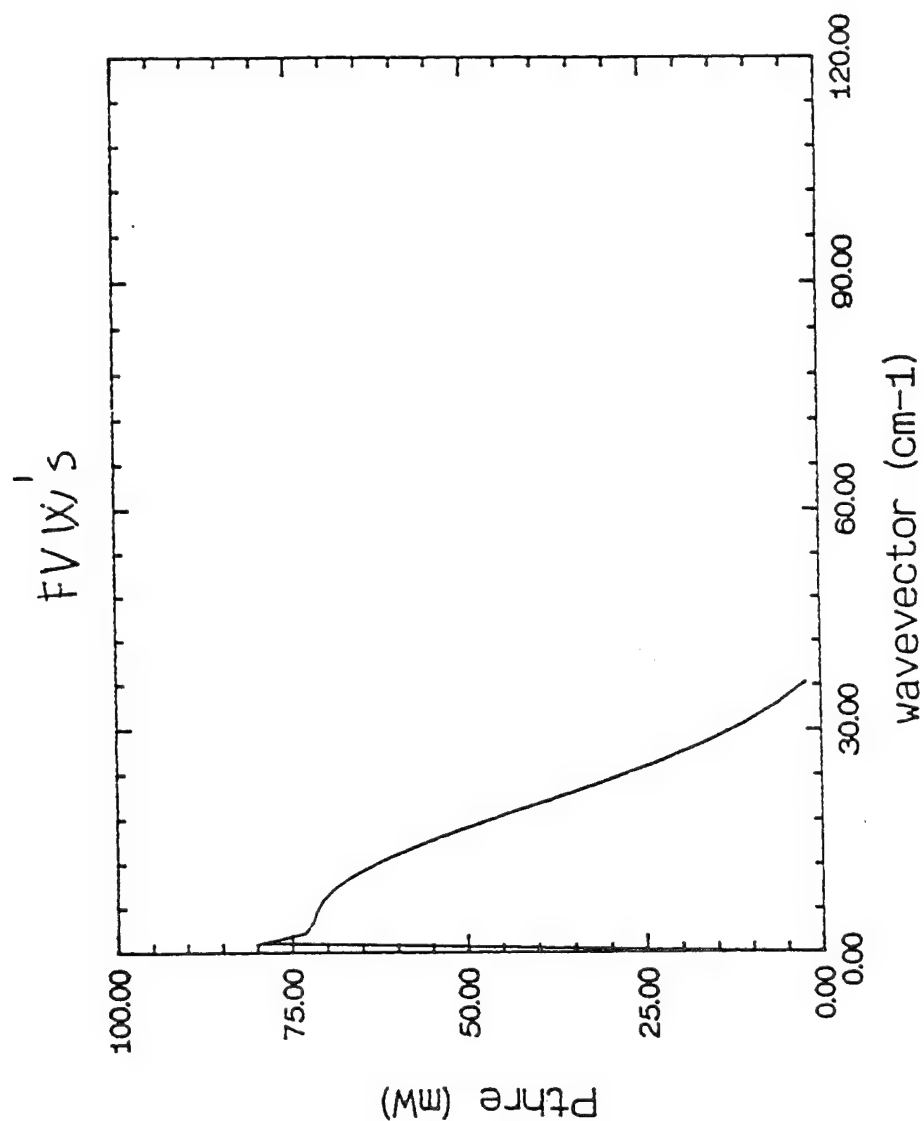
$h_1 = 254 \mu m$

$w = \infty$

$d = 10 \mu m$

$\tau = 20 \text{ nsec}$

$H_0 = 4180 \text{ Oe}$



THRESHOLD POWERS -3

FROM THE COMPUTATION OF THE THRESHOLD POWER P_{thre} FOR THE MSW SOLITONS, IT TURNS OUT THAT:

(i) P_{thre} DEPENDS ON THE k -VALUE AND ON THE APPLIED FIELD, AND IT IS PARTICULARLY EVIDENT IN THE LIMIT FOR VANISHING k .

(ii) A DRASTIC CHANGE IS PREDICTED IN THE TREND AND IN THE ABSOLUTE VALUE OF P_{thre} PASSING FROM THE NO GROUND PLANES CONDITION TO THE ONE GROUND PLANE GEOMETRY.

- (i) IS MAINLY DUE TO THE DISPERSION TREND AND TO THE ABSOLUTE WORKING FREQUENCY DEPENDENCE OF P_{thre} . THAT IS ALSO A FACT TO BE ACCOUNTED FROM AN ENGINEERING POINT OF VIEW, BECAUSE THE SAME WAVEVECTOR WILL HAVE NOT THE SAME THRESHOLD AT DIFFERENT FREQUENCIES. THIS IS ONLY A VIRTUAL PROBLEM IN THE APPLICATION OF SOLITONS TO MSW DELAY LINES, BECAUSE IT IS SUFFICIENT TO TAKE INTO ACCOUNT THE P_{thre} INCREASE VS THE OPERATIVE FREQUENCY.

- THE (ii) EFFECT IS TIGHTLY RELATED TO THE GEOMETRY OF REAL DEVICES, AND IT HAS TO BE CAREFULLY ACCOUNTED FOR APPLICATIONS.

THRESHOLD POWERS -4

- TO ACCOUNT FOR BOTH THE OUTLINED CONTRIBUTIONS, A DIFFERENT H_0 VALUE HAS BEEN IMPOSED FOR THE SIMULATION, LEAVING UNAFFECTED THE GEOMETRY. THE TREND OF P_{thre} VS k IS UNCHANGED, BUT A FACTOR CLOSE TO 10 MAKES THE DIFFERENCE BETWEEN THE TWO CURVES.

Fig. 5A

1 gnd

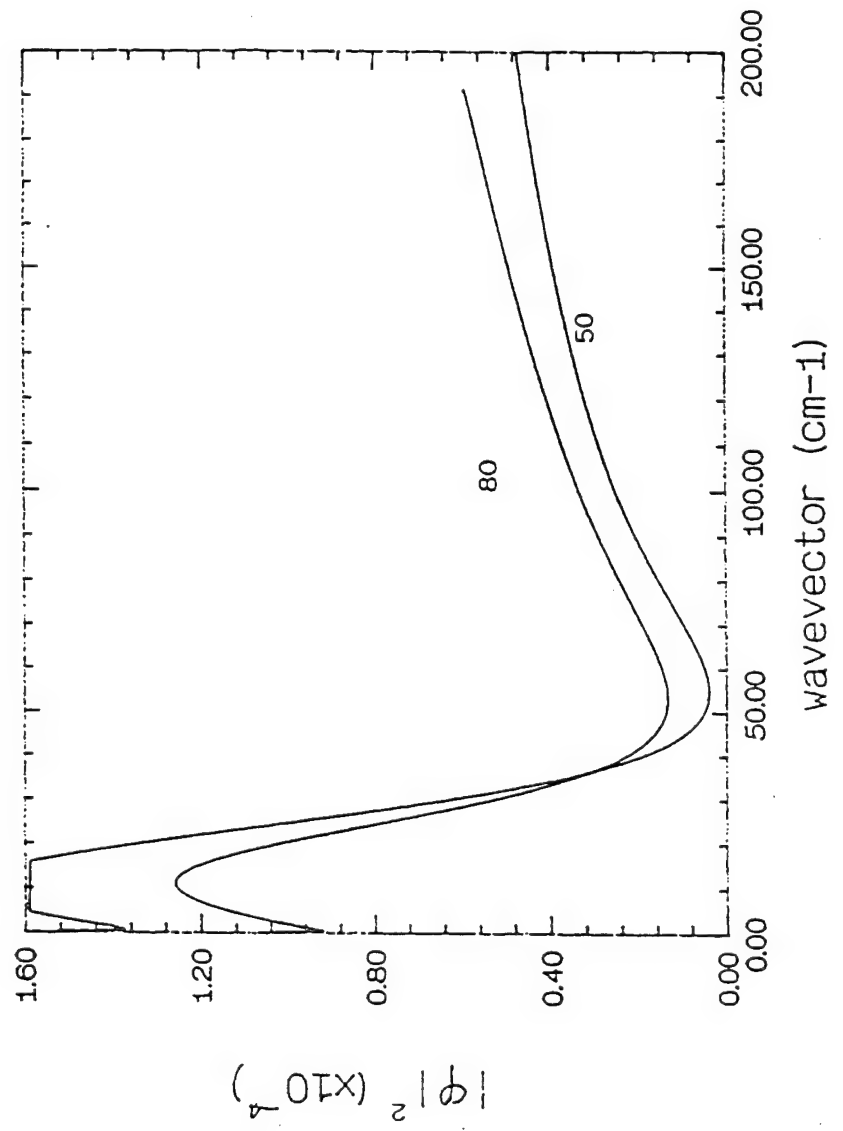
$h = 254 \mu m$

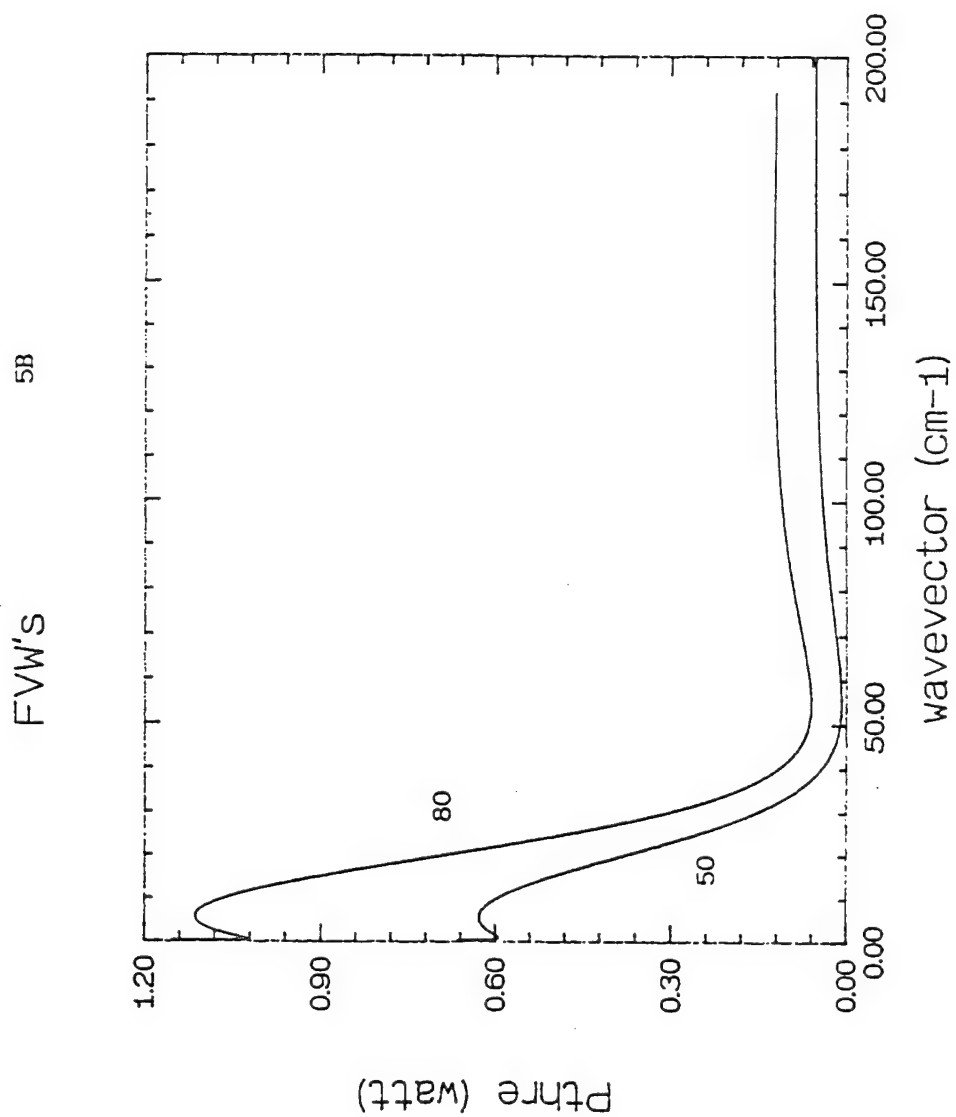
$\omega = \infty$

$H_0 = 5000 \text{ Oe}$

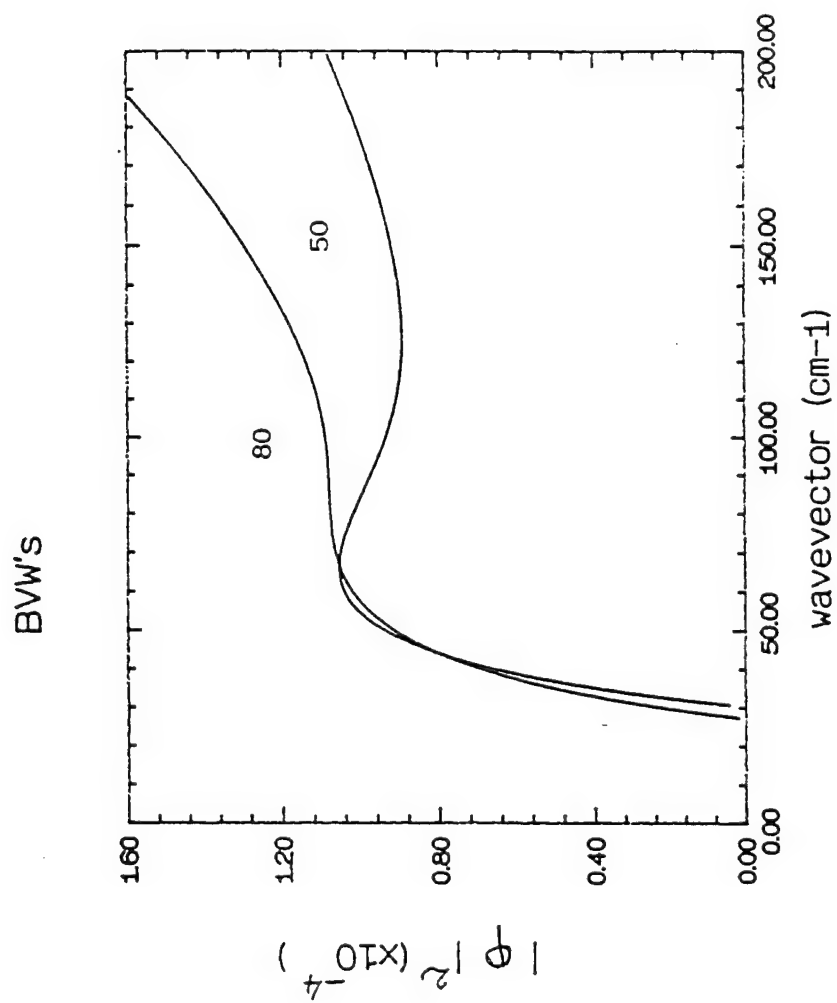
5A

FVW's

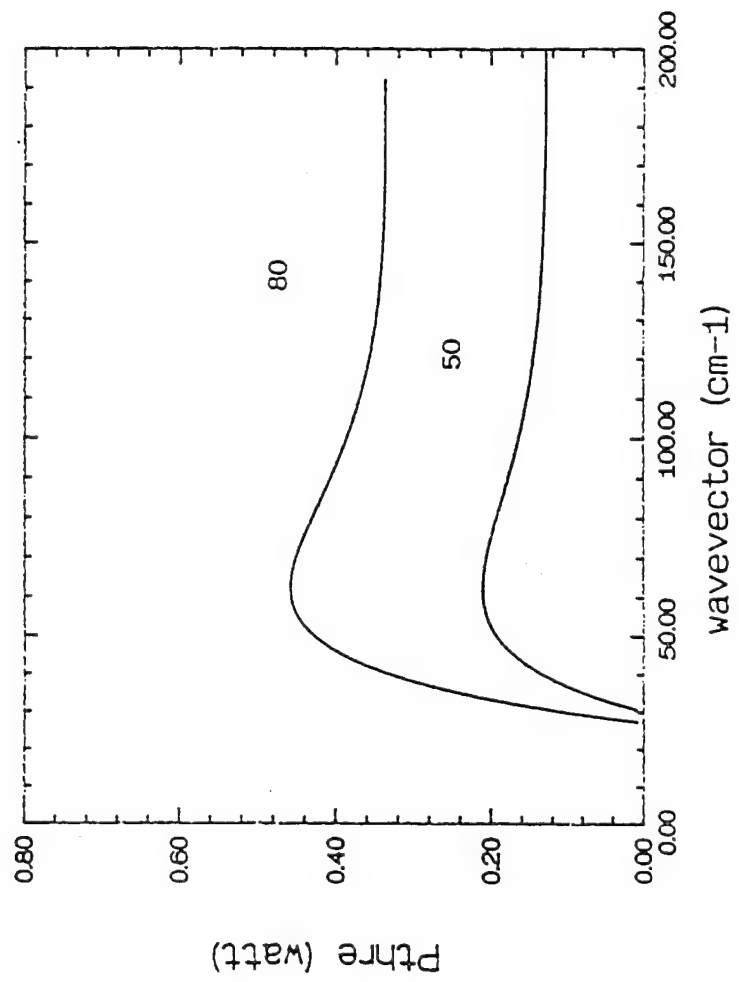




1 and 2 gnd's
 $h = 2.54 \mu\text{m}$
 $\omega = \infty, 1 \text{ mm}$
 $H_0 = 3240 \text{ De}$



BVW's



THRESHOLD POWERS AND ELECTRICAL COUPLING

- THE MICROSTRIP TRANSDUCERS USED TO EXCITE THE MSW DELAY LINE ARE

- 1) BIDIRECTIONAL
- 2) COUPLED TO MSW UP TO A MAXIMUM ALLOWED EFFICIENCY.

- ENERGY IS LOST IN THE COUPLING, THUS ENHANCING THE INPUT POWER NECESSARY TO HAVE AT LEAST THE FIRST THRESHOLD VALUE IN THE FILM.

- FROM THE ELECTRICAL QUANTITIES INVOLVED IN THE ELECTRICAL MATCHING, A COUPLING COEFFICIENT CAN BE DERIVED WHICH MUST BE ACCOUNTED IF THE REAL THRESHOLD FOR THE DEVICE HAS TO BE ACCOUNTED.

- AS AN ORDER OF MAGNITUDE, A DELAY LINE LOSSING -10 dB MUST BE EXCITED BY A PULSE TEN TIMES HIGHER WITH RESPECT TO THE THRESHOLD POWER NECESSARY TO CREATE THE FIRST SOLITON.

CONCLUSIONS

- THE BASIC CONDITIONS FOR DISPERSION AND NONLINEARITY TO EXCITE MAGNETOSTATIC VOLUME WAVE SOLITONS IN DELAY LINE CONFIGURATIONS HAVE BEEN DISCUSSED. PARTICULAR CARE HAS BEEN DEDICATED TO THE GROUND PLANES CONTRIBUTION.
- THE MODULATION IN FREQUENCY INDUCED BY THE SOLITONS CREATION HAS BEEN EVALUATED.
- THE THRESHOLD POWERS FOR BOTH, FORWARD AND BACKWARD WAVES HAVE BEEN DERIVED.
- THE THRESHOLD DEPENDS ON THE GEOMETRY AND ON THE ABSOLUTE FREQUENCY.
- BVW'S BEHAVIOUR IS NOT CHANGED BY THE PRESENCE OF A SECOND GROUND PLANE.

MAGNETIC SUPERLATTICES

D Mills

University of California

MAGNETIC SUPERLATTICES :

GROWN FROM ULTRATHIN (FEW ATOMIC LAYER)
FILMS ;

EXAMPLES OF SYSTEMS FABRICATED TO DATE :

(a) FERROMAGNET + NONMAGNETIC PARTNER :

Ni Mo , Co Ru , Gd Y , Fe Ag ,
Fe Pd , . . .

(b) TWO MAGNETICALLY ORDERED MATERIALS :

Fe Cr , Fe Gd , Gd Dy , . . .

(c) ANTIFERROMAGNETIC INSULATORS :

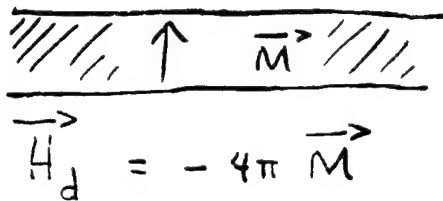
FeF_2 / CoF_2 ; NiO / CoO

BULK Fe

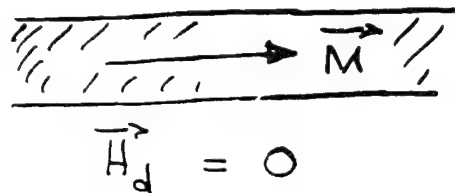
- ① $T_c = 1043 \text{ K}$
- ② $4\pi M_s = 21.5 \text{ kG} \cong 2.5 \text{ K}$
- ③ $H_A \sim 100 \text{ gauss} \cong 0.01 \text{ K}$

THIN FILMS (MANY LAYERS)

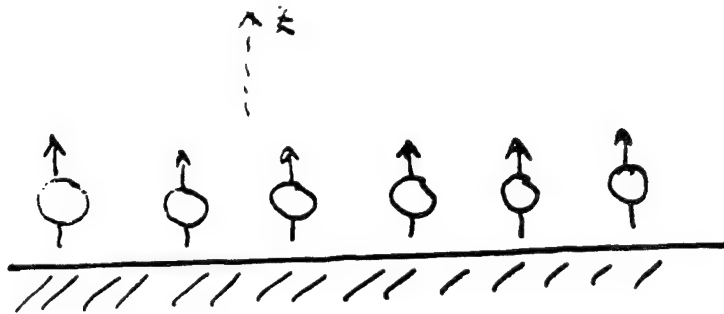
(a)



(b)



ULTRATHIN FILMS :



$$H_A = -K \sum_l S_l^2(l)$$

($H_s = 2KS = \text{EFFECTIVE FIELD}$)

(a) $2K > 4\pi M_s$: AXIS \perp TO SURFACE IS AN EASY AXIS.

(b) $2K < 4\pi M_s$ (POSSIBLY $K < 0$) :

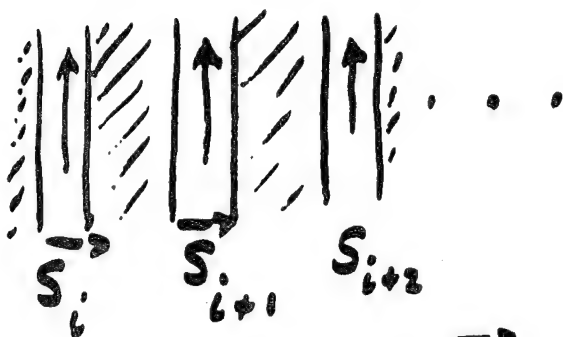
ONE HAS AN EASY PLANE MAGNET.

* ANISOTROPY VERY MUCH STRONGER THAN BULK *

(TWO ORDERS OF MAGNITUDE, ROUGHLY)

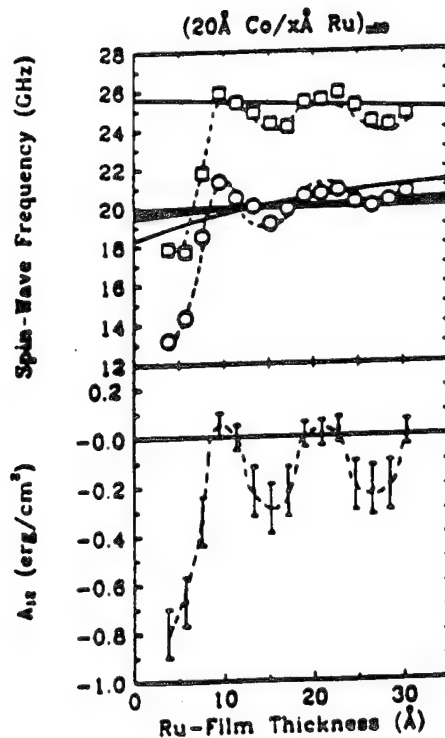
MAGNETIC MULTILAYERS:

SIMPLEST CASE: FERROMAGNETS WITH
NON FERROMAGNETIC SPACERS -



$$H_{eff} = -J \sum_i \vec{S}_i \cdot \vec{S}_{i+1}$$

(a) $J > 0$: ... $\uparrow \uparrow \uparrow \uparrow$... (b) $J < 0$ $\uparrow \downarrow \uparrow \downarrow$...
(ARTIFICIAL ANTIFERROMAG.)

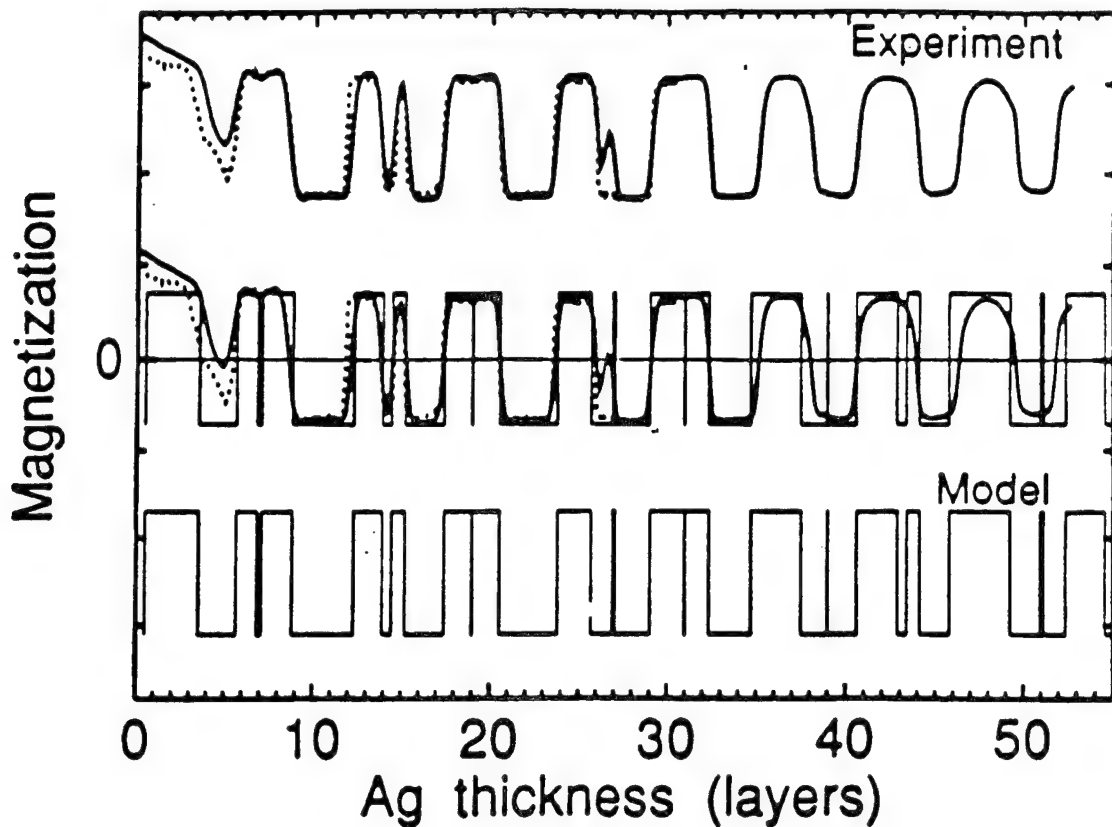


$10^{-16} \text{ ERG/CM}^2$
 $\approx 1^\circ \text{ KELVIN.}$

FROM: J. FASSBENDER, F. NORTEMANN, R. STAMPS,
R. CAMLEY, B. HILLERBRANDS, G. GÜNTHERODT,
& S.P.S. PARKIN (Phys. Rev. B 46, 5810 (1992))

INTERFILM EXCHANGE & STATIC SPIN STRUCTURES

Fe / Ag / Fe TAILAYER.



J. UNGURIS, R. J. CELOTTA

& D. T. PIERCE (TO BE PUBLISHED)


THEORY (THIRD LINE) :

* RKKY COUPLING THROUGH CONDUCTION
ELECTRONS OF THE Ag.

P. BRUNO & C. CHAPPERT *PHYS. REV. LETTERS*
67, 1602 (1991)

ANTI FERROMAGNETS IN AN EXTERNAL (5)

MAGNETIC FIELD :



$$H = +|J| \vec{S}_1 \cdot \vec{S}_2 - H(S_1^2 + S_2^2)$$

$$E(\theta) = |J| S^2 \cos(2\theta) - 2H \cos \theta$$

$$\frac{\partial E}{\partial \theta} = 0 \Rightarrow \cos \theta = \frac{H}{|J|S}$$

GIANT MAGNETORESISTANCE

M.N. BARICH ET AL., Phys. Rev. Letts 61, 2472 (1988)

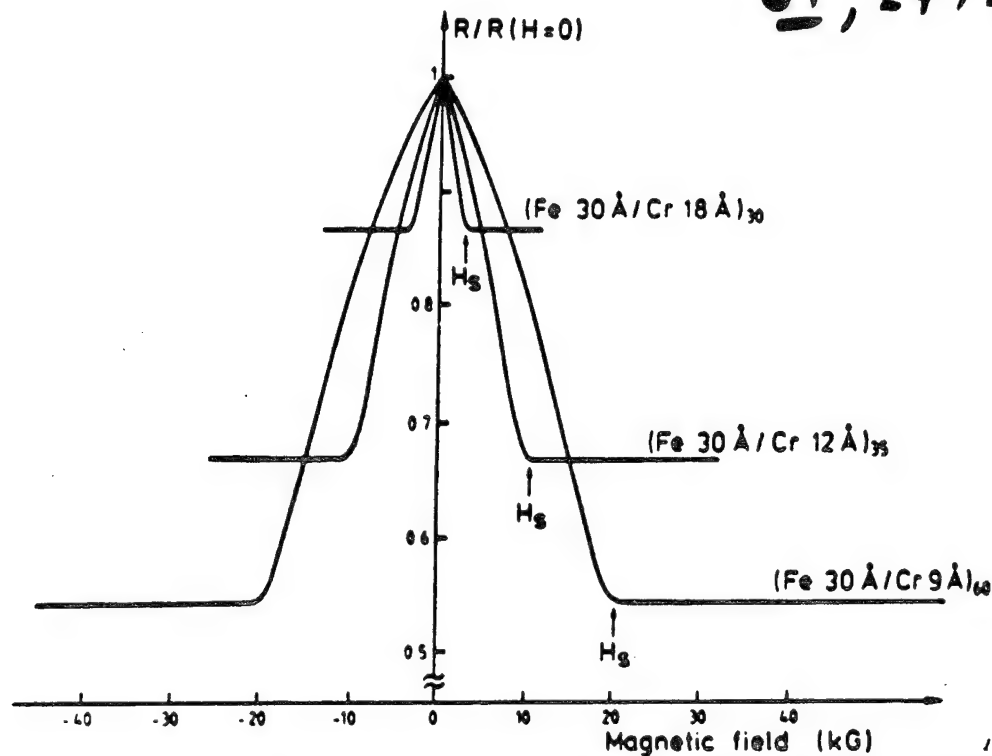


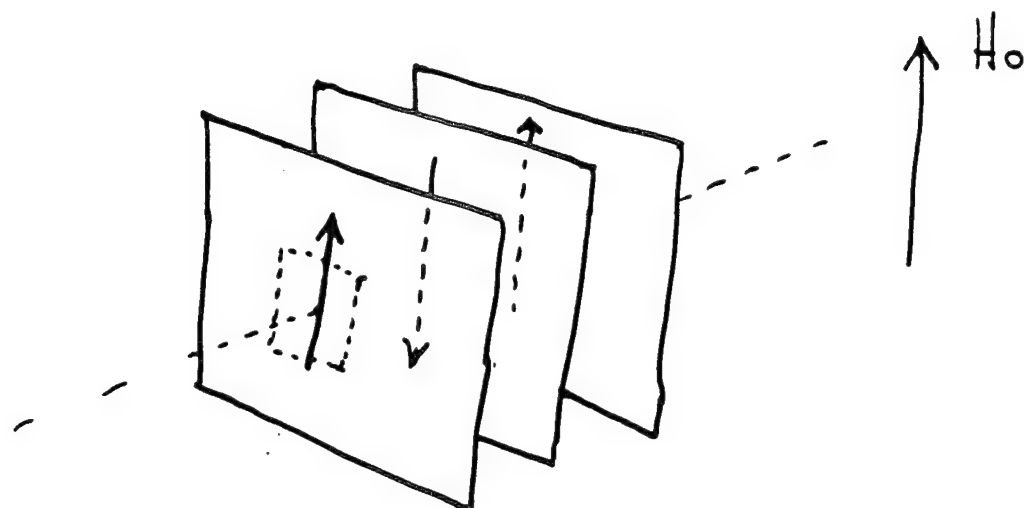
FIG. 3. Magnetoresistances of three Fe/Cr superlattices at 4.2 K. The current and the applied field are along the same [110] axis in the plane of the layers.

THEORY: R.E. CAMLEY & J. BARNAS, PRL 63, 664. (1989)

B.L. JOHNSON & R.E. CAMLEY, Phys. Rev. B44 9007/1001.

Fe/Cr (211) SUPERLATTICES :

(ERIC E. FULLERTON ET AL., ARGONNE LAB.)



* GROWN ON $MgO(110)$ -

\Rightarrow TWO FOLD IN PLANE ANISOTROPY

* OSCILLATORY IN PLANE COUPLING -

* Fe MAGNETIZATION LIES IN PLANE -

APPLY AN EXTERNAL FIELD

PARALLEL TO EASY AXIS :

SYSTEM RESPONDS LIKE MnF_2 .

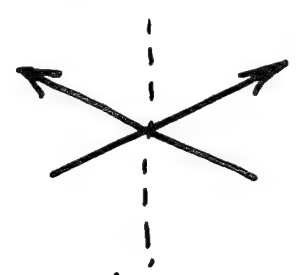
MAGNETIC PHASE DIAGRAM :

Low FIELD STATE :



$$0 < H_0 < (2H_E H_A)^{\frac{1}{2}}$$

SPIN FLOP STATE :

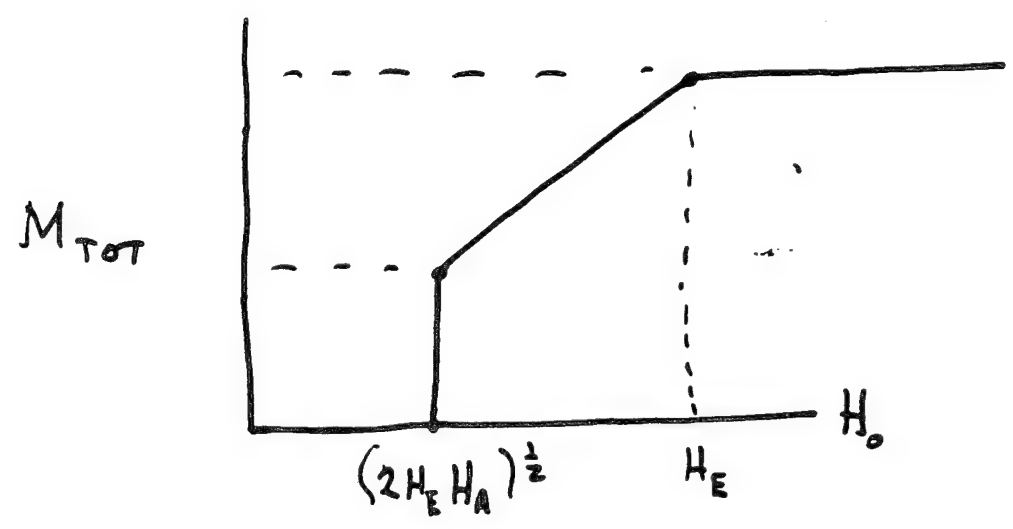


$$(2H_E H_A)^{\frac{1}{2}} < H_0 < H_E$$

High FIELDS :



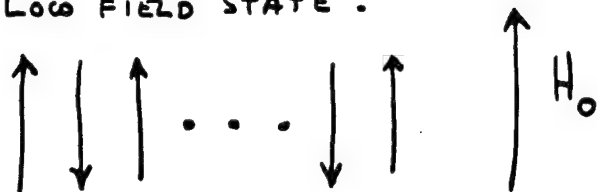
$$H_E < H_0 < \infty$$



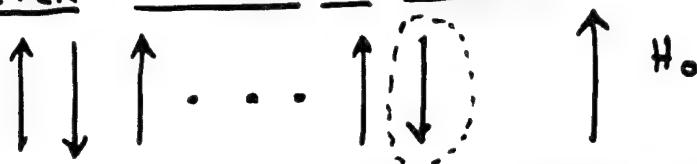
THE FINITE SUPERLATTICE :

(a) Odd NUMBER OF LAYERS :

LOW FIELD STATE :



(b) EVEN NUMBER OF LAYERS :



SURFACE LAYER GOES
UNSTABLE BELOW BULK SPIN

FLOP FIELD (D.L. MILLS, P.R.L. 20, 18(1968))

PREDICTIONS :

(a) ONE HAS A SURFACE SPIN FLOP TRANSITION :

$$\frac{H_{SF}}{H_{BF}} = \frac{1}{\sqrt{2}} \quad (H_A \ll H_E).$$

(b) THERE IS A 'SOFT SURFACE SPIN WAVE' WITH
FREQUENCY THAT VANISHES JUST ABOVE H_{SF}

(W. SASLOW & D. L. MILLS, PHYS. REV. 171, 488(1968))

UNSUCCESSFUL SEARCH FOR SURFACE MODES:

W.E. TENNAUT, R.B. BAILEY & P.L. RICHARDS,

INT'L CONF. ON MAG. & MAG. MATERIALS, SAN FRANCISCO, 1974

(c) SURFACE SPIN FLOP STATE EVOLVES CONTINUOUSLY
INTO BULK SPIN FLOP STATE (NO DETAILED
CALCULATIONS)

F. KEPPER & H. CHOW, PHYS. REV. LETT. 31, 1061(1973)

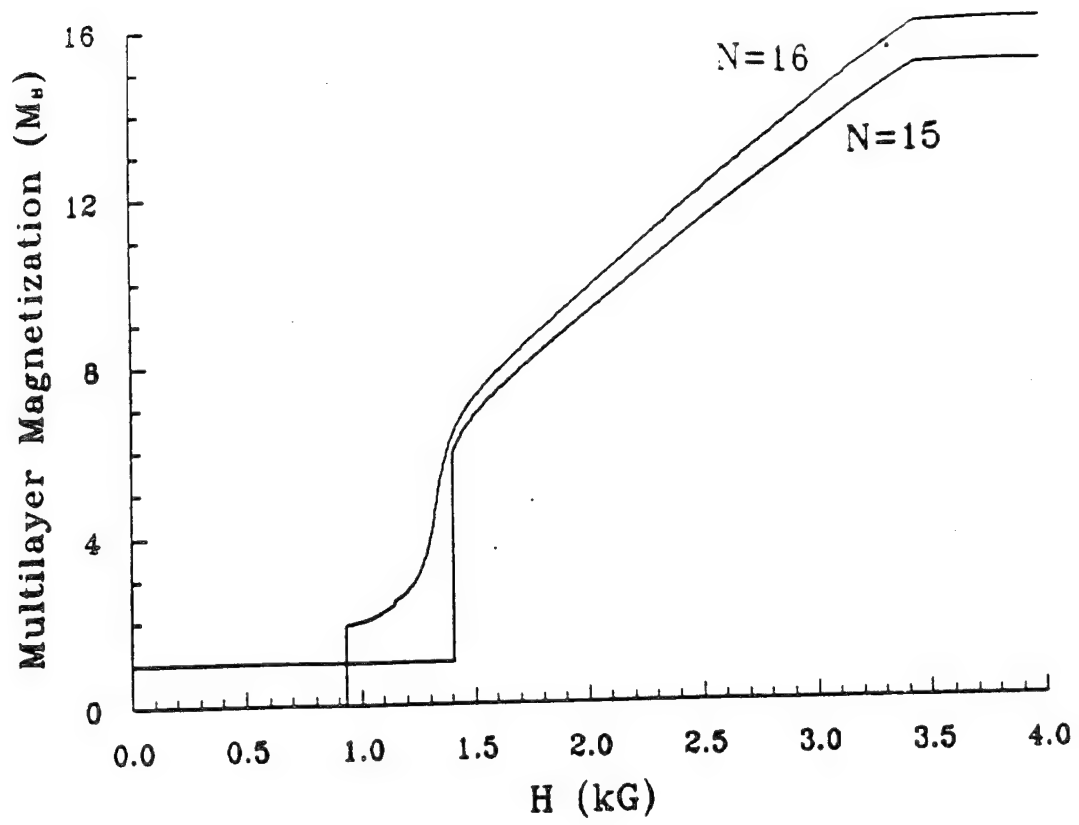


Fig.1(a)

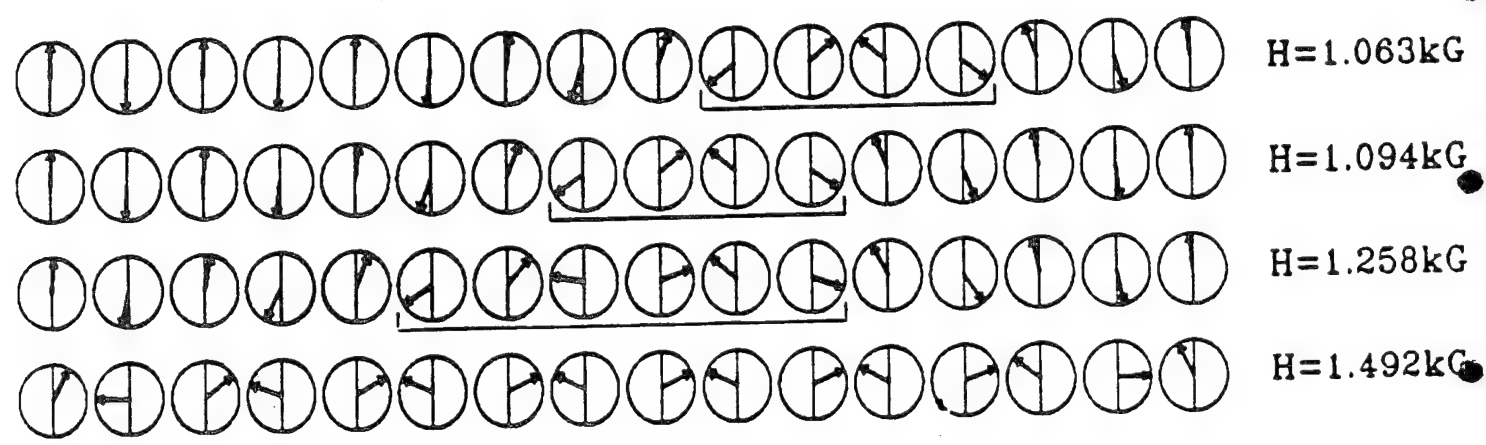


Fig.1(b)

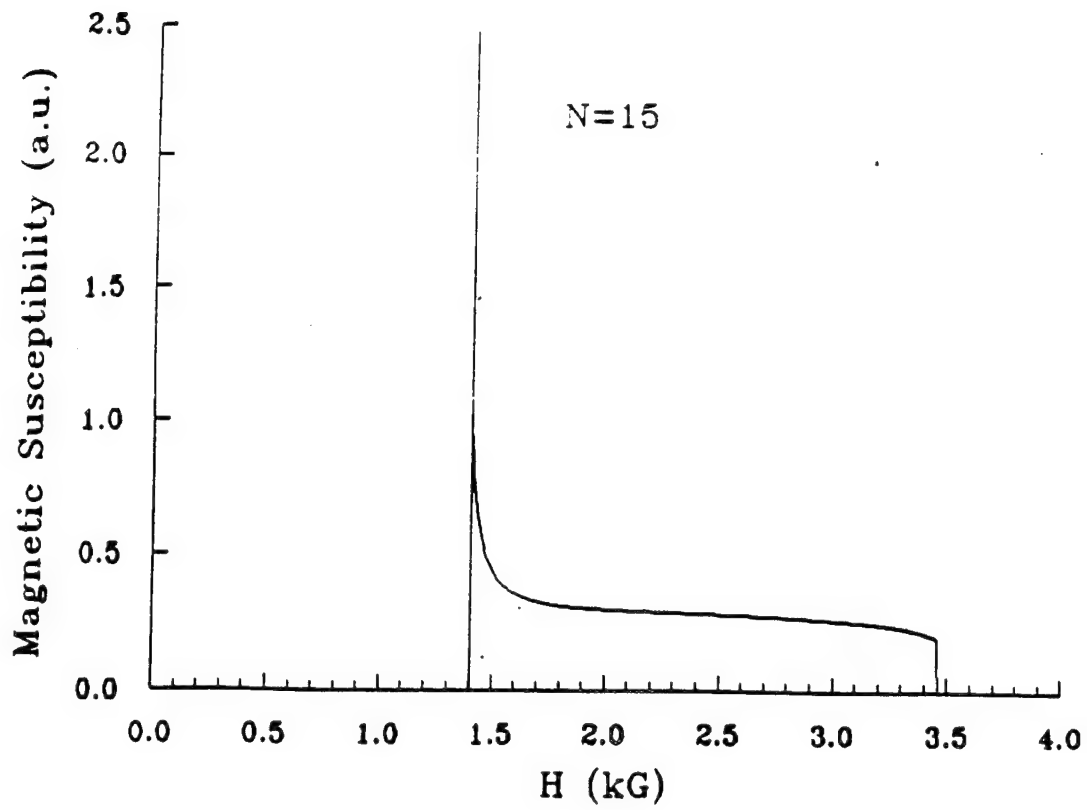


Fig.2(a)

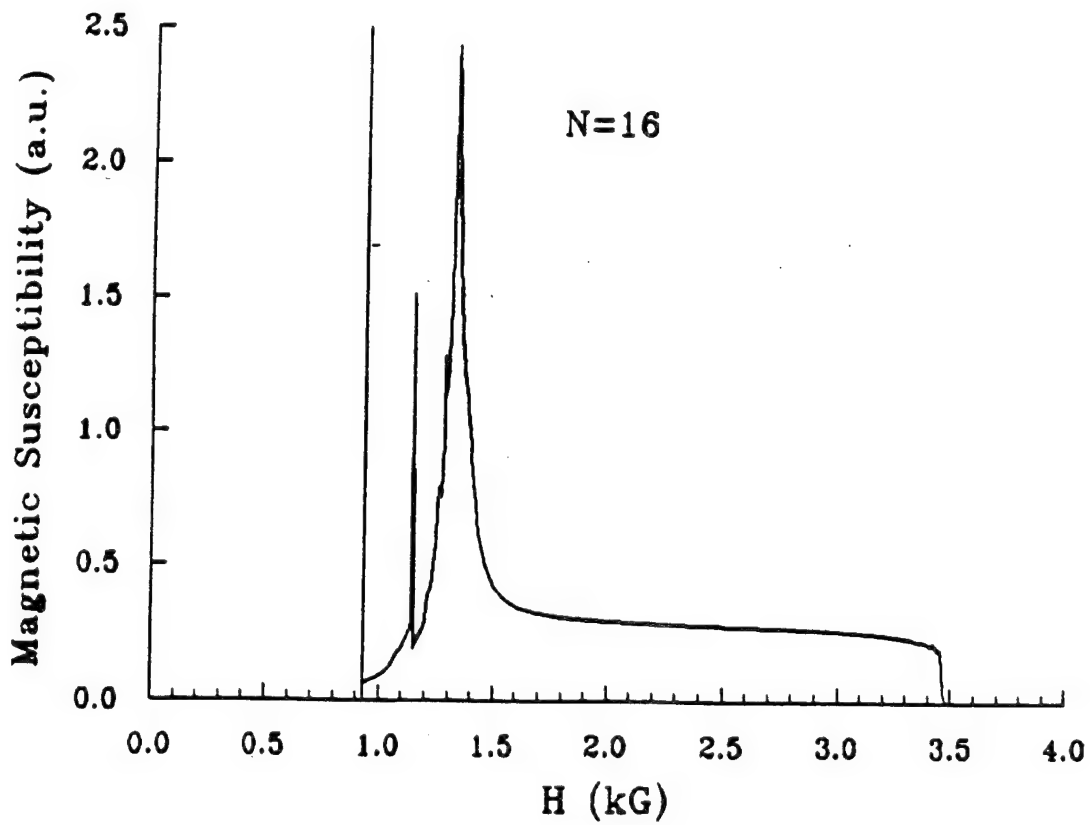
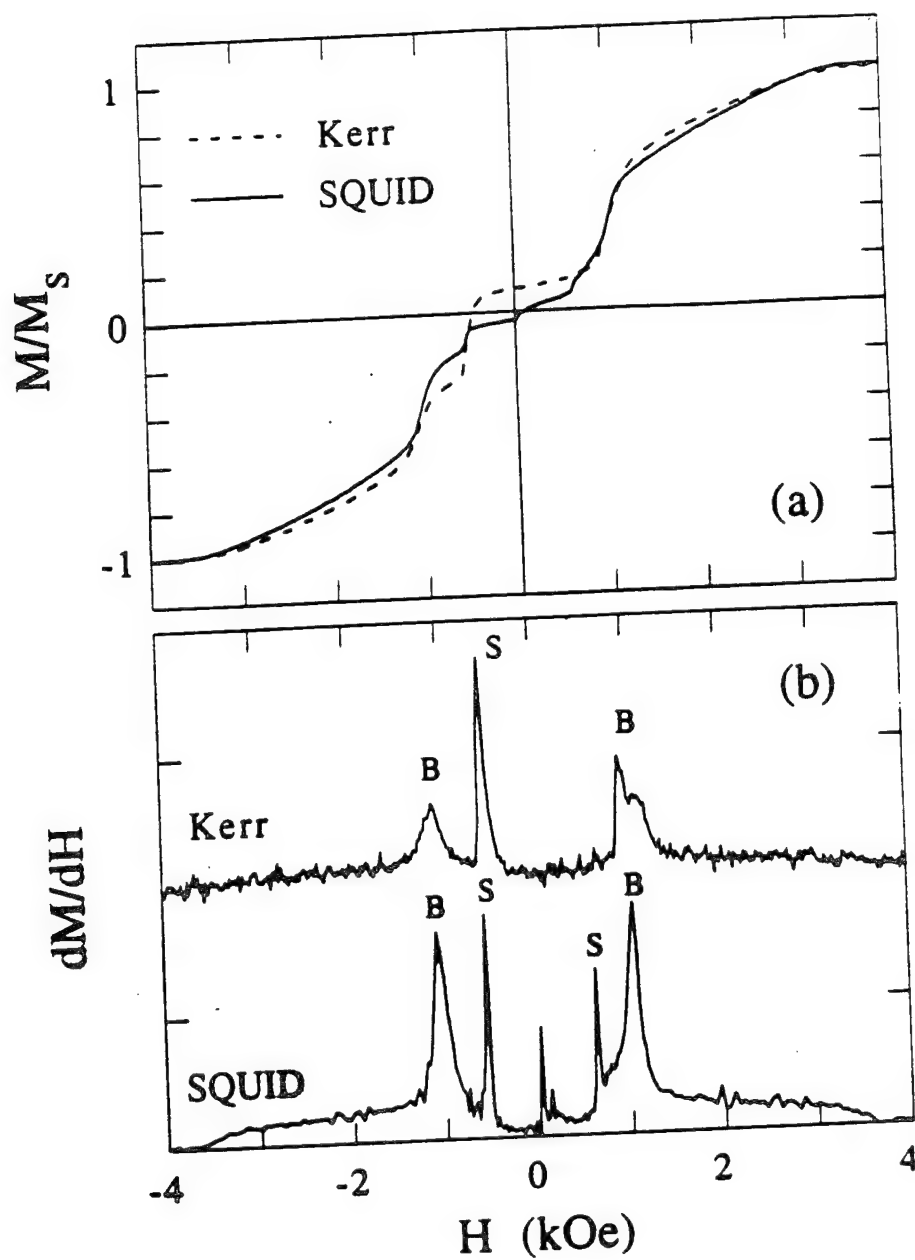
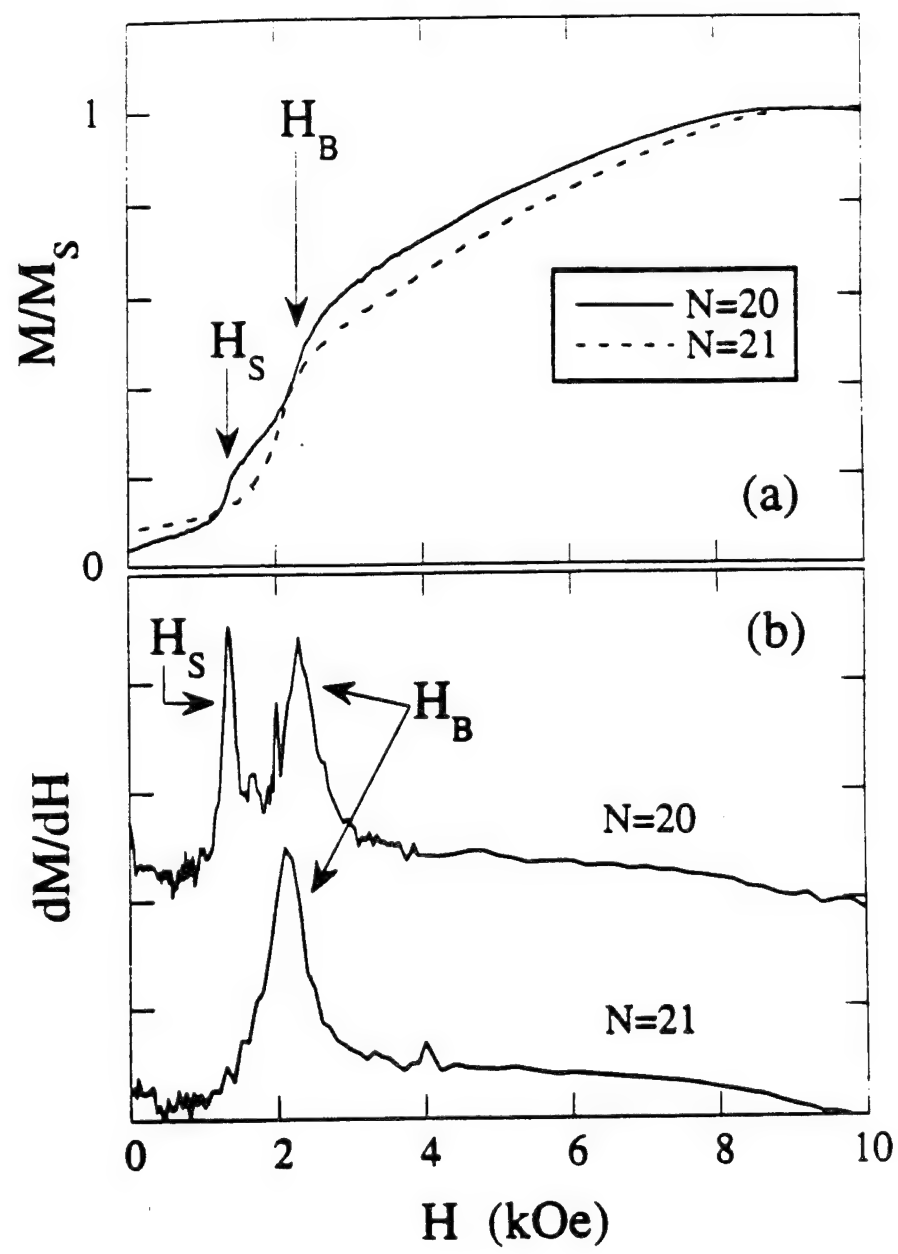
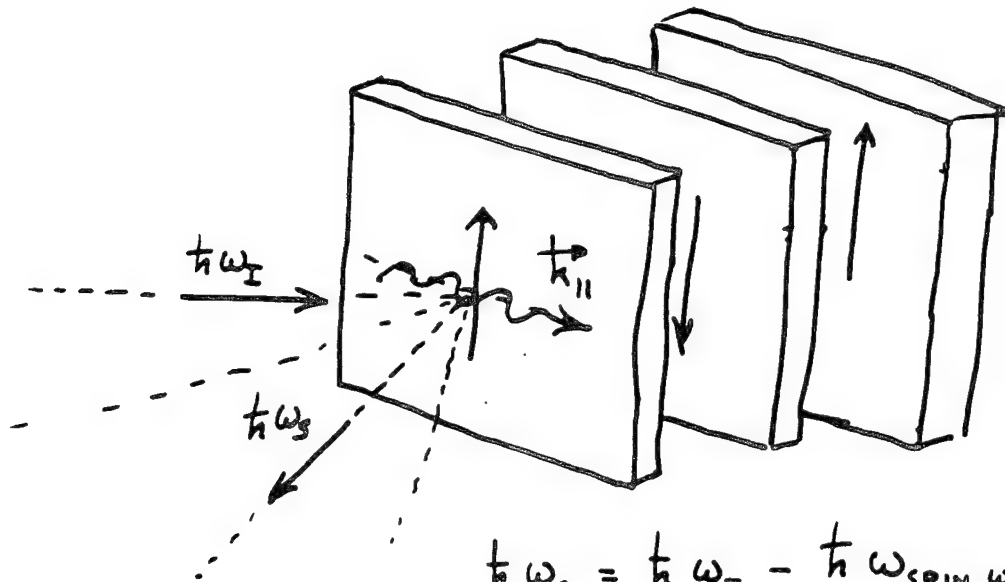


Fig.2(b)





DYNAMIC RESPONSE OF SUPERLATTICES ; THE SPIN WAVE REGIME



$$\hbar \omega_S = \hbar \omega_I - \hbar \omega_{\text{SPIN WAVE}}$$

$$k_{||}^{(S)} = k_{||}^{(I)} - k_{||}$$

VALUES OF $k_{||}^{(S)}$: $k_{||}^{(S)} \approx 10^5 \text{ cm}^{-1}$

* SPIN WAVES ARE COLLECTIVE EXCITATIONS OF ENTIRE STRUCTURE —

SOURCES OF INTERFILM COUPLING :

- ① INTERFILM EXCHANGE
- ② DIPOLAR FIELDS GENERATED BY FILM MOTION.

COMMENTS ON DIPOLAR COUPLING :

CONSIDER A SINGLE FILM :

(a) $k_{||} \equiv 0$: (MAGNETIC RESONANCE)

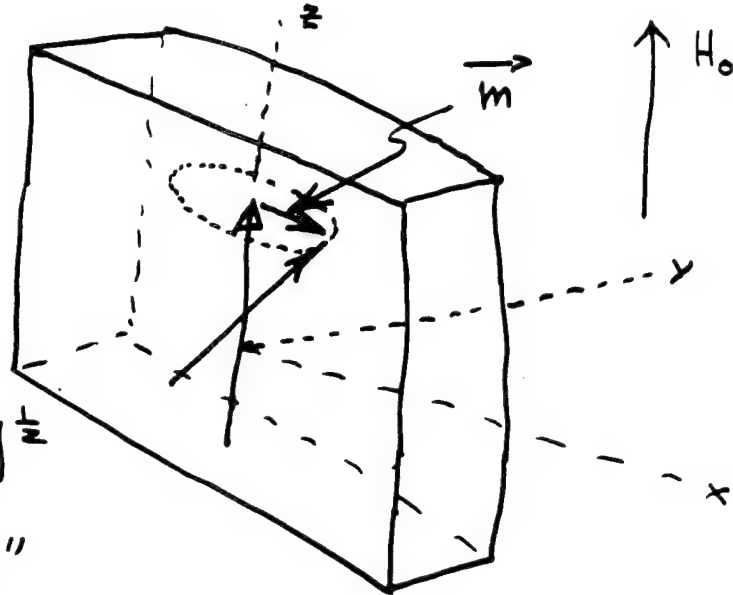
ONE HAS AN
INTERNAL DIPOLE
FIELD

$$\vec{h}_d = -4\pi m_s \hat{y}$$

THE RESONANCE
FREQUENCY IS

$$\omega = \gamma [H_0 (H_0 + 4\pi M_s)]^{\frac{1}{2}}$$

"DIPOLAR
STIFFENING"

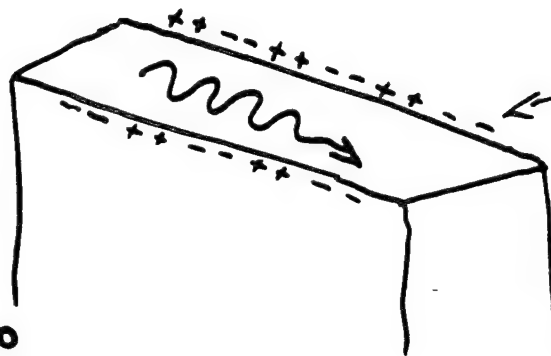


(b) $k_{||} \neq 0$:

OUTSIDE THE FILM,

$$\vec{h}_d \sim (k_{||} d) 4\pi M_s e^{-k_{||}(y-d)}$$

LONG RANGED
FIELD GIVES
RISE TO LONG
RANGED INTERFILM
COUPLINGS.

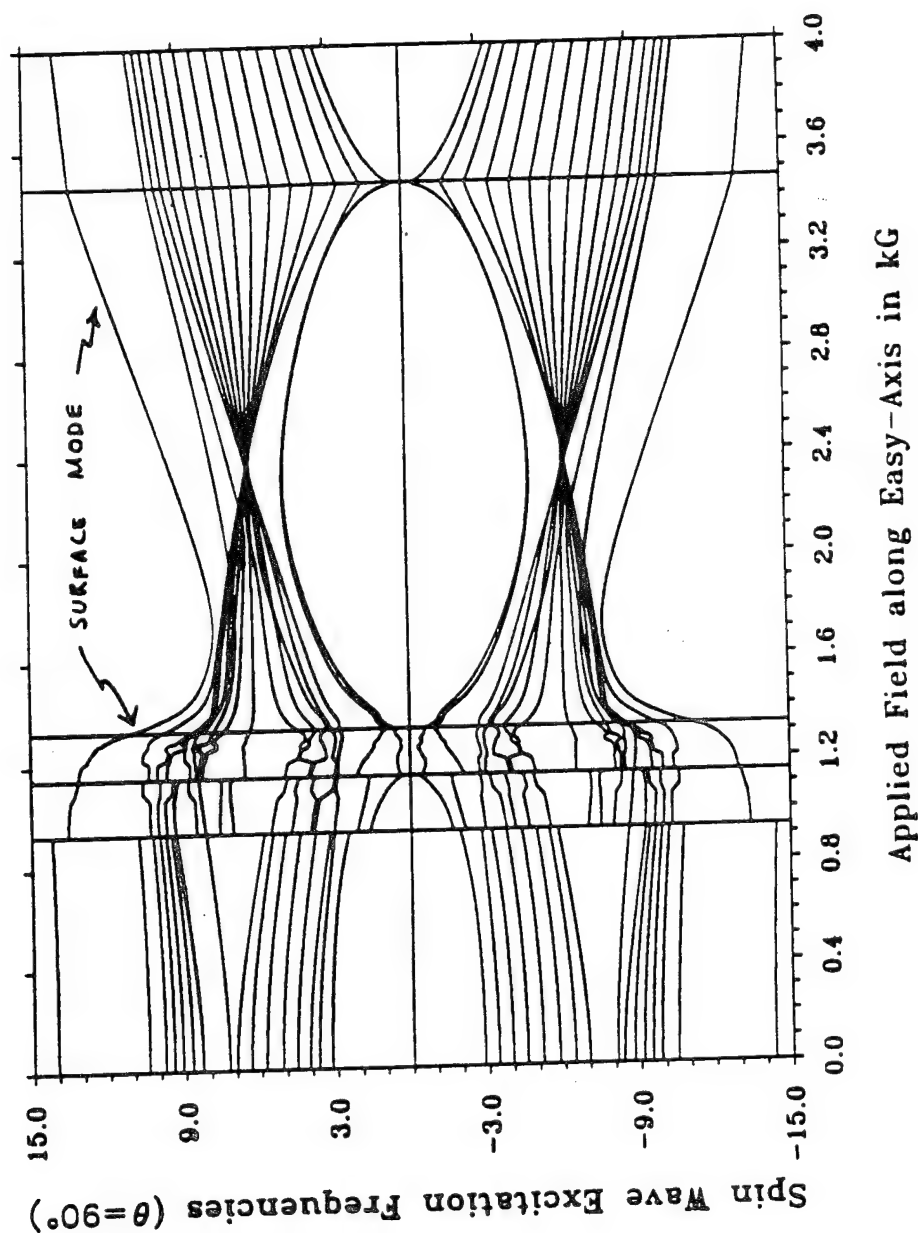


SURFACE
CHARGES
GIVE DIPOLAR
FIELDS OUTSIDE
FILM.

16 LAYERS Fe/Cr(211) :

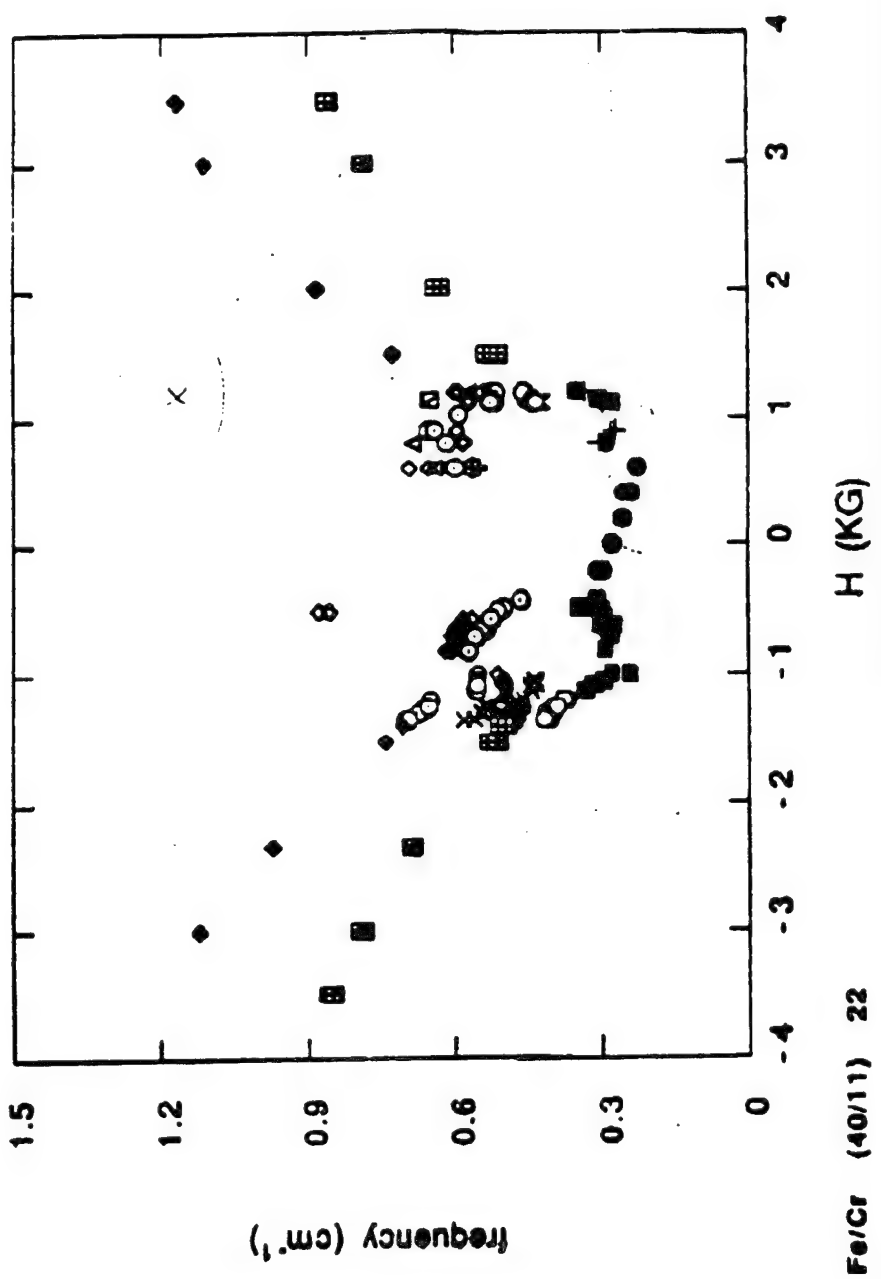
$$k_{||} \cong 10^5 \text{ cm}^{-1}$$

$k_{||} D \sim 1$ $D = \text{sample thickness}$

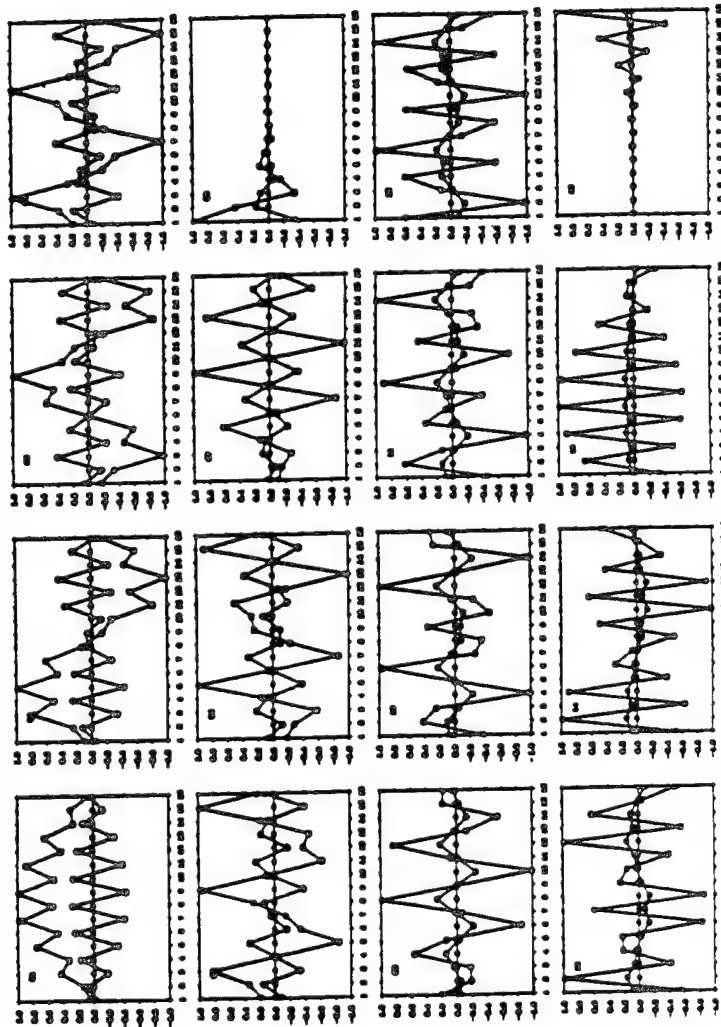


$N=16$
 $4\pi M_s=21 \text{ kG}$
 $J_A \times M_s=1.0 \text{ kG}$
 $K \times M_s=0.25 \text{ kG}$
 $d_1=25 \text{ \AA}$
 $d_2=8 \text{ \AA}$
 $k_{||} d=0.05$
 $H_{\text{min}}=0.0 \text{ kG}$
 $H_{\text{max}}=4.0 \text{ kG}$

- fr0 △ fr4 + fr8 ○ fr3'
- fr1 ▢ fr5 ● fr0' + fr8'
- x fr2 ○ fr6 ▢ fr1' ▢ l.mode
- fr3 ○ fr7 x fr2' ◆ h.mode



EIGENVECTORS JUST BELOW
SURFACE SPIN FLOP FIELD
 $\lambda_0 = 0.8 \text{ kg } 0-00'$

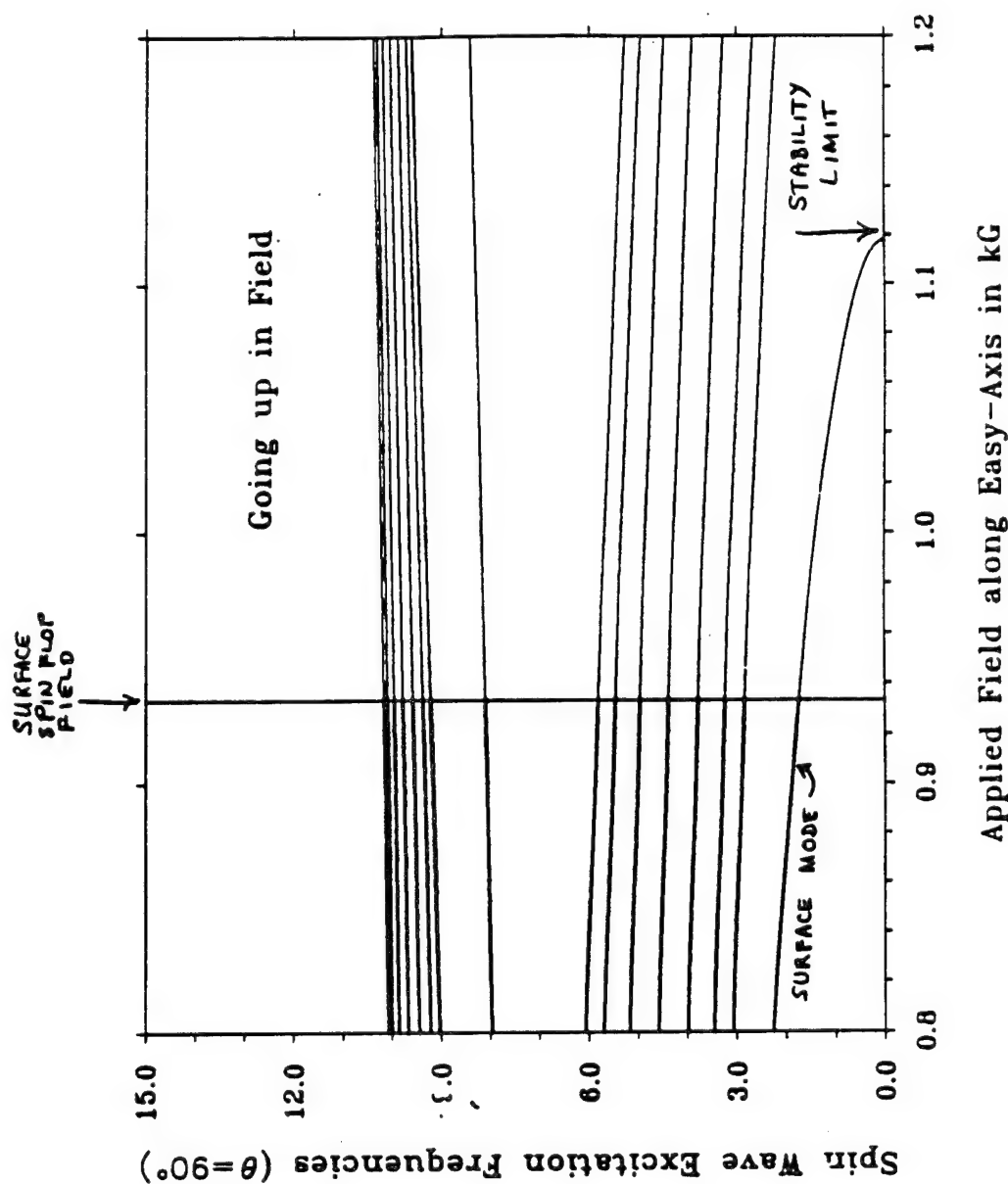


Spln Wave Amplitudes versus Film Indices

4 4 4
 . . .
 . . .

16 LAYERS Fe/Cr(211)

$k_{||} D \ll 1$

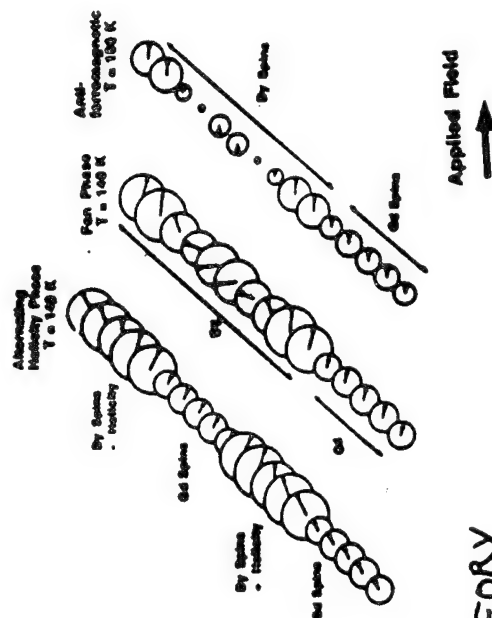
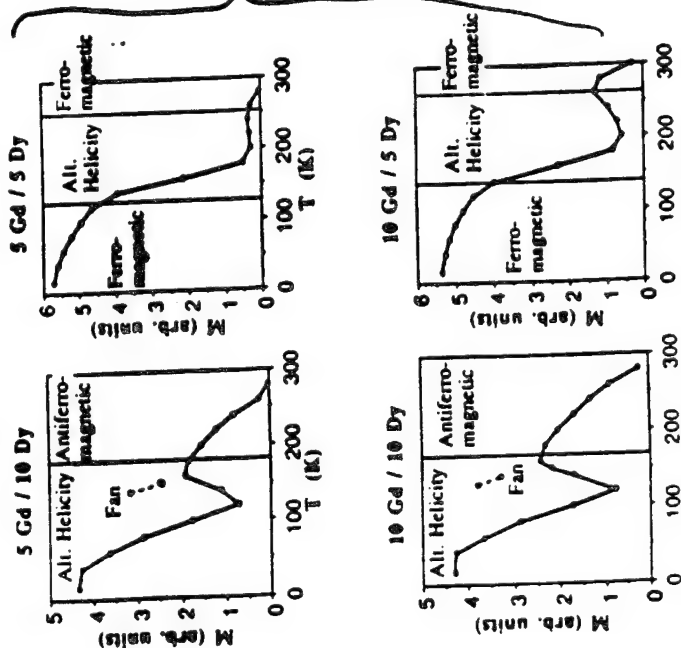
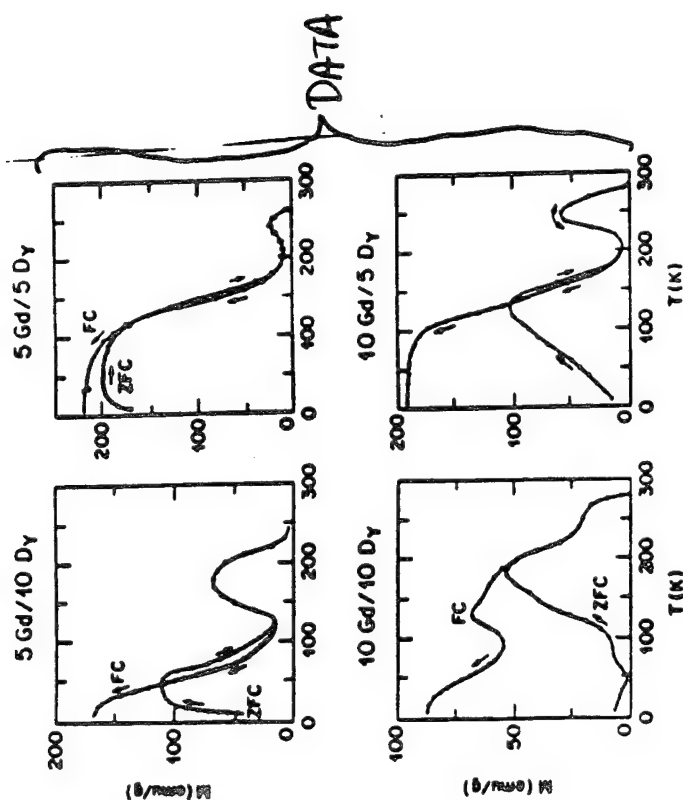


$N=16$
 $4\pi M_s=21\text{kG}$
 $J_A \times M_s=1.0\text{kG}$
 $K \times M_s=0.25\text{kG}$
 $d_1=40\text{\AA}$
 $d_2=11\text{\AA}$
 $k_{||}d=1d-8$
 $H_{min}=0.8\text{kG}$
 $H_{max}=1.2\text{kG}$

EXOTIC SPIN STRUCTURES

Gd/Dy

R.E. CAMLEY, J. KWO, M. HONG
& C.L. CHEN, PHYS. REV. LETTERS
64, 2630 (1990)



SPIN-WAVE CHAOTIC TRANSIENTS

F. M. de Aguiar, S. M. Rezende and F. C. S. da Silva

Departamento de Física, Universidade Federal de Pernambuco,

50732-970 Recife, Brazil

ABSTRACT

We report the observation of transient chaotic spin-wave auto-oscillations in X-band pulsed subsidiary-resonance experiments in a YIG sphere. Chaotic transients to a periodic attractor have been observed near a critical microwave power $p_c \sim 10$ dB relative to the Suhl instability threshold. By an averaging of 100 randomly chosen initial conditions at each power, we estimate a critical exponent $\gamma \sim 0.57$. In addition, we demonstrate that the results can be qualitatively understood within the framework of the standard two-mode model. Numerical simulations yield, for a particular set of parameters, chaotic transients obeying the predicted scaling law with a critical exponent $\gamma \sim 0.54$.

1. INTRODUCTION

The transition to sustained chaotic behavior via chaotic transients was discovered by Yorke and Yorke in the Lorenz model in the late 70s.¹ Several years later, Oseleci, Ott and Yorke² identified transient chaos as a particular manifestation of a rather general phenomenon that occurs in dissipative dynamical systems, the so called *crisis*. Three types of crisis have been characterized², namely, attractor *destruction*, attractor *mergin* and attractor *widening*. A chaotic attractor is destroyed when, as a system parameter p reaches a critical value p_c , it collides with the stable manifold of an unstable periodic orbit. The characteristic behavior in this case is the existence of chaotic transients suddenly followed by periodic orbits. The duration of a chaotic transient depends sensitively on the initial conditions and can be remarkably long. The average lifetime depends upon the system control parameter as $\langle T \rangle \sim |p - p_c|^{-\gamma}$, where γ is the critical exponent of the chaotic transient.

Finite-time chaotic behavior has been observed in a number of physical systems.³ However, only a few experiments have been analysed in detail. As far as spin waves are concerned, the only results available on such transients were obtained by Carroll, Pecora and Rachford⁴ a few years ago, in subsidiary-resonance experiments in a YIG sphere. At driving frequencies between 2.0 and 3.4 GHz, their experimental findings suggested the existence of "multiple attractors", while numerical simulations suggested the need of more than three interacting spin-wave modes to explain the long-lived transients they had observed in the experiments.

In this paper we report on transient chaos in YIG spheres at higher driving frequencies (8.0 - 10.0 GHz) at room temperature. Pulsed experiments have revealed the existence of long-lived chaotic transients involving "single attractors" in the spin-wave auto-oscillations (~ 1 MHz), 9 to 10 dB beyond the Suhl instability threshold. In addition, we present numerical results of a two-spin-wave-mode calculation in good

qualitative agreement with the experiments. By an averaging of N randomly chosen initial conditions at each power, we estimate a critical exponent in the range $0.5 < \gamma < 0.6$ both in the experiments ($N = 100$) and in the numerical simulations ($N = 400$).

2. EXPERIMENTAL RESULTS

Our experiments were carried out with single-crystal samples of yttrium iron garnet (YIG) at room temperature. Here we present results in a 1-mm YIG sphere, which is placed at the center of a critically coupled rectangular TE_{102} microwave cavity ($Q \sim 2000$). An electromagnet provides the static magnetic field H_0 perpendicular to the microwave magnetic field h , in the subsidiary resonance region. The power is provided by a 10-W traveling-wave-tube (TWT) amplifier fed by a solid-state tunable YIG oscillator. The frequency ($f_p = 8.9$ GHz) is stabilized by an external crystal oscillator and manually adjusted to the center of the cavity resonance. The radiation power is controlled with a variable precision attenuator and directed by a circulator to the cavity, where it drives spin waves in the sample. The reflected microwave signal is then detected with a sensitive Schottky-barrier diode at the output port of the circulator and recorded at intervals of $0.1 \mu s$ using a commercial digitizer. In order to study the transient response, the microwave is pulsed by a p-i-n modulator placed before the TWT amplifier. Pulses up to $800 \mu s$ long were comfortably used with no detectable heating effects. The results presented here were observed at a fixed magnetic field $H_0 = 1830$ Oe, parallel to the $[100]$ crystal axis. At low-power levels the pulse reflected from the cavity has essentially the same shape as the incoming microwave pulse. As the power is increased, abrupt changes in the pulse shape occur due to spin-wave instabilities at subsequent thresholds, namely, the Suhl instability threshold (SIT), h_c , the spin-wave auto-oscillation threshold, h_c' , and a sequence of bifurcations that lead to spin-wave chaos.⁵ Henceforth we will consider $R \equiv h/h_c$ as our control parameter.

Well above the SIT ($R = 1$), we have observed the destruction of the strange attractor due to the collision between the chaotic attractor and a coexisting unstable periodic orbit. This collision occurs at the critical value $R_c = 2.88$. For $R > R_c$ we observe an intermittent signal with laminar (periodic) regions interrupted by chaotic bursts. For $2.82 < R < R_c$, the steady-state response is periodic after a chaotic transient whose duration swings intermittently, as we observe on the screen of an oscilloscope. Figure 1 shows a frozen digitized version of a chaotic transient with duration $T \sim 618 \mu\text{s}$, with $R = 2.84$. The measured average duration as a function of the control parameter is shown in the log-log plot of Figure 2 (solid circles). From a linear regression (solid line) we estimate a critical exponent $\gamma = 0.57$.

3. NUMERICAL SIMULATIONS AND DISCUSSION

The efforts in modelling the instabilities observed in high-power ferromagnetic resonance experiments are based on a theory introduced by Suhl⁶ in the mid 50s, and have been phrased in terms of the excitation and the nonlinear interaction of spin waves in the sample. The number and the nature of the excited modes are essentially the hitherto unsolved problems in this longstanding subject. We have recently provided experimental results that strongly support the two-mode model (TMM),⁵ at least for the interval $h_c < h < h_c'$. In this section we present numerical results with the TMM in good qualitative agreement with the transient experiments described above. The particular set of parameters are the same we have originally used to explain the unusual spectra observed in parallel-pumping experiments.⁷ In this case, the model gives higher values for the auto-oscillation frequency and threshold, but shares interesting qualitative features with the experiments. We refer to reference [5] for a detailed description on the microscopic approach with the TMM. Figure 3a shows a chaotic transient in the phase plane n_1 vs. n_2 , where n_1 and n_2 are the populations of the two excited spin-wave

modes, for $R = 8.10000506$. We have chosen an initial condition inside the strange attractor for which the solutions are attracted during a time interval $\gamma_1 T \sim 87.7$, where γ_1 is the phenomenological relaxation rate of mode 1. The steady-state solution is the period-3 attractor shown in Figure 3b for $90.0 < \gamma_1 t < 3000.0$. This scenario is quite similar to the experiments: By decreasing R , an intermittent (chaos \leftrightarrow period-3) solution is destroyed at the critical value $R_c = 8.100055\dots$ below which there is a sharp period-3 window. Within this window the chaotic bursts no longer exist and the steady-state solution is reached after a chaotic transient, whose duration is very sensitive to the initial conditions. By an averaging of 400 randomly chosen initial conditions within a small volume on the strange attractor at each value of the control parameter, we have obtained the result shown in Figure 4 (solid circles). The straight line is a fit from which we estimate a critical exponent $\gamma = 0.54$. One might guess at first that we are, in both experiment and simulation, close to a situation where the system could be described by a one-dimensional map with a quadratic extremum, since in this case γ has the universal value 0.5. However, we stress that preliminary studies with return maps do not point in this direction and further investigations are under way.

This work has been supported by the Brazilian agencies CNPq, FINEP, and FACEPE.

FIGURE CAPTIONS

FIG. 1: Detected microwave absorption vs. time in a YIG sphere at subsidiary resonance with $H_0 = 1830$ Oe, $R = 2.84$ and $f_p = 8.9$ GHz.

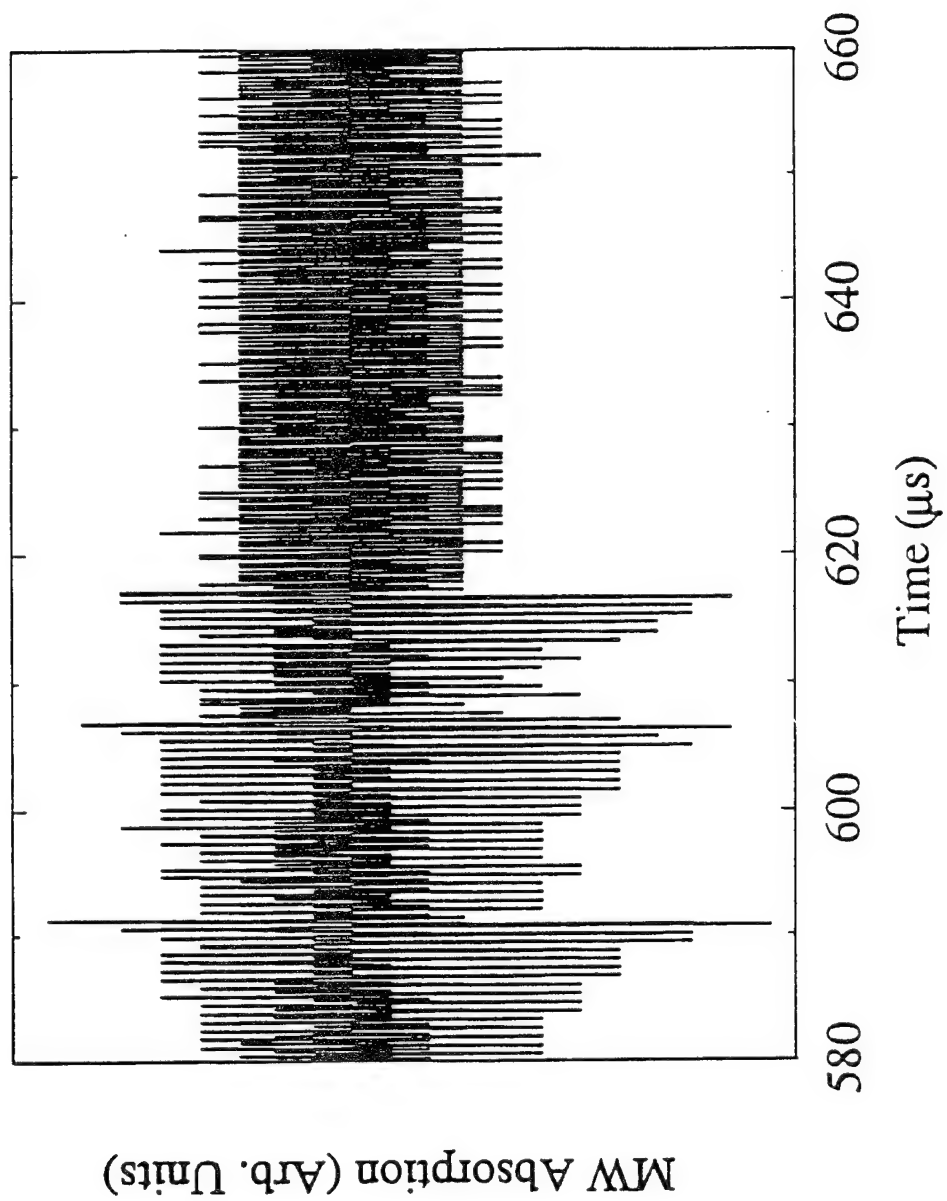
FIG. 2: Measured average duration of chaotic transients as a function of the control parameter. The straight line is a fit with a slope $-\gamma = -0.57$.

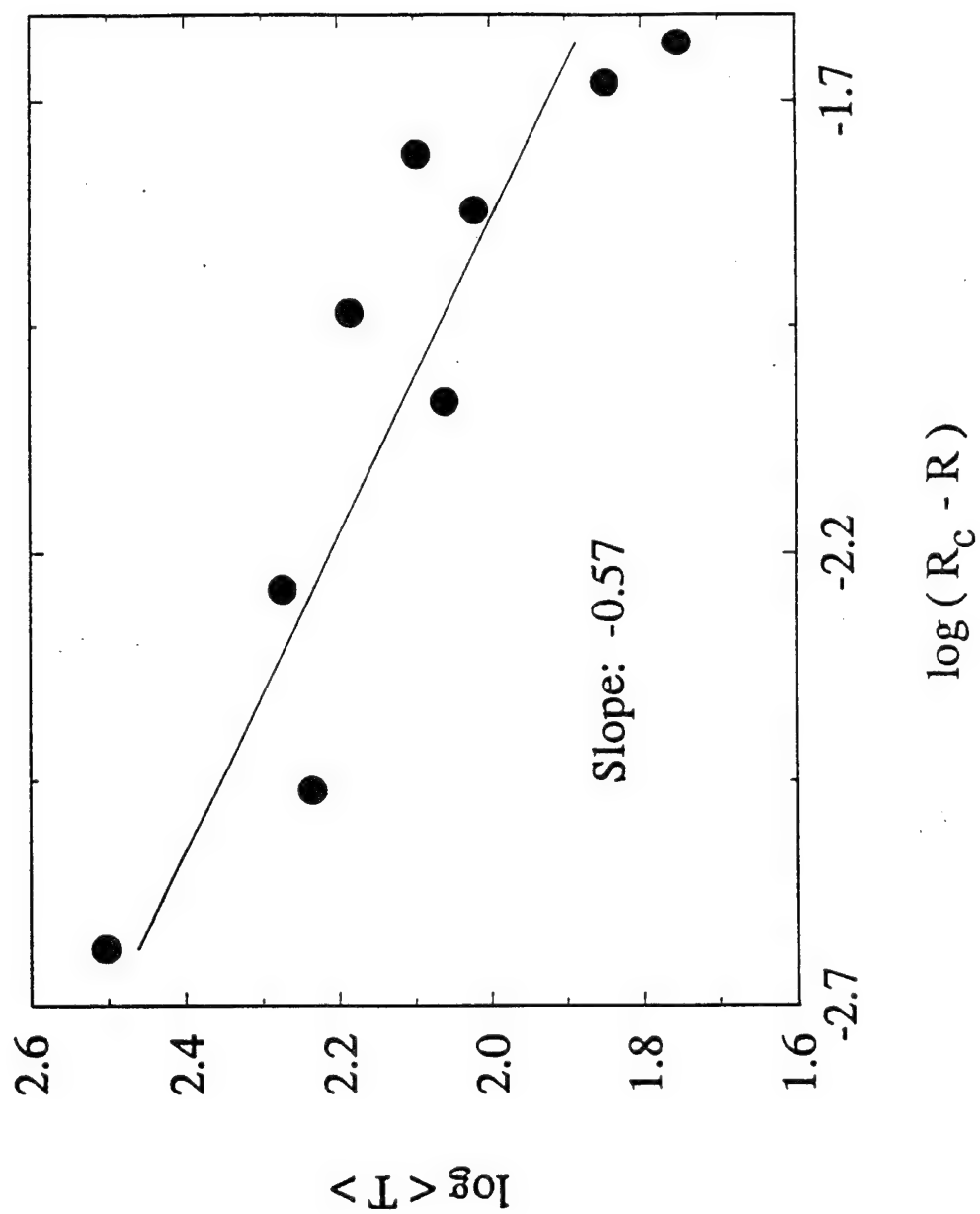
FIG. 3: Phase plane n_1 vs. n_2 showing numerical solutions of the two-mode model, as described in ref. [7], with $R = 8.10000506$: (a) transient strange attractor for $0 < \gamma_1 t < 88.0$ and (b) period-3 limit cycle for $90.0 < \gamma_1 t < 3000.0$.

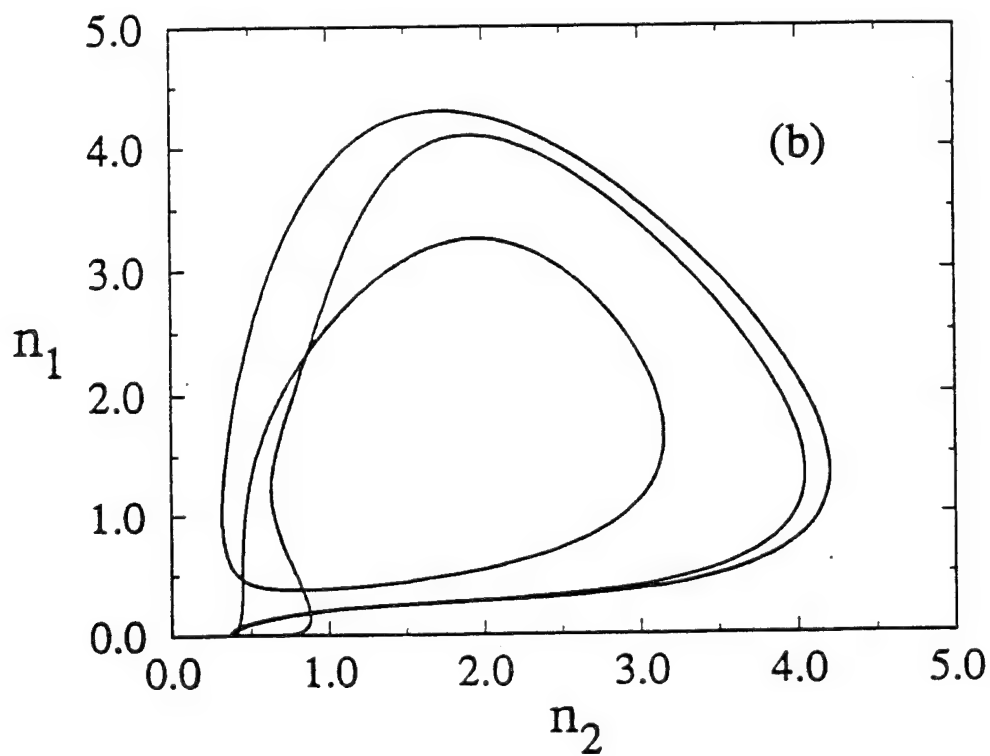
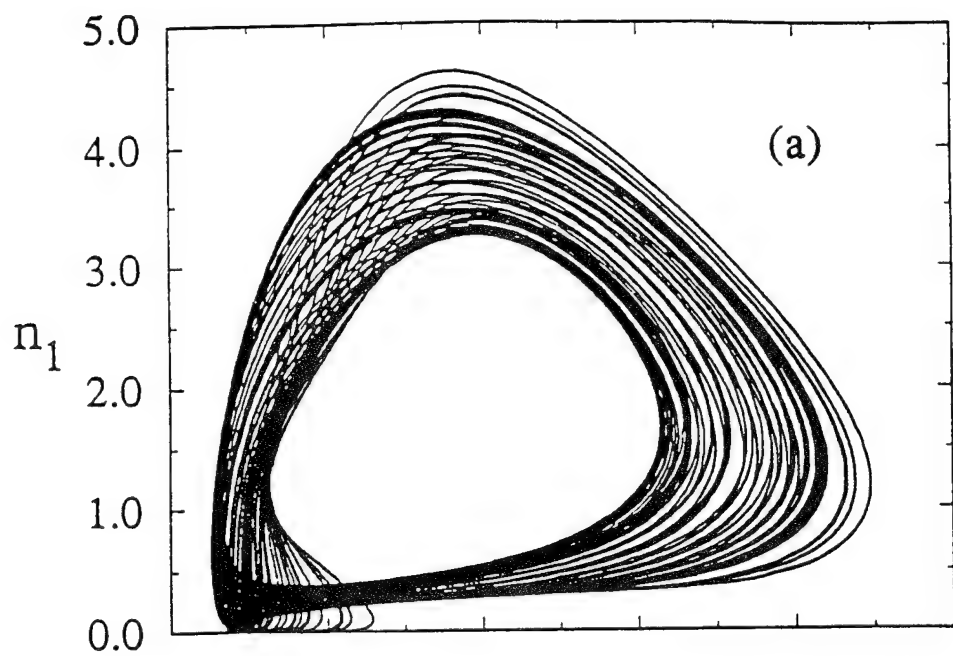
FIG 4: Calculated average duration of chaotic transients as a function of the control parameter. The straight line is a fit with a slope $-\gamma = -0.543$.

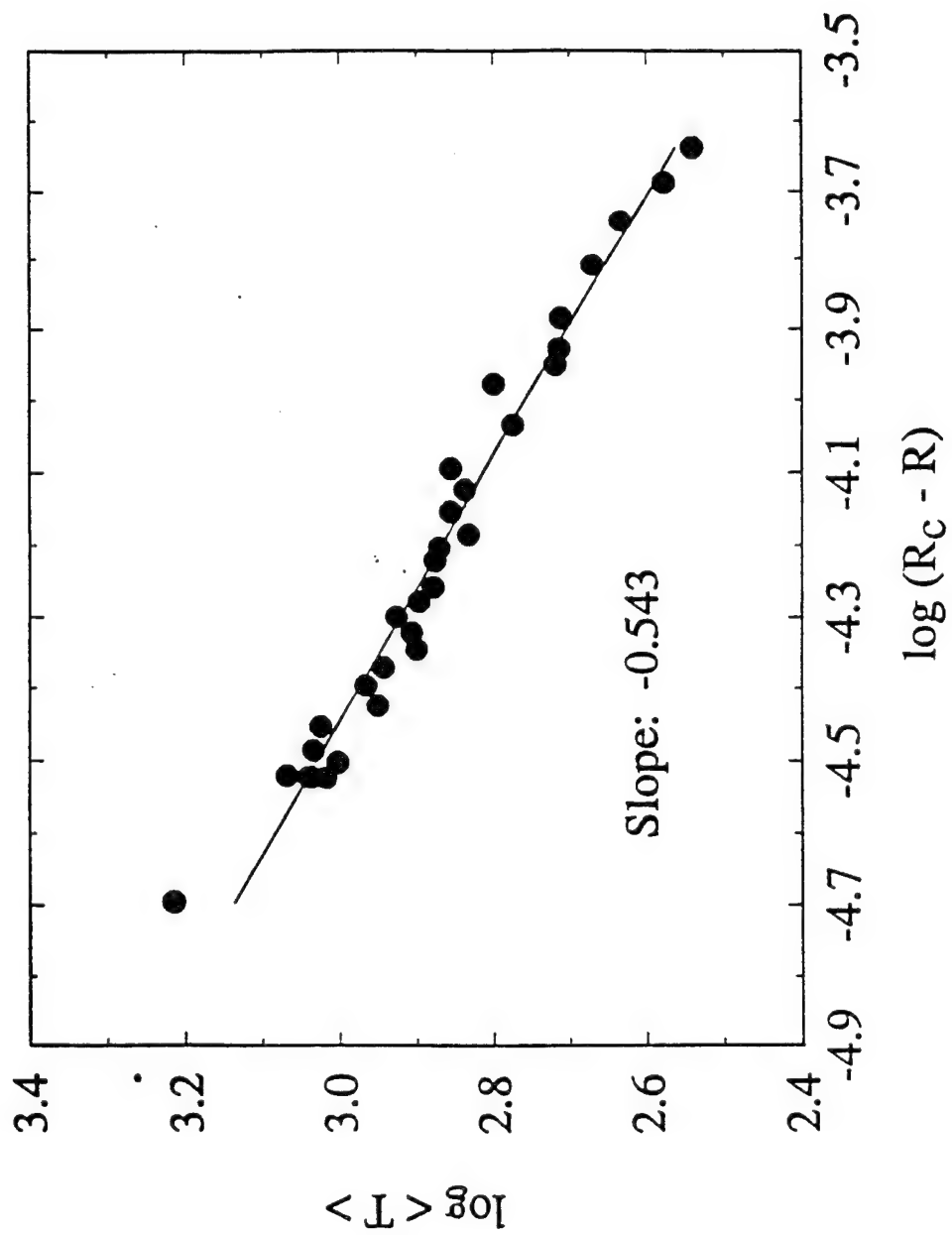
REFERENCES

- ¹ J. A. Yorke and E. D. Yorke, *J. Stat. Phys.* **21**, 263 (1979).
- ² C. Grebogi, E. Ott and J. A. Yorke, *Physica* **7D**, 181 (1983); *Phys. Rev. Lett.* **57**, 1284 (1986); *Phys. Rev. A* **36**, 5365 (1987).
- ³ T. Tél, in *Directions in Chaos*, vol. 3, (World Scientific, Singapore, 1990), edited by Hao Bai-lin, pp. 149-211.
- ⁴ T. L. Carroll, L. M. Pecora and F. J. Rachford, *Phys. Rev. Lett.* **59**, 2891 (1987); *Phys. Rev. A* **40**, 377 (1989).
- ⁵ For a review, see: S. M. Rezende, F. M. de Aguiar and A. Azevedo, *J. Appl. Phys.* **73**, 6805 (1993); *Braz. J. Phys.* **22**, 301 (1992).
- ⁶ H. Suhl, *J. Phys. Chem. Solids* **1**, 209 (1957).
- ⁷ F. M. de Aguiar and S. M. Rezende, *Phys. Rev. Lett.* **56**, 1070 (1986).









Controlling Spin-Wave Chaos

S.M Rezende, F.M. de Aguiar and A. Azevedo

*Departamento de Física,
Universidade Federal de Pernambuco
50670-901 Recife-PE, Brasil*

ABSTRACT

Microwave pumped spin-wave instabilities in YIG spheres were one of the first experimental systems used to demonstrate that chaos can be suppressed by small periodic modulations in an accessible system parameter. Here we show that the equations describing two interacting spin-wave modes account satisfactorily for the experimental results, as long as the field modulation is appropriately introduced in the model. The finite detuning parameters expressing the boundary conditions of the sample provide a natural way for introducing the field modulation. Thus the present results constitute additional evidence of the validity of the two-mode model with momentum-non-conserving driving Hamiltonian used to explain the sample size dependence of the self-oscillations.

INTRODUCTION

Microwave pumped spin-wave instabilities in YIG spheres were one of the first experimental systems used to demonstrate¹ that chaos can be suppressed by small time-dependent variations in an accessible system parameter. This method of controlling chaos is based on the fact that a chaotic attractor usually has embedded within it an infinite number of unstable periodic orbits. As shown by Ott, Grebogi, and Yorke² (OGY) it is possible to tailor the time-dependence of a relevant parameter so as to stabilize a chosen unstable orbit. In systems with relatively slow dynamics, the parameter variation necessary to stabilize the orbit can be determined at each cycle according to the prescription of OGY and the result fed back into the system^{3,4}. In the case of spin-wave instabilities, where the self-oscillation frequencies lie in the range of $100\text{kHz} - 10\text{MHz}$, a closed-loop feedback experiment is difficult to implement⁵. So the stabilization of the orbits has been achieved¹ with a periodic modulation signal provided by an independent oscillator. In general terms the parametric perturbation scheme of Lima and Pettini⁶ accounts for the observed suppression of chaos, however there is no specific model for the spin-wave case.

In this paper we show that the control of chaos in the spin-wave experiments can be explained satisfactorily by the two-mode model employed to describe spin-wave nonlinear dynamics. The field modulation used in experiments to control the chaotic state is naturally introduced in the model through the detuning parameters expressing the boundary conditions which have been shown to account for the sample size dependence of the self-oscillations^{7,8}.

EXPERIMENTS

The experiments have been previously described¹ in detail and we only present here some of its main features and results. They were carried out with a polished sphere (diameter 1.0mm) of the prototype ferromagnet yttrium iron garnet (YIG) at room temperature pumped with X-band radiation in the "subsidiary-resonance" configuration. The experimental arrangement is the same used in spin-wave pumping experiments^{7,11} except for a loop placed inside the microwave cavity to allow the modulation of the sample biasing field $H = H_0 + \delta H \cos(2\pi f_m t)$ over a broad frequency range 0 – 10MHz, typically with $\delta H/H_0 \sim 10^{-4}$.

The usual experiment to study spin-wave phenomena is done with fixed values of H_0 and varying microwave power. At low power levels the steady-state reflection from the critically coupled cavity is negligible. As the microwave driving field h is increased, an abrupt change in reflection occurs at the Suhl threshold h_c , due to the parametric excitation of a magnon pair with frequency $\omega_k \simeq \omega_p/2$ and wave vector \vec{k} and $-\vec{k}$. The value of k is determined by the frequency ω_p , the field H_0 , and the condition for minimum threshold, which depends on the pumping configuration.

The suppression of chaos has been observed at many points of the $h \times H_0$ diagram. The results presented here were observed after the system has been driven to a full chaotic regime with $h = 1.1$ Oe and $H_0 = 1750$ Oe, with the field applied in the [110] crystal direction. Fig.1(a) shows the power spectrum of a chaotic auto-oscillation for $\delta H = 0$, displaying a characteristic broadband feature. By increasing δH , the spectrum becomes progressively cleaner, with sharp lines characteristic of a periodic signal. Fig.1(b) shows the result for $\delta H = 0.435$ Oe and $f_m = 1480$ kHz. The spectrum in this case corresponds to a quasiperiodic signal with fundamental frequencies $f_0 = 740$ kHz and $f_1 = 1975$ kHz, and a subharmonic component at $f_0/2$. In Fig.2

we show the variation of the critical amplitude δH^* necessary to control chaos with the modulation frequency f_m . Notice that δH^* has minima at values commensurate with the fundamental frequency f_0 , i.e., $f_0/f_m = p/q$, where p and q are integers. In addition, for the f_m range shown in Fig.2, the minima are strikingly ordered according to the devil's staircase, i.e., the values between p/q and p'/q' are characterized by the ratio $(p+p')/(q+q')$. The suppression of chaos in the shaded regions of Fig.2 was also confirmed by the behavior of the information dimension D_1 and the metric entropy K of the attractor. As h increases at fixed f_m and crosses the boundaries in the $\delta H \times f_m$ diagram, D_1 and K approach the values 1 and 0 respectively, characteristic of a periodic orbit¹.

THEORETICAL MODEL AND RESULTS

The usual two-mode model^{9,11} for describing the nonlinear dynamics considers that the interacting spin-wave system is driven by a uniform microwave field in an infinite medium, so that the driving Hamiltonian $\mathcal{H}'(t)$ preserves momentum. However, in a finite medium, $\mathcal{H}'(t)$ can be nonzero for pairs $\vec{k}, -\vec{k}'$ for which k and k' differ by an amount of the order of the reciprocal of the sample size L . In this case, it can be shown⁷ that a new driving term is introduced in the spin-wave equations, having magnitude proportional to a factor $\alpha_{\Delta k}$ which depends on the wave-vector mismatch $\Delta \vec{k} = \vec{k} - \vec{k}'$. For instance, for two neighbouring standing waves along x with $\Delta k_x = \pi/L_x$, $\alpha_{\Delta k}$ attains its maximum value $2/\pi \simeq 0.64$. In an infinite medium, $\alpha_{\Delta k} = 0$. With this new momentum non-conserving driving term, the equations of motion for the slowly varying spin-wave variables c_k for two neighboring

modes become⁷

$$\begin{aligned}\dot{c}_1 = & (\gamma_1 + i\Delta\omega_1) c_1 - ih\rho_1 (c_1^* + \alpha e^{i\beta/2} c_2^*) \\ & - i2 (S_1 c_1^2 c_1^* + S_{12} c_1^* c_2^2 + 2T_{12} c_2 c_2^* c_1) \quad ,\end{aligned}\quad (1)$$

$$\begin{aligned}\dot{c}_2 = & (\gamma_2 + i\Delta\omega_2) c_2 - ih\rho_2 (c_2^* + \alpha e^{-i\beta/2} c_1^*) \\ & - i2 (S_2 c_2^2 c_2^* + S_{12} c_2^* c_1^2 + 2T_{12} c_1 c_1^* c_2) \quad ,\end{aligned}\quad (2)$$

where $\Delta\omega_k = \omega_k - \omega_p/2$, $\alpha \equiv \alpha_{\Delta k}$ and $\beta \equiv \beta_{12}$ is the phase difference between modes 1 and 2, γ_k is the relaxation rate, ρ_k the coupling factor between mode k and the pumping field h and the S_i and T_i are the nonlinear coupling parameters⁷.

The presence of one mode in the pumping term of the other represents a modulation with the frequency difference $\Delta\omega = \omega_1 - \omega_2$, leading to self-oscillations with frequency that depends not only on the relaxation rate but also on $\Delta\omega$. For two neighboring modes in k space, $\Delta\omega \simeq \pi/L$, which accounts for the observed size dependence of the spin-wave self-oscillations. When a small ac field variation is superimposed to the static field, the spin-wave detuning parameters become

$$\Delta\omega_k = \omega_k - \frac{\omega_p}{2} + \gamma\delta H \cos(2\pi f_m t) \quad . \quad (3)$$

Equations (1) and (2) with the time-dependent detunings (3) constitute our model to explain the suppression of chaos. Those equations have been integrated numerically in a SUN Sparc 2 workstation with a Runge-Kutta subroutine. Chaotic dynamics and control of chaos with field modulation are observed with many sets of parameters. The results described below were obtained with $\gamma_1 = \gamma_2$, $\rho_1 = \rho_2$, $\Delta\omega_1/\gamma_1 = 0.2$, $\Delta\omega_2/\gamma_1 = -0.5$, $S_1/\gamma_1 = S_2/\gamma_1 = 0.5$, $S_{12}/\gamma_1 = -0.2$, $T_{12}/\gamma_1 = -0.4$, $\alpha = 0.65$ and $\beta = \pi$. With these parameters, auto-oscillations with frequency $f_0 \simeq 0.49\gamma_1$ (with no field modulation, $\delta H = 0$) develop at a normalized microwave amplitude

$R \equiv h\rho_1/\gamma_1 = 1.32$ (the Suhl threshold is $R = 1.0$) and chaos sets in at $R = 1.808$. Fig.3(a) shows the power spectrum of mode 1 amplitude, $n_1 = c_1^* c_1$, for $R = 1.83$ and $\delta H = 0$, characterizing a chaotic state. With the modulation turned on at some frequency values, if δH exceeds a critical amplitude δH^* , chaos is suppressed after a transient time. Fig.3(b) shows the power spectrum for $f_m = 0.56\gamma_1$ and $\delta H = 0.4\gamma_1/\gamma$ (γ is the gyromagnetic ratio), demonstrating that the signal has become periodic with frequency $0.56\gamma_1$. The boundaries of the stability regions in the modulation-amplitude \times frequency plane, shown in Fig.4, display tongues like the experimental results of Fig.2.

The results shown in Figs. 3 and 4 were obtained by integrating the equations of motion with the field modulation on for a length of time on the order of 200 cycles of the oscillation, so that the response has reached steady-state. Actually, the stable orbit resulting from the field modulation is preceded by a chaotic transient in which orbits similar to those of the uncontrolled chaotic attractor dominate². The duration τ of such chaotic transient depends sensitively on the initial conditions. For a given modulation, we calculate the average duration $\langle \tau \rangle$ for 256 randomly chosen initial conditions. For $f_m = 0.56\gamma_1$ this average time is found to scale with the modulation amplitude as $\langle \tau \rangle \sim (\delta H - \delta H^*)^{-\gamma}$, where $\gamma \simeq 0.287$. A scaling relation of this type was predicted by OGY, though with a different value of the critical exponent.

CONCLUSIONS

The experimental observations on controlling chaos in spin-wave instabilities driven by microwave radiation in YIG spheres, by means of a small periodic variation in the applied magnetic field, are explained by a two-mode model. The field modulation is introduced in the model through the same detuning parameters used to explain

the sample size dependence of the self-oscillations. Hence, the present results provide additional evidence of the validity of the two-mode model with momentum-non-conserving driving Hamiltonian for describing spin-wave dynamics.

ACKNOWLEDGEMENTS

This work was supported by FINEP, CNPq, PADCT, CAPES and FACEPE.

REFERENCES

1. A. Azevedo and S.M. Rezende, Phys. Rev. Lett. 66, 1342 (1991).
2. E. Ott, C. Grebogi, and J.A. Yorke, Phys. Rev. Lett. 64, 1196 (1990).
3. W.L. Ditto, S.N. Rauser, and M.L. Spano, Phys. Rev. Lett. 65, 3211 (1990).
4. E.R. Hunt, Phys. Rev. Lett. 67, 1953 (1992).
5. M. Ye, D.E. Jones, and P.E. Wigen, J. Appl. Phys. 73, 6822 (1993).
6. R. Lima and M. Pettini, Phys. Rev. A41, 726 (1990).
7. S.M. Rezende and A. Azevedo, Phys. Rev. B45, 10387 (1992).
8. S.M. Rezende, F.M. de Aguiar, and A. Azevedo, J. Appl. Phys. 73, 6805 (1993).
9. K. Nakamura, S. Ohta, and K. Kawasaki, J. Phys. C 15, L143 (1982).
10. P.H. Bryant, C.D. Jeffries, and K. Nakamura, Phys. Rev. A 38, 4223 (1988).
11. S.M. Rezende and F.M. de Aguiar, Proc. IEEE 78, 893 (1990).

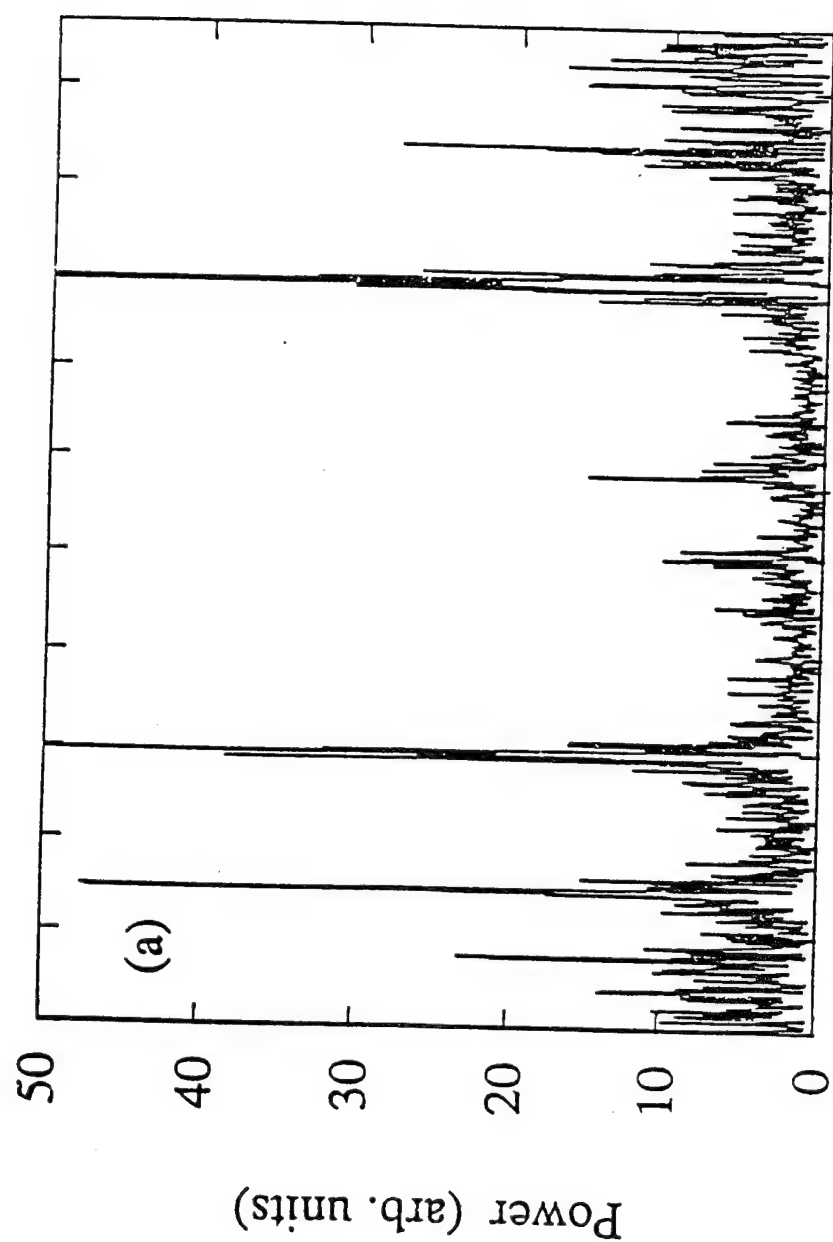
FIGURE CAPTIONS

FIG. 1. Power spectra of observed auto-oscillations for different values of the amplitude δH of the field modulation. (a) Chaos for $\delta H = 0$. (b) Chaos under control with $\delta H = 0.435$ Oe and $f_m = 1480$ kHz [Ref.1].

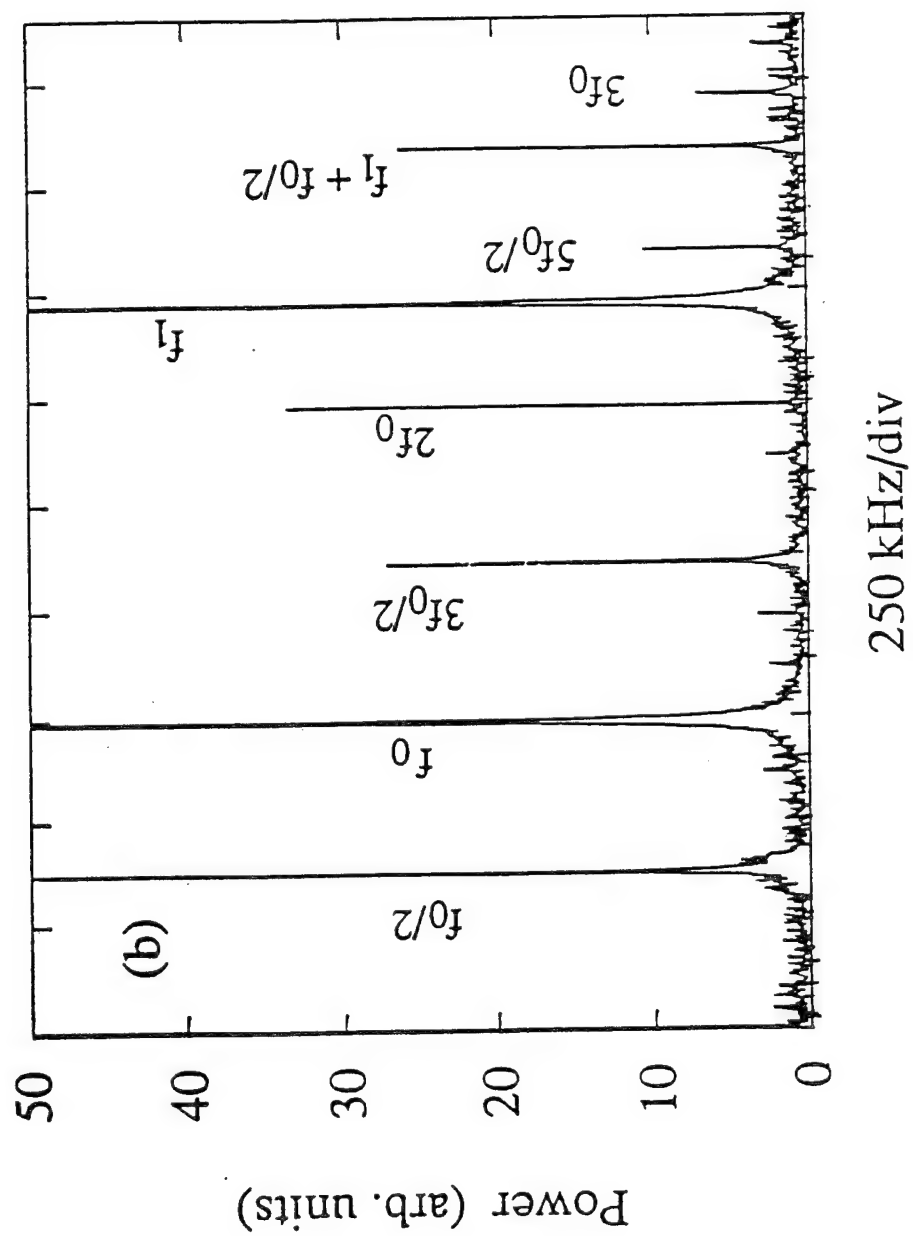
FIG. 2. Critical modulation amplitude δH^* vs. modulation frequency f_m . The boundaries between the chaotic and controlled regions have minima at values of f_m commensurate with the fundamental frequency f_0 at ratios indicated at the top [Ref.1].

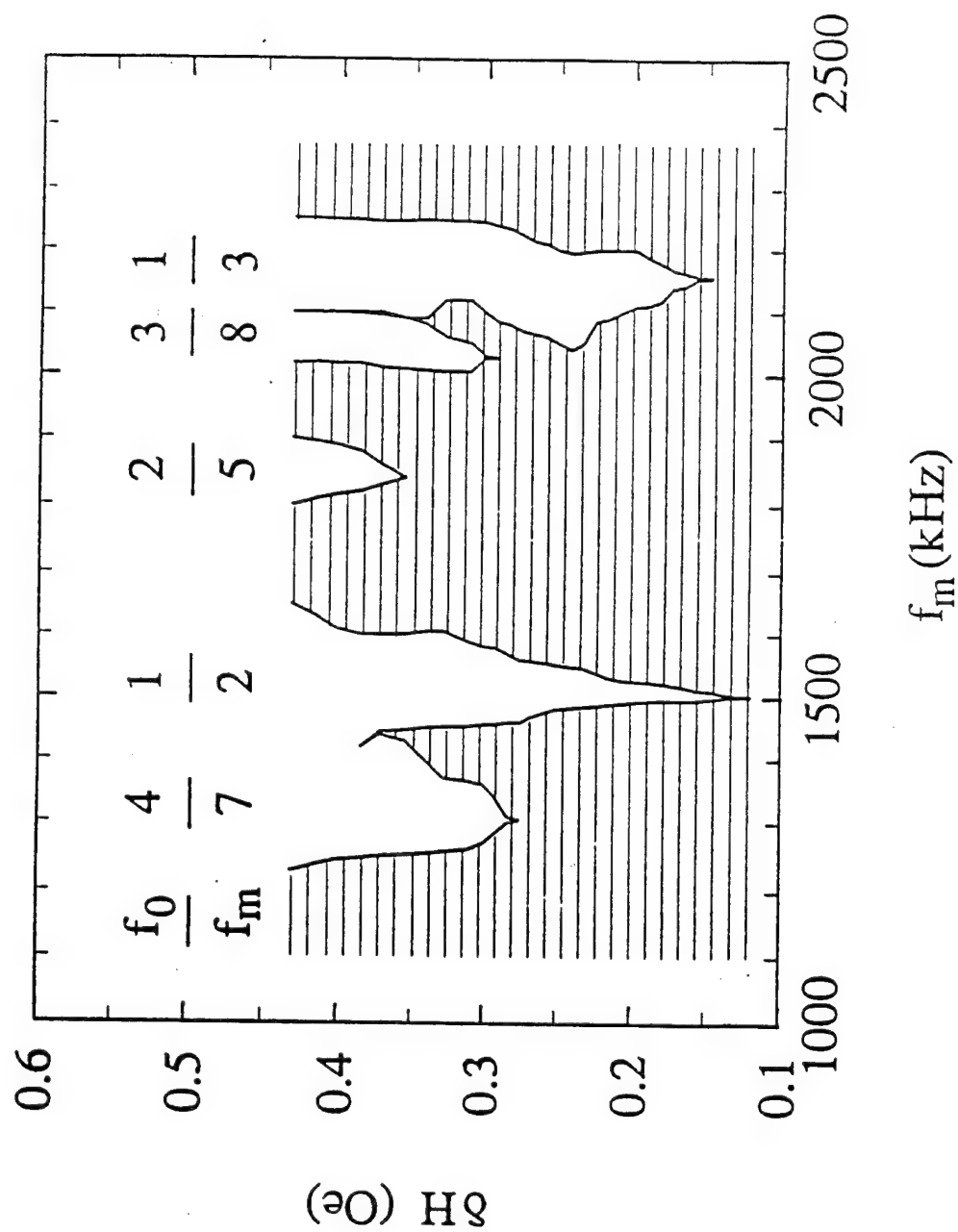
FIG. 3. Fourier transform of mode 1 amplitude without (a) and with field modulation (b), $\delta H = 0.4 \gamma_1/\gamma$, $f_m = 0.56 \gamma_1$. The clean spectrum in (b) demonstrates suppression of chaos with the two-mode model.

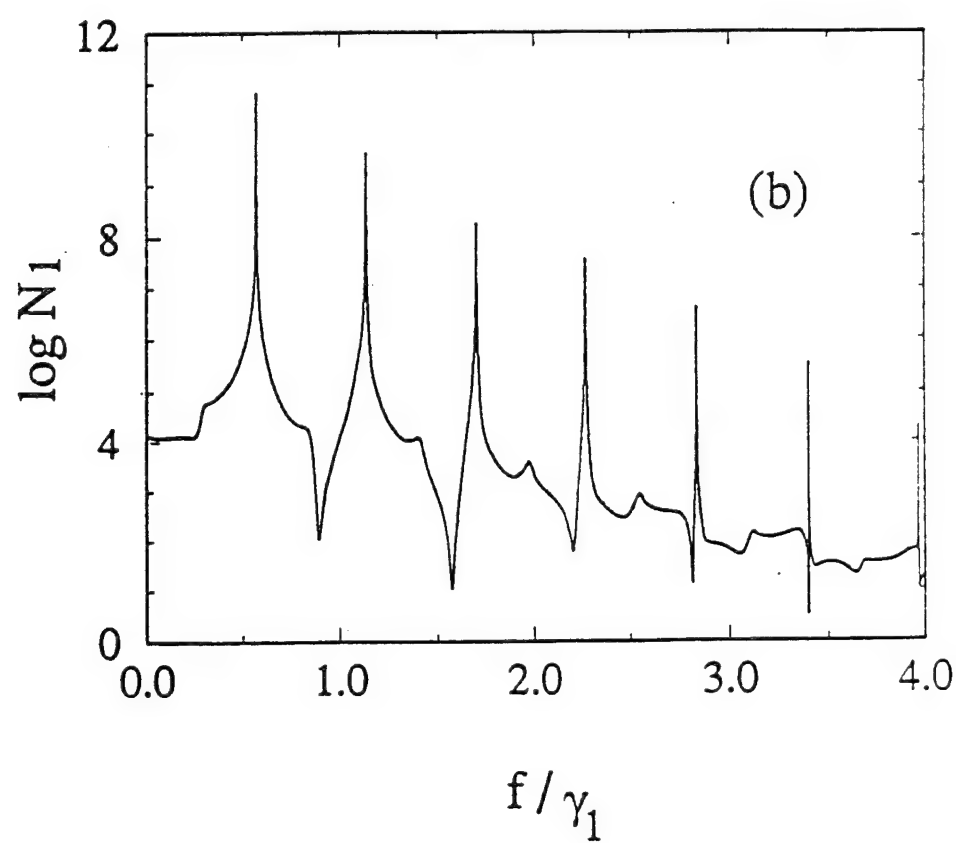
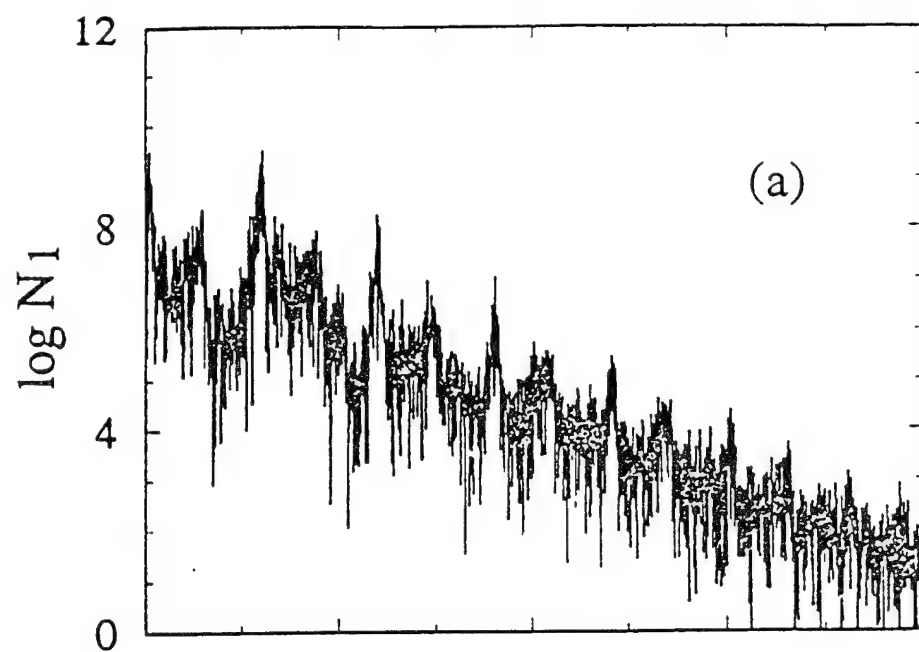
FIG. 4. Critical amplitude δH^* in units of γ_1/γ obtained with the model and parameters described in the text.

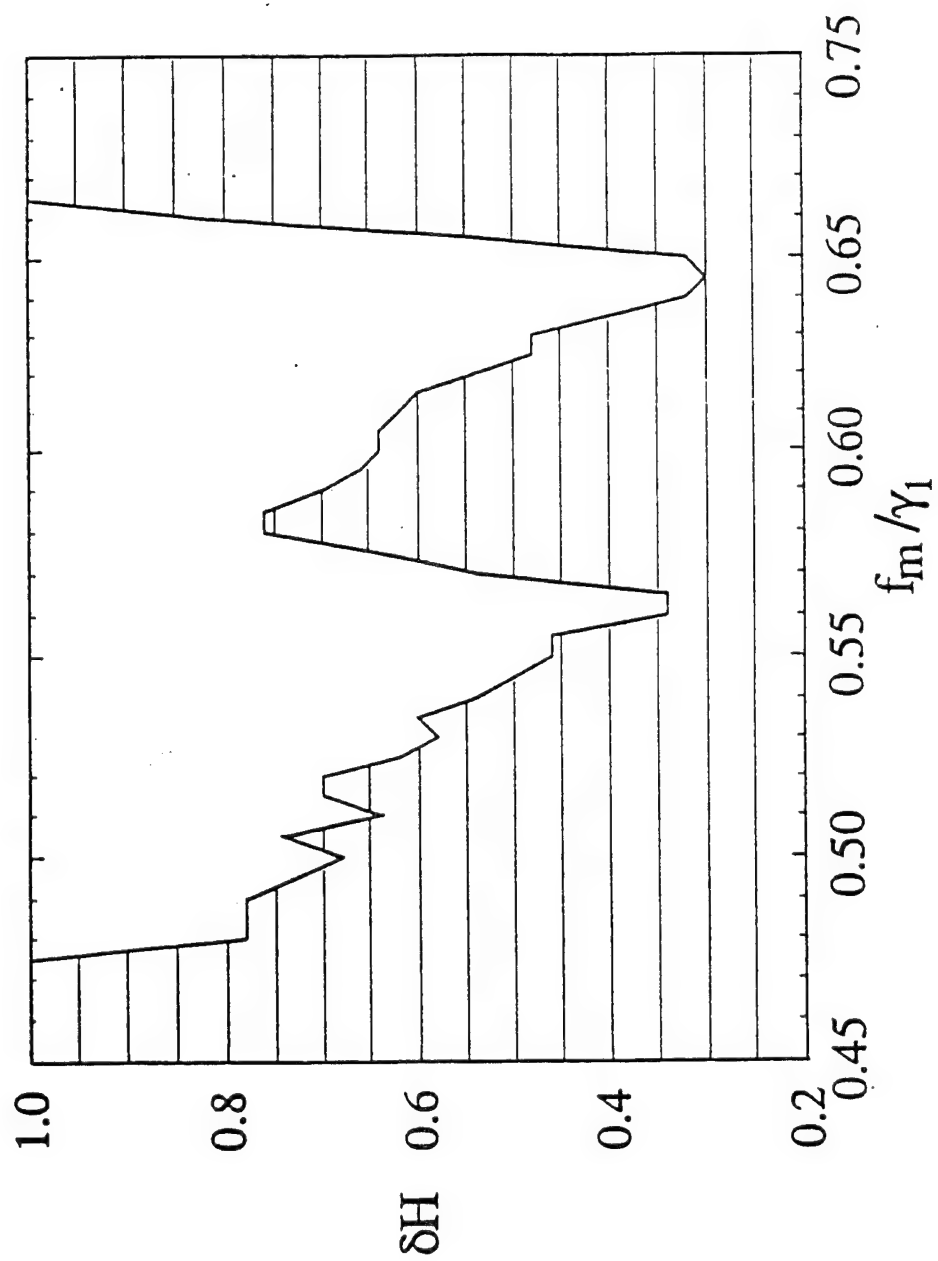


250 kHz/div









SAMPLE-SIZE EFFECT IN SPIN WAVE AUTO-OSCILLATIONS

A.N. Slavin

Department of Physics, Oakland University,
Rochester, MI 48309, USA

ABSTRACT

The theoretical model of spatially inhomogeneous unstable collective oscillations in a system of spin waves parametrically excited in a finite magnetic sample is used to explain the **sample-size effect in spin wave auto-oscillations under parallel pumping** observed in yttrium-iron garnet (YIG) spheres and films.

It is shown that in the **axially symmetric case (YIG sphere)** the model demonstrates **good quantitative agreement with the experiment** for both auto-oscillation threshold and frequency.

In the **absence of axial symmetry (tangentially magnetized YIG film)** the instability criterion for collective oscillations is fulfilled only for sufficiently small values of the bias magnetic field H (large values of parametric spin wave wave number k). In this case the model gives **only qualitative description of the size dependence** of the auto-oscillation threshold, but correctly describes the size dependence of the auto-oscillation frequency.

1. Introduction

Spin wave auto-oscillations in ferrites above the threshold of parametric excitation discovered in [1] were studied intensively during the last decade mostly because of interesting chaotic dynamics they demonstrate in a strongly nonlinear regime (see e.g. [2, 3, 4, 5]).

The experiments performed by Rezende et al. [6, 7] demonstrate a pronounced sample-size dependence of auto-oscillation frequency and threshold that was not explained by the traditional theory of spin wave auto-oscillations [8, 9].

In our previous work [10, 11] we have developed a model of spin wave auto-oscillations under parallel pumping in finite-size ferromagnetic samples taking into account the boundary conditions for the envelope of the packet of parametrically excited spin waves at the boundaries of a magnetic sample. This model explains the sample-size dependence of auto-oscillation frequencies and thresholds observed YIG spheres in [6, 7].

In our present paper we make a detailed comparison of this model with the experiments performed by Rezende et al. in YIG spheres [6, 7], describe our own experiments on sample-size dependence of auto-oscillations performed in tangentially magnetized rectangular YIG film samples, and discuss the applications of our theoretical model to the case of film samples.

2. Theoretical model

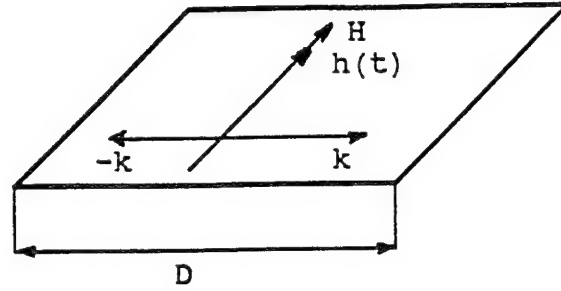
The theoretical model [10, 11] that we are using to describe the sample-size effect in spin wave auto-oscillations is an **extension of the S-theory** of auto-oscillations in unlimited ferromagnetic samples [8]. In the framework of this theory **spin wave auto-oscillations are interpreted as unstable collective oscillations in the system of parametrically excited spin waves**. These oscillations are originated from the **four-wave interaction** between parametric spin waves. The criterion of instability of collective oscillations (i.e. appearance of auto-oscillations) can be formulated as (see [8])

$$2R + 1 < 0, \quad (1)$$

where $R = T/S$, and **S and T are the coefficients of four-wave interaction** between spin waves.

In the case of a **finite** magnetic sample we assume that the collective oscillations in the system of parametrically excited spin waves can be **spatially inhomogeneous** (i.e. can propagate in the sample) and the amplitudes A_k of these oscillations (or secondary waves) must satisfy certain **boundary conditions** at the sample boundaries.

For simplicity we assume that only one size of the sample is relevant - the size **D** in the direction of propagation of parametric spin waves excited at the threshold.



In the case when the mean free path $l = v_g/\gamma_k$ of spinwaves in a sample is much smaller than the sample size D ($l \ll D$) the boundary conditions for the oscillation amplitudes must be the conditions of "no reflection" at the boundary ($\mathbf{A}_k = 0$). In this particular case the model [10, 11] yields the following expressions for the auto-oscillation threshold h_{osc} and the auto-oscillation frequency ω_{osc} at this threshold

$$\frac{h_{osc}^2}{h_{th}^2} - 1 = \frac{1}{2} \left(\frac{\pi v_g}{D \gamma_k} \right)^2 \frac{1}{|2R + 1|} \quad (2)$$

$$\frac{\omega_{osc}}{\gamma_k} = \frac{1}{2} \left(\frac{\pi v_g}{D \gamma_k} \right)^2 \left(\frac{5R + 1}{2R + 1} \right)^{\frac{1}{2}} \quad (3)$$

where h_{th} is the threshold of parametric excitation of spin waves, γ_k is the relaxation parameter, and v_g is the group velocity of parametric spin waves.

The four-wave interaction coefficients **T** and **S** (and their ratio) can be calculated from the general expressions presented in [12]. We note, that both **values and signs of the four-wave interaction coefficients S and T depend strongly on the crystallographic orientation of the sample** even in cubic crystals like YIG, where spin wave spectrum is practically isotropic. This property of **T and S** the giant crystallographic anisotropy of auto-oscillations observed in experiments.

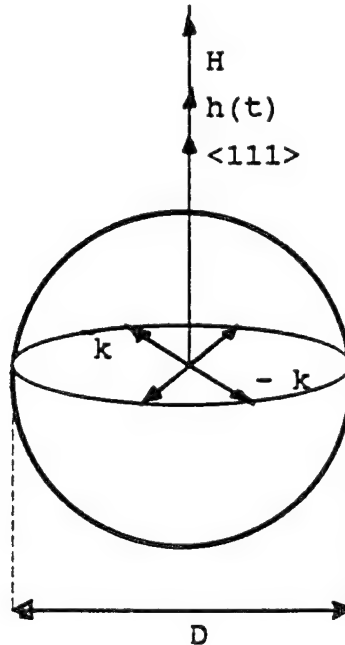
Another..interesting feature of the expressions (2), (3) is that in the axially symmetric case (**sphere**) the **ratio** of these two expressions is **independent of both the sample size D and the bias magnetic field H**.

$$G = \frac{\left(\frac{h_{osc}^2}{h_{th}^2} - 1 \right)}{\left(\frac{\omega_{osc}}{\gamma_k} \right)} = \frac{1}{\sqrt{|2R + 1||5R + 1|}} \quad (4)$$

The model Eqs.(2), (3) is applicable when parametric spin waves with wave numbers **k > 0 (H < H_c)** are excited in the sample and describes all the characteristic features of the spin wave auto-oscillations under parallel pumping (including the sample-size effect).

3. Sample-Size Effect In Spheres

The most complete experimental investigation of the sample-size effect in spin wave auto-oscillations under parallel pumping in YIG spheres has been reported by Rezende et al. in [6]. The results for the threshold of parametric excitation of spin waves h_{th} , the threshold of spin wave auto-oscillations h_{osc} , and the auto-oscillation frequency f_{osc} ($f_{osc} = \omega_{osc}/2\pi$) as functions of a bias magnetic field H are presented in Fig.7 of Ref.[6] for YIG spheres of diameters $D = 1$ mm and 0.52 mm.



Using expressions for T and S from [12] we calculated the ratio G Eq.(4) for the conditions of the experiments [6]. The parameter $R = T/S$ in this case was equal to $R = -1.42$, while the ratio G turned out to be equal to

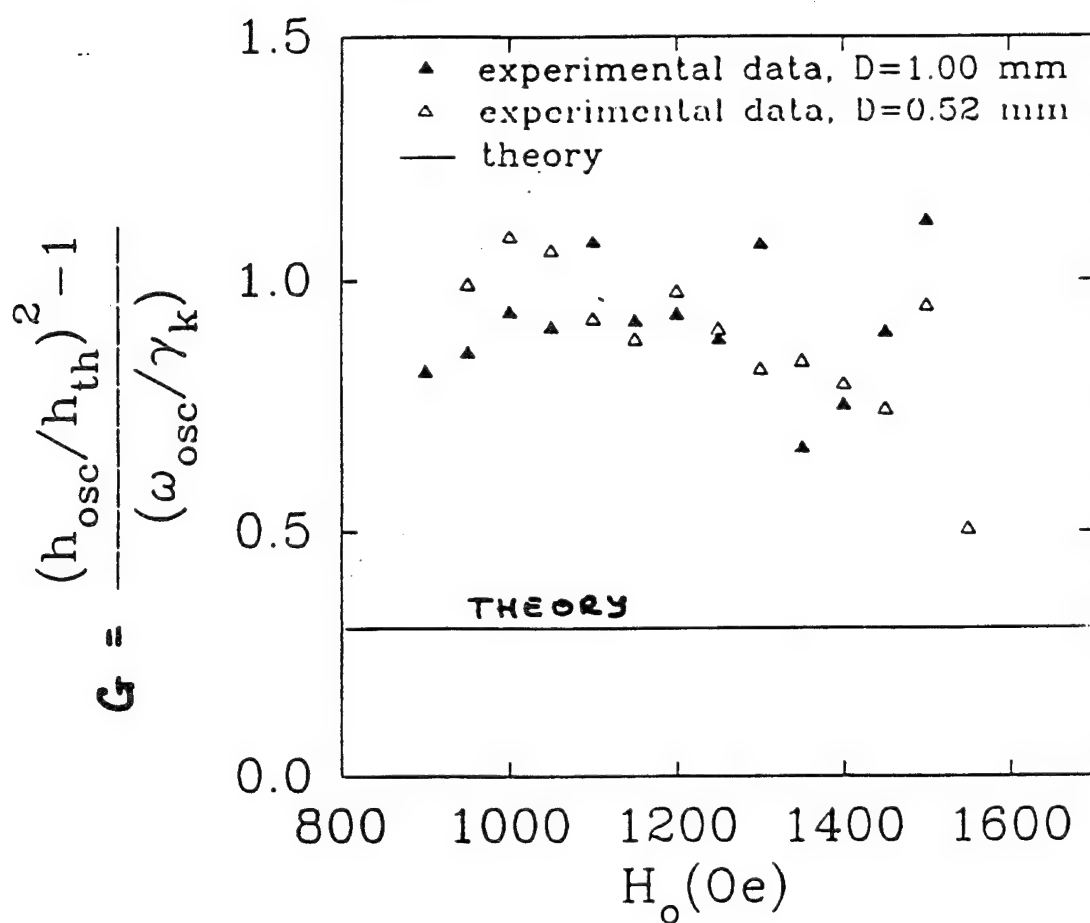
$G = 0.3$. We also calculated the same ratio G from the experimental data presented in [6]. . The theoretical and experimental values of G are presented in Fig.1.

It is clear from Fig.1 that although the numerical values of theoretical and experimental ratio G are different, the behavior of G with variation of D and H is similar : in both theory and experiment G does not depend on either the sample size D or the bias field H .

Using Fig.1 we determined the value of the parameter R for which the theoretical value of the ratio G is equal to the mean average of experimental values $G = 0.8$. This value turned out to be equal to $R = - 0.765$. We note, that the instability criterion (1) is still fulfilled for this value of R .

Below we used $R = - 0.765$ in Eqs.(2), (3) to calculate the theoretical curves $h_{osc}(H)$ and $\omega_{osc}(H)$. The results of comparison of these calculations with the experimental data from [6] are presented in Fig.2.

It is clear from Fig.2 that our model Eqs.(2), (3) demonstrates good quantitative agreement with the results of the experiment [6] and explains the sample-size effect in spin wave auto- oscillations under parallel pumping in YIG spheres.



$$\bar{G}_{exp} = 0.8$$

$$(R_{exp} = -0.765)$$

$$G_{THEOR} = 0.3$$

$$(R_{THEOR} = -1.4)$$

Fig.1 Comparison of theoretical and experimental values of the ratio G in the axially symmetric case (YIG spheres of diameters $D = 1$ mm and $D = 0.52$ mm [6]).

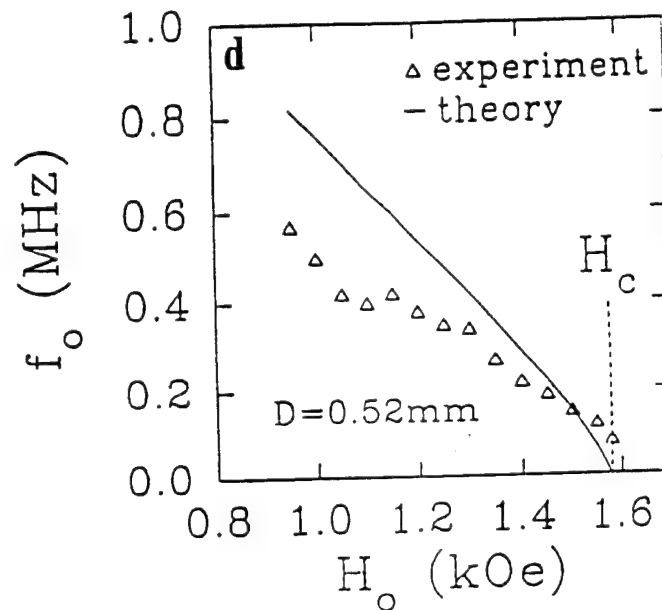
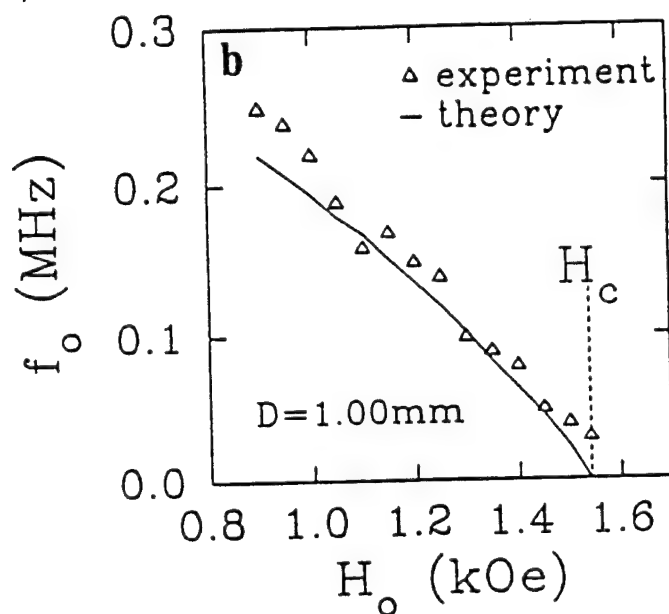
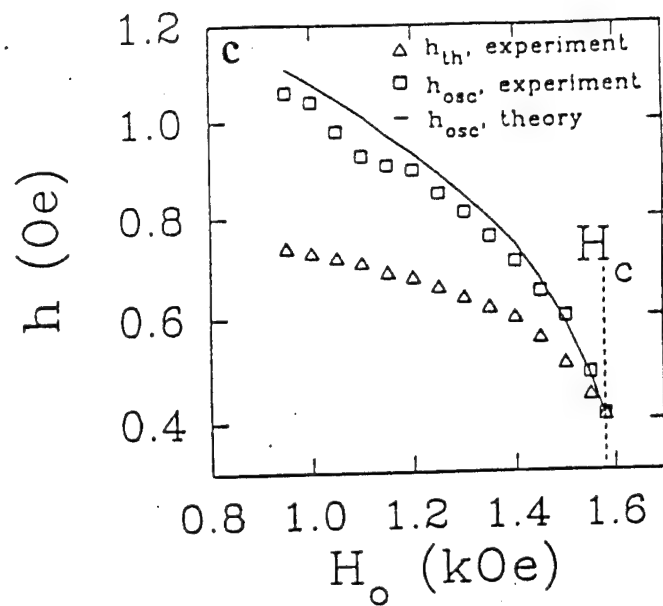
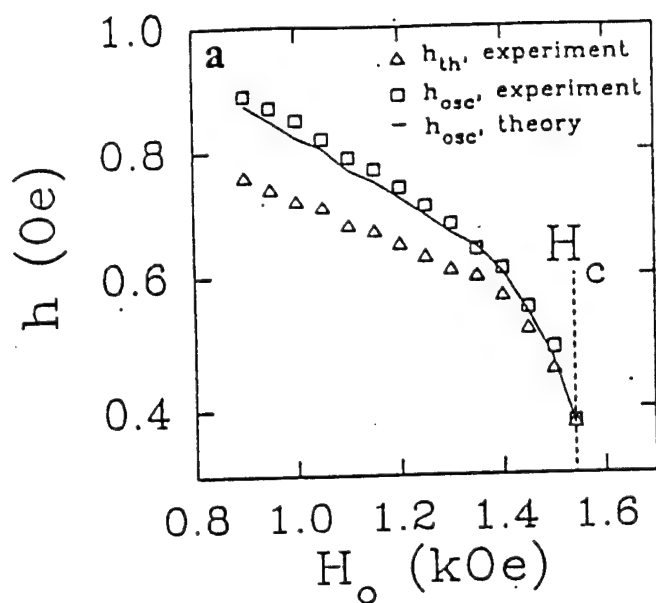
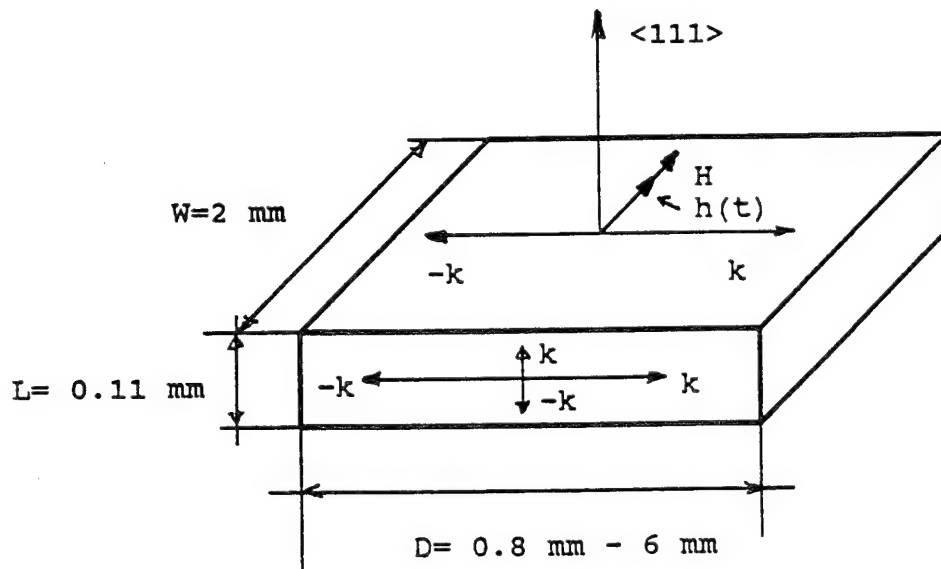


Fig.2 Comparison of the results of experimental measurements of auto-oscillation threshold and frequency performed on two YIG spheres ($D = 1$ mm and 0.52 mm) in [6] with the results of theoretical calculations of these characteristics done using the model Eqs.(2), (3) for $R = T/S = -0.765$.

3. Sample-Size Effect in Films

To make a further check of our theoretical model we performed a series of experiments on rectangular YIG film samples magnetized in the film plane along the sample width ($W = 2 \text{ mm}$). The idea of the experiment was to change the length of the sample ($D = 0.8 - 6 \text{ mm}$) and to see how it affects the frequency of spin wave auto-oscillations ω_{osc} . The samples were cut from an epitaxial YIG film (thickness $L = 0.11 \text{ mm}$) of the orientation $\langle 111 \rangle$ to get the minimum crystallographic anisotropy in the film plane. The spin waves were excited by parallel pumping in a TE reflection type cavity at the frequency $\omega / 2\pi = 9.24 \text{ GHz}$ [14, 15]. The microwave pumping field was parallel to the bias magnetic field (and to the width W of the sample).



The experimental results for tangentially magnetized YIG film samples of different lengths D are presented in Fig.3 a-d. It is easy to see, that, contrary to the case of spherical samples, in film samples the sample-size effect is observed **only for sufficiently small values of the bias magnetic field $H < 700$ Oe** (or for sufficiently large values of spin wave wave number $k > 3 \cdot 10^5 \text{ cm}^{-1}$). Theoretical interpretation of the size effect in films is more complicated than in spheres for the following reasons

- (i) in films we have **two effective sample sizes (D and L)**;
- (ii) distribution of parametric spin waves in the film is **not axially symmetric**, so the **coefficients S and T are dependent on the bias field H** .

To apply our **one-dimensional model** to the case of a tangentially magnetized film sample we made a naive assumption that the auto-oscillation frequency in this sample can be represented in the form

$$\omega_{osc}(L, D) = \sqrt{\omega_{osc}^2(D) + \Omega^2(L)}, \quad (5)$$

where the first term depends on the sample length D and is given by Eq.(3), while the second term is determined by the film thickness L and by small effects like scattering of auto-oscillations on each other and on random inhomogeneities of the medium. These effects are described in detail in [16].

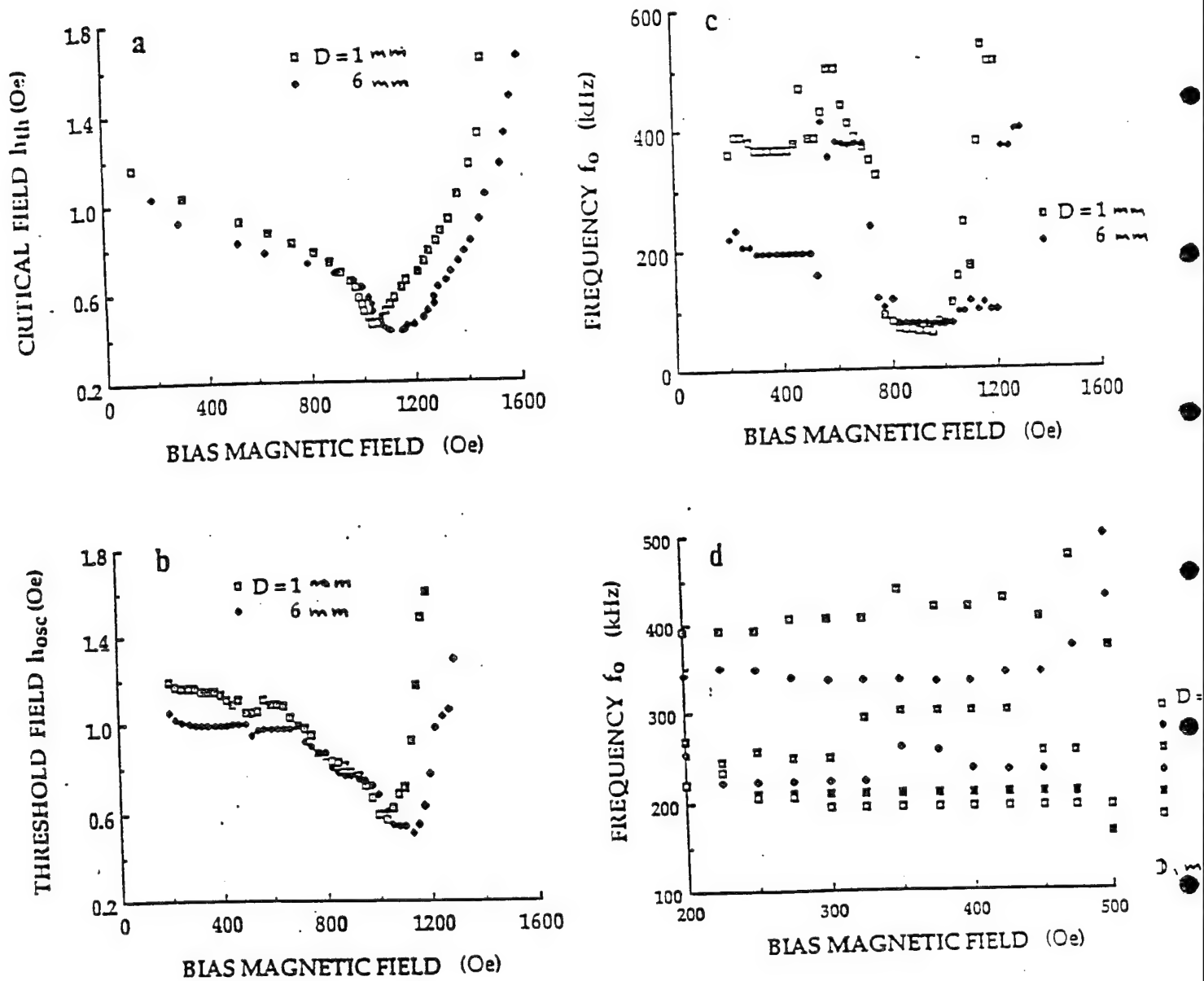


Fig.3 Experimental characteristics of spin wave auto-oscillations in tangentially magnetized YIG film samples (thickness $L = 0.11$ mm, width $W = 2$ mm, orientation (111)) of different lengths $0.8 \text{ mm} < D < 6 \text{ mm}$:
 (a) threshold of parametric excitation ; (b) threshold of spin wave auto-oscillations ; (c) frequency of spin wave auto-oscillations; (d) frequency of spin wave auto-oscillations for several intermediate sample lengths D in the bias field region ($H < 700$ Oe) where the sample-size effect was observed.

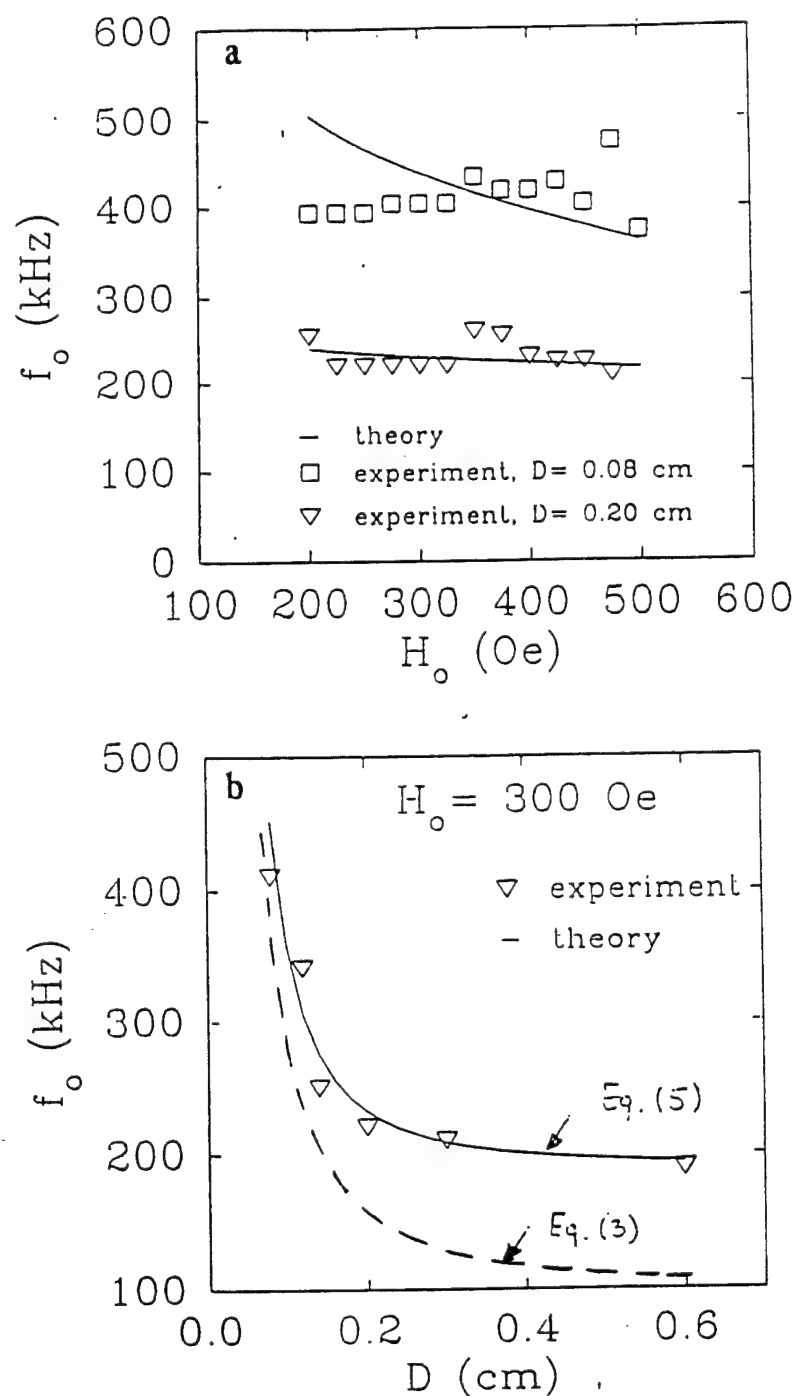


Fig.4 Comparison of theoretical and experimental results for frequency of spin wave auto-oscillations in tangentially magnetized YIG film samples:

- (a) dependence of the frequency on the bias field H ,
 (b) dependence of the frequency on the sample length D

We did not calculate $\Omega(L)$ here and assumed that this term is equal to the auto-oscillation frequency 190 kHz in the sample having the largest length $D = 6$ mm (see Fig.3 c,d).

It is clear from Fig.3 b, c that the sample-size effect in film samples manifest itself only for $H < 700$ Oe. (The nature of auto-oscillations observed in the bias field region $H > 700$ Oe will be discussed elsewhere.)

To explain this fact we assumed that for $H > 700$ Oe the instability criterion Eq.(1) is broken and the coefficient $S(H)$ changes its sign from positive to negative at $H = 700$ Oe. Using this assumption we calculated theoretical dependencies of auto-oscillation frequency $f_{osc} = \omega_{osc}/2\pi$ on the sample length D (at a fixed $H = 300$ Oe) and on the bias field H (at two fixed lengths $D = 0.8$ mm and $D = 2$ mm) from Eqs.(3), (5).

The results of comparison of these calculations with the experimental results from Fig.3 c, d are presented in Fig.4 a,b. It is clear that Eqs. (3), (5) give good qualitative explanation of the sample-size effect on auto-oscillations in films.

CONCLUSION

The above presented comparison of theoretical and experimental results for the characteristics of spin wave auto-oscillations demonstrate that our simple **one-dimensional theoretical model** of spin wave auto-oscillations in finite-size magnetic samples works well in spheres, but gives only limited qualitative description of the sample-size effect on spin wave auto-oscillations observed in tangentially magnetized **YIG** films. Presently, efforts are in progress to develop a two-dimensional theoretical model of spin wave auto-oscillations in magnetic films capable to give the quantitative description of the above reported sample-size effects.

References

1. T.S. Hartwick, E.R. Peressini, and M.T. Weiss, J. Appl. Phys. 32, 223 (1961) .
2. G. Gibson and C. Jeffries, Phys.Rev.A 19, 811 (1984).
3. F.M. de Aguiar and S.M. Rezende, Phys. Rev. Lett. 56 1070 (1986).
4. C.D. Jeffries, P.H. Bryant, and K. Nakamura, J. Appl. Phys. 64 5382 (1988) .
5. H. Yamazaki, J. Appl. Phys. 64, 5391 (1988)
6. S.M. Rezende and A. Azevedo, Phys.Rev.B 45, 10 387 (1992).
7. S.M. Rezende, F.M. de Aguiar, and A. Azevedo, J.Appl.Phys. 67, 5624 (1990); 73, 6805 (1993).
8. V.S. L'vov, S.L. Musher, and S.S. Starobinets, Sov.Phys.- JETP 37, 546 (1973).
9. X. Zhang and H. Suhl, Phys.Rev.B 38, 4893 (1988).
10. V.B. Cherepanov and A.N. Slavin, Phys.Rev.B 47, 5874 (1993).
11. V.B. Cherepanov and A.N. Slavin, J.Appl.Phys. 73, 6811 (1993).
12. V.S. L'vov, Wave Turbulence under Parametric Excitation (Springer Verlag, Berlin, 1993).
13. V.E. Zakharov, V.S. L'vov, and S.S. Starobinets, Sov.Phys.- Usp. 17, 896 (1975).
14. G. Srinivasan, Solid State Comm. 80, 5 (1991).
15. A.N. Slavin, G.Srinivasan, and V.B.Cherepanov, Abstracts of MMM-92,GE-04, 371 (1992).
16. V.S. L'vov and V.B. Cherepanov, Sov.Phys.- JETP 48, 822 (1978).

Internal Fields in the Ferromagnetic Resonance
of Soft Ferromagnetic Materials

R. F. Soohoo
University of California at Davis and
Soohoo Associates, Inc.
568 Reed Drive, Davis, CA 95616

Our experiments at VHF/UHF frequencies and at low applied fields with Soohoo Associates Magnetic Domain Spectrometer 103 showed that Kittel's resonance equation should be modified with the addition of H_i to read:

$$\omega = |\gamma| \sqrt{[H_z + H_i + (N_x - N_z)M_s][H_z + H_i + (N_y - N_z)M_s]} \quad (1)$$

where the applied field H_z may include anisotropy fields. In Eq. (1), N_x , N_y and N_z are demagnetizing factors in the x,y,z directions and M_s is the saturation magnetization. We found that H_i is a fraction of an oersteds for permalloy films and 10's of oersteds for ferrite discs.

The origin of H_i has been attributed by E. Schlomann to the directional distribution of anisotropy axes in a polycrystal and to sample porosity.¹ Our experimental

FIGURE CAPTIONS

- Fig. 1 Modified Kittel's Resonance Formula.
- Fig. 2 Experimental Setup - Soohoo Associates' Magnetic Domain Spectrometer System MDSS103.
- Fig. 3 Sample Absorption vs. Applied Field Parallel and Perpendicular to Easy Axis.
- Fig. 4 M-H Loops.
- Fig. 5 Absorption vs. Easy-Axis Field for Ni/Fe Film.
- Fig. 6 Single-Pass Barkhausen Transitions for Ni/Fe Film.
- Fig. 7 Multiple-Pass Barkhausen Transitions for Ni/Fe Film.
- Fig. 8 Absorption vs. Hard-Axis Field for Ni/Fe Film.
- Fig. 9 Easy-Axis M-H Loop for Ni/Fe Film.
- Fig. 10 Hard-Axis M-H Loop for Ni/Fe Film.
- Fig. 11 Hard-Axis M-H Loop for Ni/Fe Film
(without domain-wall motion).
- Fig. 12 Internal Field for Ni/Fe Film t2.
- Fig. 13 Internal Field for Ni/Fe Film Si.
- Fig. 14 Absorption vs. Applied Field for Polycrystalline Ferrite Disc.
- Fig. 15 Barkhausen Transitions for Ferrite Disc.
- Fig. 16 Internal Field H_i for Ferrite Disc.
- Fig. 17 Origin of Internal Field.
- Fig. 18 Resonance Field for Different Crystalgraphic Orientations.
- Fig. 19 Internal Fields Expressions due to Random Crystallite Orientation and Porosity.

results show that there are additional contributions to H_i when the sample is unsaturated. Whereas our experiments at VHF/UHF frequencies are performed at low fields of 0 to 100 oe which encompass non-saturation and changes in magnetic states, other experiments^{2,3} were typically performed at x-band ($\sim 10\text{GHz}$) and above where resonance fields were in the 1000's of oersteds corresponding to magnetic saturation. For H_i of a fraction of an oersted that we measured, it would not be possible to discern at these high fields.

1. E. Schlomann, Proc. Conf. Mag. and Mag. Materials, Boston T-91, 600 (1956).
2. T. Okamura, Y. Torizuka, and Y. Kojima, Phys. Rev. 88, 1425 (1952).
3. Y. Kojima, Sci. Rept. Tohoko Univ. A-6, 614 (1954); T. R. McGuire, Proc. Conf. Mag. and Mag. Materials, Pittsburg T-78, 43 (1955).

Kittel's Resonance Formula

$$\omega_n = \gamma \sqrt{[H_z + H_k + (N_x - N_z)M_s][H_z + H_k + (N_y - N_z)M_s]}$$

Modified Formula

$$\omega_n = \gamma \sqrt{[H_z + H_k + H_i + (N_x - N_z)M_s][H_z + H_k + H_i + (N_y - N_z)M_s]}$$

Fig. 1

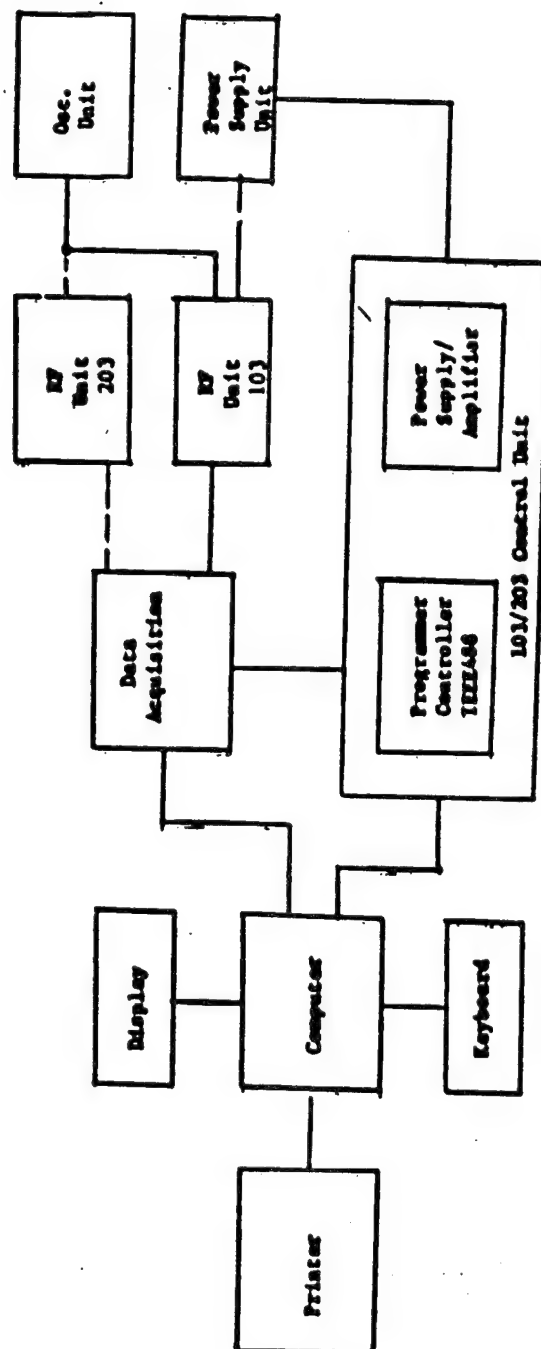


Fig. 2

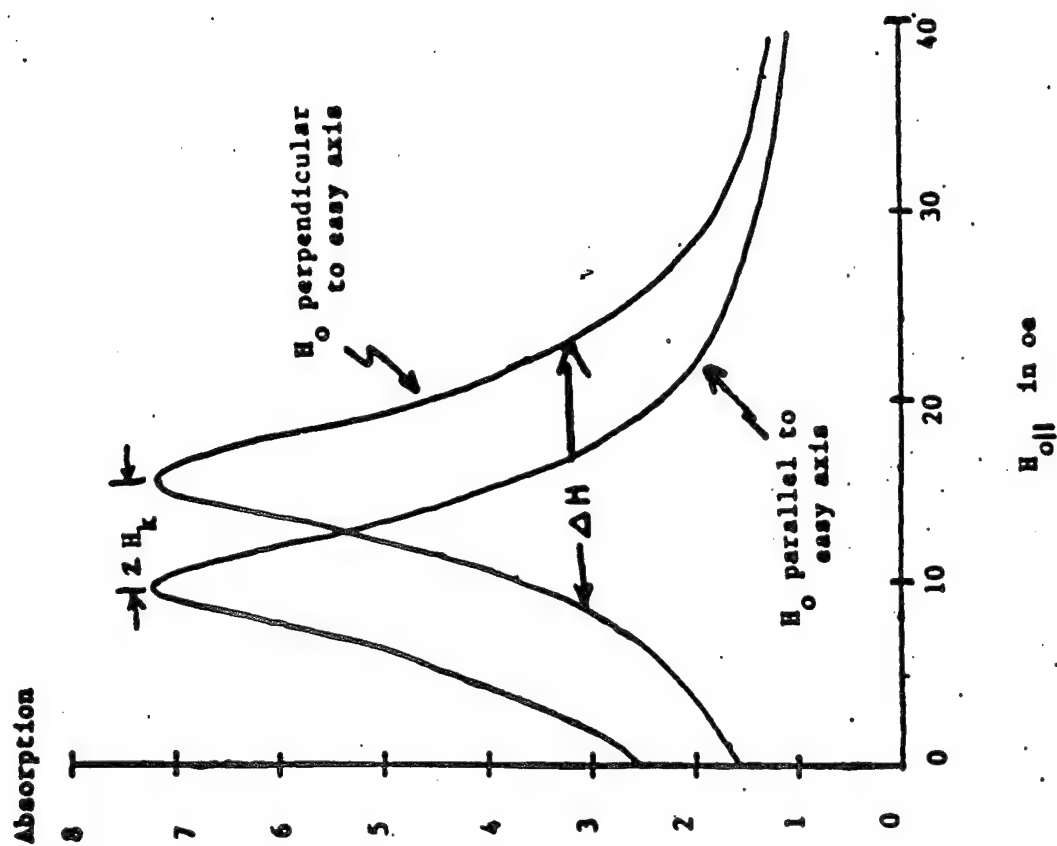
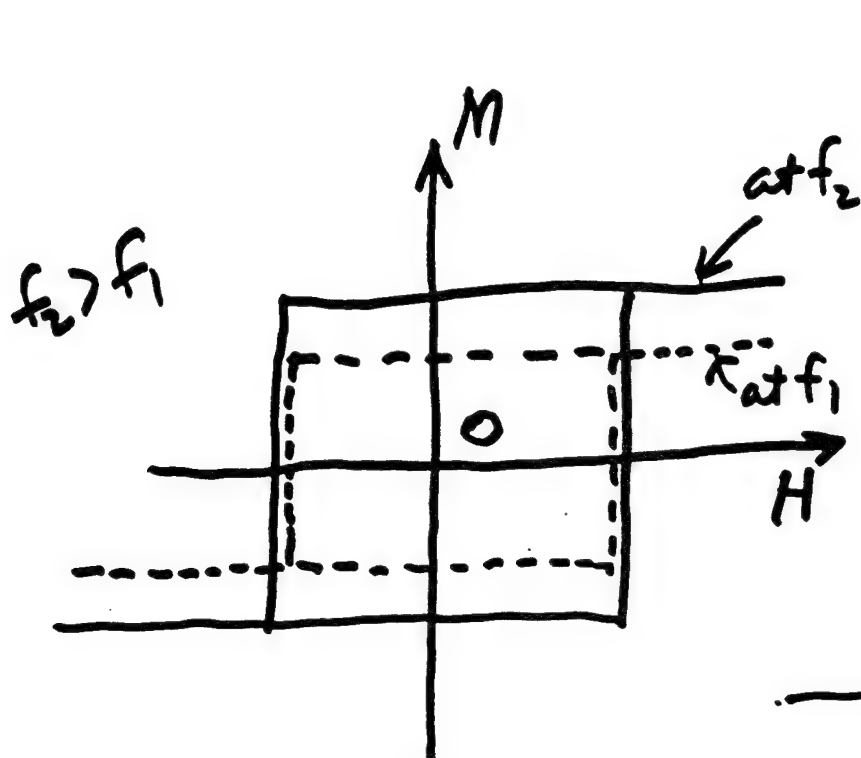
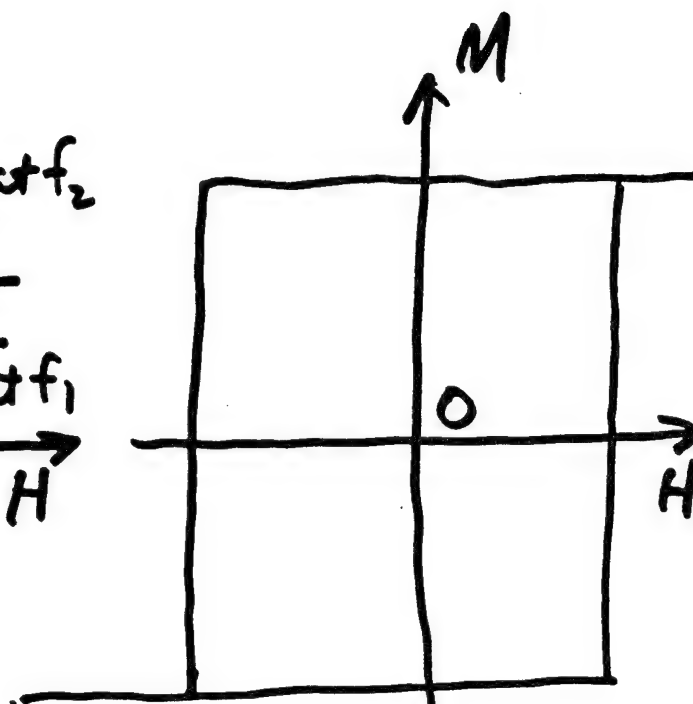


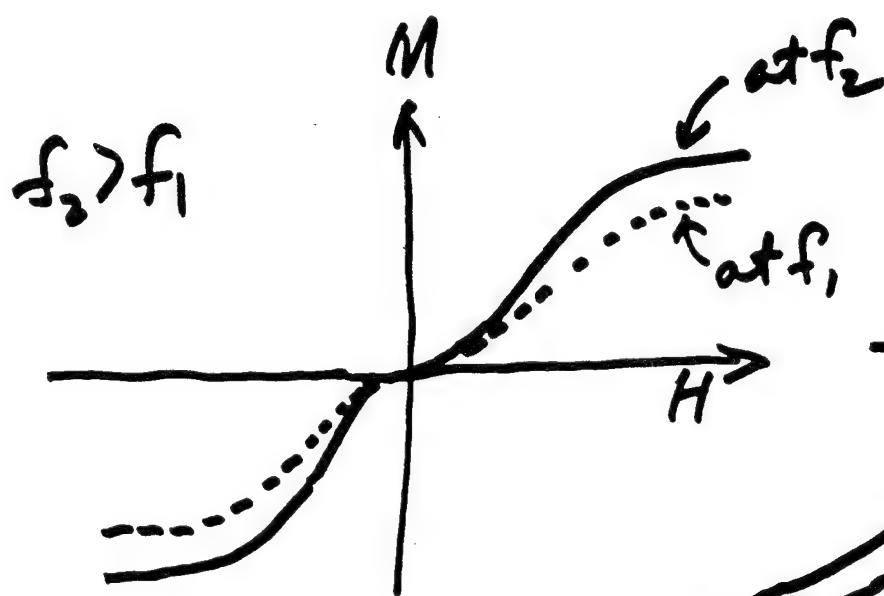
Fig. 3



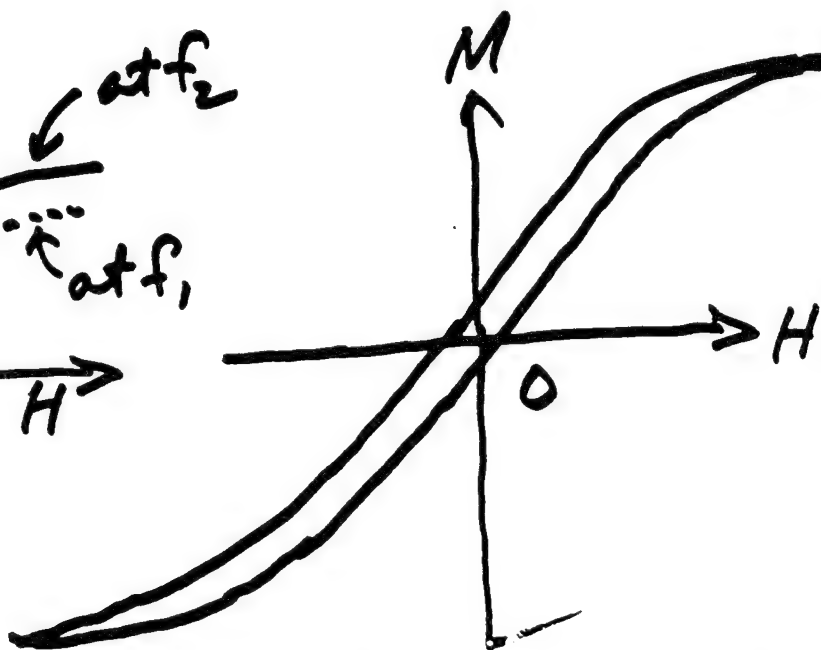
E.A. Loop from FMR



E.A. Loop from Loop or VSM



H.A. Loop from FMR

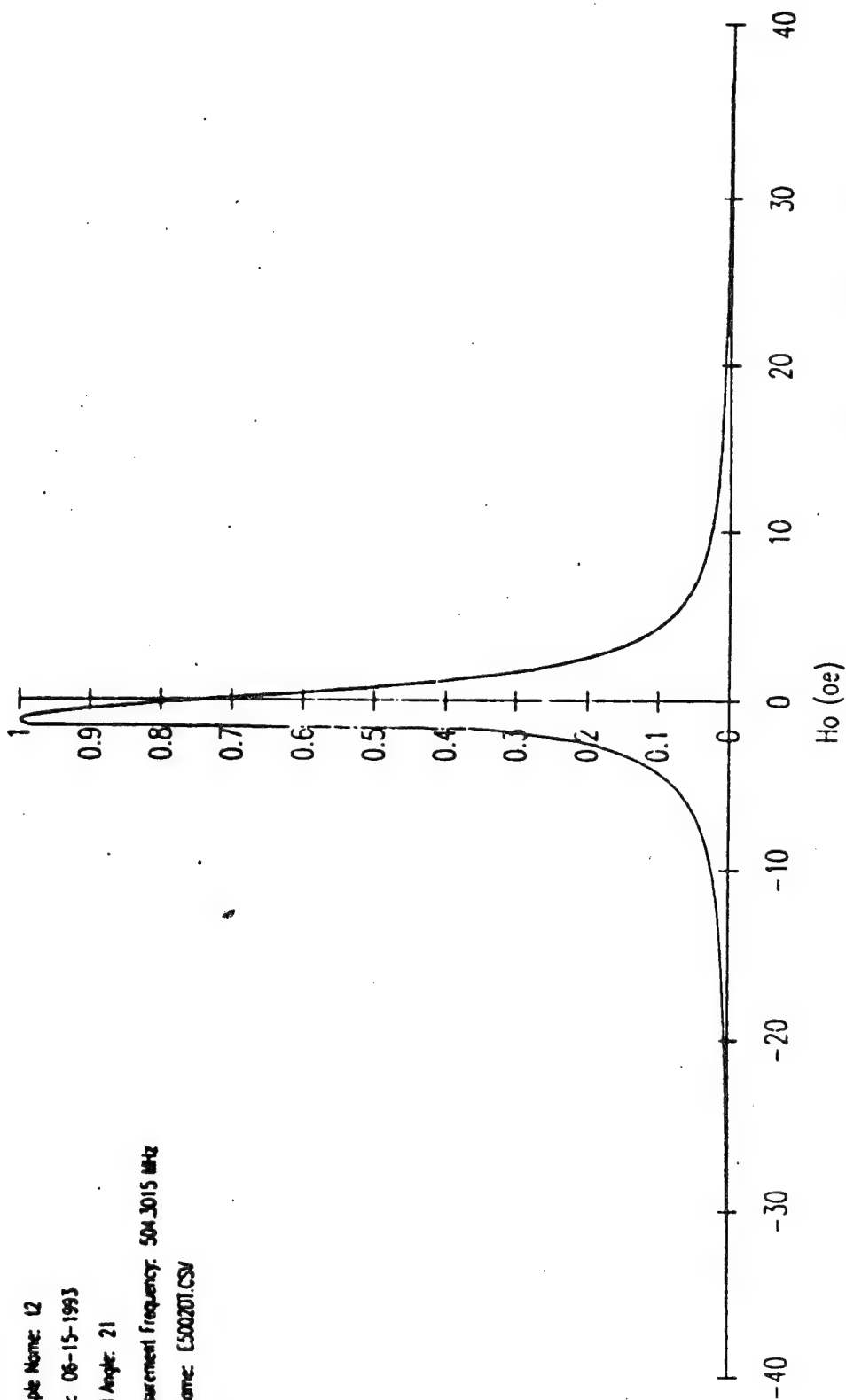


H.A. Loop from Loop or VSM

Im(Mu) vs Ho

Sample Name: L2
 Date: 06-15-1993
 Field Angle: 21
 Measurement Frequency: 504.3015 MHz
 Filename: L500201.CSV

Im(Mu) / (8piMs/Delta-H)

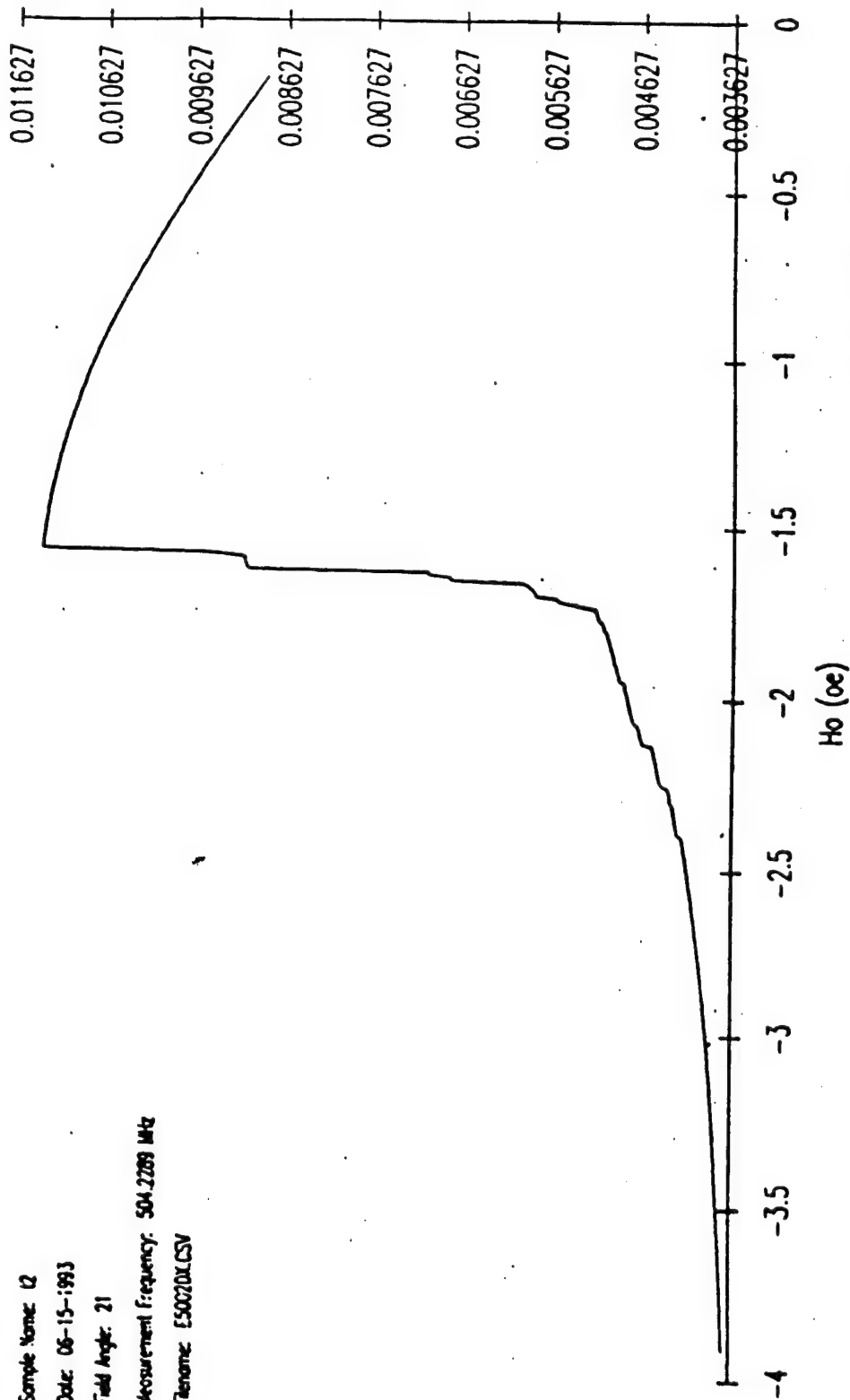


500-00 Associates - MOSS 103

Fig. 5

Absorption vs Field

Sample Name: 12
 Date: 06-15-1993
 Field Angle: 21
 Measurement Frequency: 504.2289 MHz
 Filename: E500201.CSV

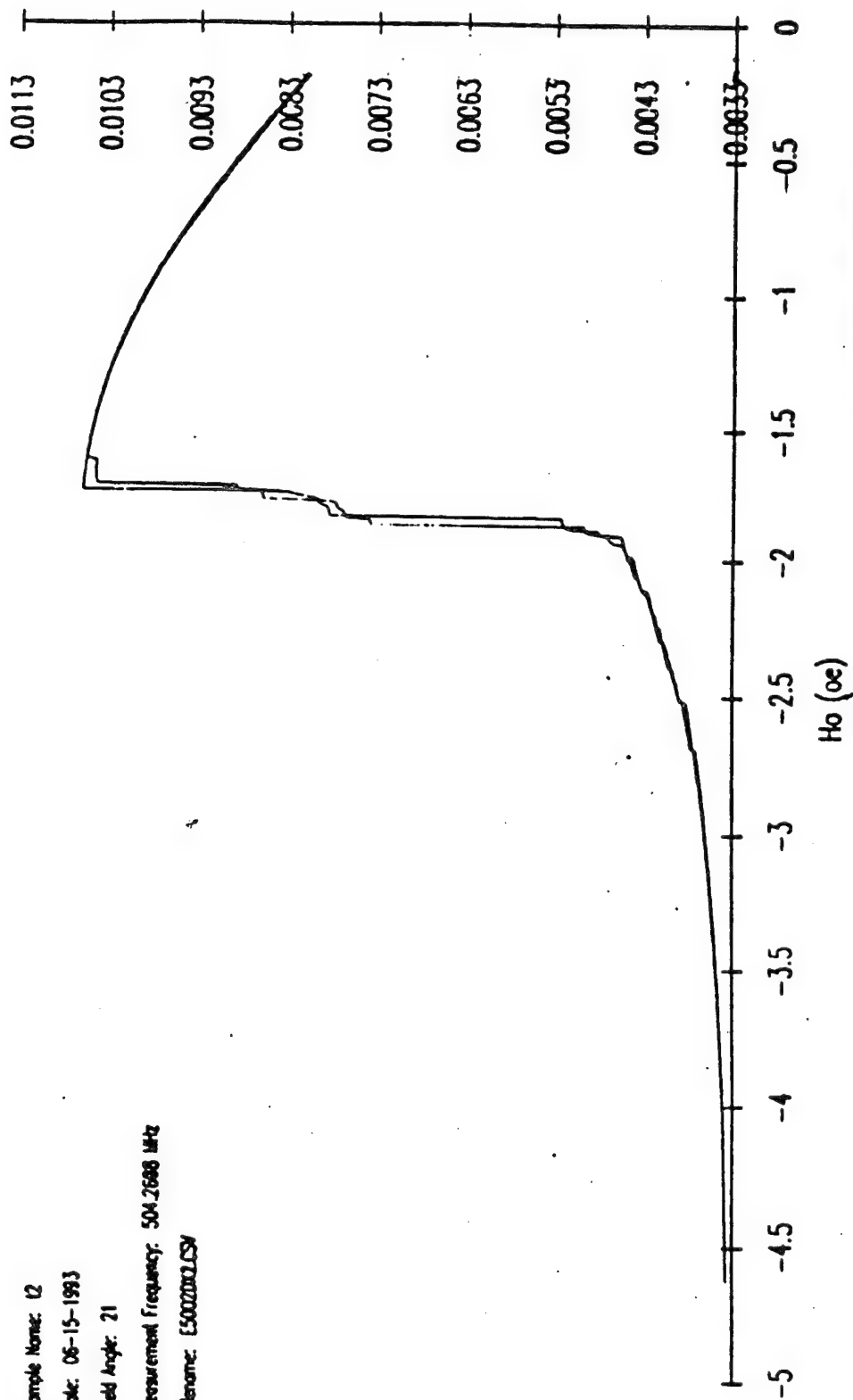


Sothos Associates - MDSS 103

Fig-6

Absorption vs Field

Sample Name: 12
 Date: 06-15-1993
 Field Angle: 21
 Measurement Frequency: 504.2688 MHz
 Filename: E5002001.CSV



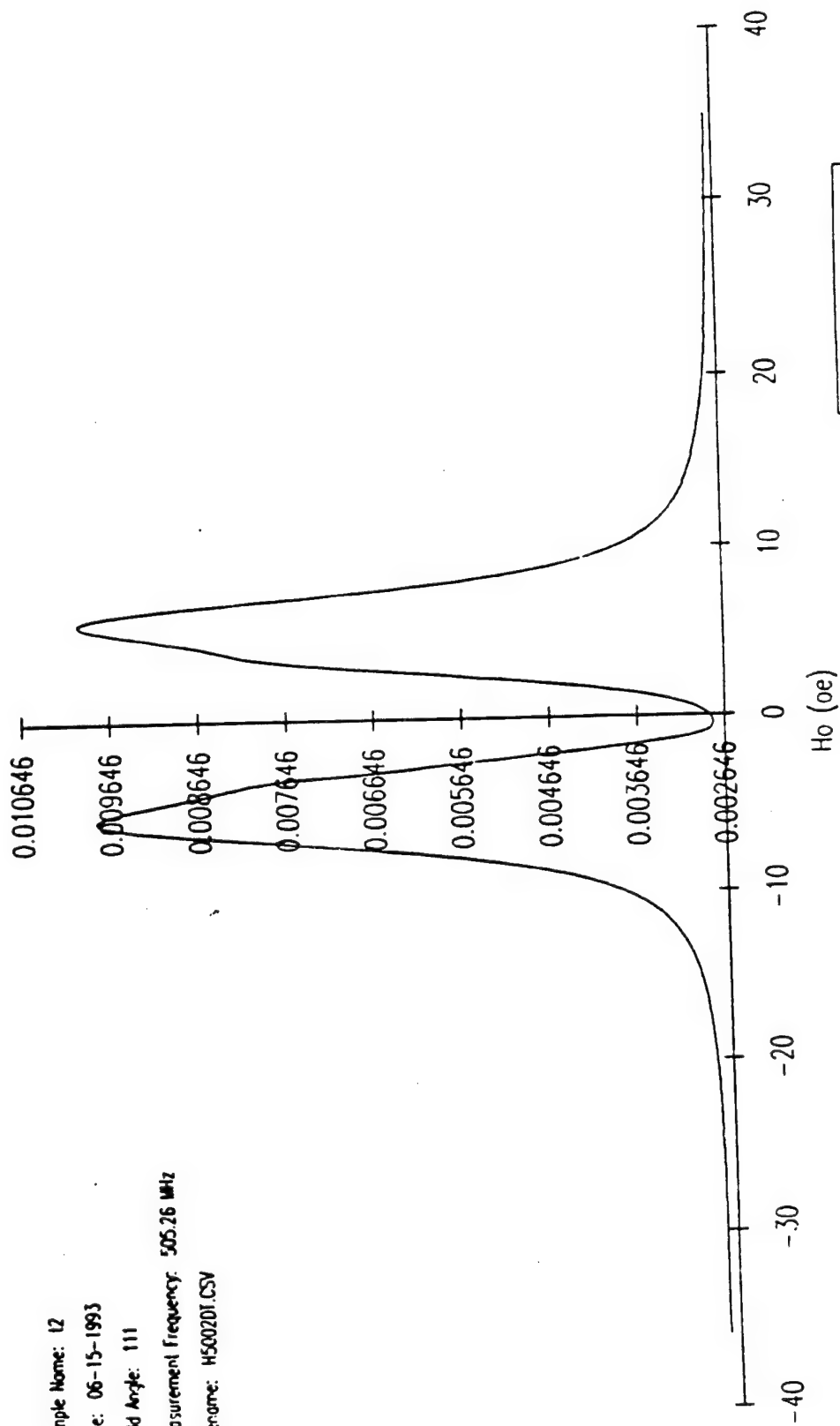
Sasha Associates - MESS ME

Fig. 7

Sample Name: 12
 Date: 06-15-1993
 Field Angle: 111
 Measurement Frequency: 505.26 MHz
 Filename: W500201.CSV

A b s o r p t i o n

Absorption vs Field



Sophoo Associates - MOSS 103

Fig. 8

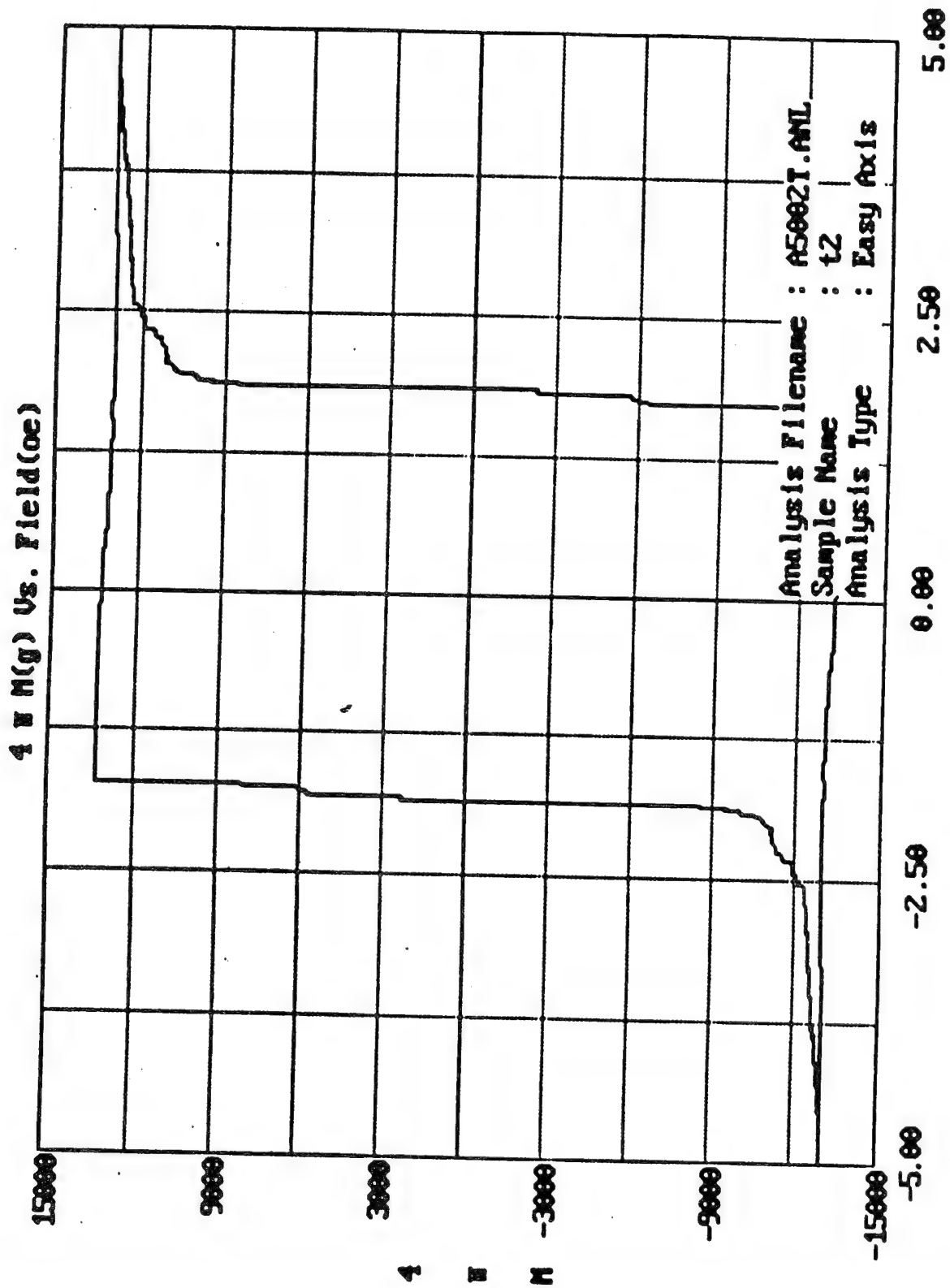


Fig. 9

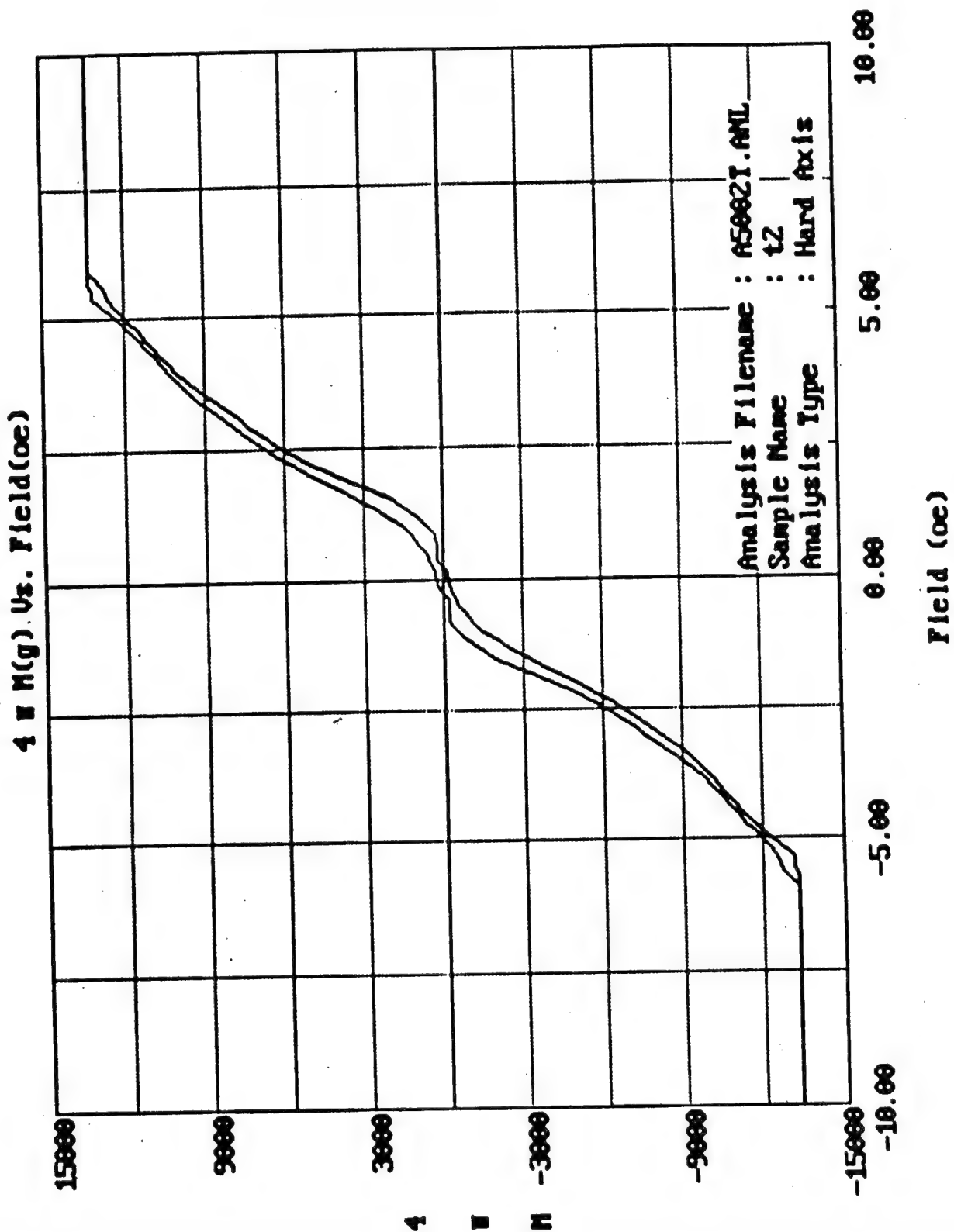
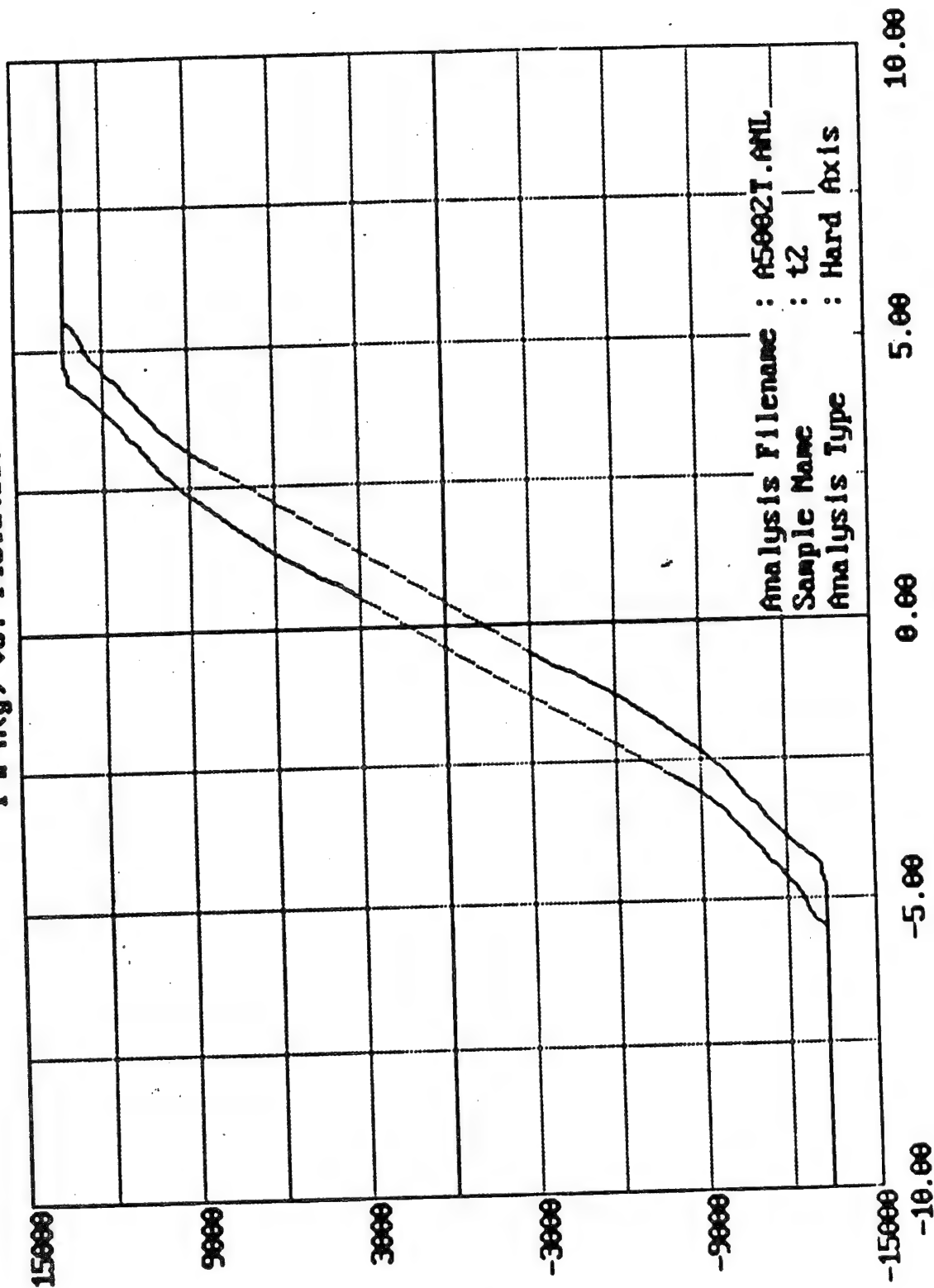


Fig. 10

4 H(g) vs. Field(oe)



Field (oe)

Fig. 11

Sample t₂, Permalloy

$$\times \delta H = 0.16 \text{ oe}$$

$$\Delta \delta H = 0.04 \text{ oe}$$

$$\odot \delta H = 0.4 \text{ oe}$$

$$4\pi M_s = 10 \text{ Kg}$$

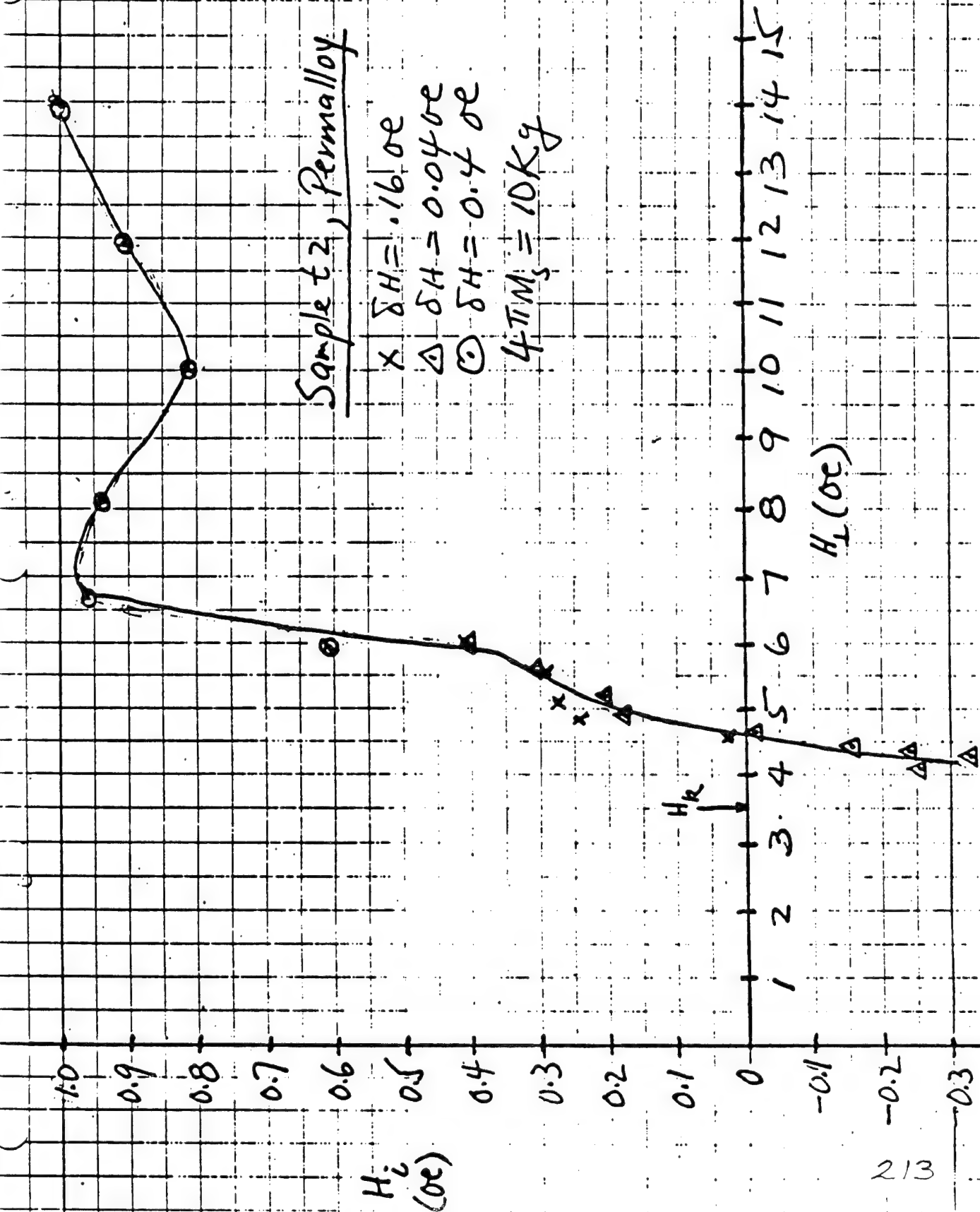
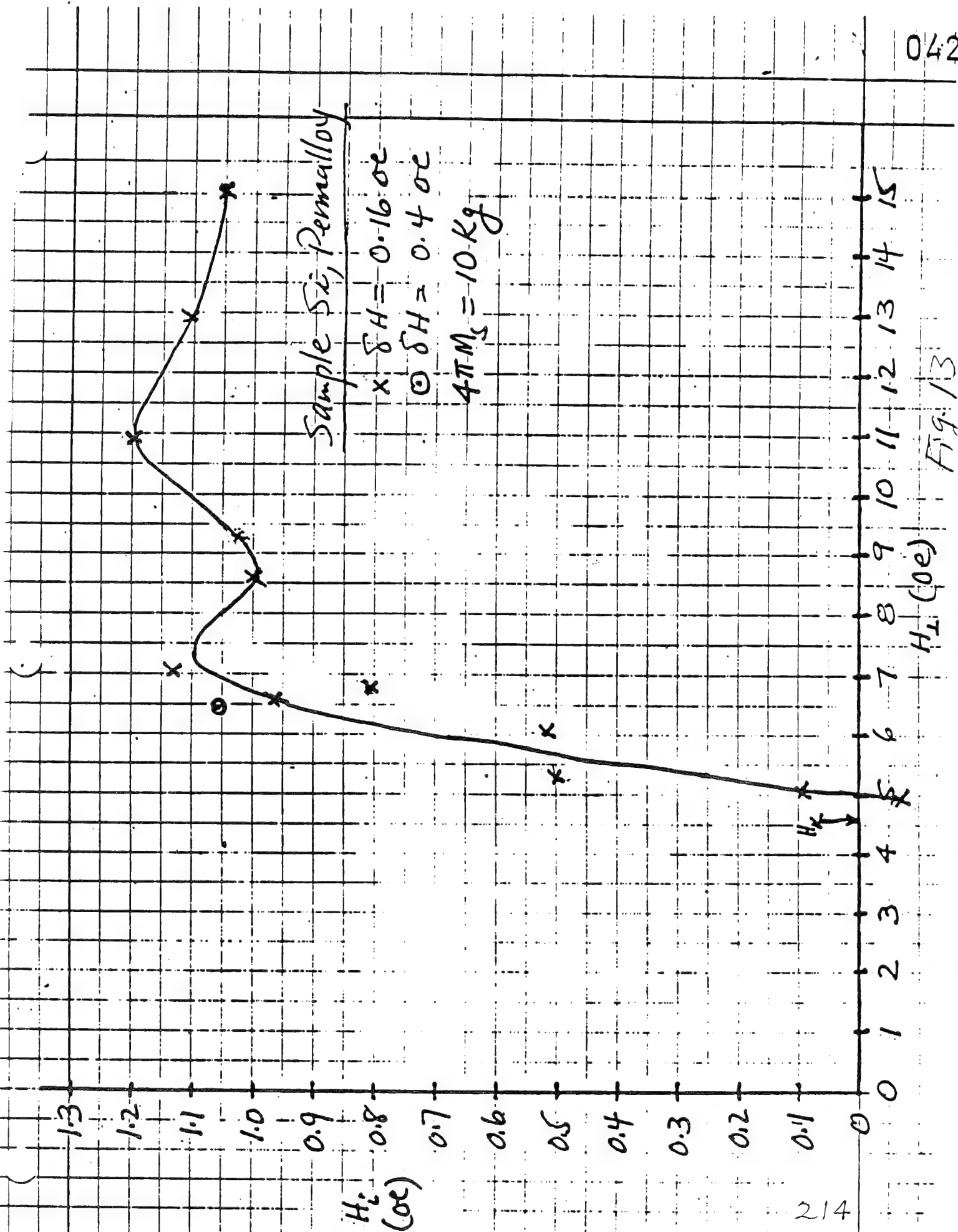
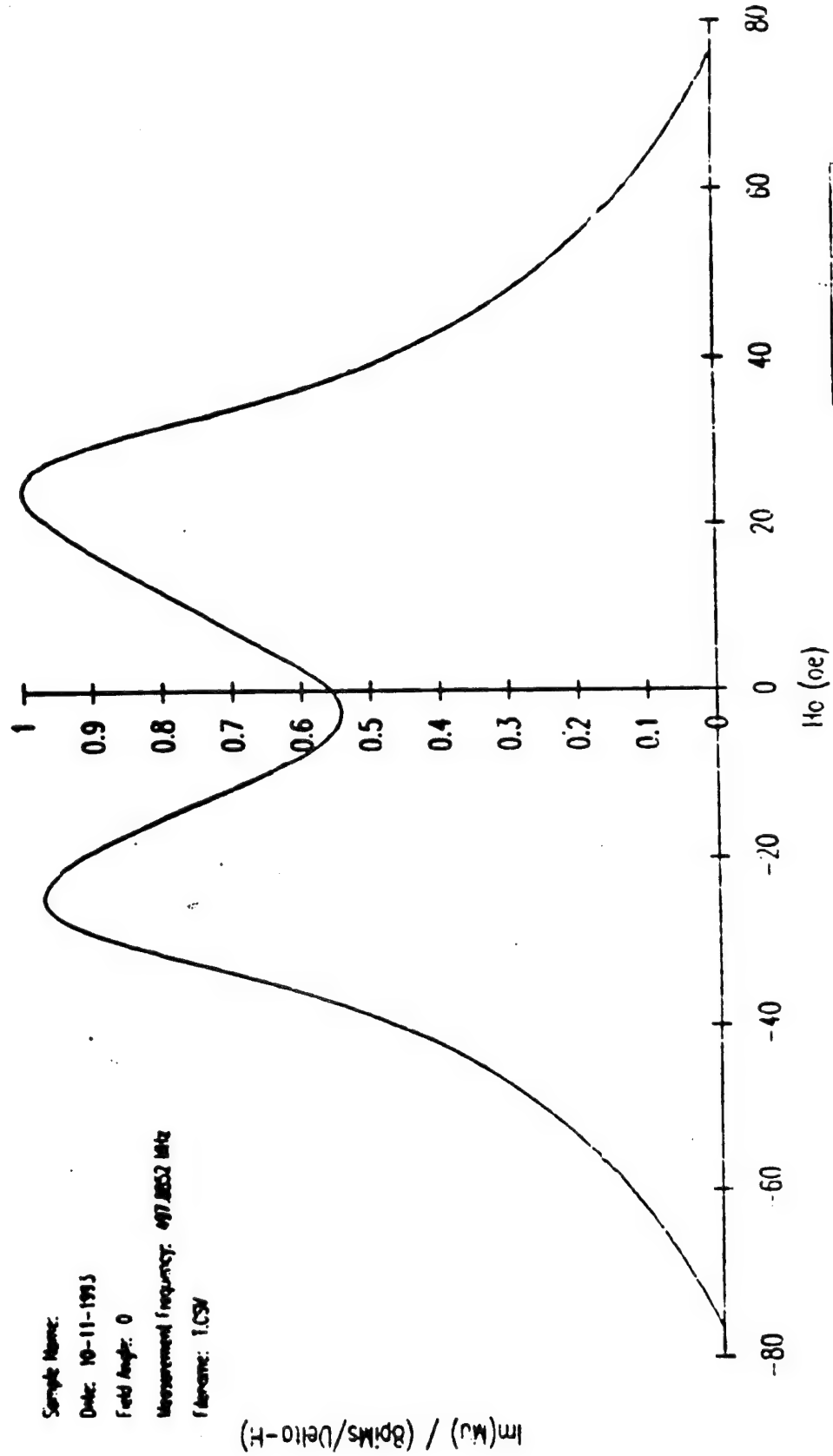


Fig. 12



$\text{Im}(\mu) \text{ vs } H_0$



Sootol Associates - MSS 103

Fig. 14

Sample Name:
Date: 10-11-1993
Field Angle: 0
Measurement frequency: 497.852 MHz
Fluxgate: 1CSU

$\text{Im}(\mu) / (\text{Gauss/Volt-H})$

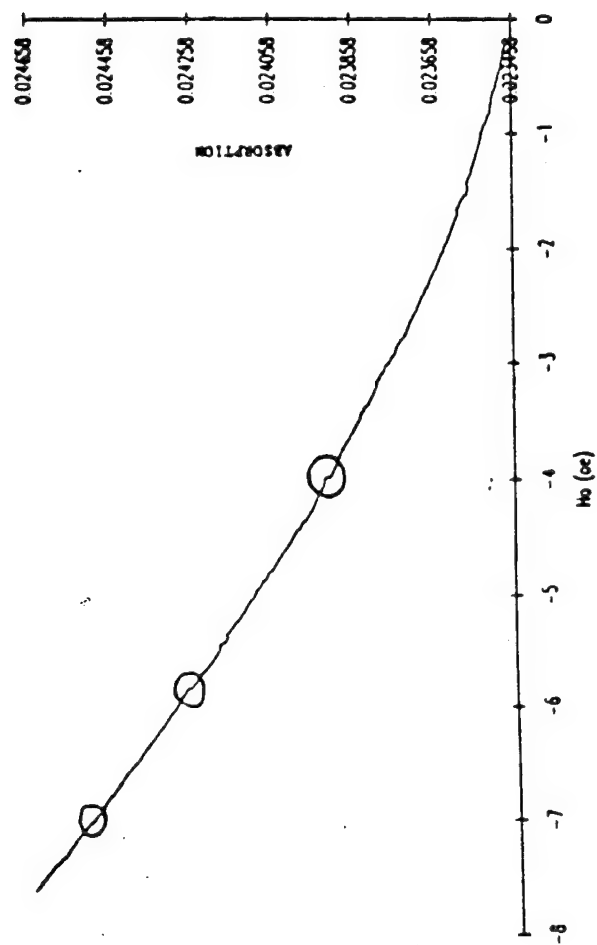
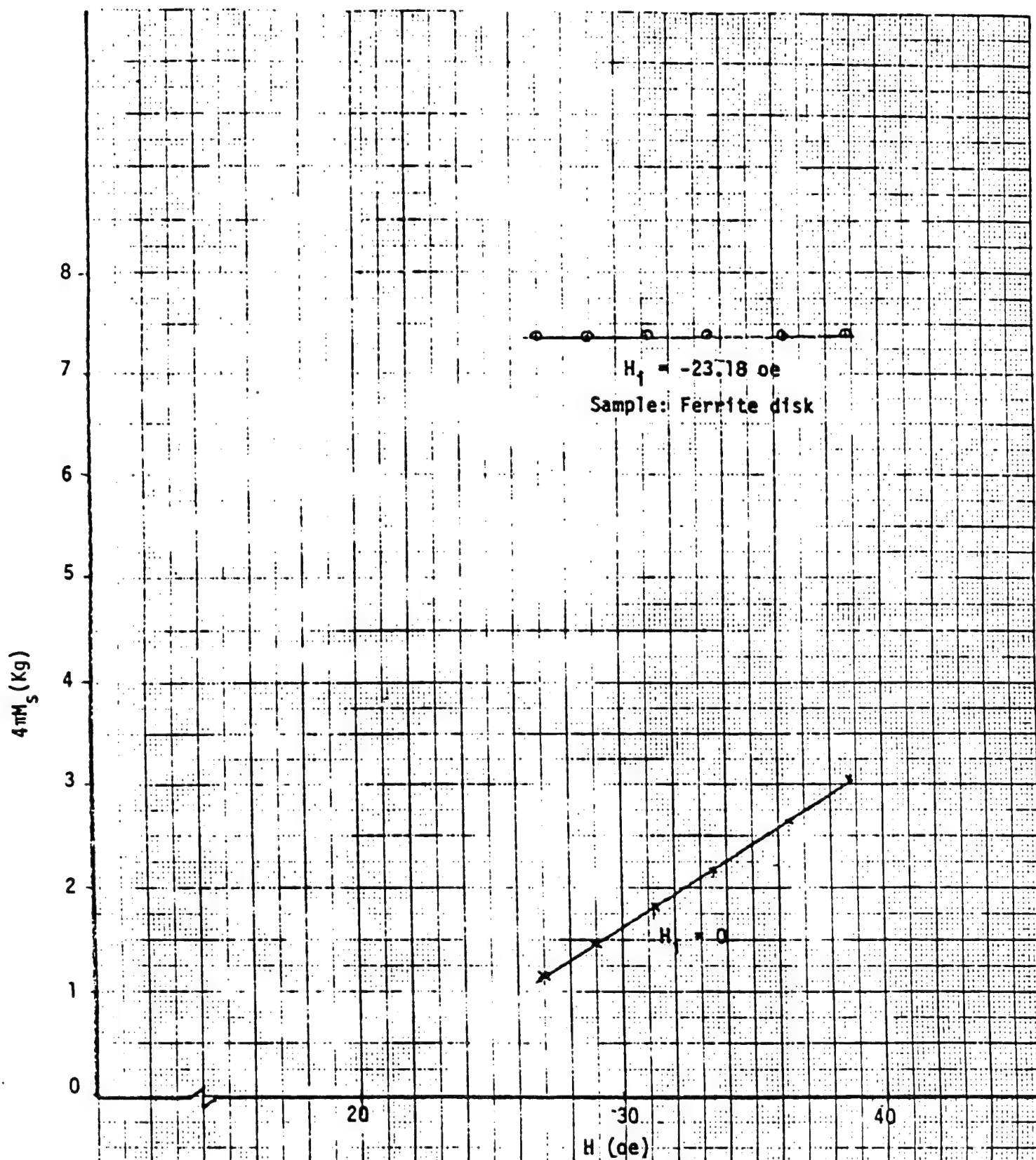


Fig. 15



Origin of Internal Field

- (1) Anisotropy Axes Distribution
- (2) Poles at grain boundaries & pores

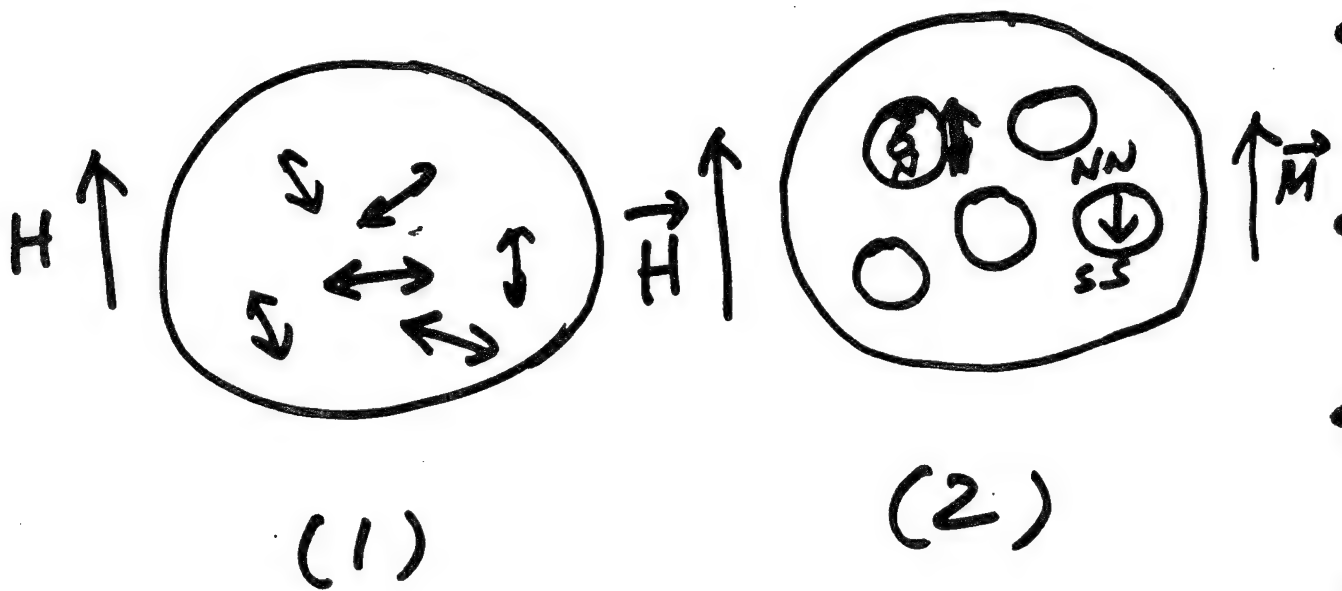


Fig. 17

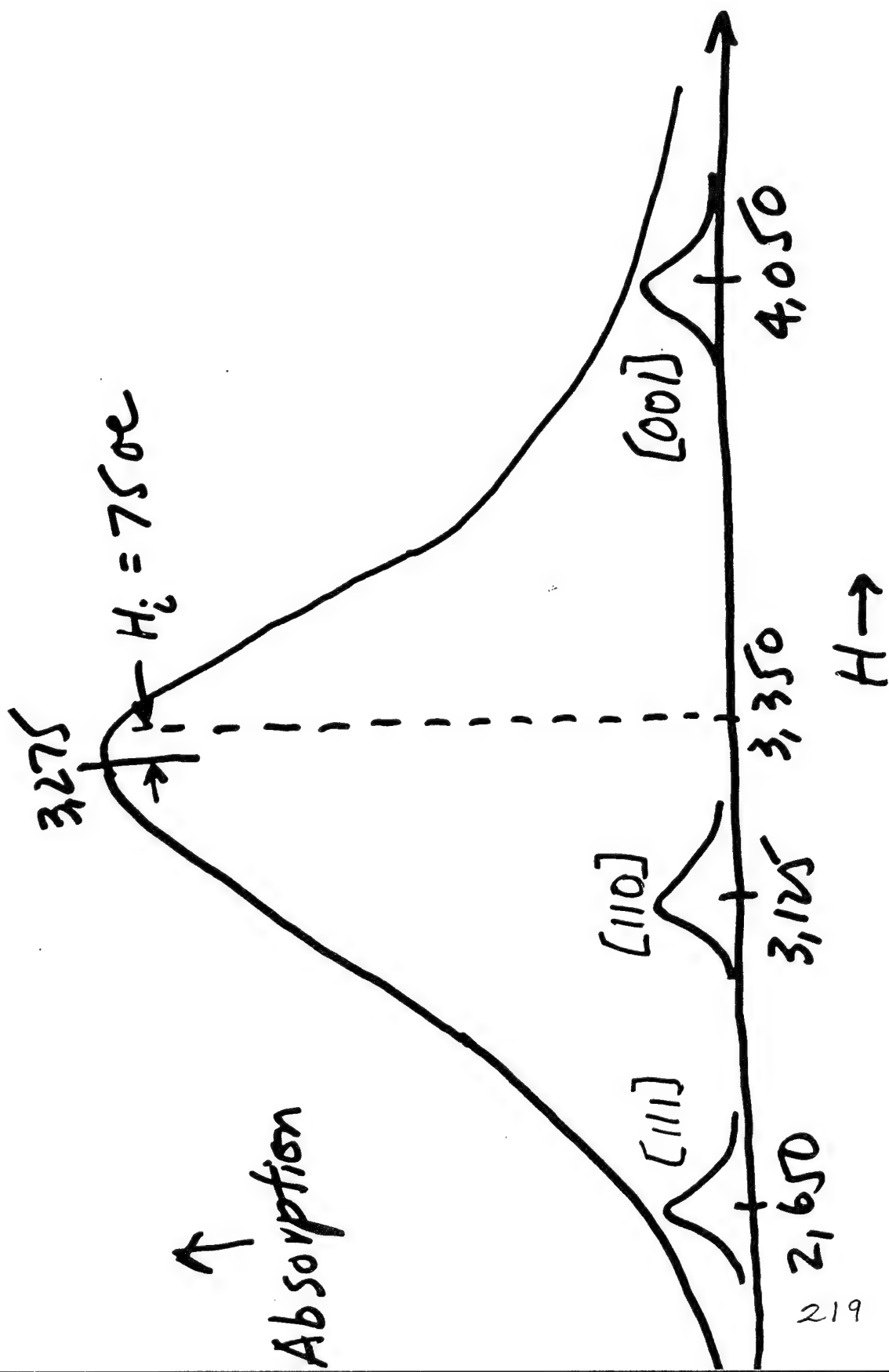


Fig. 18

$$W = \gamma (H + H_i)$$

(a) Where for randomly-oriented noninteracting spherical Xallites with Cubic anisotropy



$$W = \gamma \left(H - \frac{K_1}{2M_s} \right)$$

(b) For spherical samples with spherical hole & no Xalline anisotropy

$$H_i = \frac{4\pi}{3} M_s \left(\frac{V}{V_s} \right)$$

where V = volume of cavity

V_s = " " sample

CRITICAL BEHAVIOR OF MAGNETIC DOMAINS

H. SUHL

University of California, San Diego

- I. Ordered systems, with a continuous degree of symmetry, invariably exhibit a singular response to a perturbation coupling to the degree of freedom with that symmetry. (Goldstone mode.) A very simple case is a ferromagnet without any kind of anisotropy: The direction of its magnetization can be changed continuously without changing the energy of the system. Correspondingly the transverse susceptibility at low field diverges as the field tends to zero. In symbols:

$$\vec{M} = \vec{H} / |\vec{H}|$$
$$\vec{H} = \vec{H}_0 + \vec{h}, \quad \vec{M} = \vec{M}_0 + \vec{m}$$

To lowest order in h

$$\vec{m} = \vec{h} / |H_0|, \quad dm/dh = 1/|H_0|$$

which goes to infinity as the biasing field goes to zero. A slightly more elaborate argument shows that the longitudinal susceptibility likewise diverges.

- II. In the case of a magnetic sample with domain walls (i.e. a sample in a subsaturating external field) there is likewise "very nearly" a continuous symmetry: the positions of the domain walls. Neglecting interaction between them, as well as pinning, they can be moved without changing the energy. The magnetization component along the field, on the other hand, can change as the result of wall motion. The response is usually quoted as a response to an internal magnetic field. In an obvious notation:

$$H_i = H_e - N_z M$$

$$\chi_e = dM / dH_e = (dM / dH_i) (dH_i / dH_e)$$

$$= \chi_i (1 - N_z \chi_e)$$

$$\chi_i = \chi_e / (1 - N_z \chi_e)$$

So if the measured χ_e equals $1 / N_z$ then χ_i is infinite

- III. The following is a sketch of a possible theory that should lead to the correct critical index α in the observed law $\chi_i \propto 1/h^\alpha$.

Hamiltonian:

$$\mathcal{H}(M) = \int d^3x \{ -\vec{H}_e \cdot \vec{M}(x) + \mathcal{H}_{dip} + \mathcal{H}_{exch} \}$$

Partition function :

$$Z = \int \Pi dM(x) e^{-\beta \mathcal{H}}$$

Constrained Partition function well below T_c :

$$Z' = \int \Pi dM(x) e^{-\beta \mathcal{H}} \delta(\vec{M} - \int d^3x \vec{M}(x)) \Big|_{\langle \vec{M}(x) \rangle = M_{sat}} \\ = e^{-\beta F(\vec{M})}$$

$$\text{where } F(\vec{M}) = -\vec{H}_e \cdot \vec{M} + \frac{1}{2} \vec{M} \mathbf{N} \vec{M} - k_B T S(\vec{M})$$

\mathbf{N} and S depend only weakly on T and \vec{H}_e and an expansion of S starts with terms of fourth order in the components of \vec{M} .

The first two terms give the infinite susceptibility below saturation, but the last term should give a finite result $\propto 1/h^\alpha$ at small but finite h .

IIIa. The unrenormalized result might be as follows:

Cylindrical Symmetry around an external field in the z-direction.

$$F = -H_e \cdot M_z + \frac{1}{2} N_z M_z^2 - k_B T S(M_z)$$

Mean field theory: $dF/dM_z = 0$, that is

$$H_e = N_z M_z - k_B T dS/dM_z$$

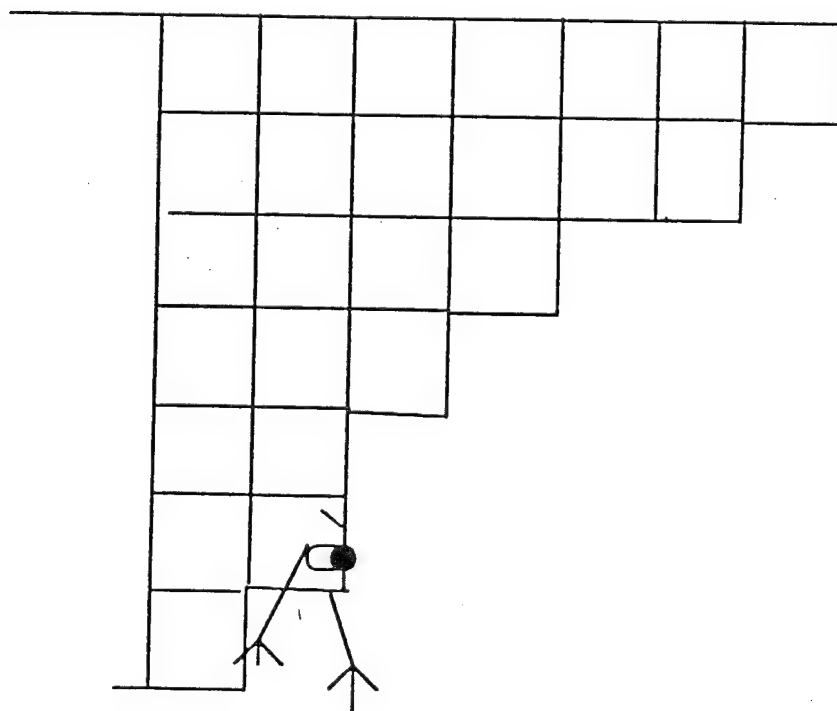
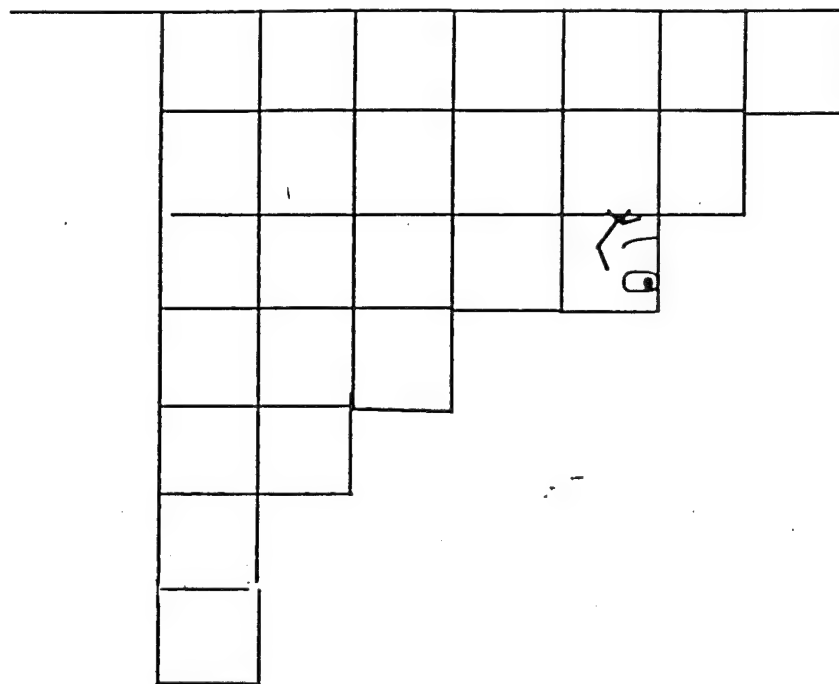
so if S is neglected, $\chi_e = 1/N_z$, $\chi_i = \infty$

If leading term in S is $-\frac{1}{4} a M_z^4$, then since

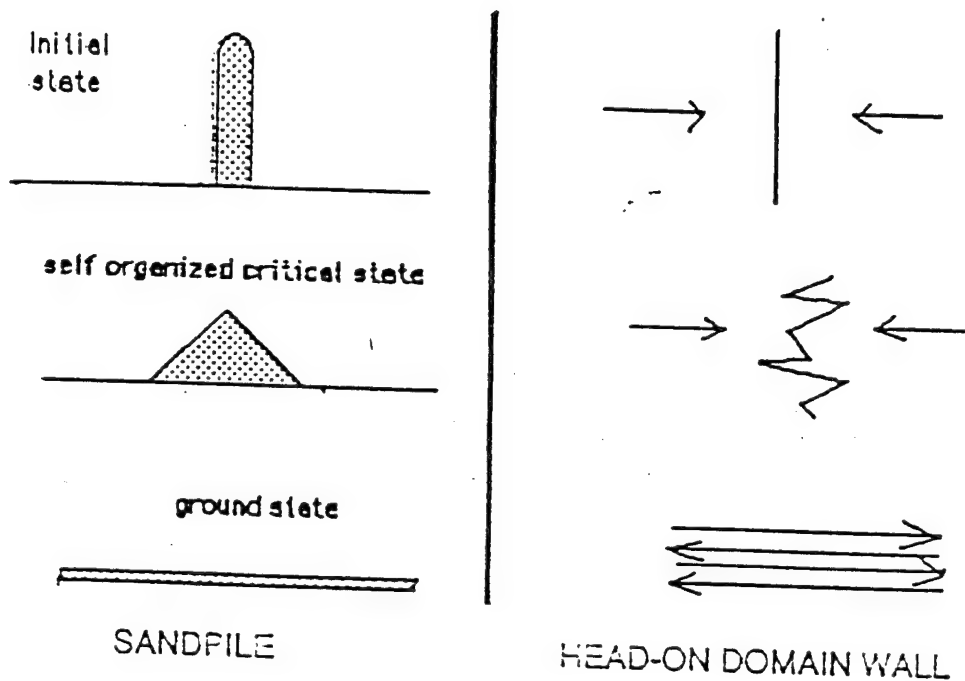
$H_i = H_e - N_z M_z$, we get

$$M_z = (H_i / (k_B T a))^{1/3}, \quad \chi_i = \frac{1}{3} \left(\frac{1}{H_i \sqrt{k_B T a}} \right)^{2/3}$$

- IV. The genesis of a zigzag pattern of the domain wall in a recording tape has certain common features with the behavior of idealized sandpiles:

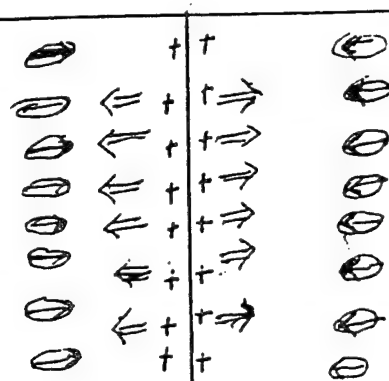




V.



Formation of zig-zag domain wall in a film of particles with easy axis aligned perpendicular to the narrow dimension of film, and with uniaxial anisotropy field less than $4\pi M$. The magnetization gets 'stuck' in a random, but essentially unchanging domain wall configuration.

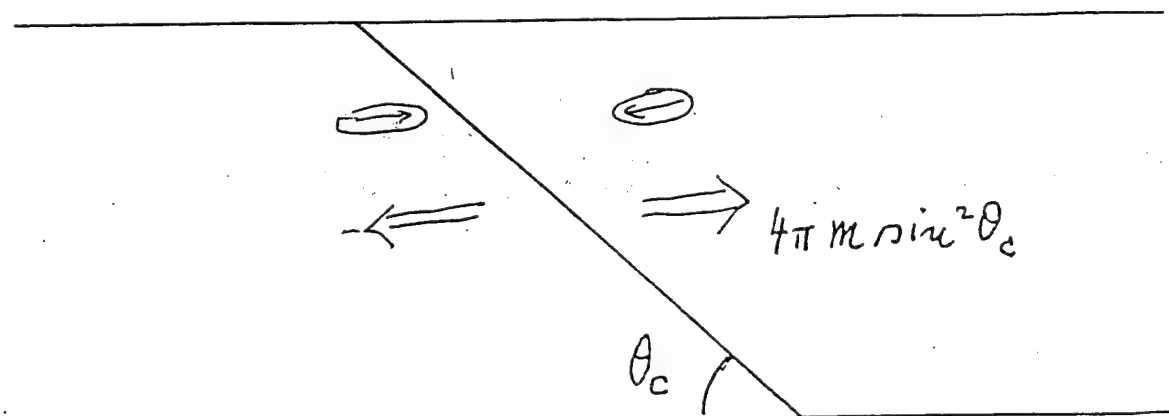
Va.



 Magnetic particle  with magnetization \rightarrow
 lined up along easy anisotropy axis

\Rightarrow Magnetic field generated by magnetic
 $H = 4\pi M$ pole accumulation at domain wall,

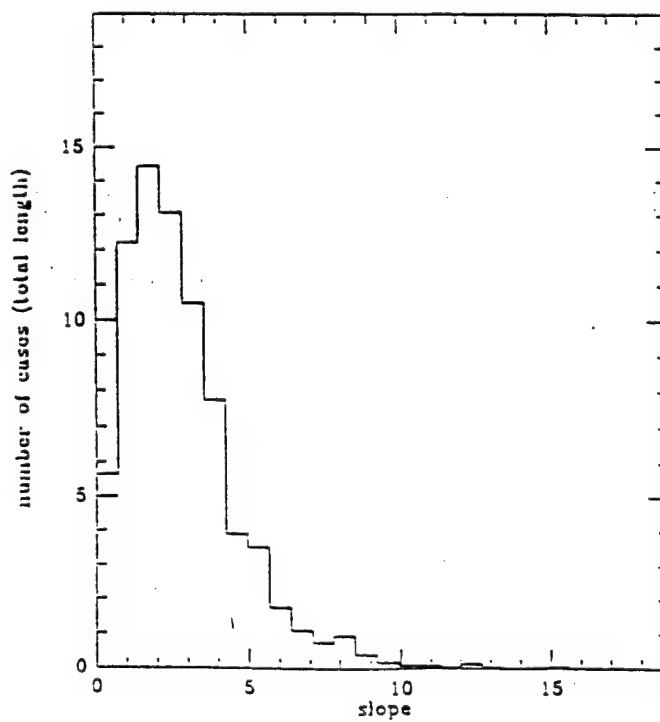
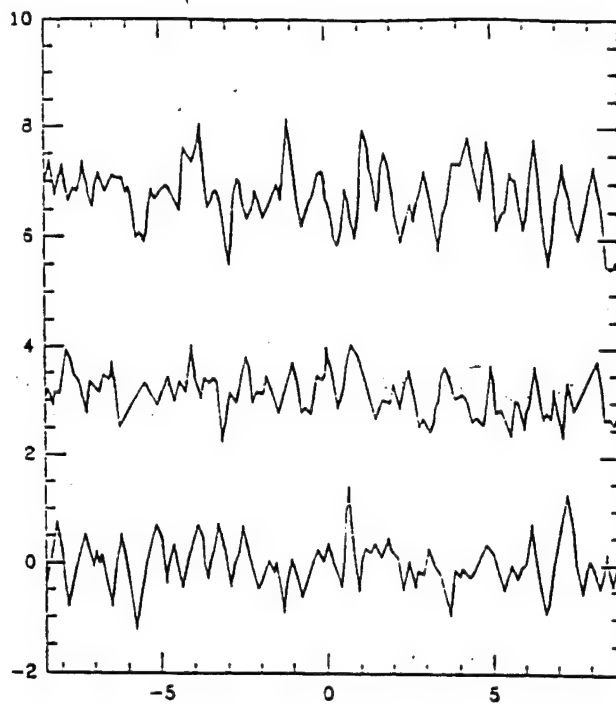
UNSTABLE IF $H > H_{\text{anisotropy}}$ (or $\frac{H_{\text{anis.}}}{4\pi M} < 1$)



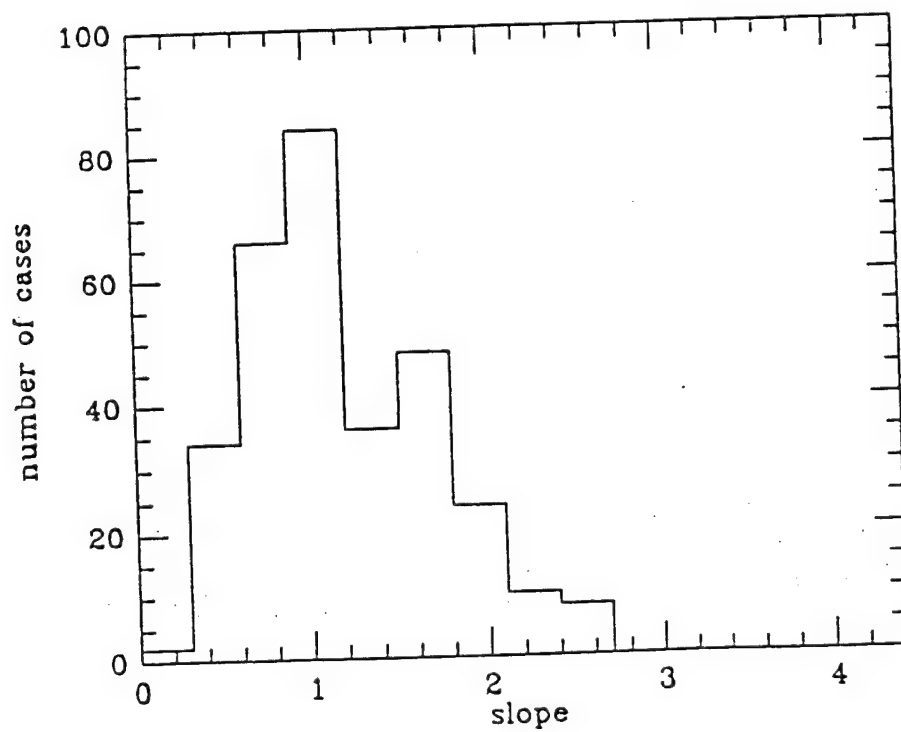
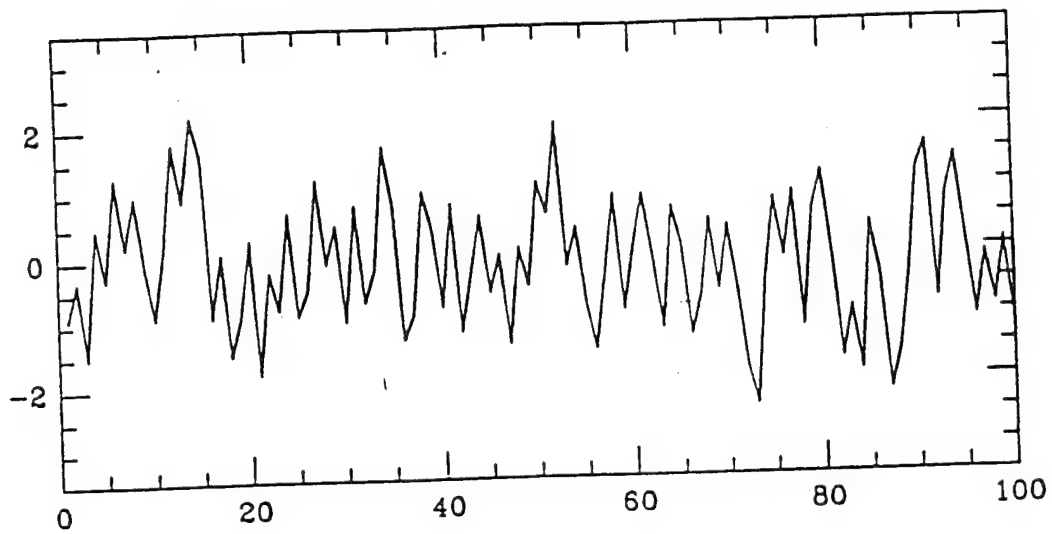
Just stable when $\sin^2 \theta_c = \frac{H_{\text{anis.}}}{4\pi M}$

Increasingly stable with further decrease of θ

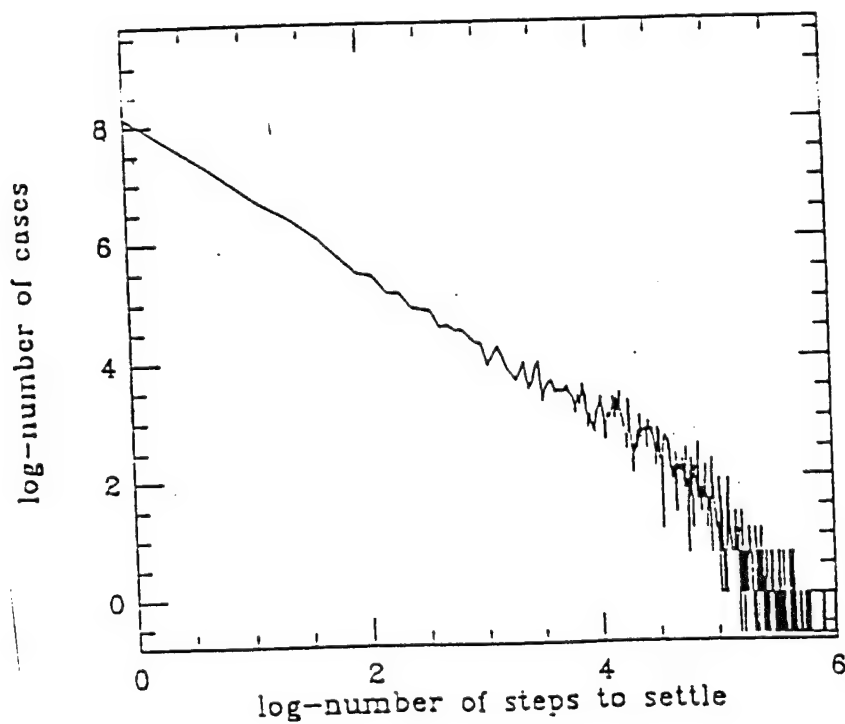
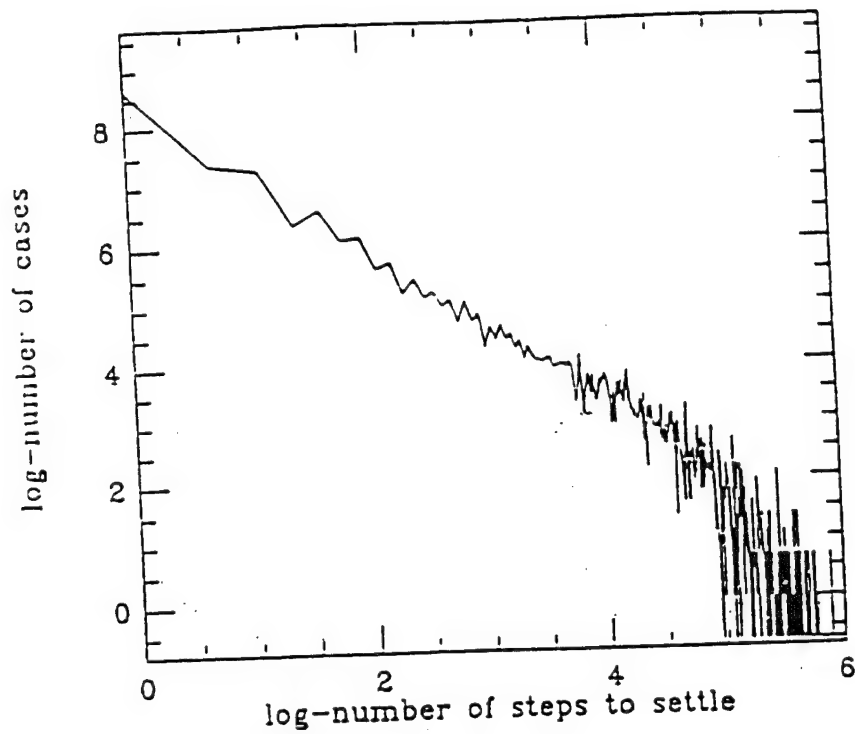
VI. Observations: Arnoldussen & Tang, IEEE Trans. Mag. 22, 889, 1986.



VII. Simulation results:



VIII. Response (probability of settling down after a given number of elementary steps) follows a power law in the infinite tape.



IX. Finite Size Scaling:

SCALING OF THE TAIL OF THE DISTRIBUTION.

THE UNIVERSAL SLOPE PERSISTS OVER TWO TO THREE DECADES, BUT AT THE HIGH END (RARE, LONG- LASTING AVALANCHES) THE CURVES FOR DIFFERENT ANISOTROPIES AND SAMPLE SIZES PART COMPANY. HOWEVER, WE CAN SCALE THE RESULTS WITH RESPECT TO THESE PARAMETERS SO THAT THE CURVES ONCE AGAIN COINCIDE APPROXIMATELY. (THIS IS KNOWN AS FINITE-SIZE SCALING.) IN THE MOST FAMILIAR PROBLEMS, THERE IS ONLY ONE PARAMETER, THE SIZE L .

IXa.

IN THE PRESENT CASE, WE HAVE TWO-PARAMETER SCALING , WITH RESPECT TO THE LENGTH, L , OF TAPE SEGMENT, AND S , THE CRITICAL SLOPE.

WE FIND THE SCALING LAW

$$P(N;S,L) = \frac{B}{S^{\gamma}} g_2(nS^{-\beta}; LS^{-\delta})$$

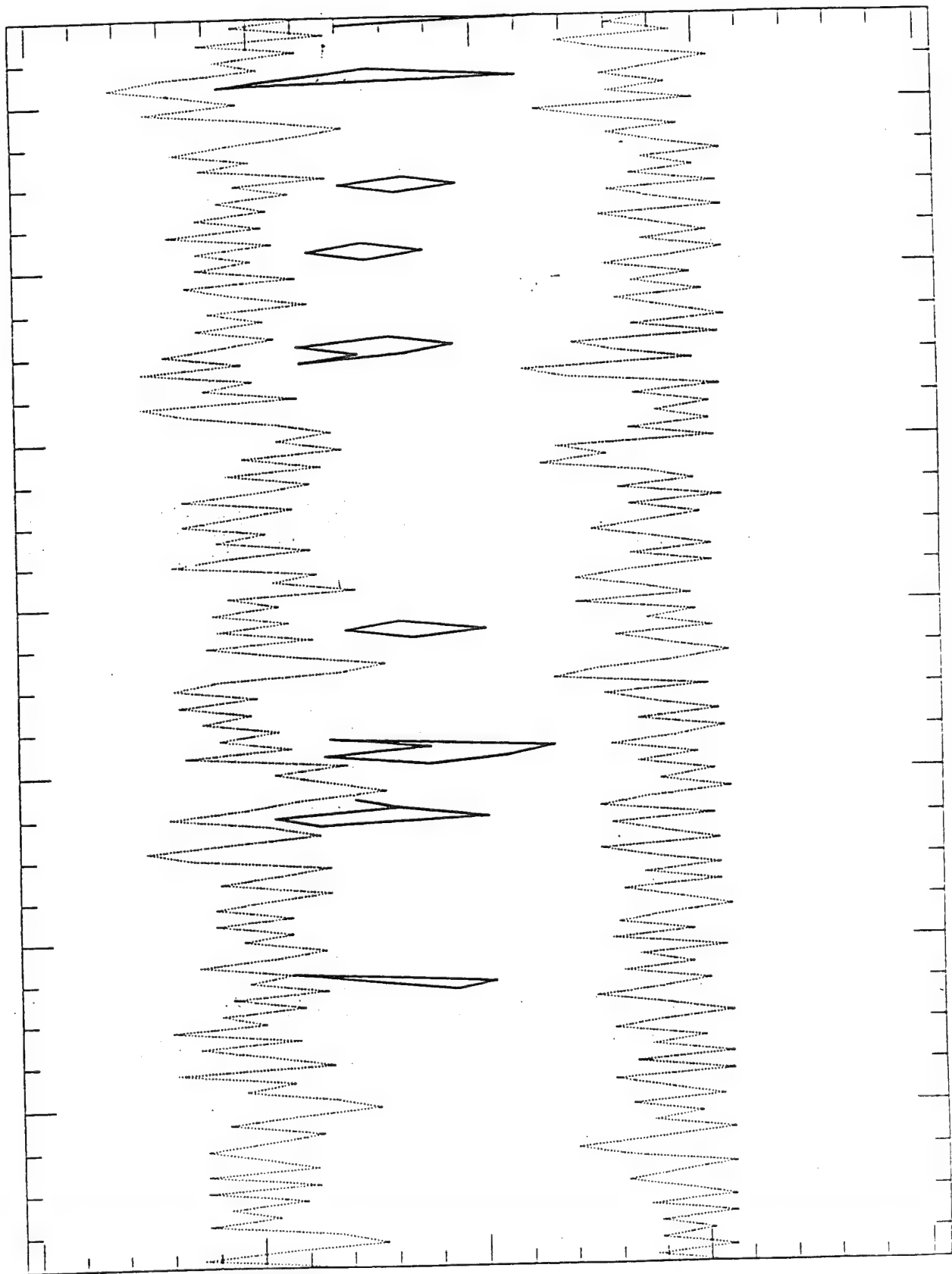
$$g_2(x;y) = x^{-\alpha} e^{-x^2(1+Cy^{-\epsilon})^2}$$

AND B AND C ARE CONSTANTS AND $\gamma = \alpha\beta$,

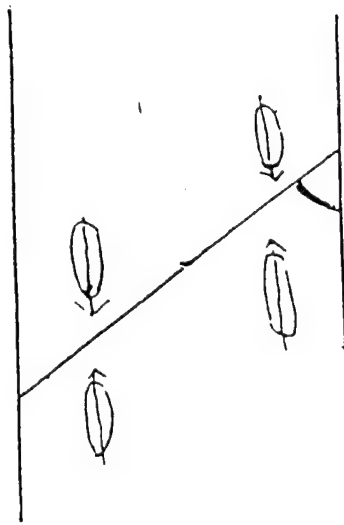
$\delta = \beta/\epsilon$. THE INDEPENDENT CRITICAL INDICES ARE

$$\alpha = 1.1, \quad \beta = 1.51, \quad \epsilon = 1.8$$

- X. Difficulty of complete DC erasure of signal using the same algorithm as in construction of the zigzag:
Initial signal = reversed magnetization between the two dotted zigzag lines
Final signal = remaining lozenge-shaped island after application of very large dc field opposing the magnetization direction between the two zigzags.

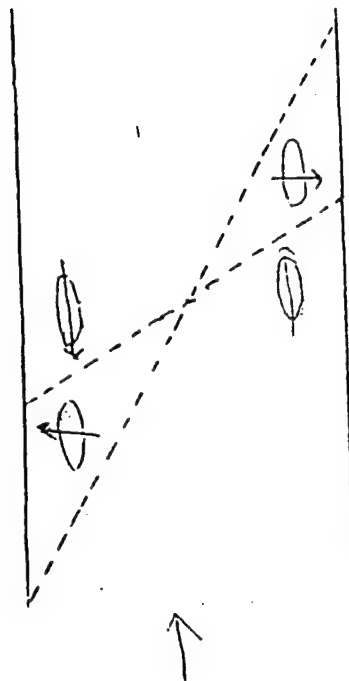


Initial State

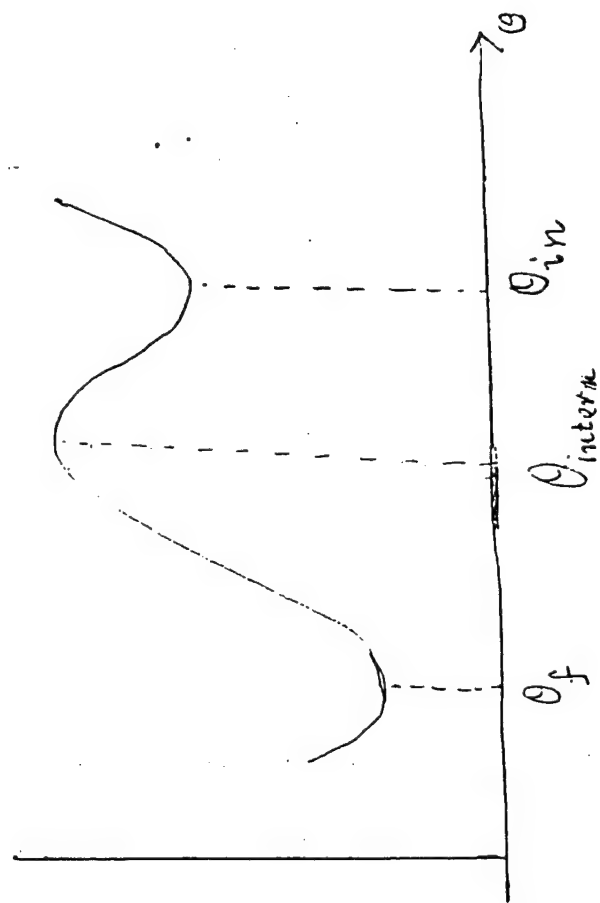
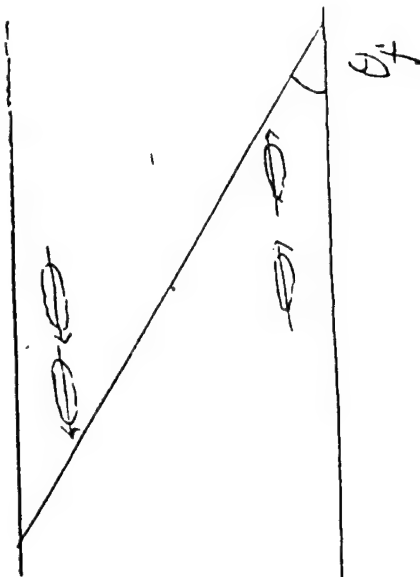


$$\theta_c < \theta_{in}$$

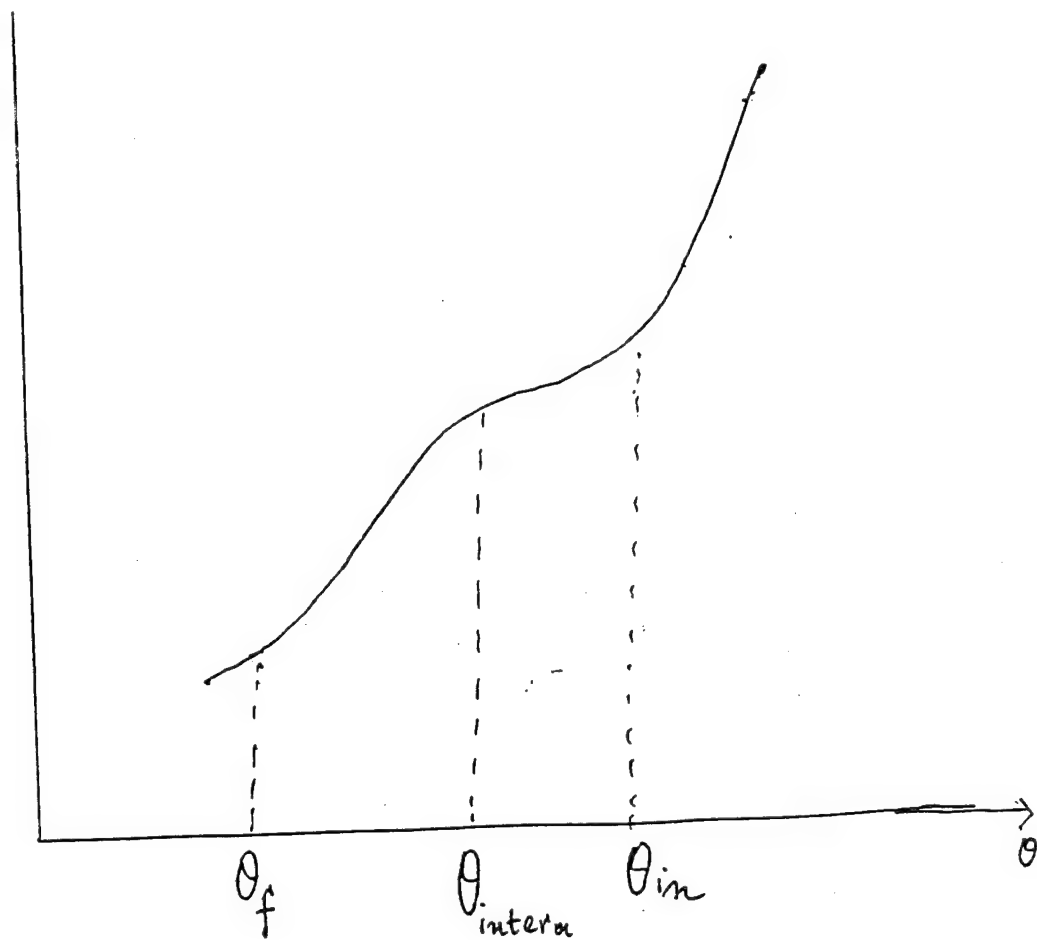
Intermediate state



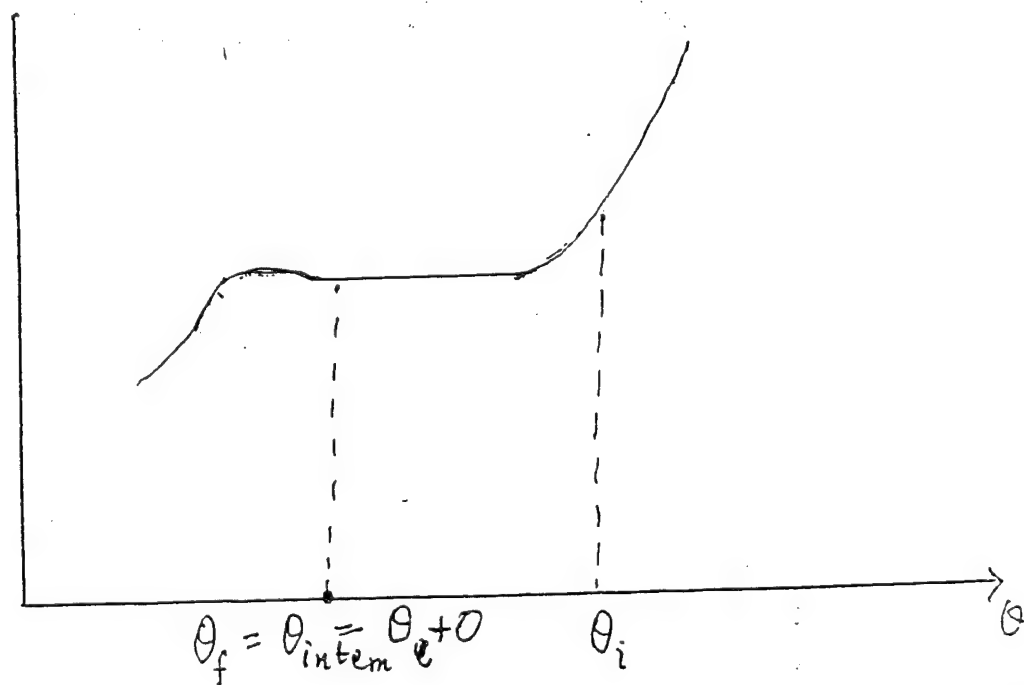
Final State



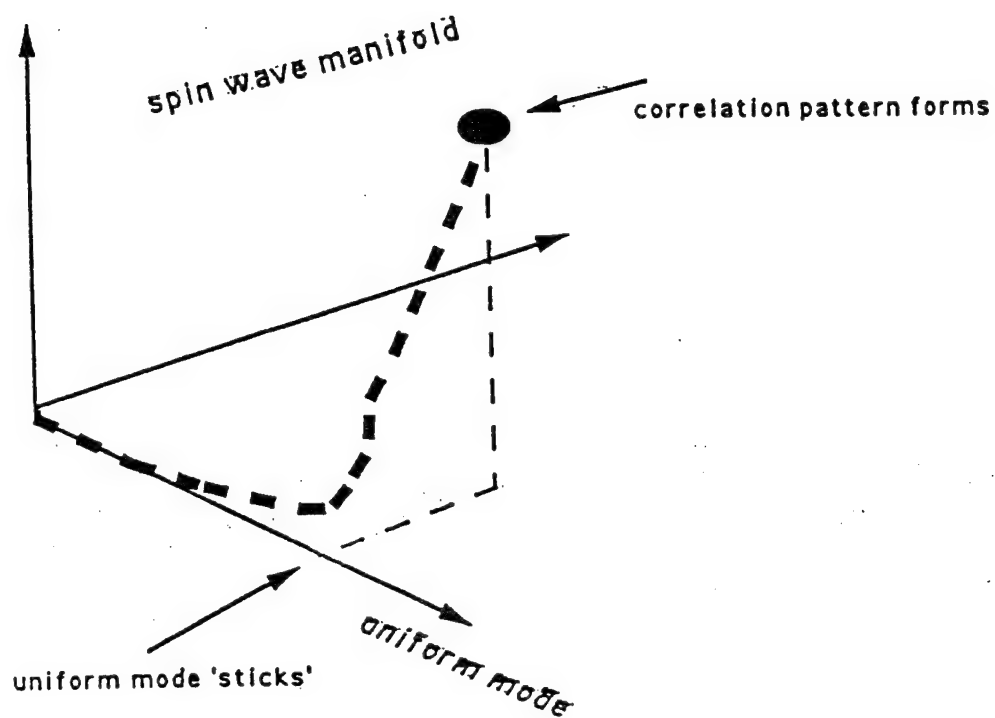
XIa.



$$\theta_{in} > \theta_f > \theta_c$$

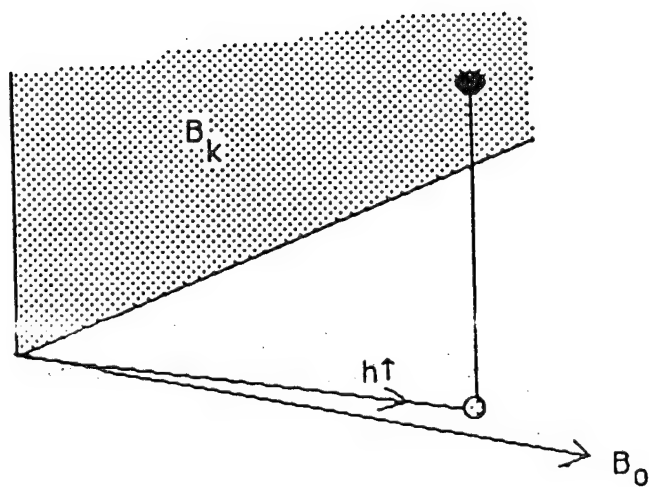


XII.



High power ferromagnetic resonance. Approach to new fixed point in the presence of thermal noise.

XIIa.



Approach to new fixed point in the limit of zero thermal noise.

XIII.

The phase of each excited spin wave b_k is random, except that it is tied to the phase of b_{-k} by the phase of the signal.

The spatial autocorrelation function of the transverse magnetization along the direction (z) of the field is

$$c(z) = \langle m^+(\vec{r} + \vec{e}z) m^-(\vec{r}) \rangle = \sum |b_k|^2 e^{ikz} \\ \approx \text{const.} \cdot e^{iqz} / \sqrt{z} \quad \text{for large } z.$$

$$q \approx \frac{1}{l} \cdot \left(\frac{\omega_0}{\omega_{exch}} \right)^{1/2}$$

Transverse correlation function:

$$c(x) \approx \text{const.} \cdot e^{iq'x} / x \quad \text{for large } x.$$

Forward Volume Wave Envelope Solitons in a Thin Unpinned Y I G Film

Mincho A. Tsankov, Ming Chen, and Carl E. Patton,

Department of Physics, Colorado State University, Fort Collins, CO 80523

Workshop on Nonlinear Interaction in Magnetic and Magneto optic Materials,

December 12-14, 1993, Costa Mesa, CA

Earlier works on FVW solitons:

Kalinikos *et al.*, Pis'ma Zh. Eksp. Teor. Fiz. **38**, 343 (1983)

(pinned film; first observation of MSW soliton in YIG)

Kalinikos *et al.*, IEEE Trans. Magn. **26**, 1477 (1990).

Kalinikos *et al.*, Phys. Rev. B **42**, 8658 (1990).

(unpinned film; observation of single and multiple solitons)

De Gasperis *et al.*, Phys. Rev. Lett. **59**, 481 (1987).

De Gasperis *et al.*, J. Appl. Phys. **63**, 4136 (1988).

(investigation of peak pulse powers)

The Present Work:

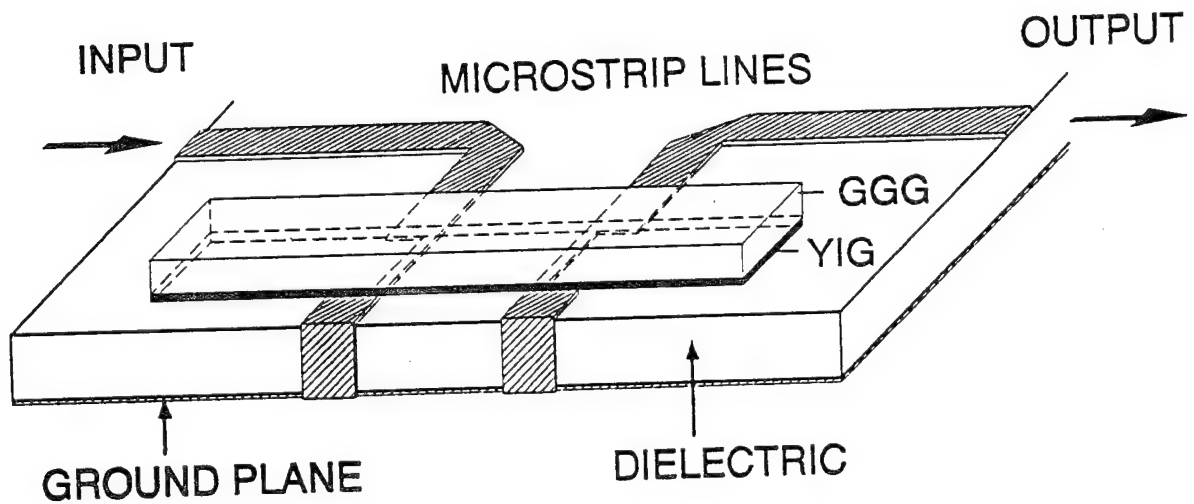
- Verifies and comments on earlier experimental results.
- Provides some new results:
 - investigation of the pulse decay rate vs. power,
 - excitation of solitons in wide frequency band,
 - soliton collision.

The Experimental Details

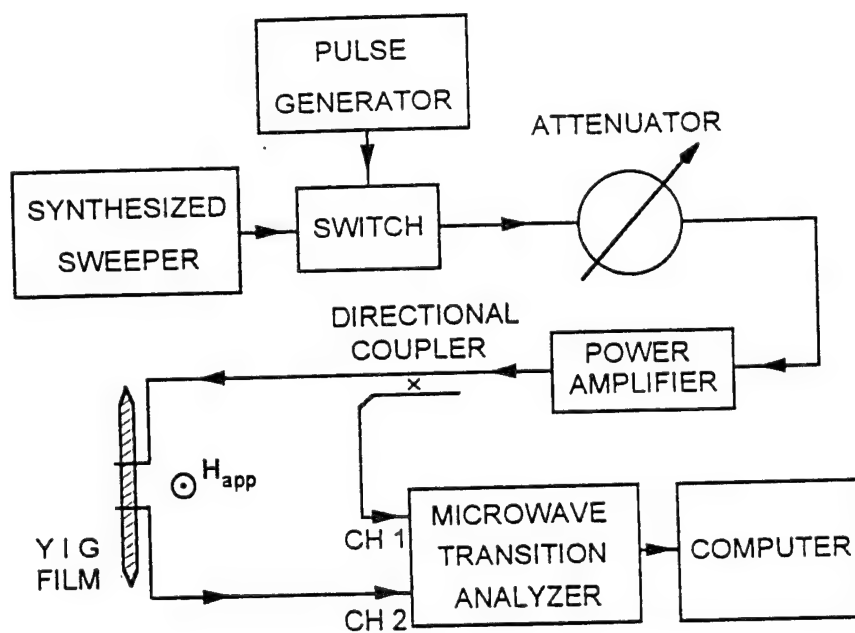
The sample: 2 mm x 15 mm x 7.2 μm single-crystal YIG film; $4\pi M_s = 1750$ G, $\Delta H = 0.6$ Oe

Applied Field: $H_{app} = 3744$ Oe; Frequency: 5.6 GHz

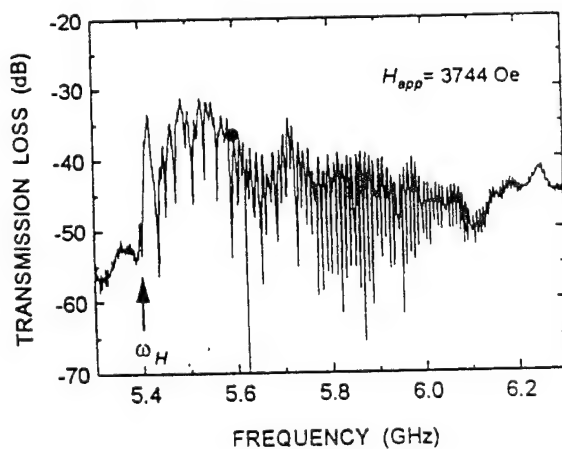
The Experimental Structure



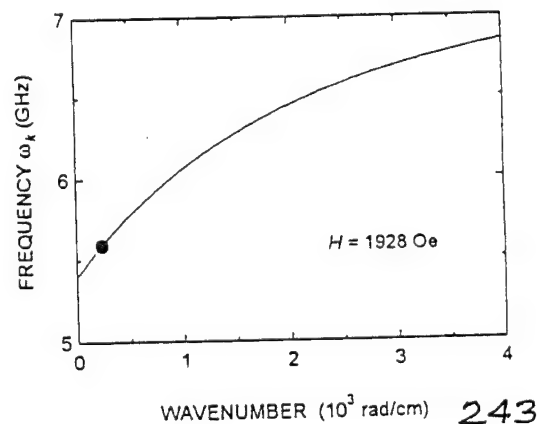
The Experimental Setup



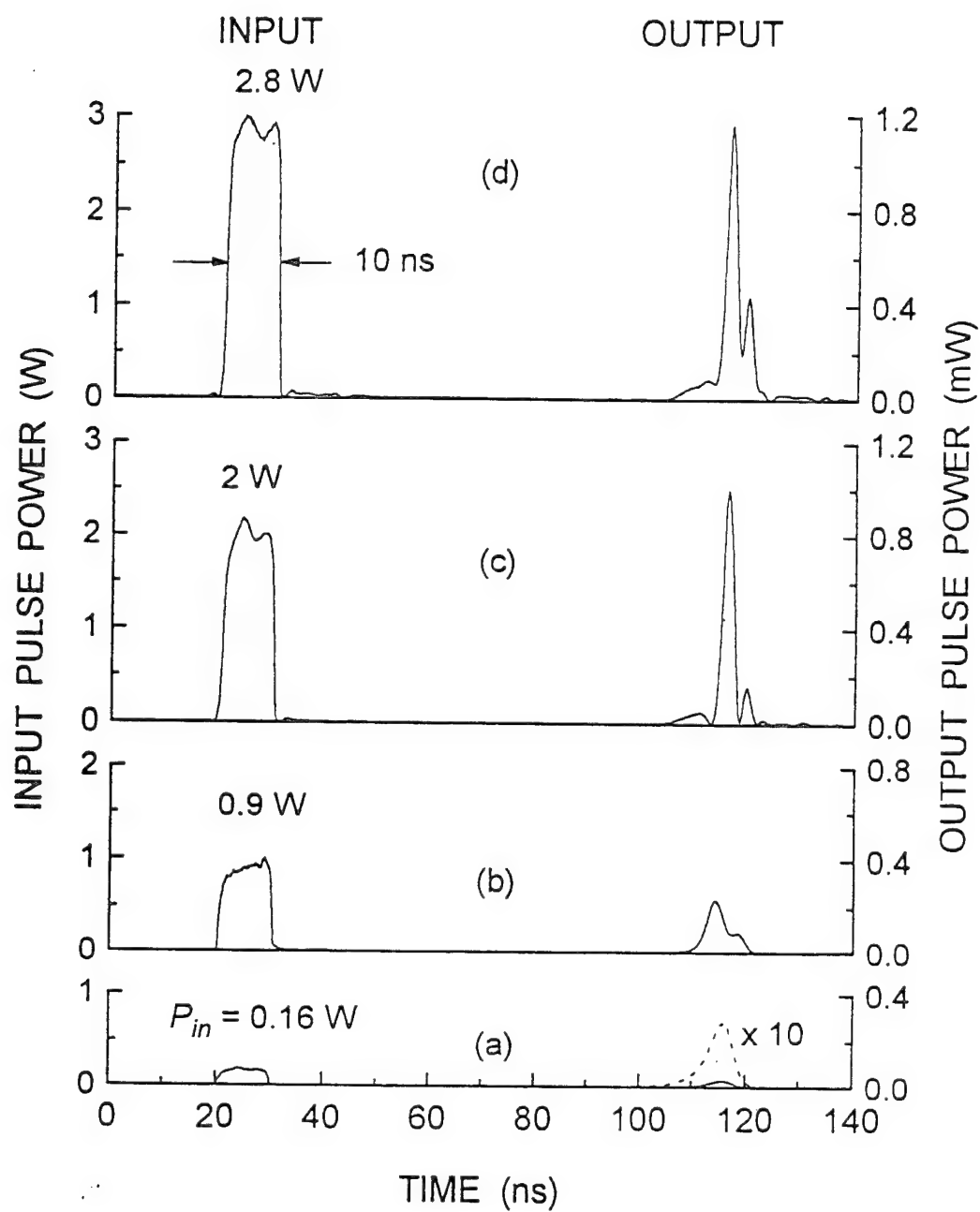
Transmission-loss Curve:



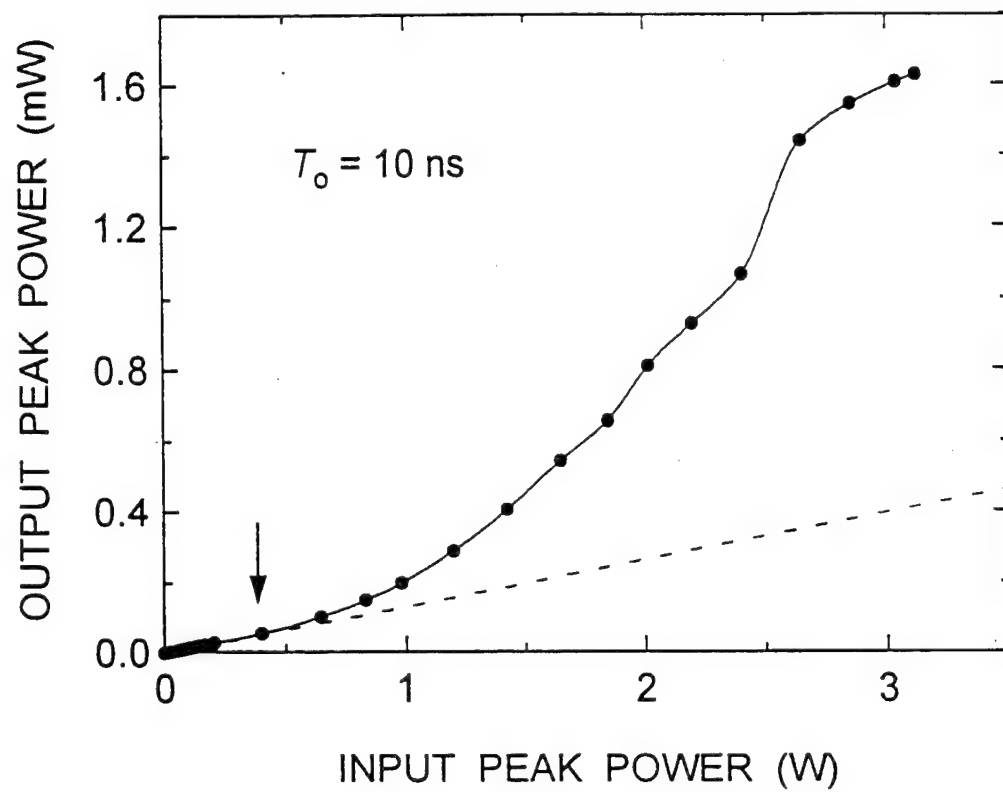
Dispersion Curve:



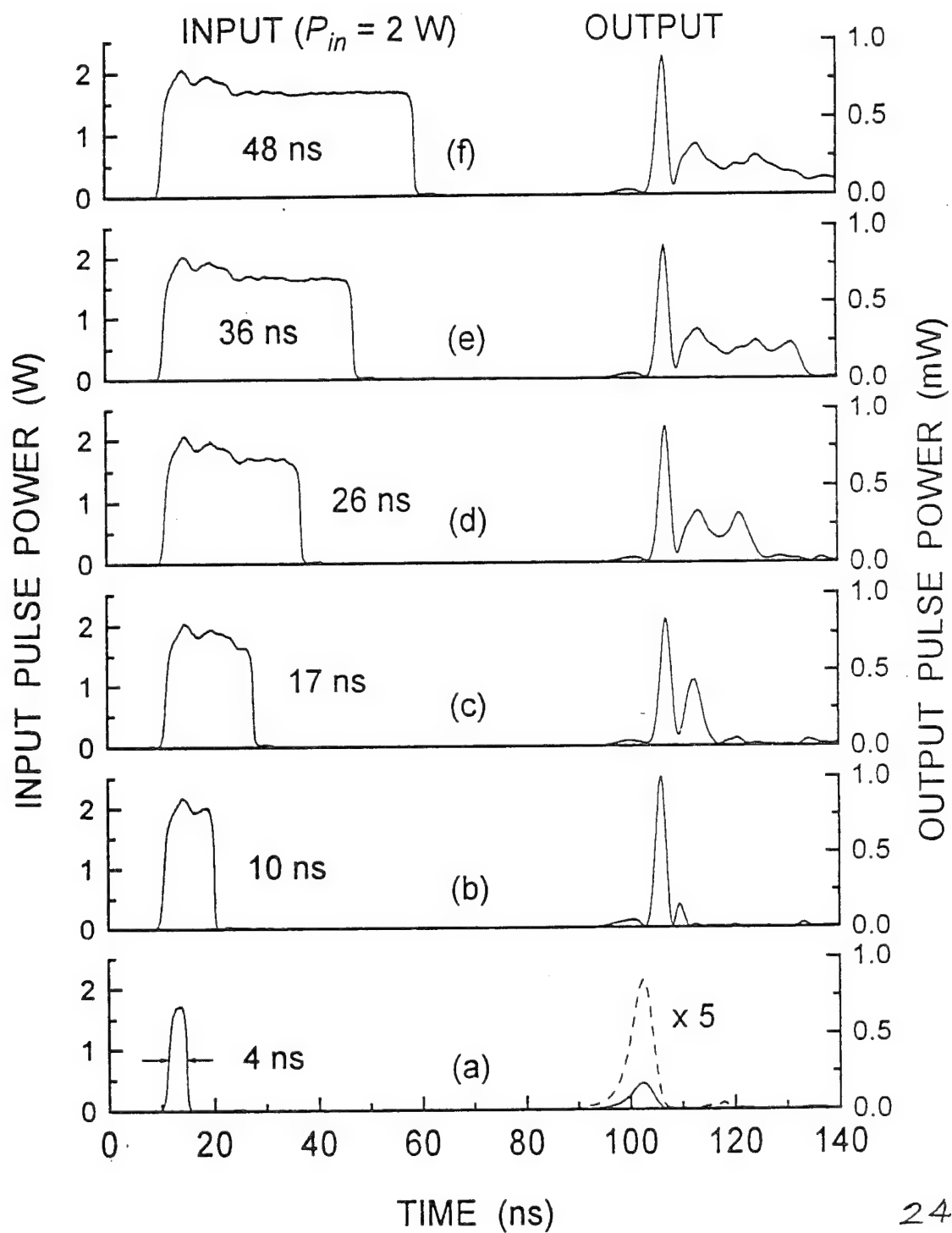
First Experiment (A)
Variable Pulse Power, Constant Pulse Width



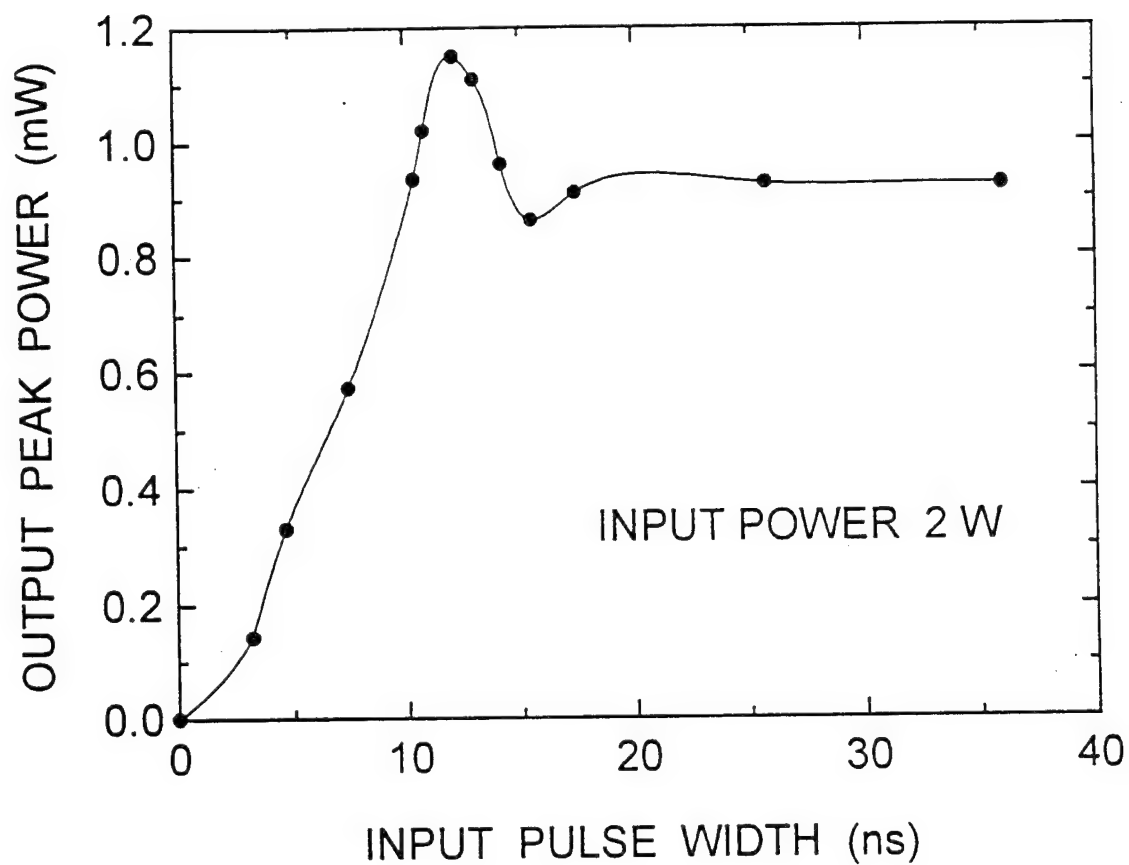
First Experiment (B)
Variable Pulse Power, Constant Pulse Width



Second Experiment (A)
Variable Pulse Width, Constant Pulse Power

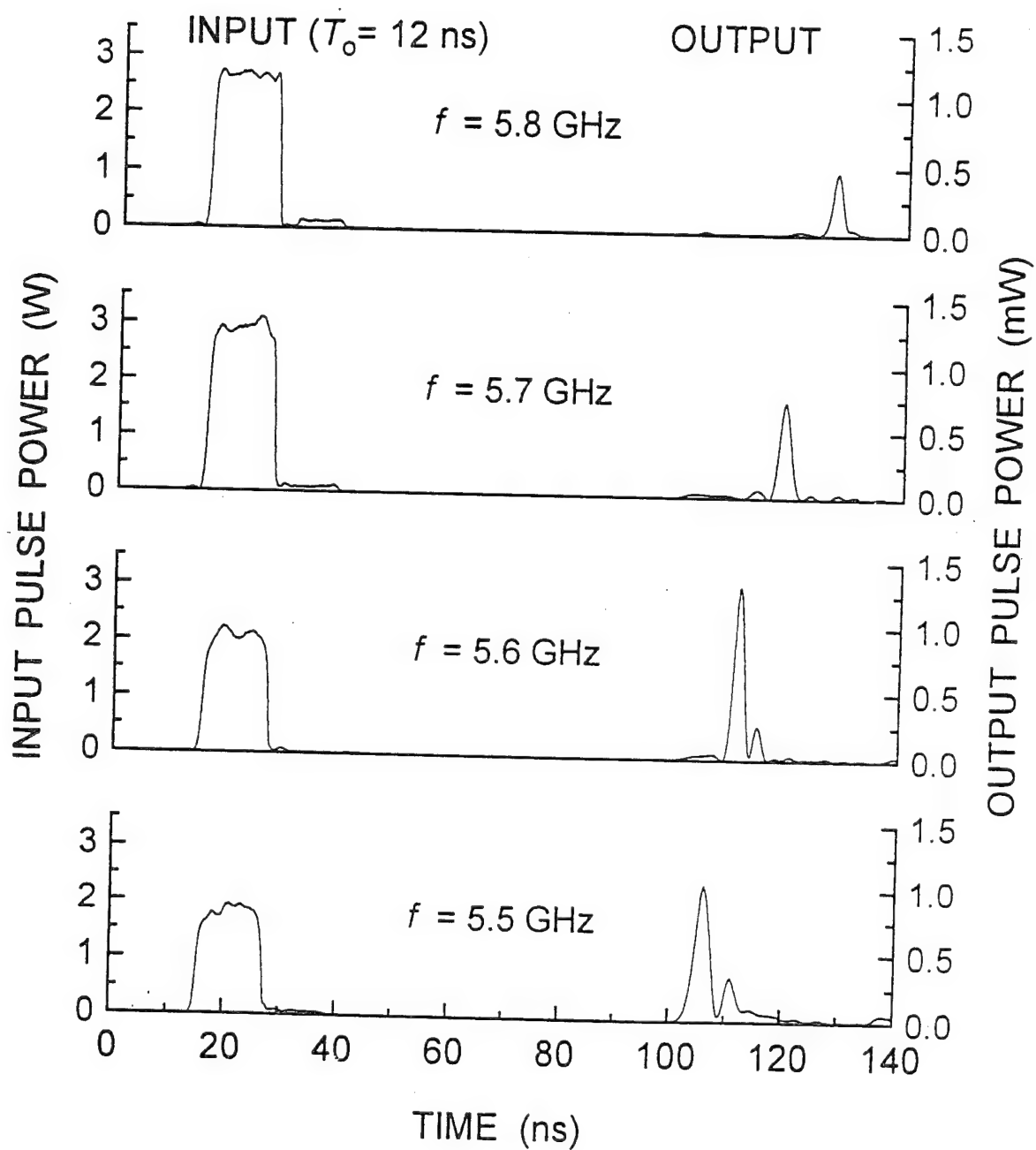


Second Experiment (B)
Variable Pulse Width, Constant Pulse Power

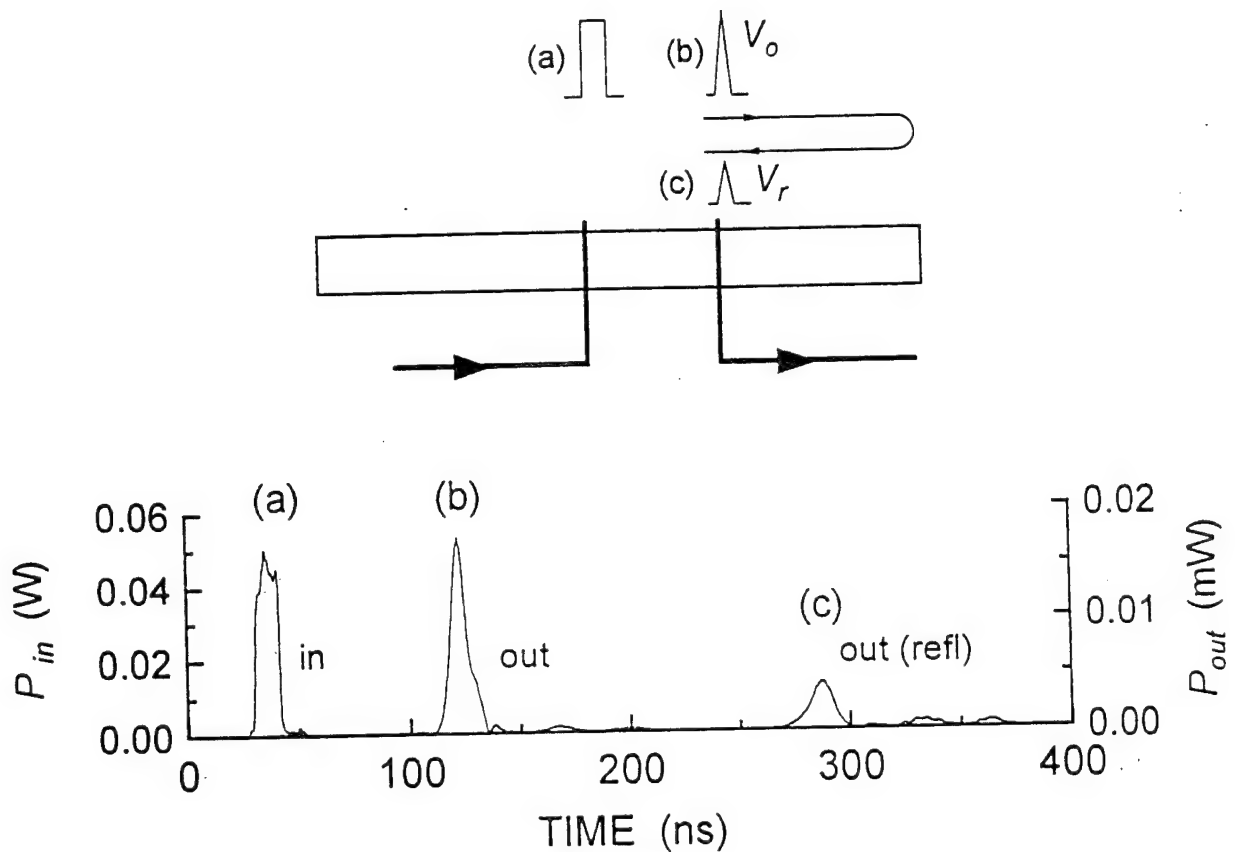


Third Experiment

Soliton Excitation in a Wide Frequency Band



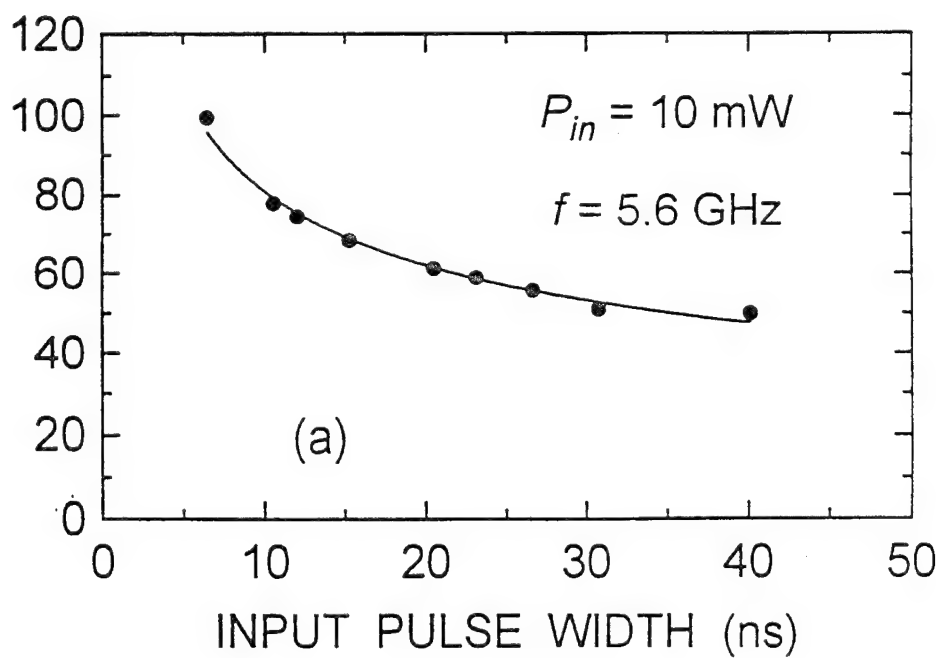
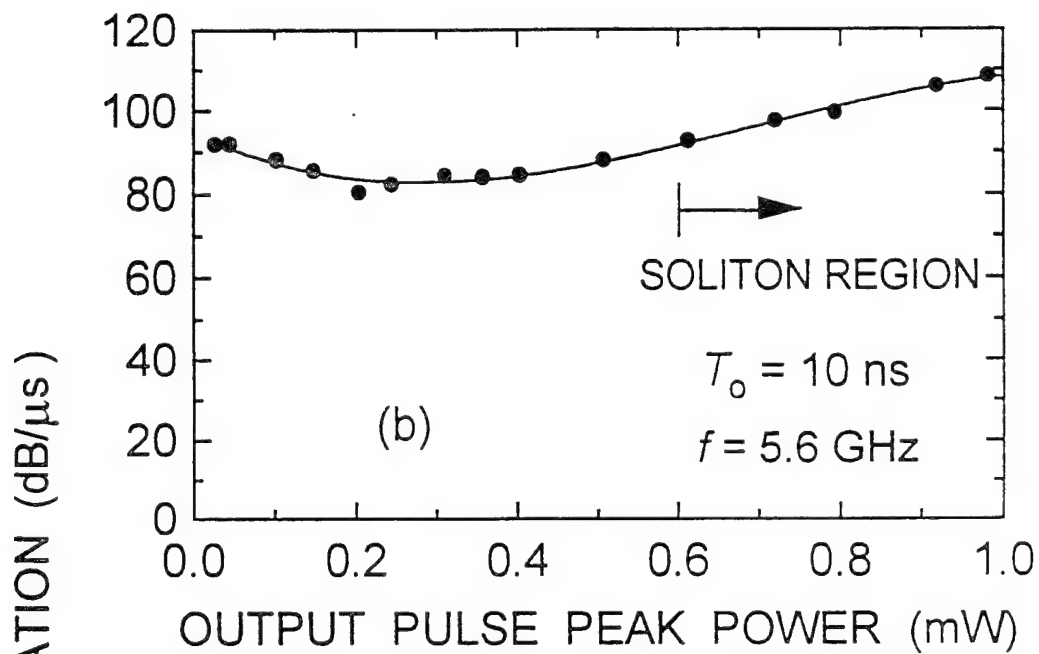
Fourth Experiment (A) Pulse Decay Rate vs. Power



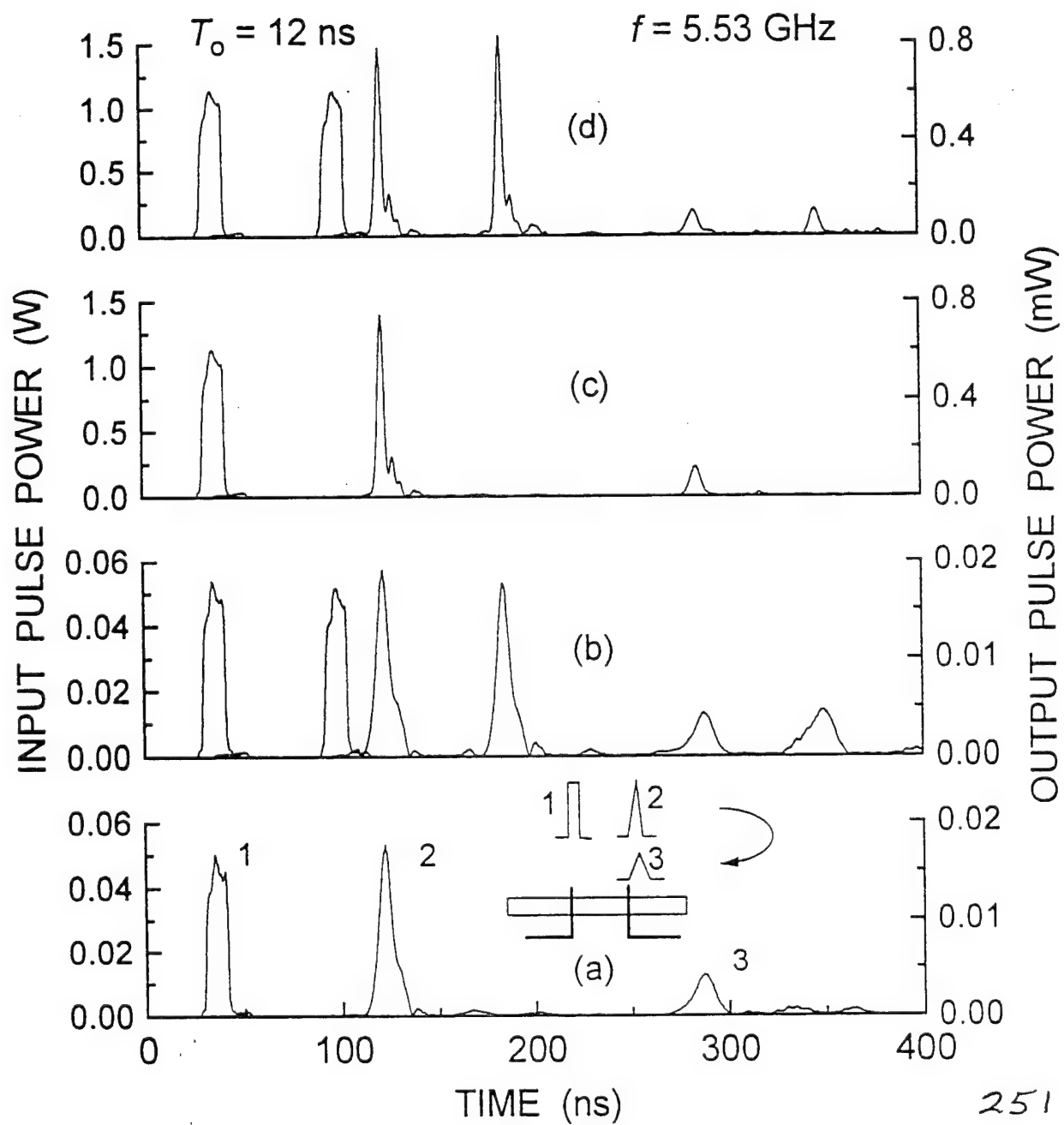
The Attenuation in dB/ μ s:

$$A = \frac{1}{0.088} 20 \log \frac{V_o}{V_r} .$$

Fourth Experiment (B)
Pulse Decay Rate vs. Power



Fifth Experiment
Soliton Collision



Theoretical Background

The Nonlinear Schrödinger Equation:

$$i \left(\frac{\partial u}{\partial t} + v_g \frac{\partial u}{\partial x} + \eta u \right) + \frac{1}{2} \omega_k'' \frac{\partial^2 u}{\partial x^2} - N |u|^2 u = 0 ,$$

$$u = \frac{m(x,t)}{\sqrt{2}M_s}; \quad v_g = \frac{\partial \omega}{\partial k}; \quad \omega_k'' = \frac{\partial v_g}{\partial k} = \frac{\partial^2 \omega}{\partial k^2}; \quad N = \frac{\partial \omega}{\partial |u|^2}$$

The necessary condition for “bright” soliton solution:

$$\omega_k'' \cdot N < 0$$

$$\omega_k'' < 0 \quad ; \quad N > 0$$

$$\omega \approx \omega_H = \gamma(H_{app} - 4\pi M_z) = \gamma[H_{app} - 4\pi M_s(1 - |u|^2)]; \quad \frac{\partial \omega_H}{\partial |u|^2} = \gamma 4\pi M_s = \omega_M$$

The analytical solution of NSE:

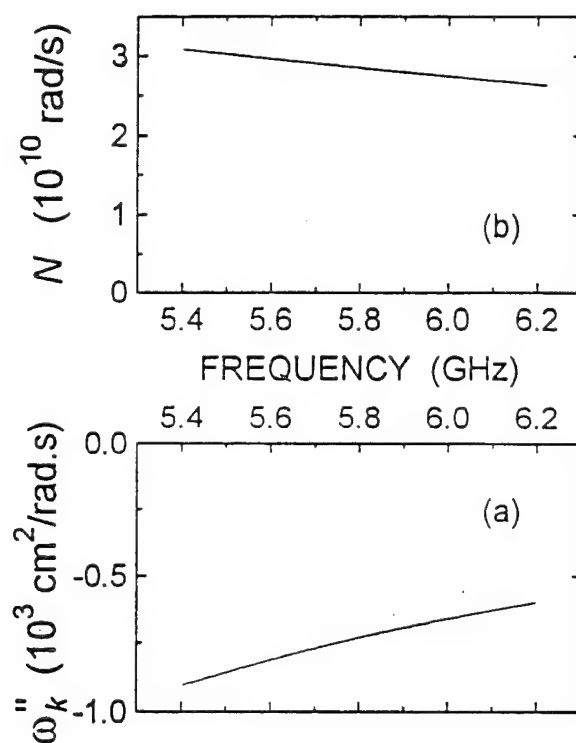
$$u(x,t) = u_o e^{-2\eta t} \operatorname{sech} \left[u_o e^{-2\eta t} \sqrt{\left| \frac{N}{\omega_k''} \right|} (x - v_s t - x_o) \right] e^{i(kx - \Omega t)}$$

Condition for multisoliton excitation:

$$T_o > (n - 1/2) \frac{\pi}{|v_g| |u_o|} \sqrt{\left| \frac{\omega_k''}{N} \right|} = (n - 1/2) \cdot C$$

Discussion

1. The $e^{-2\eta t}$ soliton decay rate.
2. The possibility of broadband soliton excitation



3. Critical pulsewidths for multisoliton excitation.

If $T_{o,crit\ 1} = 5 \text{ ns}$, then $C = 10 \text{ ns}$ and

$T_{o,crit\ 2}$	$= 15 \text{ ns}$
$T_{o,crit\ 3}$	$= 25 \text{ ns}$
$T_{o,crit\ 4}$	$= 35 \text{ ns}$

Conclusions:

Old experiments were verified and extended.

Soliton attenuation rate was confirmed to be close to $e^{-2\eta t}$.

Solitons were excited in a wide frequency band.

Collision of solitons was observed.

EXISTENCE OF SPIN WAVE SOLITONS IN AN ANTIFERROMAGNETIC FILM

A D Boardman,^{*} S A Nikitov⁺ and N A Waby^{*}

*Joule Laboratory,
Department of Physics,
University of Salford,
Salford, M5 4WT.
England.

+Institute of Radioengineering and Electronics,
Russian Academy of Sciences,
Mokhovaya St., 11,
103907, Moscow.
Russia.

Plan of the Talk

- Introduction
- Bright soliton conditions
- Surface waves on an antiferromagnetic film
 - Group velocity dispersion
 - Nonlinear coefficients
- Volume waves
 - Tangentially magnetized film
 - Perpendicularly magnetized film
- Conclusions

Introduction

- magnetostatic envelope solitons in thin ferromagnetic films have received a significant degree of attention.
- high quality antiferromagnetic films made by molecular-beam-epitaxy are now available.
- antiferromagnetic films may have many new applications.
- antiferromagnetic resonance frequencies and the frequencies of excited spin waves belong to the infra-red.
- this fact makes the use of antiferromagnetic media for applications very attractive.
- here we discuss the formation of spin wave envelope solitons for different combinations of external magnetic field and spin wave propagation directions.
- Reference: A D Boardman, S A Nikitov and N A Waby. Phys. Rev. B48, 1 November 1993.

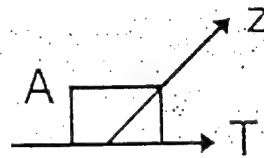
General Bright Soliton Conditions.

- Use coupled set of the Maxwell and Landau-Liftshitz equations.

- Nonlinear Schrödinger Equation

$$i \frac{\partial A}{\partial z} = \frac{1}{2} \text{sgn}(\beta_2) \beta_2 \frac{\partial^2 A}{\partial T^2} - \gamma \text{sgn}(\gamma) |A|^2 A$$

- A: amplitude of the envelope of the pulse



- T: time measured in a frame of reference that moves with the pulse

- $\beta_2 = \frac{\partial^2 k}{\partial \omega^2}$: group-velocity dispersion

- $\text{sgn}(\beta_2)$: sign of β_2

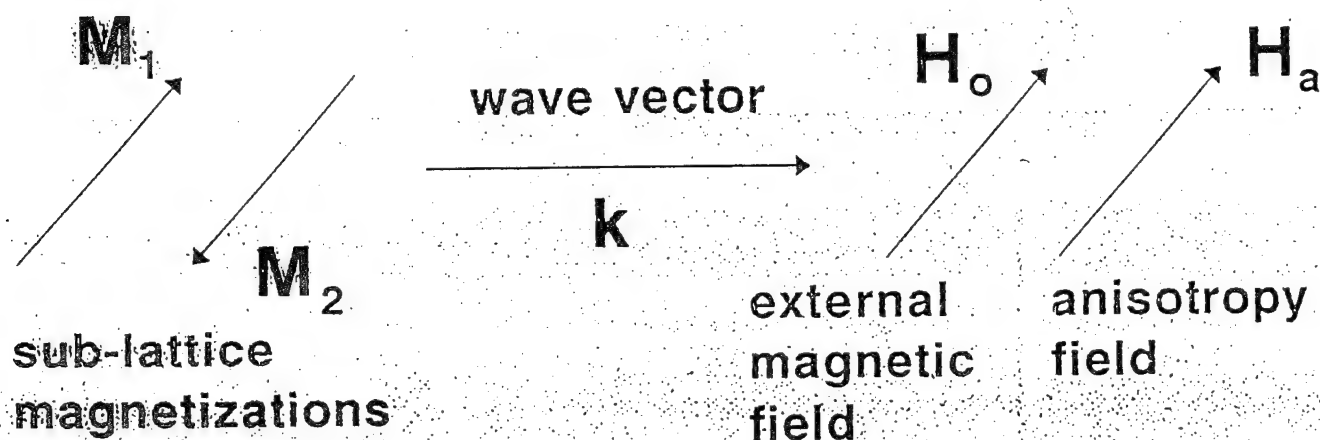
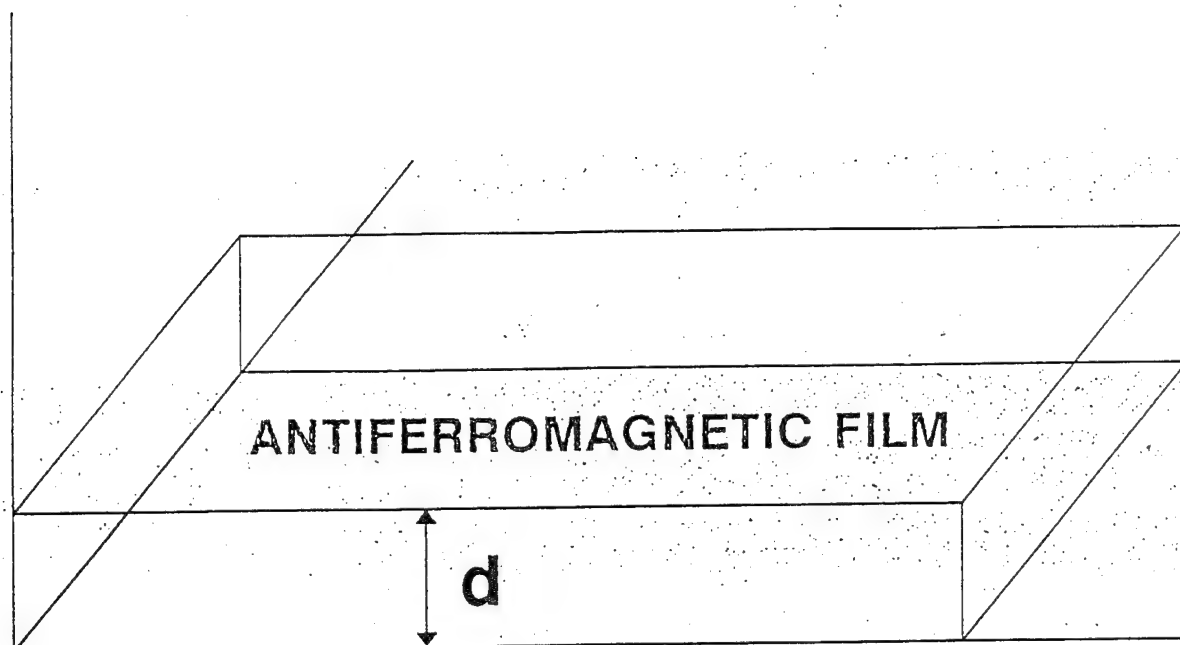
- $\gamma = \frac{\partial k}{\partial |A|^2}$: nonlinear coefficient

- $\text{sgn}(\gamma)$: sign of γ

- Necessary condition for the formation of bright solitons is

$$\beta_2 \gamma < 0$$

Lighthill Criterion



PROPAGATION OF SURFACE WAVES

Surface Waves on an Antiferromagnetic Film

- The dispersion relation

$$\exp(2kd) = \frac{(\mu_1 - 1)^2 - \mu_2^2}{(\mu_1 + 1)^2 - \mu_2^2}$$

- μ_1 and μ_2 are the magnetic permeability tensor components

$$\mu_1 = 1 + \frac{R^2 g^2 (\omega_+ \omega_- - \omega^2)}{(\omega_+^2 - \omega^2)(\omega_-^2 - \omega^2)}$$

$$\mu_2 = \frac{R^2 g^2 (\omega_- - \omega_+) \omega}{(\omega_+^2 - \omega^2)(\omega_-^2 - \omega^2)}$$

$$R^2 = 8\pi M_o H_a$$

$$\omega_{\pm} = g(H_c \pm H_o)$$

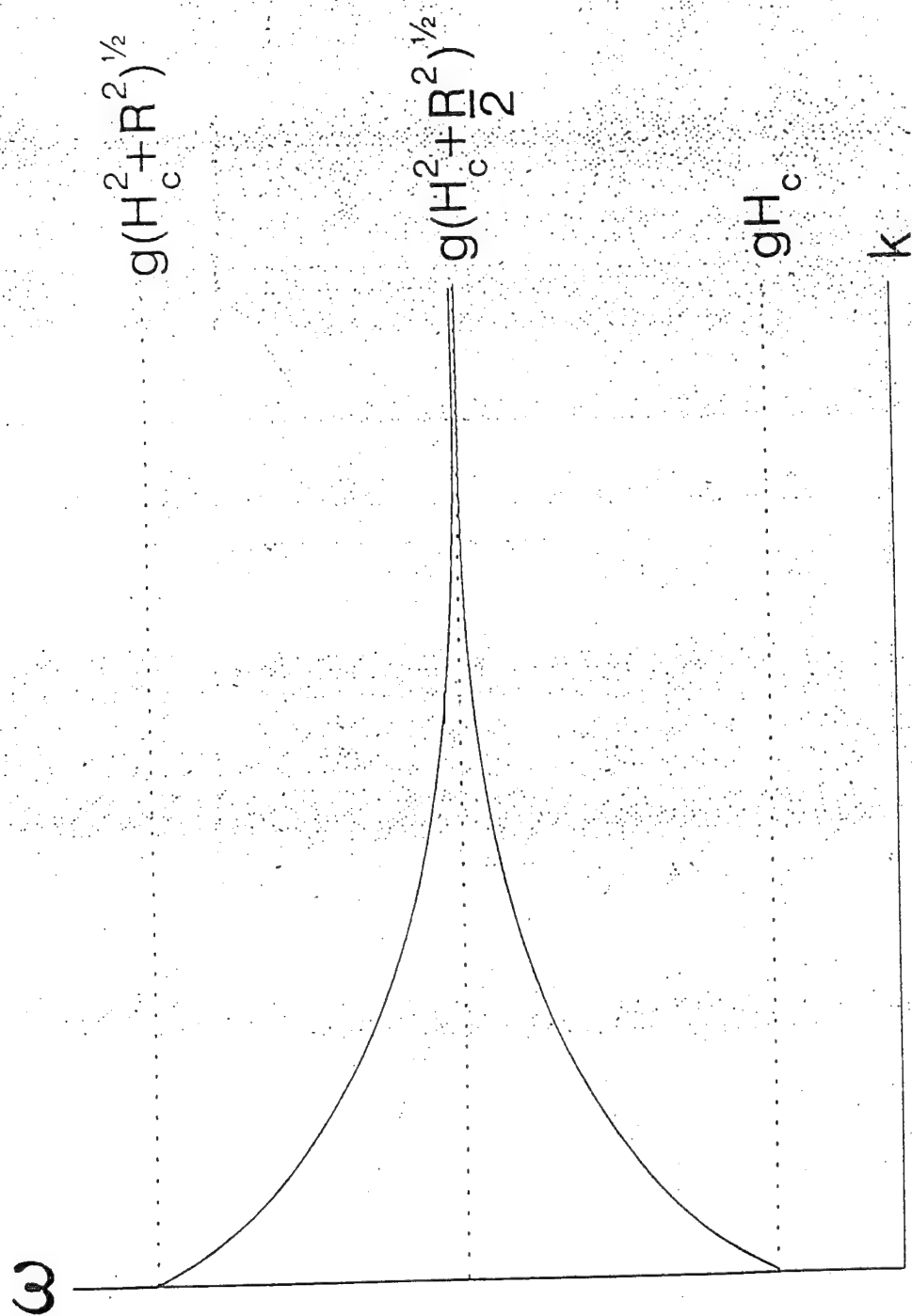
$$H_c^2 = H_a(2H_E + H_a) \quad H_E = -\lambda M_o \quad H_a = (\beta - \beta_1) M_o$$

- λ : exchange constant

- M_o : NET magnetization

- β, β_1 : anisotropy constants

- g : gyromagnetic ratio



Surface Waves

- If $H_0=0$ the surface waves propagate within the two frequency regions

$$gH_c < \omega < g(H_c^2 + \frac{R^2}{2})^{1/2}$$

$$g(H_c^2 + \frac{R^2}{2})^{1/2} < \omega < g(H_c^2 + R^2)^{1/2}$$

- Group velocity dispersion

$$\beta_2 = \frac{\partial^2 k}{\partial \omega^2}$$

Surface Waves

Lower branch

$$\beta_2 = \frac{1}{V^3} \frac{g^2 R^2 d^2 \exp(-kd)}{2\omega_0} > 0$$

$$V = \frac{g^2 R^2 d \exp(-kd)}{2\omega_0} \quad (\text{Group Velocity})$$

$$\omega_0 = g \left(H_c^2 + \frac{R^2}{2} (1 - \exp(-kd)) \right)^{1/2}$$

Upper branch

$$\beta_2 = -\frac{1}{V_1^3} \frac{g^2 R^2 d^2 \exp(-kd)}{2\omega_{01}} < 0$$

$$V_1 = \frac{g^2 R^2 d \exp(kd)}{2\omega_{01}} \quad (\text{Group Velocity})$$

$$\omega_{01} = g \left(H_c^2 + \frac{R^2}{2} (1 + \exp(-kd)) \right)^{1/2}$$

$$R^2 = 8\pi M_0 H_a$$

Nonlinear Coefficients

- use method of A K Zvezdin and A F Popkov [Sov. Phys. JETP 57, 350 (1983)]
- for small ac deviations (due to the wave) from equilibrium

$$M_z \approx M_0 \left[1 - \frac{|m_x|^2 + |m_y|^2}{2M_0^2} \right]$$

- in the limit $kd \ll 1$ $M_z \approx M_0 - M_0 |A|^2$

■ A is dimensionless amplitude of magnetostatic potential

- nonlinear coefficients for the lower and upper branches are

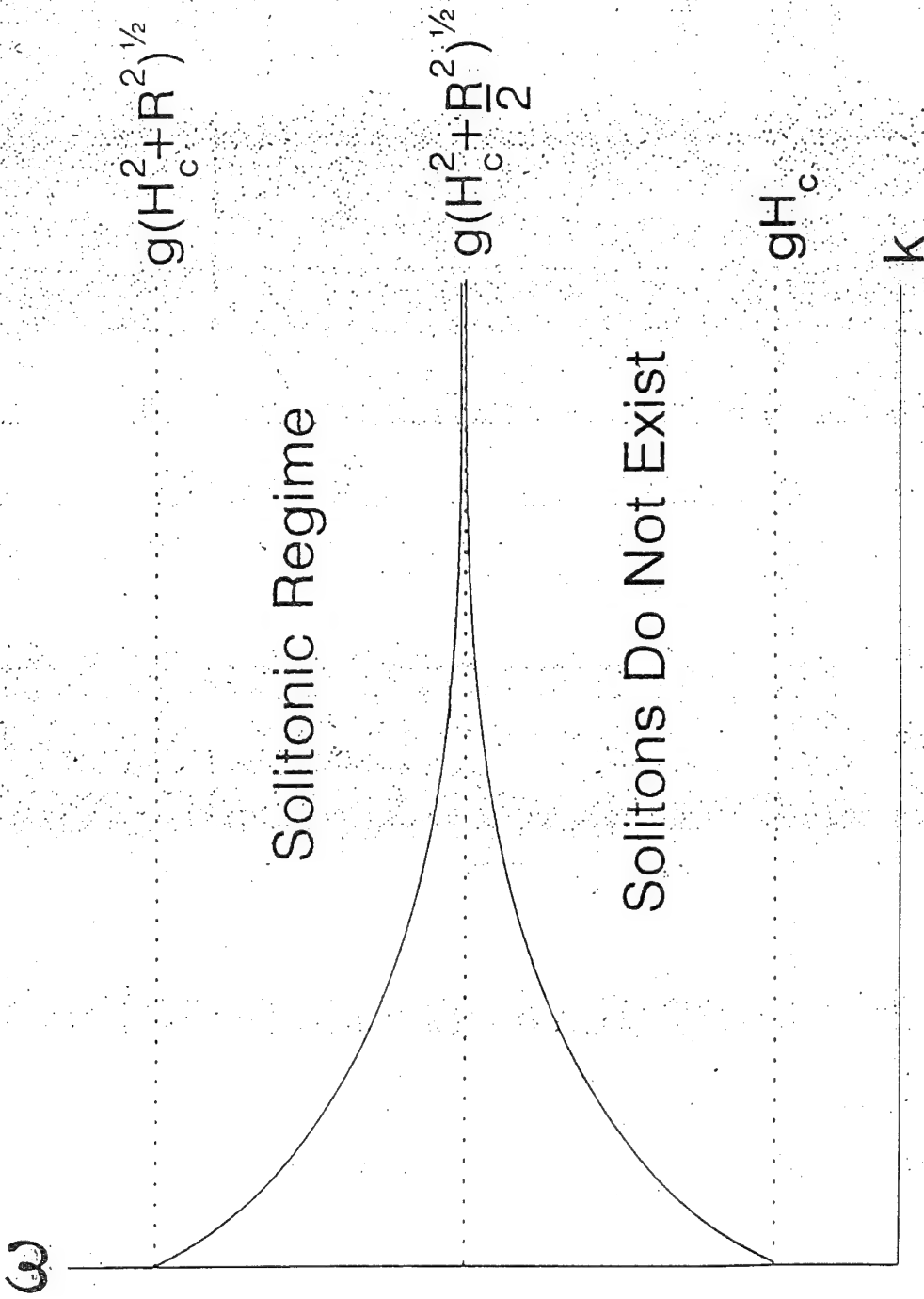
$$\gamma \approx \frac{2}{V} \frac{gH_a H_e}{(2H_a H_e + H_a^2)^{1/2}}$$

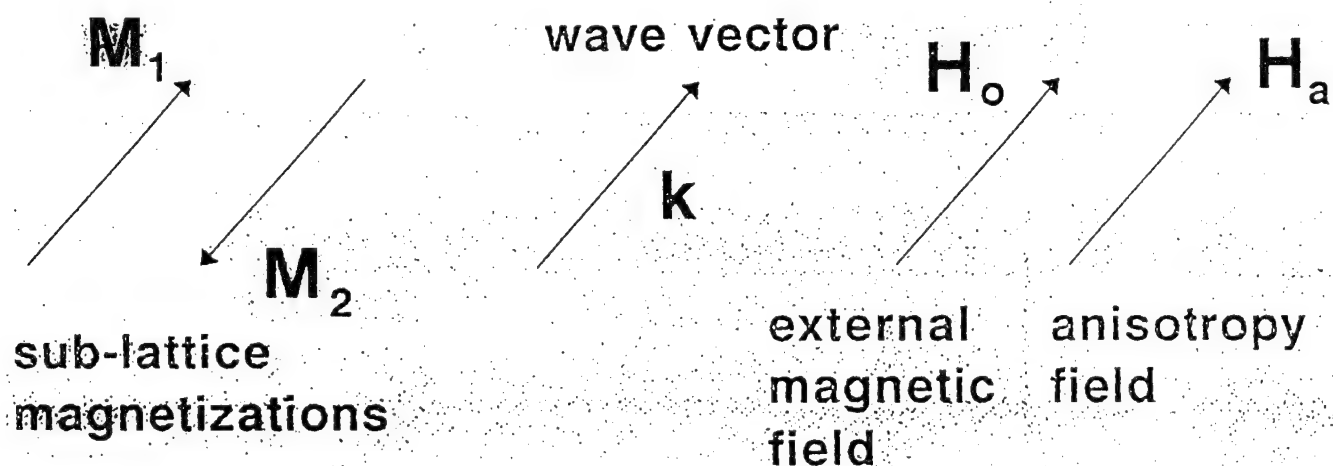
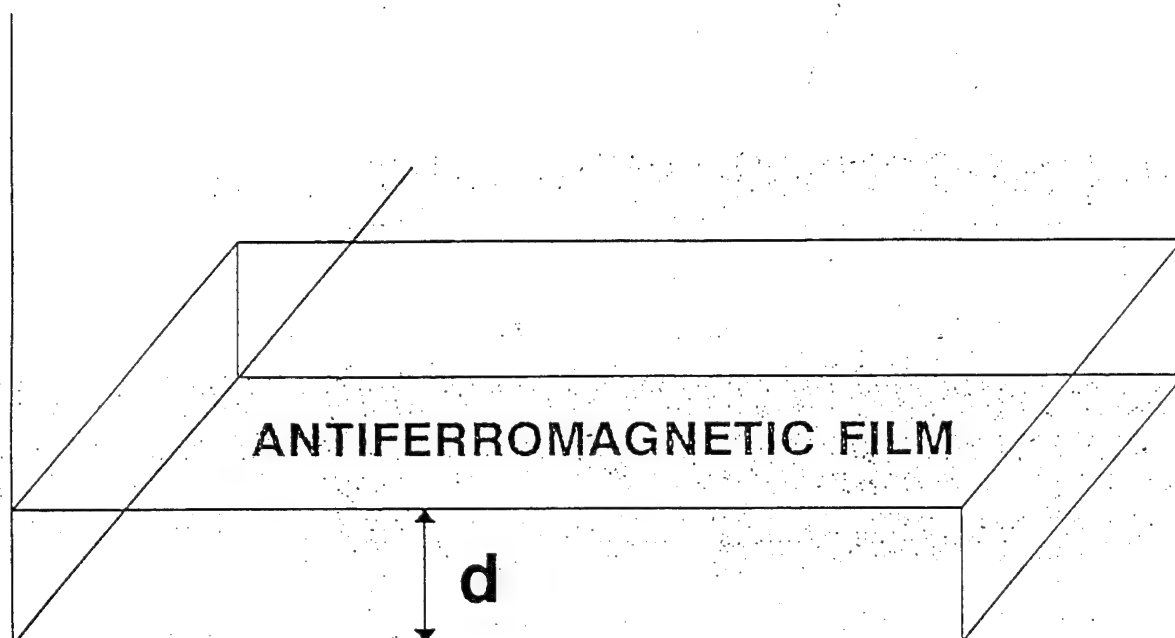
Lower Branch

$$\gamma \approx \frac{2}{V_1} \frac{gH_a H_e}{(2H_a H_e + H_a^2)^{1/2}}$$

Upper Branch

- Lighthill criterion satisfied for upper branch
- Lighthill criterion not satisfied for the lower branch





PROPAGATION OF TANGENTIALLY MAGNETIZED VOLUME WAVES

Volume Waves

Tangentially Magnetized Antiferromagnetic Film

- dispersion relation

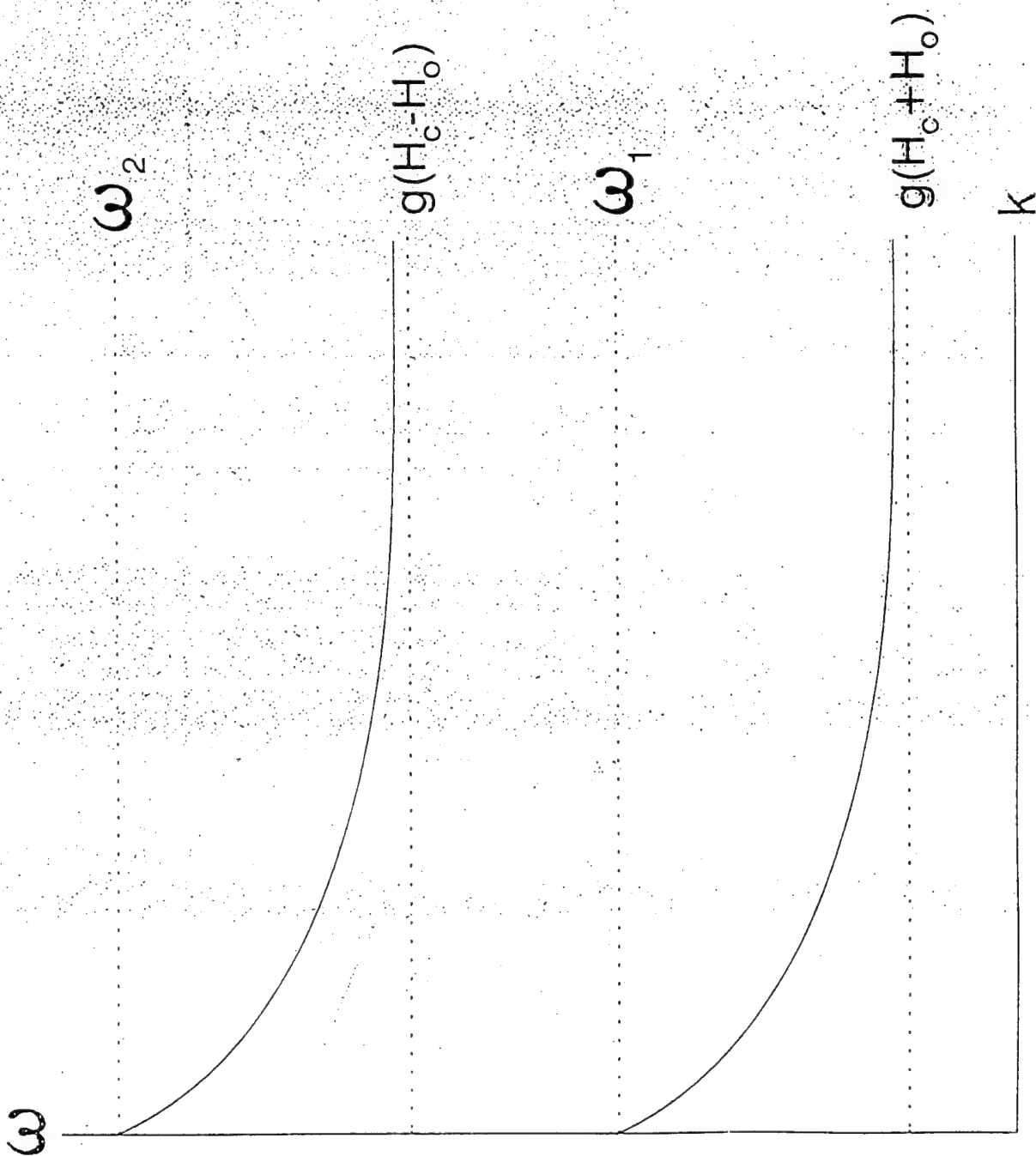
$$\tan(kd/\sqrt{\mu_1}) = \frac{2\sqrt{\mu_1}}{\mu_1 - 1}$$

- spin wave spectrum (for $H_0 \neq 0$) consists of two branches

$$g(H_c + H_0) < \omega < \omega_1 \quad \boxed{\text{Lower Branch}}$$

$$g(H_c - H_0) < \omega < \omega_2 \quad \boxed{\text{Upper Branch}}$$

$$\omega_{2,1} = \frac{1}{\sqrt{2}} (2g^2(H_c^2 + H_0^2) + g^2 R^2 \pm (g^4 R^4 + 8R^2 g^4 H_0^2 + 16g^4 H_0^2 H_c^2)^{1/2})^{1/2}$$



Volume Waves

Tangentially Magnetized Antiferromagnetic Film

- $H_0=0$: only one branch exists with anomalous dispersion frequency region

$$gH_c < \omega < g(H_c^2 + R^2)^{1/2}$$

- Group Velocity Dispersion

$$\beta_2 = -\frac{1}{V_2^3} \frac{g^2 R^2 d^2}{4g(H_c^2 + R^2)^{1/2}} < 0$$

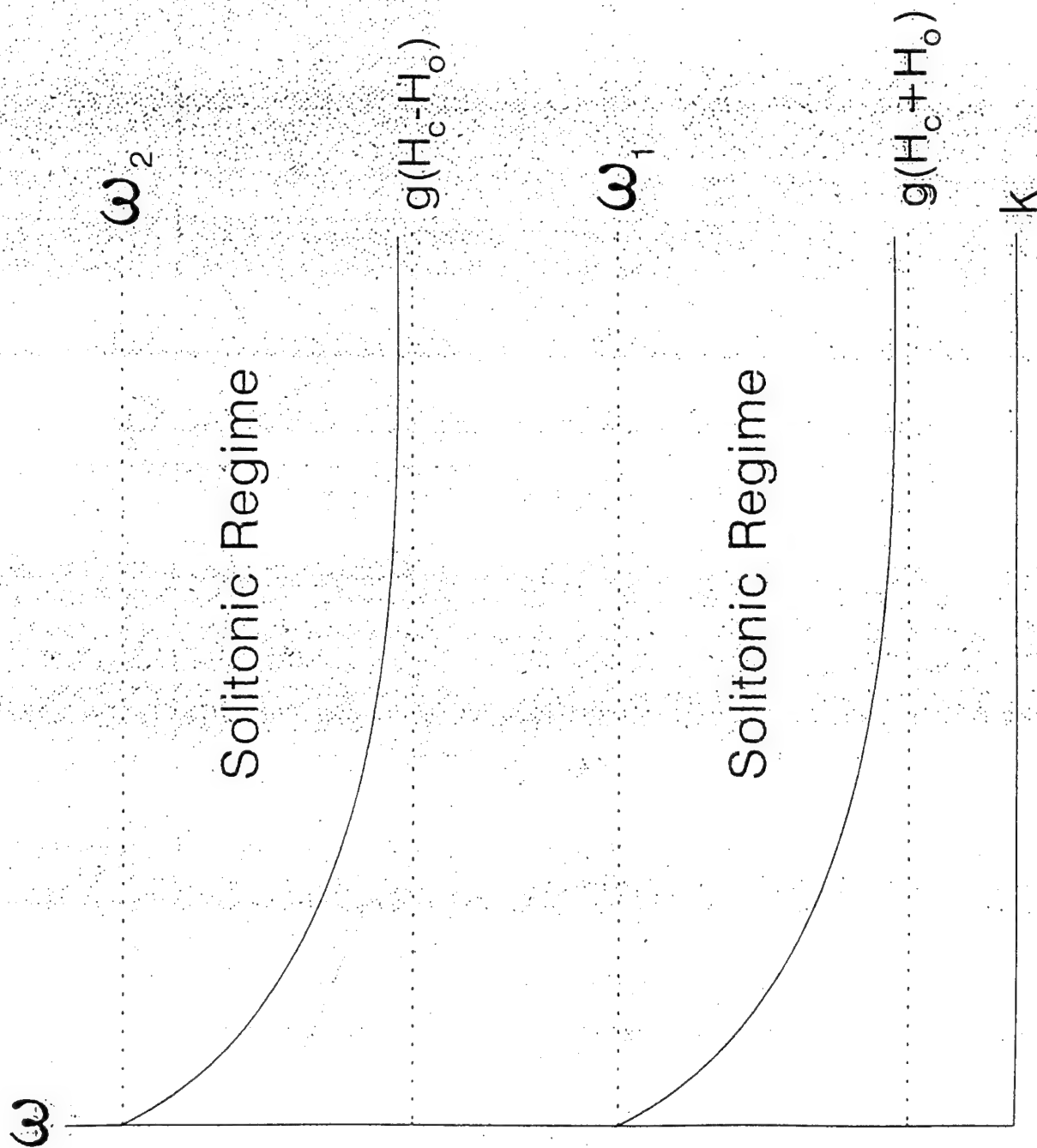
- Group Velocity

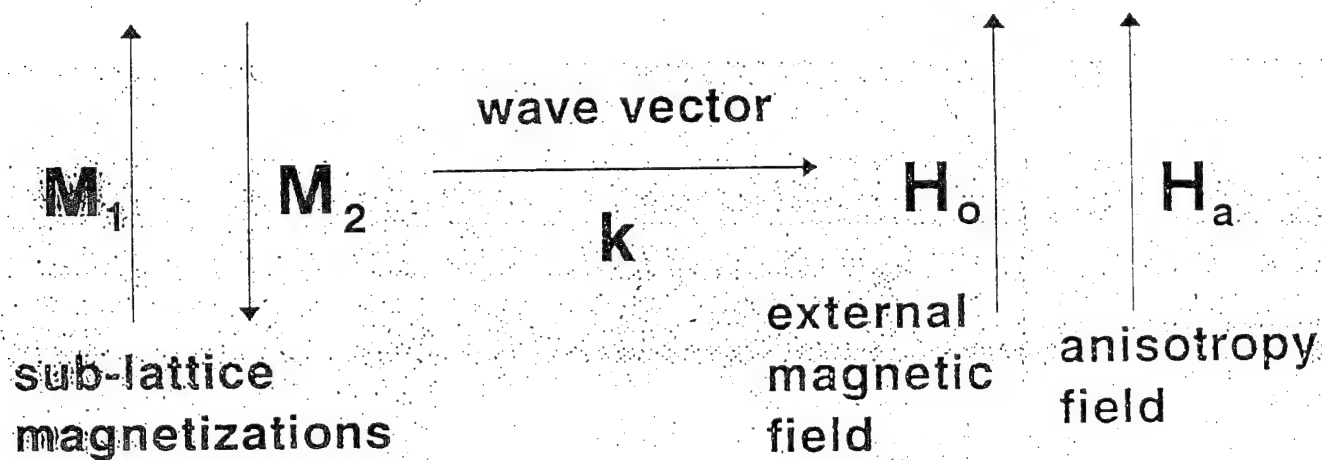
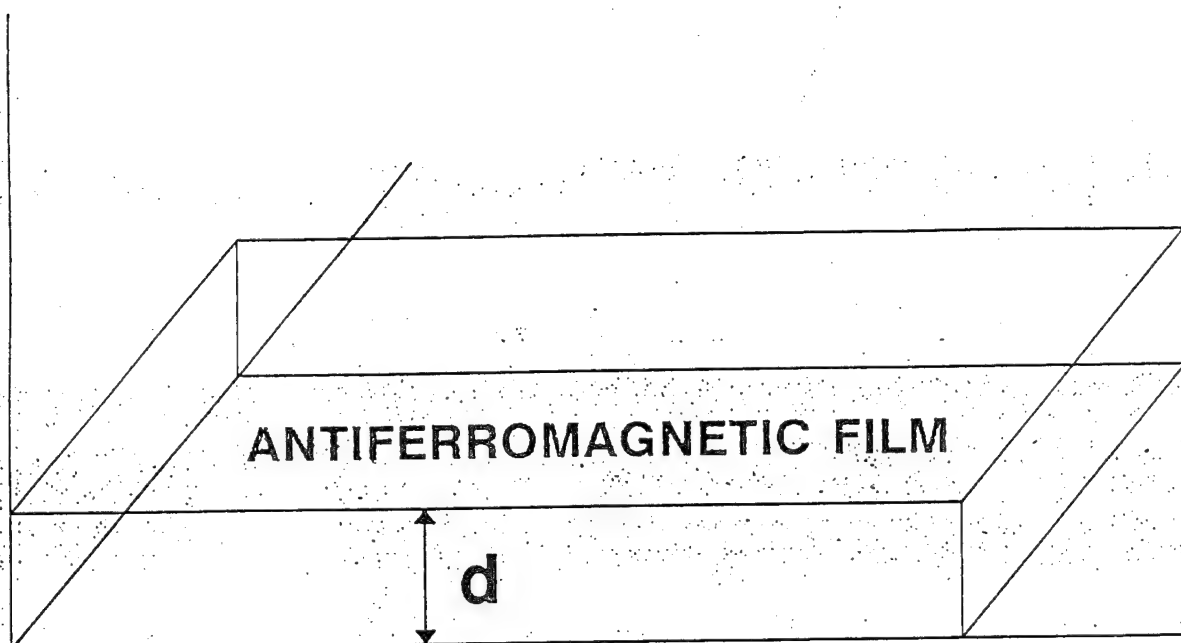
$$V_2 = \frac{-g^2 R^2 d}{2(g^2 H_c^2 + R^2)^{1/2}}$$

- Nonlinear Coefficient

$$\gamma \approx \frac{2}{V_2} \frac{gH_a H_e}{(2H_a H_e + H_a^2)^{1/2}}$$

- Lighthill criterion fulfilled





PROPAGATION OF PERPENDICULARLY MAGNETIZED VOLUME WAVES

Volume Waves

Perpendicularly Magnetized Antiferromagnetic Film

- dispersion relation

Symmetric modes

$$\cot \sqrt{\mu_1} kd = \sqrt{\mu_1}$$

Antisymmetric modes

$$\tan \sqrt{\mu_1} kd = -\sqrt{\mu_1}$$

- spectrum, again, consists of two branches

Lower branch

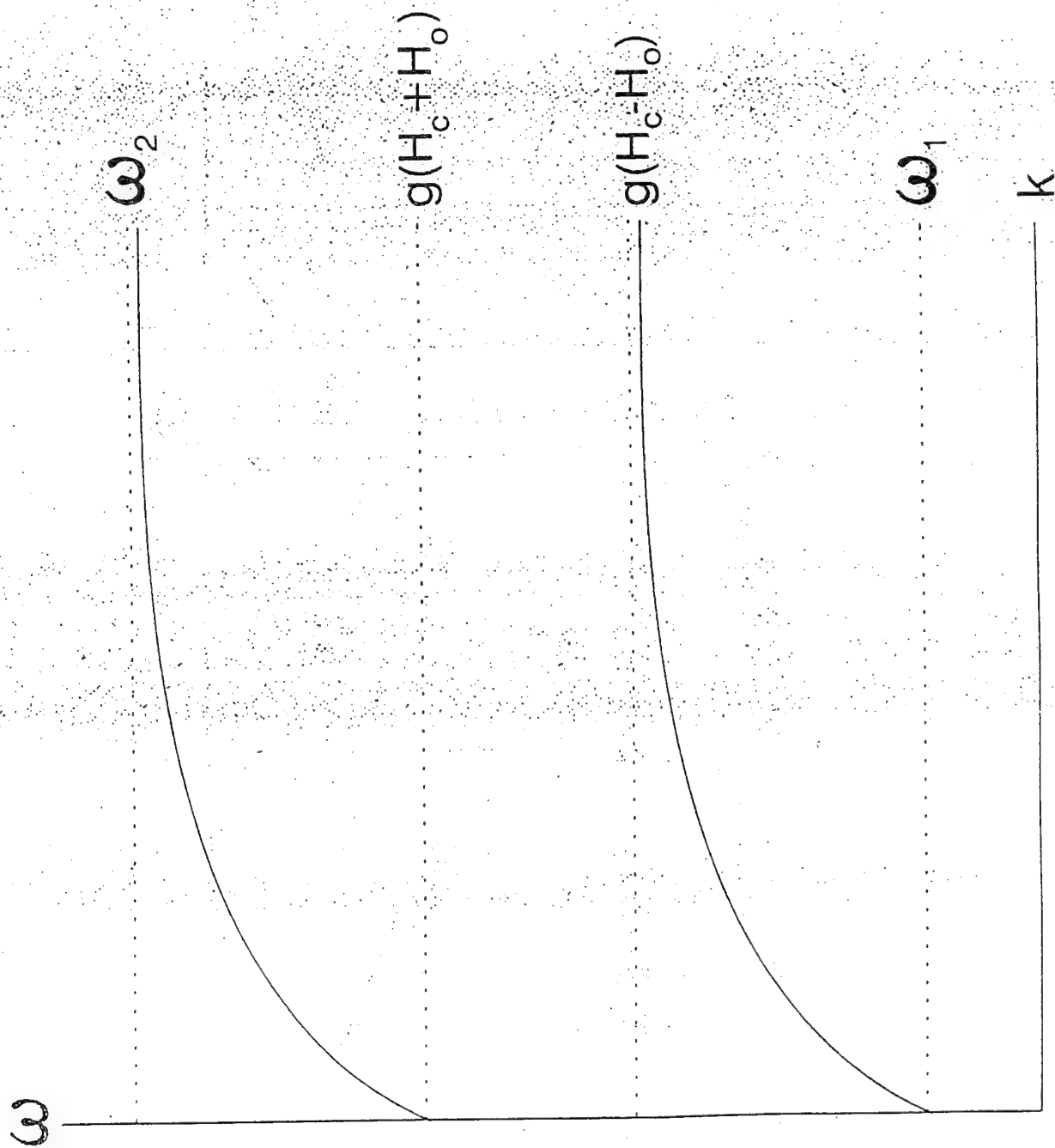
$$\omega_1 < \omega < g(H_c - H_o)$$

Upper branch

$$g(H_c + H_o) < \omega < \omega_2$$

- zero external field ($H_o = 0$): only one branch in range

$$gH_c < \omega < g(H_c^2 + R^2)^{1/2}$$



Volume Waves

Perpendicularly Magnetized Antiferromagnetic Film

- group-velocity dispersion for this ($H_0=0$) branch is

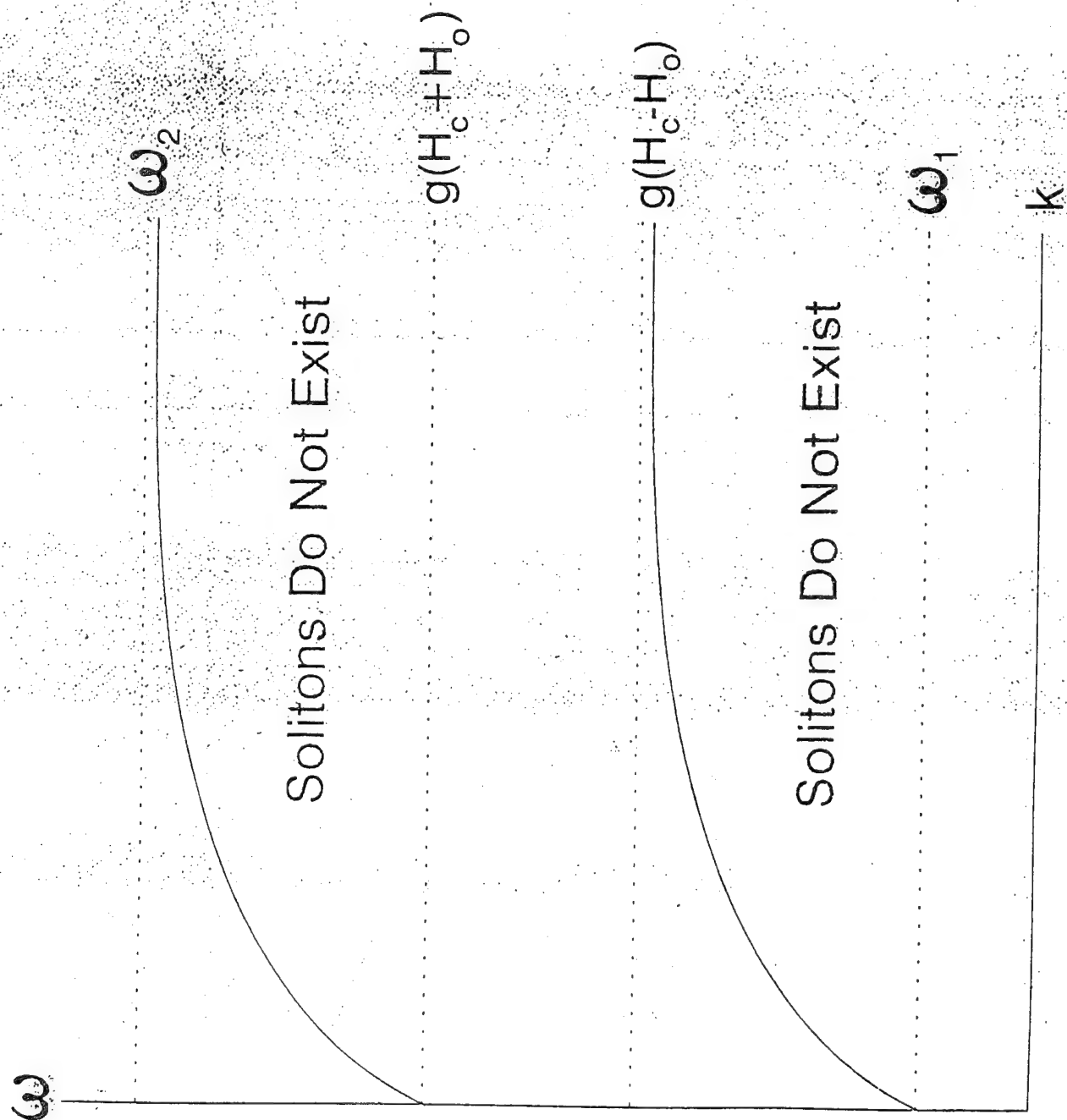
$$\beta_2 = -\frac{1}{V_3} \frac{gH_c d^2}{4} < 0 \quad \text{GVD}$$

$$V_3 = \frac{gH_c d}{2} \quad \text{Group Velocity}$$

- nonlinear coefficient

$$\gamma \approx -\frac{2}{V_3} \frac{gH_e H_a}{H_c} < 0$$

- Lighthill criterion not satisfied



Conclusions

- Envelope solitons of dipole spin-wave type are possible in two-sublattice uniaxial antiferromagnetic films.
- If the external magnetic field is parallel to the axis of anisotropy, and is in the plane of the film, surface and volume dipole spin waves propagate within the film.
- If the external magnetic field is perpendicular to the film surface, and parallel to the anisotropy axis, volume dipole spin waves can exist in the antiferromagnetic film, for rather weak fields ($H_0 < H_c$).
- For the tangentially magnetized antiferromagnetic film, the necessary and sufficient conditions for envelope soliton formation are satisfied.
- Hence, solitons can exist for the surface waves belonging to the upper branch of the spectrum. Solitons can exist for volume waves belonging to both branches of the spectrum.
- It is explained, simply, why solitons cannot exist for volume waves propagating in a normally magnetized antiferromagnetic film.

Controlling Chaos in Nonlinear Magnetic Thin Films*

by P.E. Wigen

with M. Ye and D.W. Peterman
Ohio State University

Workshop on Nonlinear Interactions in Magnetic and
Magneto optic Materials

Costa Mesa, CA
12-14 December 1993

* supported in part by NSF

Controlling Chaos in Nonlinear Magnetic Films

Outline

- I Chaos in Bulk Ferromagnets
- II Chaos in Thin Film YIG Disks
- III Controlling Chaos
- IV Concluding Remarks

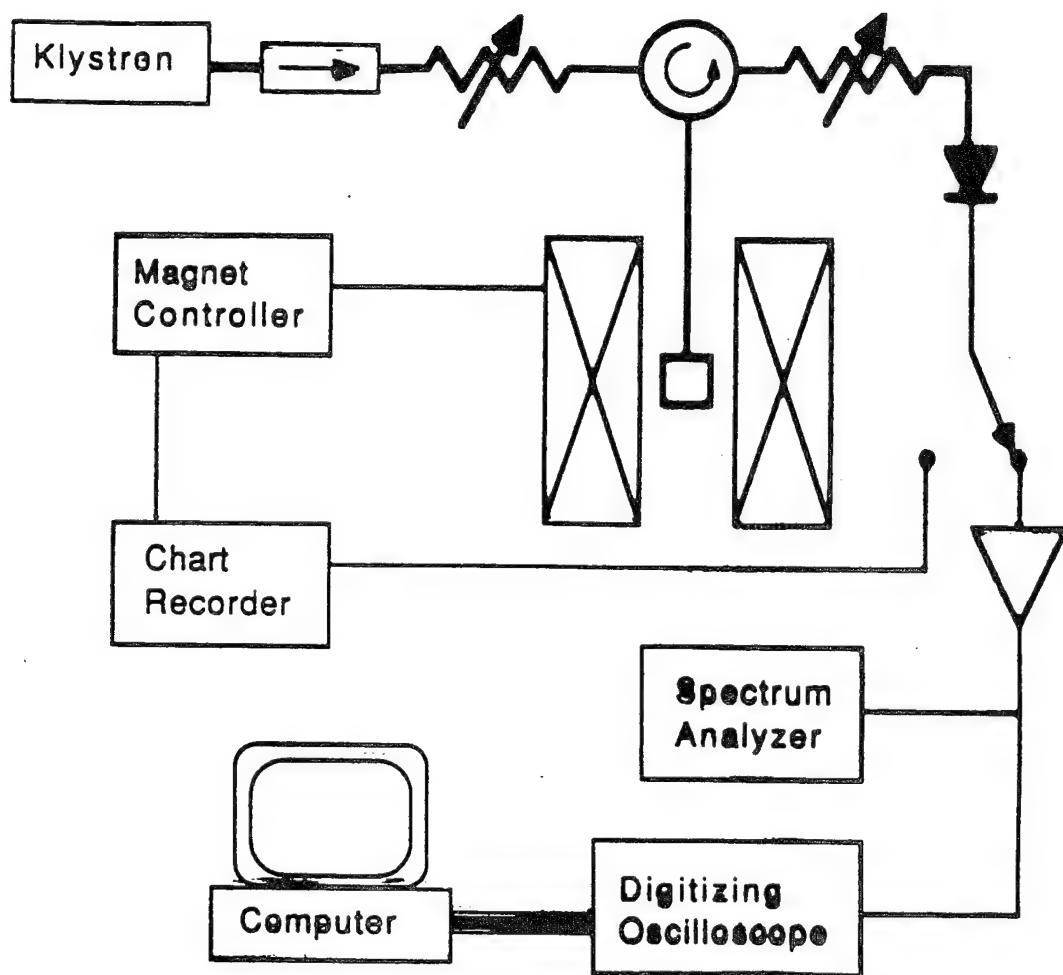
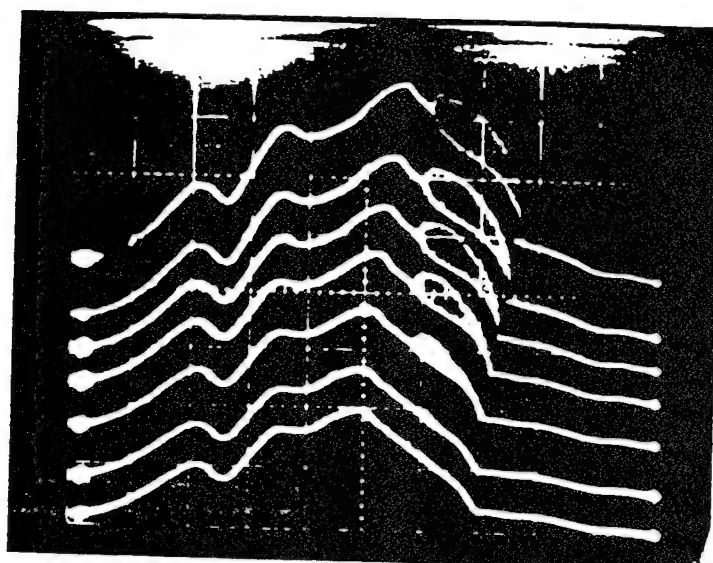


Diagram of the experimental setup used for nonlinear ferromagnetic resonance. The magnetic field is supplied by a Varian 15" magnet controlled by the magnet controller. X-band microwave power is supplied by a Varian X-13 klystron which produces about 50 mW of power at about 9.2 GHz. After passing through an isolator, precision attenuator, circulator and slide screw tuner, the microwaves are incident on a TE₁₀₂ cavity. The cavity is nearly critically coupled so only a small amount of microwave power is reflected from the cavity at its resonant frequency. The reflected power is routed via the circulator to a crystal detector, and from there, the absorption signal is analyzed electronically.

Perpendicular Resonance



→ f

$$f_c = 983.4 \text{ MHz}$$

$$\Delta f = 15 \text{ MHz}$$

$$H = 59.8 \text{ mT}$$

$$P_7 = 0.26 \text{ m}$$

$$P_6 = -0.5$$

$$P_5 = -1.0$$

$$P_4 = -1.5$$

$$P_3 = -2.0$$

$$P_2 = -2.5$$

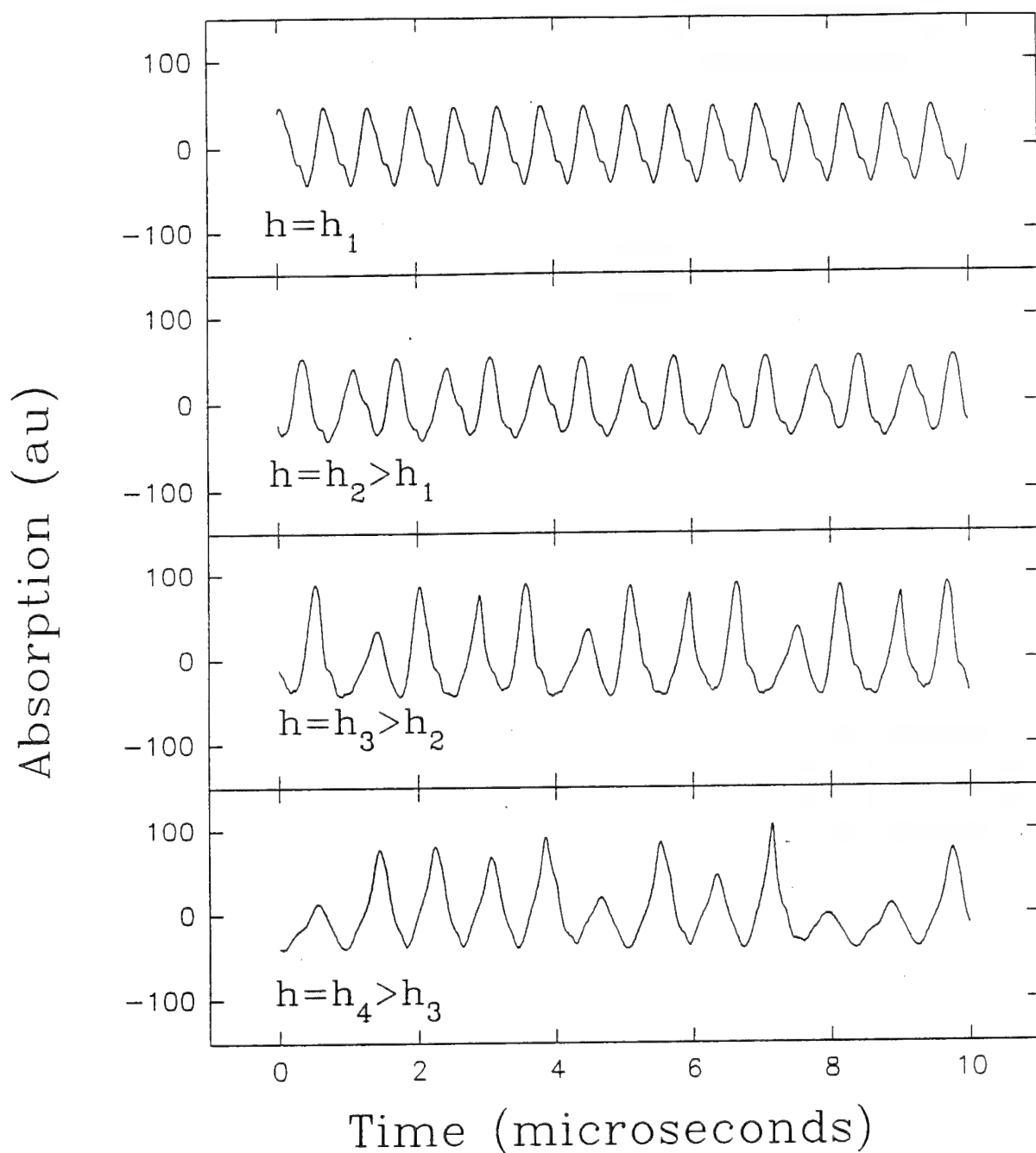
$$P_1 = -2.6$$

with H. Dötsch

1988

Ferromagnetic resonance spectra at varying microwave power. The microwave power increases from the bottom spectrum to the top. The fuzzy bulge at the high frequency side of the spectra indicate an instability in the microwave absorption called auto-oscillation.

Bifurcation Route to Chaos in the FMR Absorption Signal as the Driving Field h is Increased



As the amplitude of the microwave driving field h is increased, the period doubles (bifurcates), and at some critical amplitude of the driving field (h_4), the sample absorption becomes chaotic.

Magnetic materials display a rich variety of nonlinear dynamic phenomena.

- Regular auto-oscillations
- Period doubling
- Irregular period oscillations
- Intermittency
- Chaos
- Periodic windows

Investigations centered on magnetic systems are motivated by several advantages:

- Magnetic resonance is a well established field.
- The chaotic response occurs in a homogeneous bulk media.
- At resonance the precession angle of the magnetization vector increases with a driving parameter.
- Nonlinear effects generate both temporal and spatial fluctuations in the media.
- The resonance occurs at GHz frequencies.
- The auto oscillations occur at 0.5-15MHz.
- A number of parameters can be readily controlled:

magnetic field

frequency

temperature

geometry

material parameters

Spin Hamiltonian

$$\begin{aligned}
 H &= H_Z + H_A + H_{dd} + H_{EX} \\
 &= -g\mu_B H \cdot S - K_1 (S_x^2 S_y^2 + S_y^2 S_z^2 + S_z^2 S_x^2) \\
 &\quad - K_u S_z^2 + D_{ij} (S_z^2 + - \frac{3}{r_{ij}^2} S_i \cdot r_{ij} S_j \cdot r_{ij}) \\
 &\quad - 2J_{ij} S_i \cdot S_j
 \end{aligned}$$

$$S_x = \frac{1}{2} (b + b^*) (2S - b^*b)^{1/2}$$

$$S_y = \frac{1}{2} (b - b^*) (2S - b^*b)^{1/2}$$

$$S_z = S - b^*b$$

The Hamiltonian involves terms associated with the interaction of the sample with the static field, the anisotropy energy, the dipole-dipole interaction energy, and the exchange interaction energy. The spin operators are expressed in terms of Bose raising and lowering operators.

$$\mathcal{H} = \mathcal{H}_Z + \mathcal{H}_A + \mathcal{H}_{dd} + \mathcal{H}_{Ex}$$

$$\mathcal{H}_i = \mathcal{H}_i(b_k b_k^* \dots)$$

$b_k + b_k^*$ satisfy Hamilton's Equations

$$\frac{db_k}{dt} = i \frac{\partial \mathcal{H}}{\partial b_k^*} = i \omega_k b_k$$

The low power spectra is equivalent to neglecting all terms beyond those that are quadratic in b_k

This determines the normal modes of the system

Higher order terms in b_k add nonlinearities and chaos

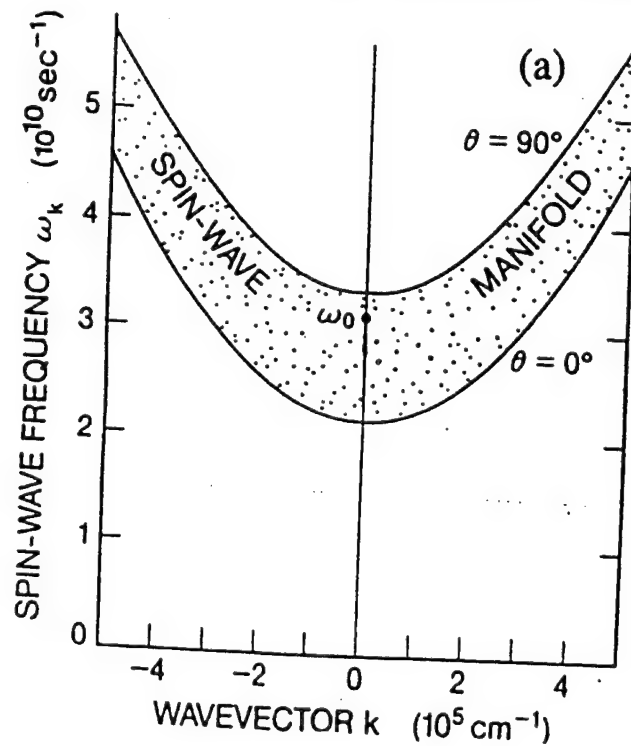
In terms of bose operators,

$$\mathcal{H}^{(2)} = \sum_k \omega_k b_k b_k^*,$$

and the spinwave dispersion relation is

$$\omega_k^2 = \left[\omega_z - \omega_M N_z + \omega_e (ak)^2 + \omega_A + \omega_M \frac{\sin^2(\theta)}{2} \right]^2 - \omega_M^2 \frac{\sin^4(\theta)}{4}$$

- $\omega_z = \gamma H_0$
- $\omega_M = 4\pi\gamma M$
- $\omega_A = 2\alpha K_A/M$ where α is the contribution of the anisotropy energy depending on the crystallographic direction of the applied field, H_0 .



The frequency values above are for a ferromagnetic sphere. The uniform resonance frequency for a sphere, ω_0 , is degenerate with approximately 10^{10} spin wave modes of the sphere.

Nonlinear terms:

Three magnon terms:

$$\mathcal{H}^{(3)} = \frac{1}{2} \sum_k A_{0k} b_0^* b_k b_{-k}.$$

Allows the uniform precession, b_0 , to excite $\pm k$ Suhl spinwave pairs in the 2nd order Suhl instability.

Four magnon terms:

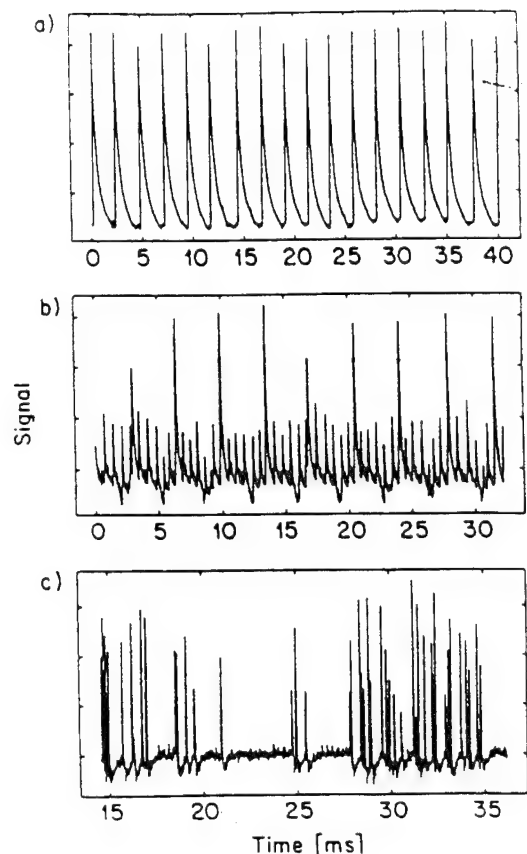
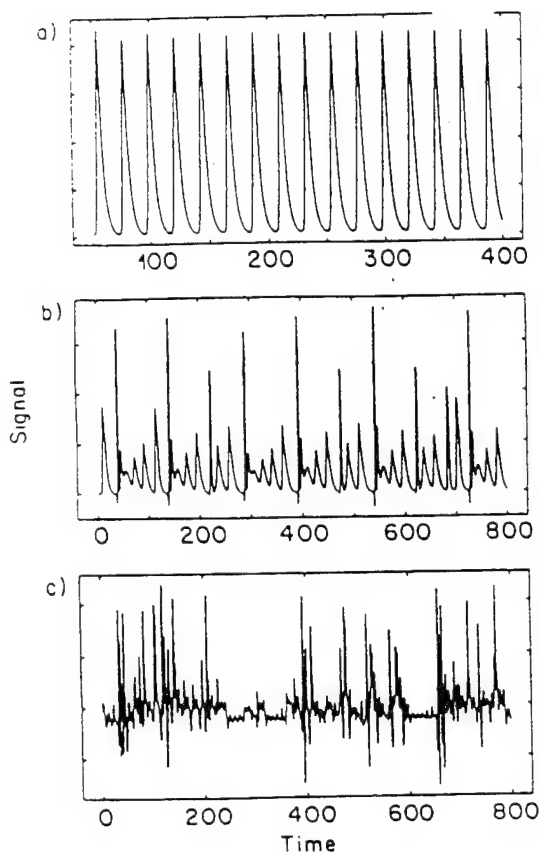
In the random phase approximation, the excited $\pm k$ spinwaves are coupled to degenerate $\pm k'$ spinwaves.

$$\mathcal{H}^{(4)} = \sum_{k,k'} T_{k,k'} b_k b_k^* b_{k'} b_{k'}^* + \frac{1}{2} \left[\sum_{k,k'} S_{k,k'} b_k b_{-k} b_{k'}^* b_{-k'}^* + c.c. \right],$$

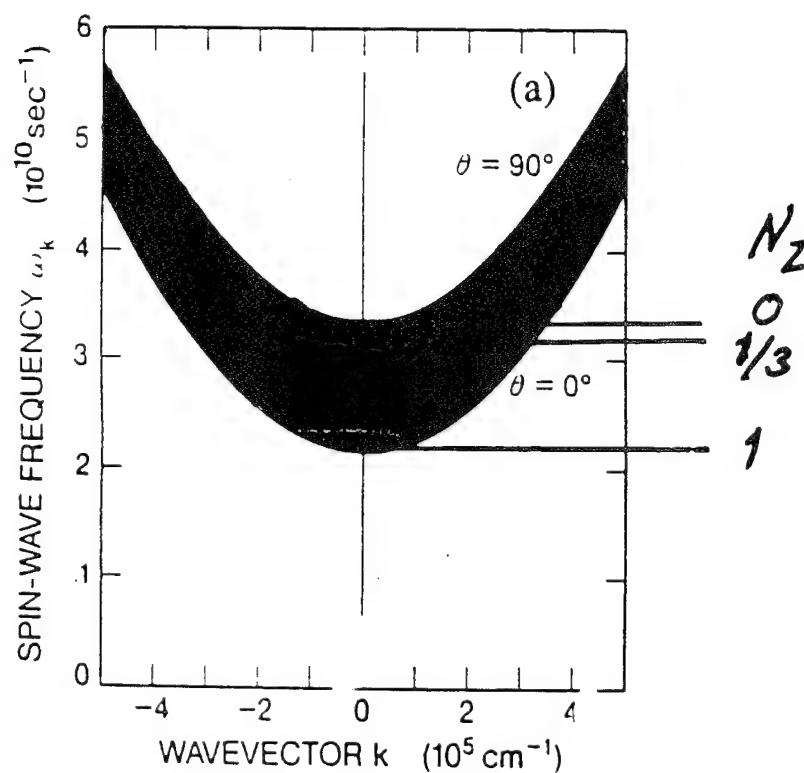
The $T_{k,k'}$ terms renormalize the spinwave frequencies,

$$\Omega_k = \omega_k + 2 \sum_{k'} T_{k,k'} |b_{k'}|^2.$$

$S_{k,k'}$ terms annihilate pairs of $\pm k$ spinwaves while creating $\pm k'$ pairs.



Truncating the number of active modes still yields qualitatively good results. On the left are signals from a truncated model compared to experimental signals on the right. From M. Warden, thesis. Despite the large number of degenerate modes, experimental chaotic signals often have fractal dimensions between 3 and 5, indicating that the system reduces the number of degrees of freedom. This suggests that cooperative modes are developed. Intensive effort is underway to determine the nature of these normal modes in bulk magnetic materials.



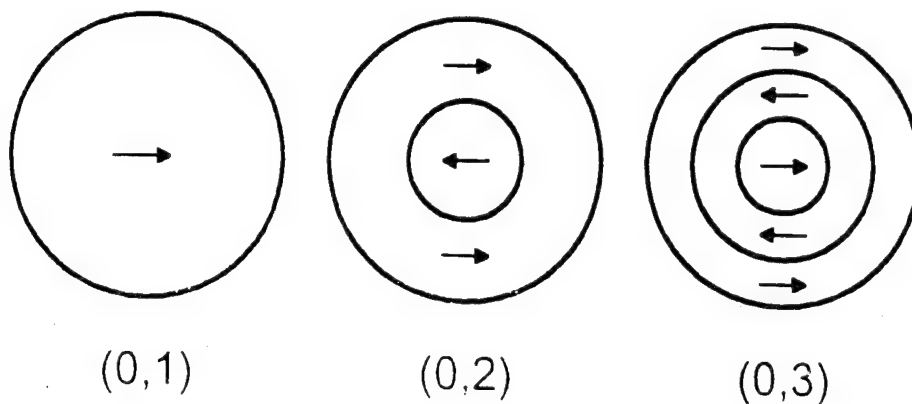
Unlike FMR in spheres where the resonance is degenerate with a large number of spin wave modes in the middle of the spin wave band, in a disk, the driven modes are at the bottom of the band, and relatively few modes are excited. This is due to the difference in the demagnetization factors between a sphere and a disk.

For a circular film, the spatial functions are of the form

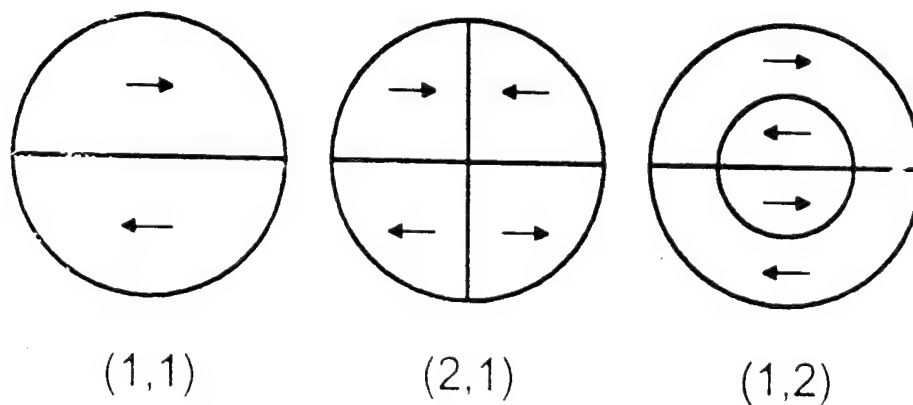
$$m_{\nu,s}(\vec{r}) = \frac{1}{J_{\nu+1}(x_{\nu,s})} J_{\nu}(x_{\nu,s}\rho/a) \begin{Bmatrix} \sin(\nu\phi) \\ \cos(\nu\phi) \end{Bmatrix}$$

where $x_{\nu,s}$ is a zero of the Bessel function J_{ν} and a is the sample radius.

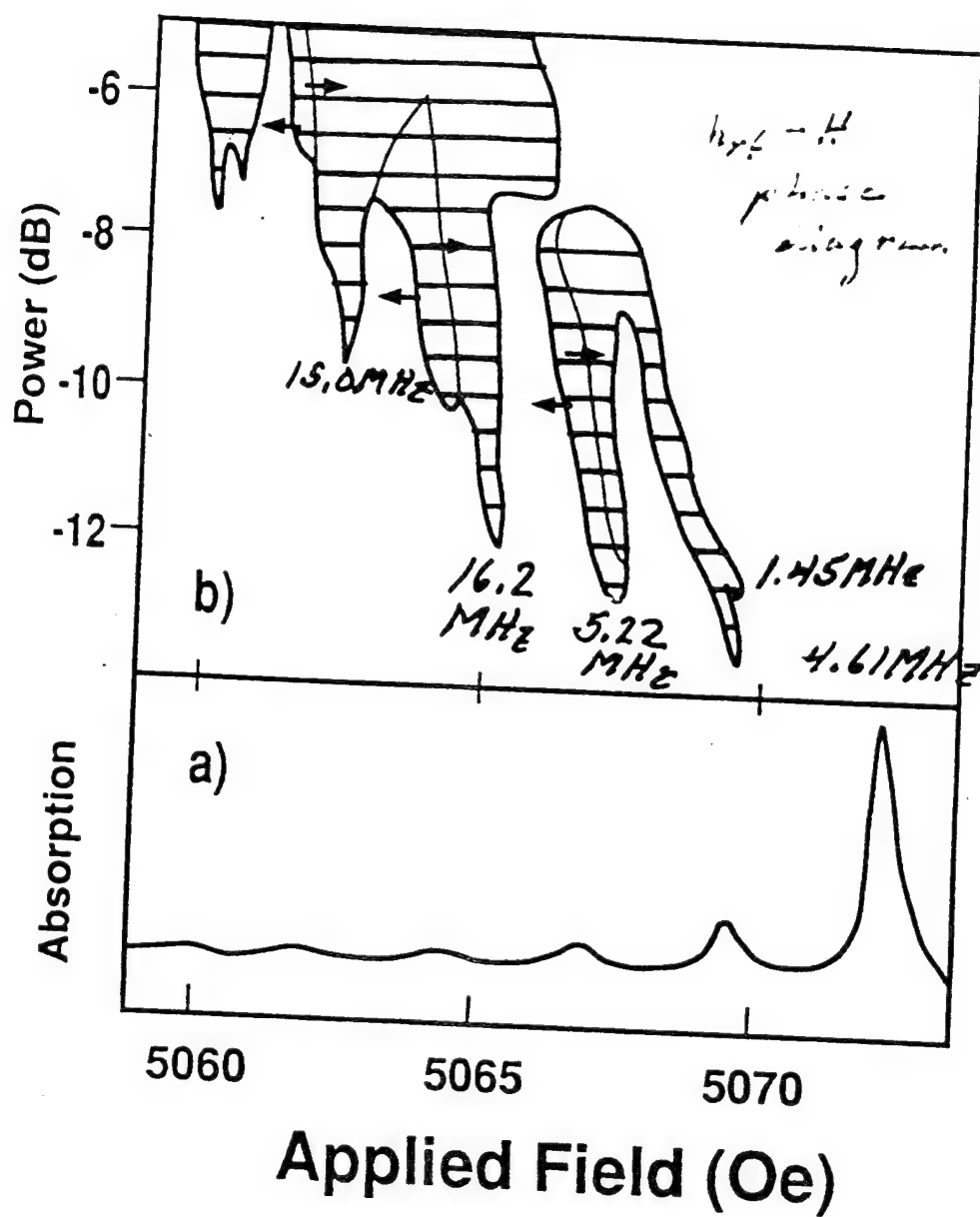
Direct Modes



Hidden Modes



Domains of the transverse component of magnetization of the lowest magnetostatic modes in a circular disk.



a) Low power FMR absorption of a thin circular YIG film as a function of the magnetic field; b) Fingers of instability oscillation in the rf pumping power-magnetic field plane. The low-field borders of fingers show hysteresis as the magnetic field was swept in the direction indicated by the arrows.

$$\mathcal{H} = \mathcal{H}_{static} + \mathcal{H}_{demag} + \mathcal{H}_{dd} + \mathcal{H}_{pump}.$$

$$M^+ = M_x + iM_y = a(2\gamma M_s - \gamma^2 aa^*)^{1/2}$$

$$a = \sum_i a_i m_i(\vec{r})$$

$$\mathcal{H} = Const + \gamma \left[(H_0 - 4\pi M_s + 2M_s D_{ii}) a_i a_i^* \right. \\ \left. + 2\pi\gamma \sum_{ijkl} A_{ijkl} a_i^* a_j^* a_k a_l \right] + \mathcal{H}_{pump}.$$

The Hamiltonian for a disk includes the interaction with the static field, the demagnetization field, the dipole-dipole interaction and the microwave pumping field. The magnetization operators are expanded in terms of the normal modes of the disk (Bessel functions). From the Hamiltonian, the equations of motion of the mode amplitudes can be derived. Note that the non-linear term arises from the dipole-dipole

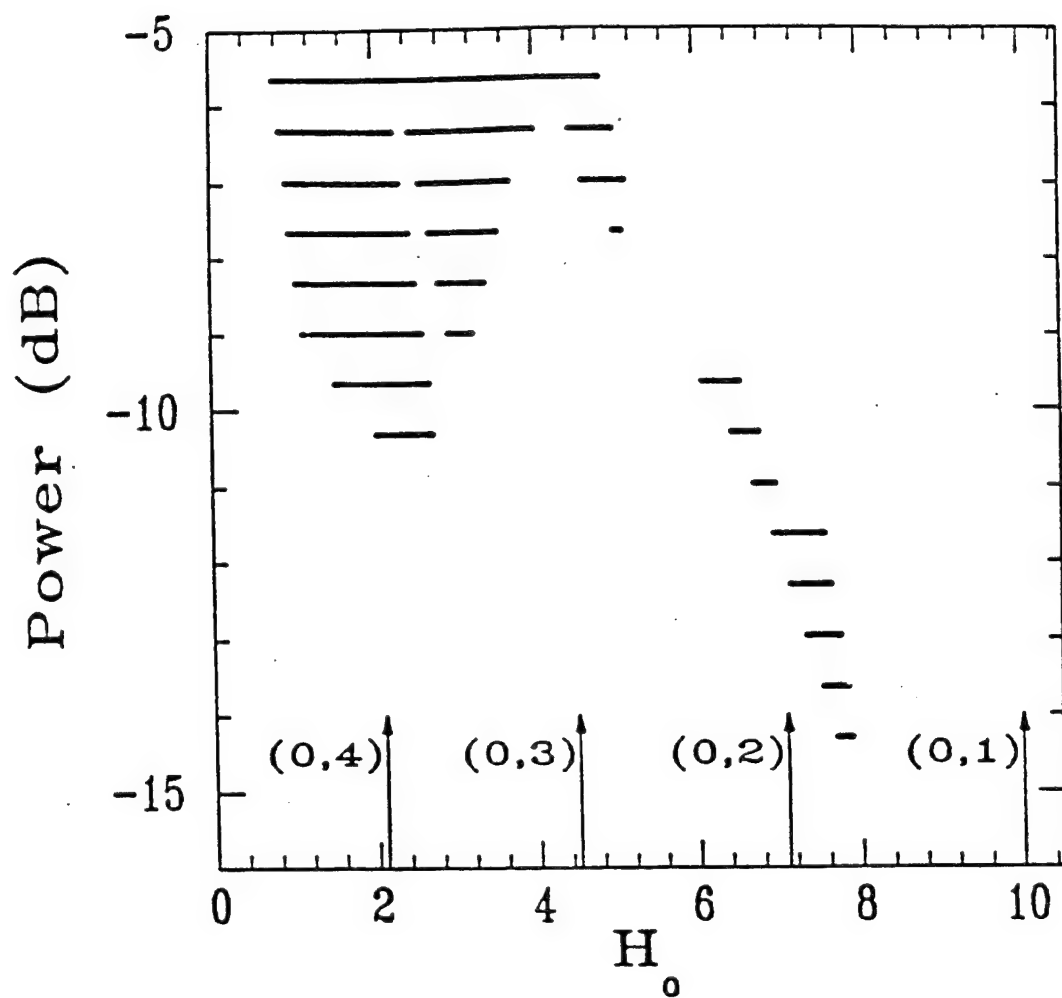
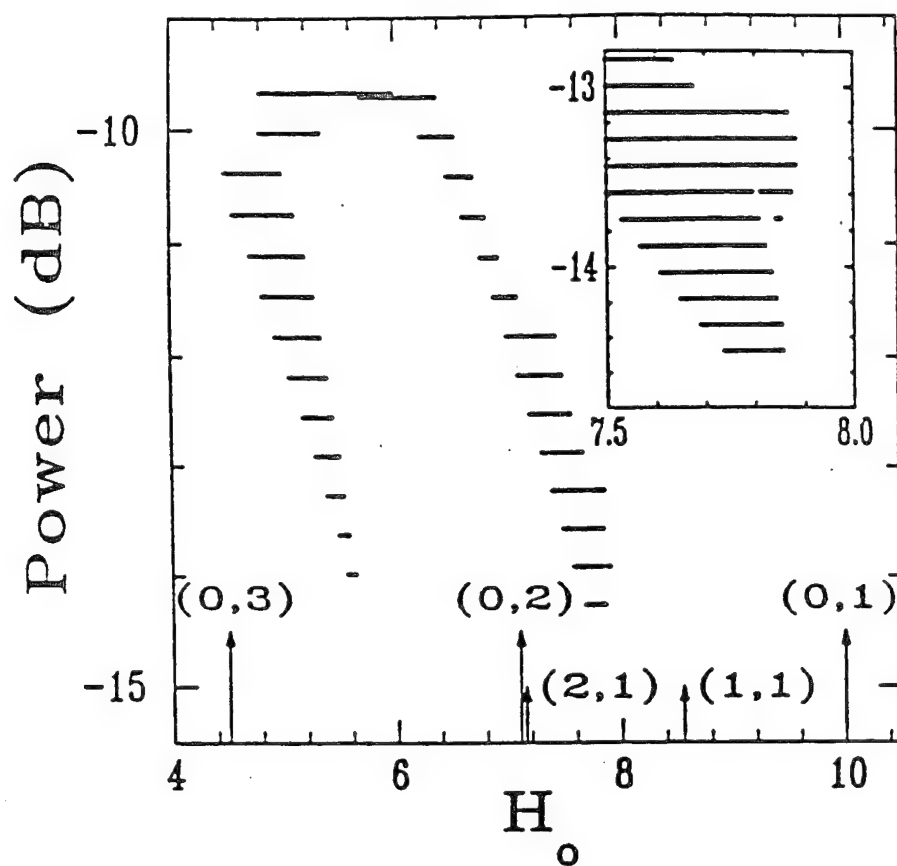


Figure 5.3: Domain of auto-oscillation in a model including only the (0,1), (0,2), (0,3), and (0,4) modes.

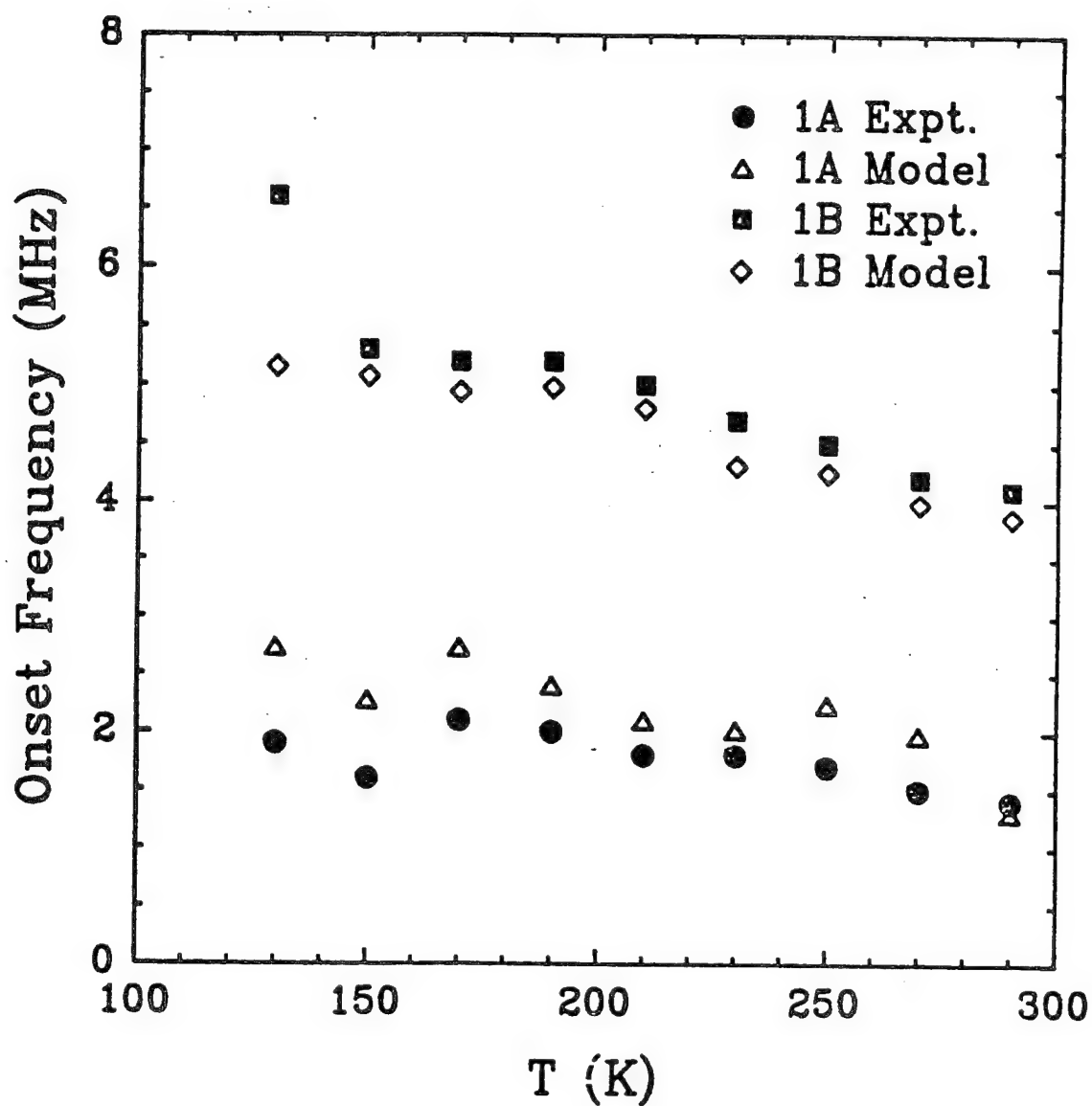


By including the (2,1) and (1,1) hidden modes along with the (0,1), (0,2) and (0,3) direct modes, "thumbs" seen in the experiment can be reproduced, suggesting that the hidden modes play a role in the system dynamics.

Finger #	frequencies (MHz)		Onset power (dB)	
	model	expt.	model	expt
1	3.97	4.61	-14.5	-13.5
	1.5	1.5	-13.7	-12.5
2	—	5.22	—	-12.5
	7.8	9.2	-14.0	-12.5

Table 5.2: Auto-oscillation frequencies calculated from the five mode model and values obtained from sample 1.

Onset Frequency vs. Temp. for the low (1A) and high (1B) frequency branches of the first finger.



CONTROLLING CHAOS

Goal - stabilize certain unstable orbits

Three recognized techniques:

1. Ott, Grebogi, Yorke (OGY) PRL '88

Discrete method of applying a perturbation at intervals determined by behavior in phase space.

2. Hunt PRL '91

Discrete method of applying a perturbation at intervals determined by behavior in time space.

3. Pyragas PL A '92

Analog method applying a continuous "feedback" perturbation.

1. OGY Method - discrete

Consider a path in N-dimensional phase space

Goal is to stabilize the orbit such that it regularly penetrates the plane at a fixed point Φ_F

A region for Φ_n near Φ_F is defined over which a linear response to a perturbation of some systematic variable is expected

Behavior is expanded in a region near Φ_F for which a linear approximation, valid for

$$\Phi_n - \Phi_F \leq \Delta\Phi$$

then

$$\Phi_{n+m} - \Phi_F = \underline{M} \cdot [\Phi_n - \Phi_F]$$

\underline{M} is a 2x2 matrix with eigen vectors along the stable manifold and the unstable manifold (saddle point) associated with the perturbation

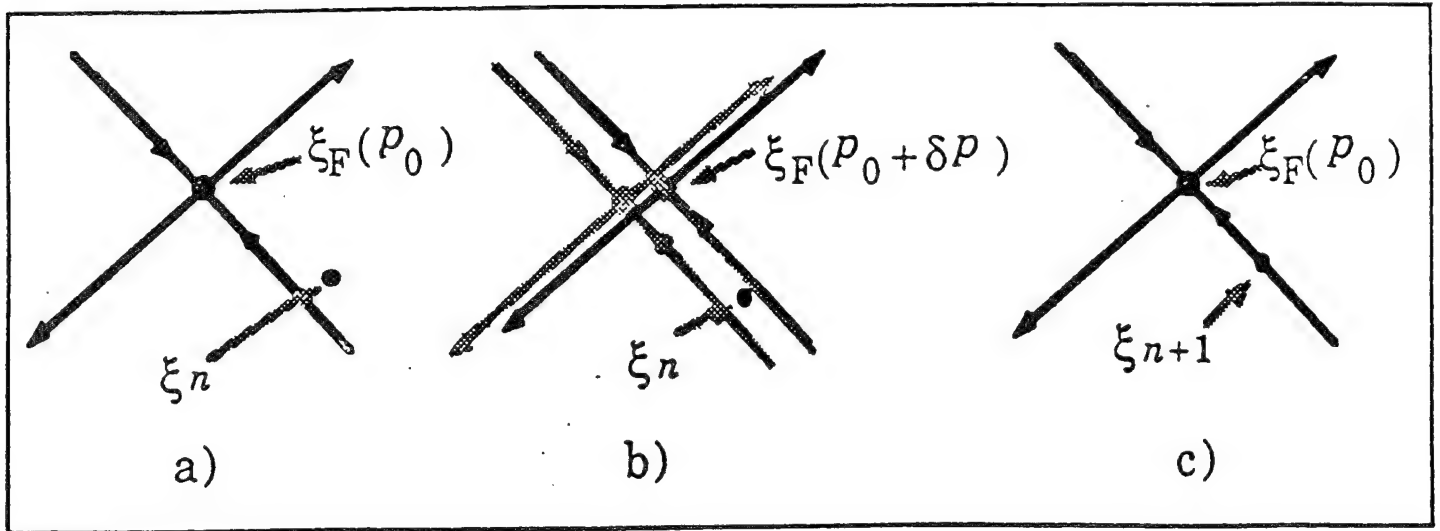
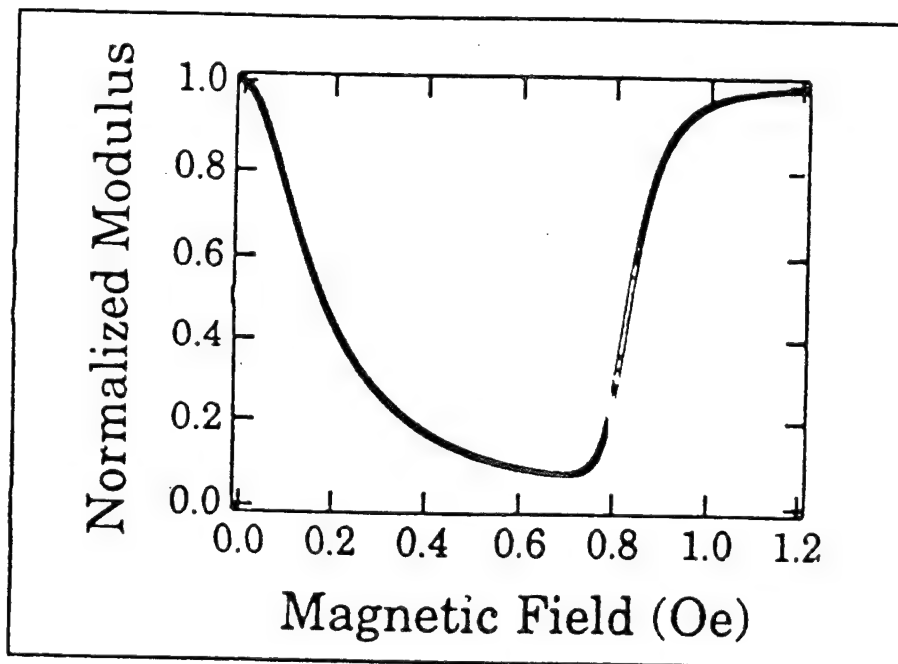
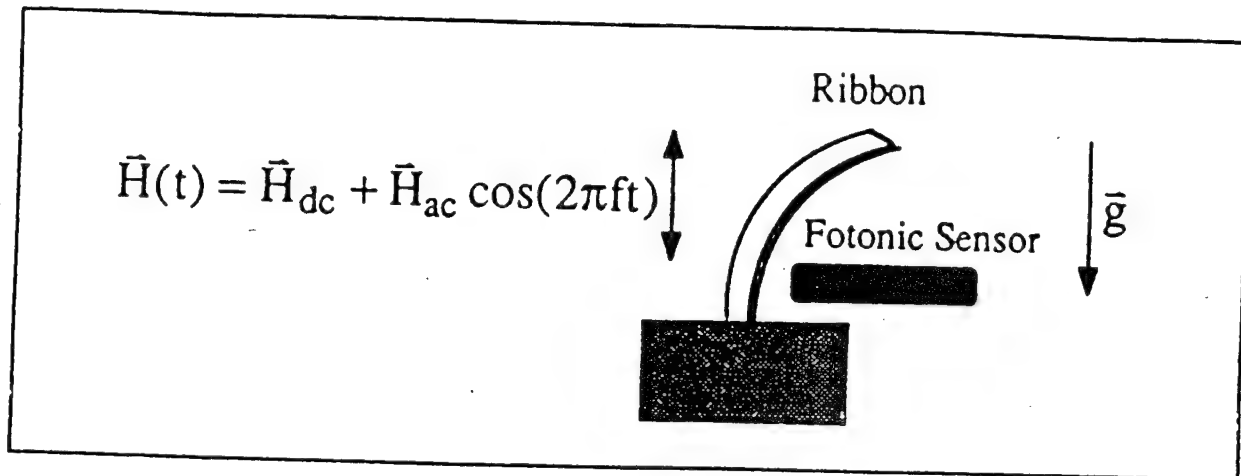


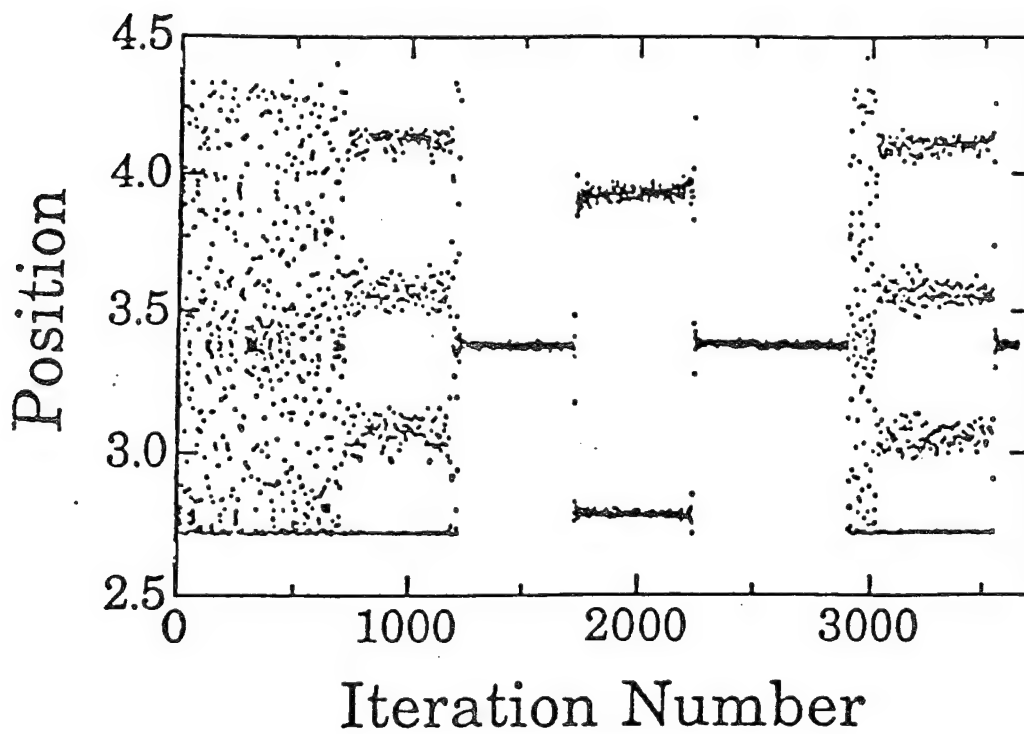
Figure 3. Outline of OGY control algorithm for a saddle fixed point: (a) the n^{th} iterate ξ_n falls near the fixed point $\xi_F(p_0)$. (b) Turn on the perturbation of p to move the fixed point. (c) The next iterate is forced onto the stable manifold of $\xi_F(p_0)$. Turn off the perturbation.

From Ditto, Rauseo, and Spano.

Controlling Chaos in a Magnetoelastic Ribbon



The experimental setup of Ditto, Rauseo and Spano who used the OGY method to stabilize the chaotic swaying of a magnetoelastic ribbon. The ribbon's Young's modulus was highly sensitive to external magnetic fields, so the external AC magnetic field induced chaotic motion. Ditto, Rauseo and Spano were able to apply discrete perturbations to the magnetic field to create a periodic motion in the ribbon under circumstances that would be chaotic without perturbation.



The ability of DRS to switch the periodicity of the ribbon. Notice the brief chaotic transients between switchings. From the Proceedings of the 1st Experimental Chaos Conference.

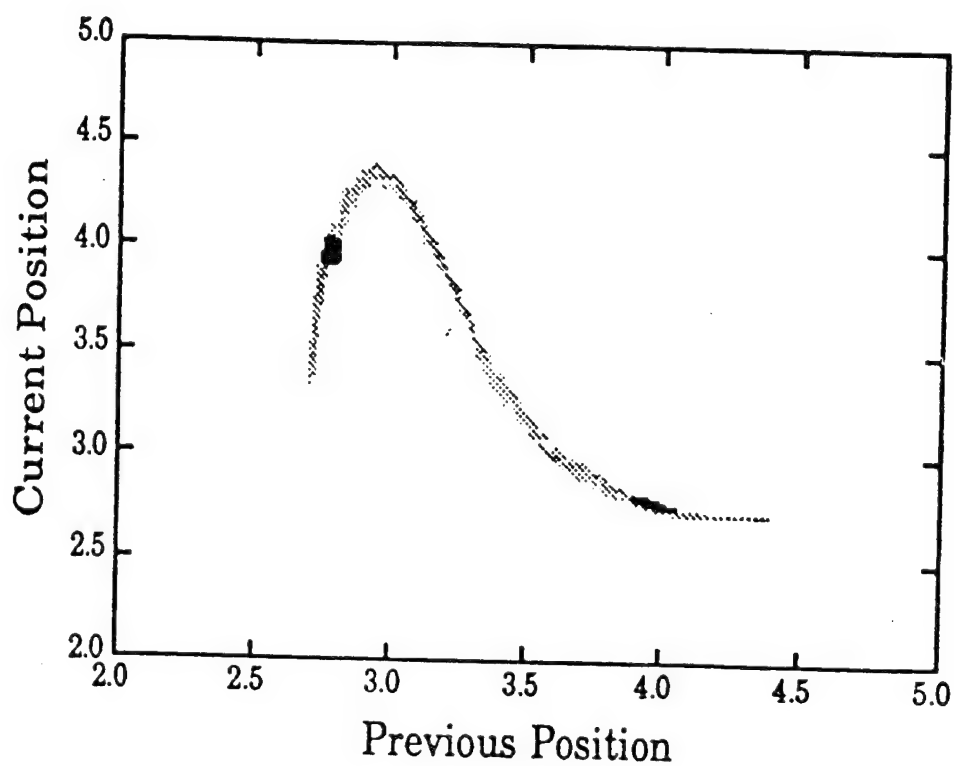
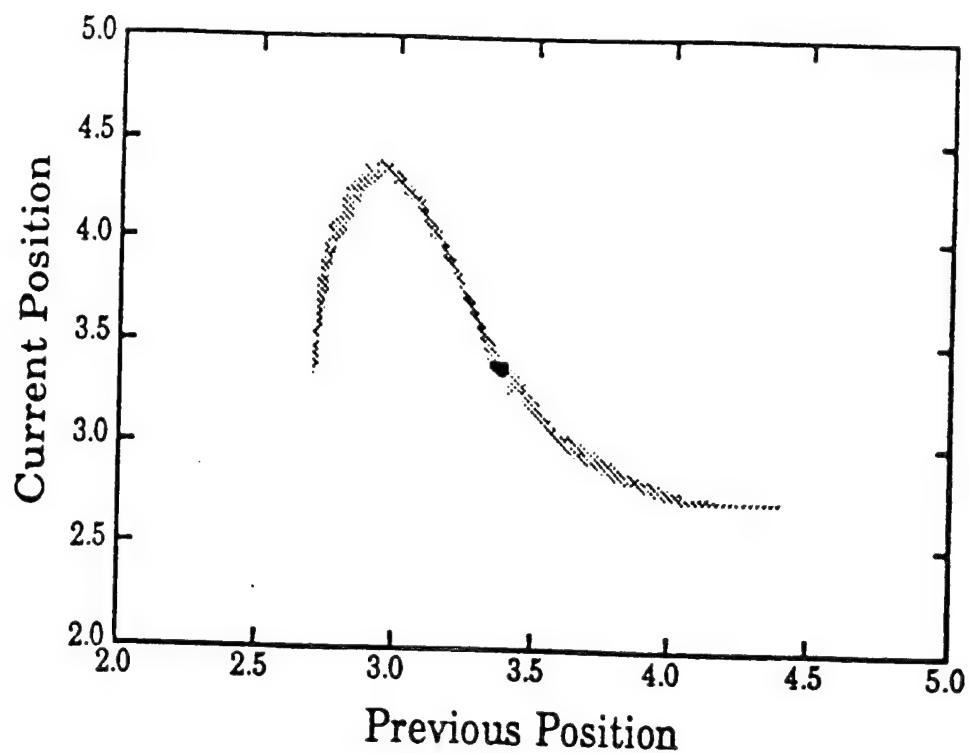


Fig. 4. The current ribbon position V_i is plotted versus the previous position V_{i-1} yielding a phase portrait of the attractor. (a) Period one control (black). (b) Period two control (black). In both cases the grey represents the uncontrolled chaotic behavior.

2. Hunt Method

A modification of OGY.

Consider an oscillatory time signal

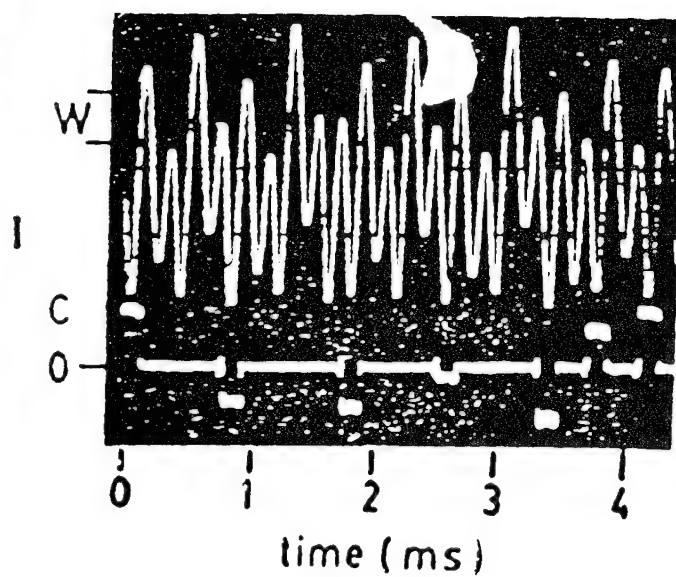
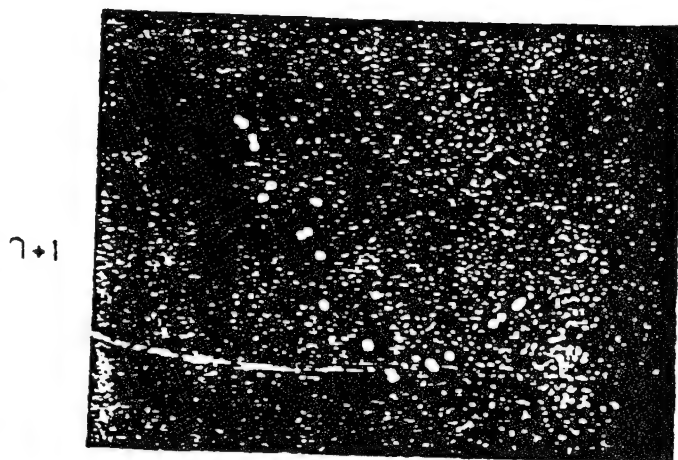
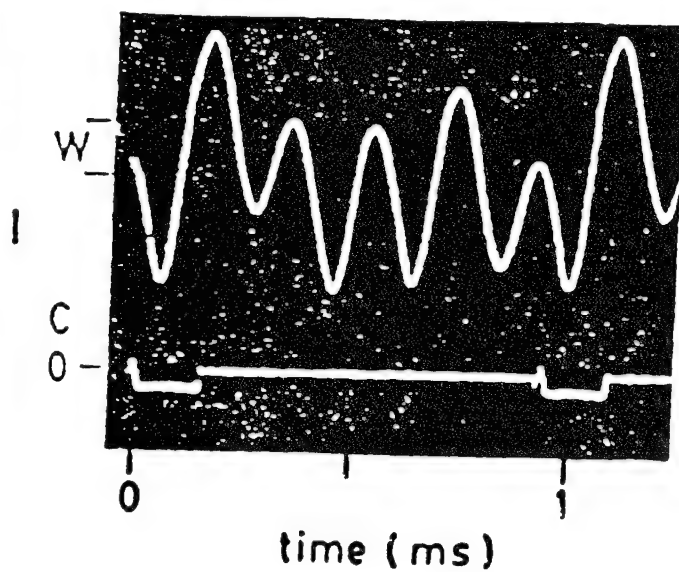
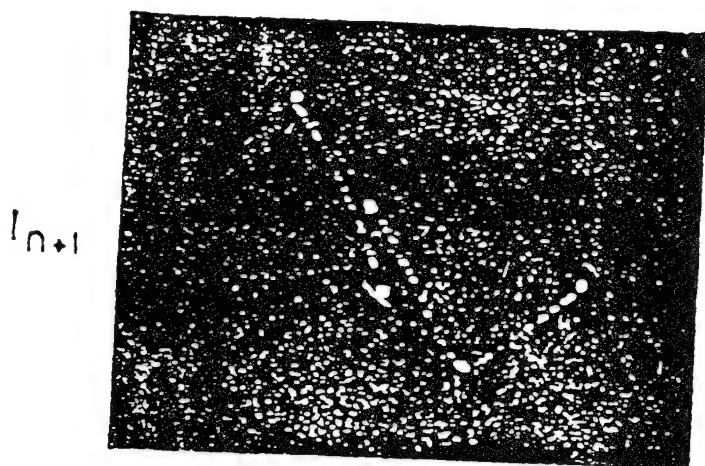
An amplitude window W establishes the application and magnitude of the perturbation

$$F = L[A_n - W_m] \delta$$

$$\delta = \begin{cases} 1 & \text{if } |A_n - W_m| \leq W/2 \\ 0 & \text{if } |A_n - W_m| > W/2 \end{cases}$$

Example is a resonator circuit driven at 53 kHz

Chaotic signals have been stabilized in periodic orbits up to period 86!



First return map (I_{n+1} vs I_n , left) and the current through chaotic oscillator (right). By applying the control signal indicated in (c), the system stabilized on period 5 (upper graphs) and period 21 (lower graphs) orbits.

3. Pyragas Method

An analog technique

$F(t)$ is a perturbation to an external control parameter

$$F(t) = K [y_i(t) - y(t)] = K D(t)$$

$y_i(t)$ is the desired behavior (stable orbit) of the system

$y(t)$ is the actual response

$D(t)$ is the difference

K is the adjustable weight/drive factor

Example is Rossler system and the Lorenz system

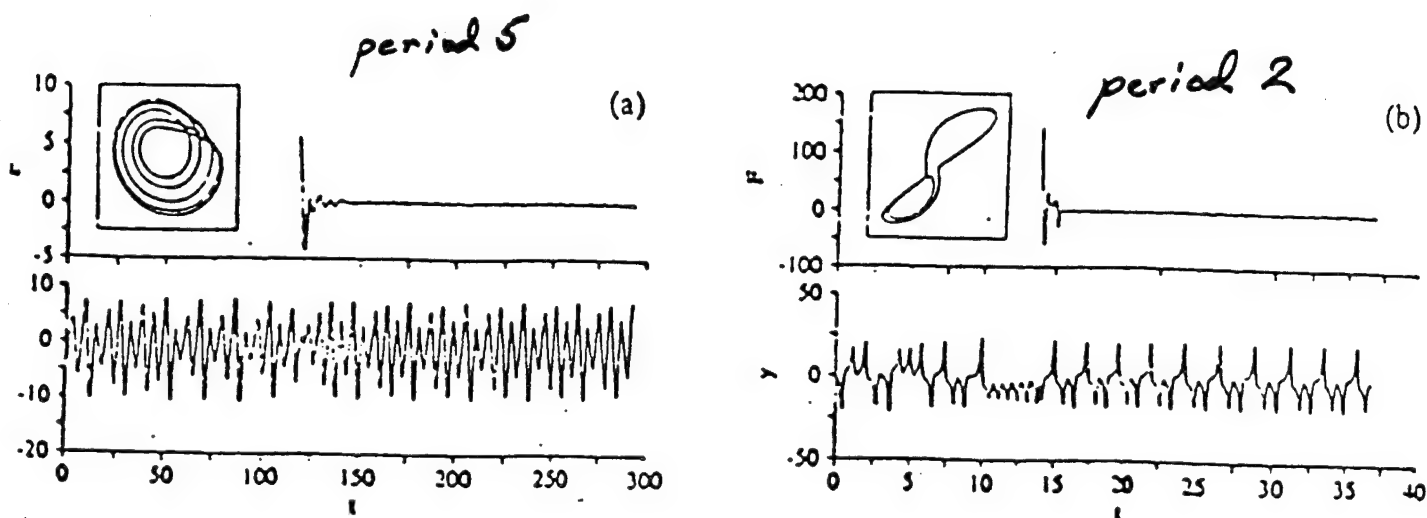


Figure 2: The output signal $y(t)$ and the forcing term $F(t)$ of the (a) Rosler system: $dx/dt = -y - z$, $dy/dt = x + 0.2y + F(t)$, $dz/dt = 0.2 + z(x - 5.7)$, stabilized to a period-5 cycle and the Lorenz system: $dx/dt = 10(x - y)$, $dy/dt = -xz + 28x - y + F(t)$, $dz/dt = xy - (8/3)z$, stabilized to period-2 motion. The inset is an x-y portrait of the stabilized system. From Pyragas

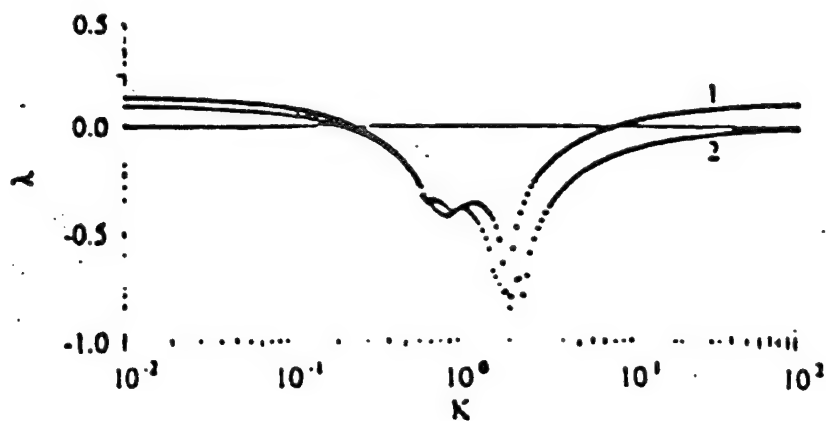


Figure 3: The graph above shows the leading Lyapunov exponent λ , a measure of the system's dependence to initial conditions, versus K in stabilizing orbital periods of 1 and 2 of the Rossler system. When λ is less than zero, the system is no longer sensitive to initial conditons. From Pyragas.

Controlling Chaos in YIG Film using Feedback Modulation

Magnetic field H_0 is modulated by the chaotic signal $S(t)$ obtained from the FMR:

$$H_0 \rightarrow H_0 + \Delta H[S(t - \tau) - \overline{S(t - \tau)}]$$

ΔH : perturbation amplitude
 τ : delay time
 $\overline{S(t)}$: DC component of FMR signal

The perturbation term is proportional to the AC component of the FMR signal.

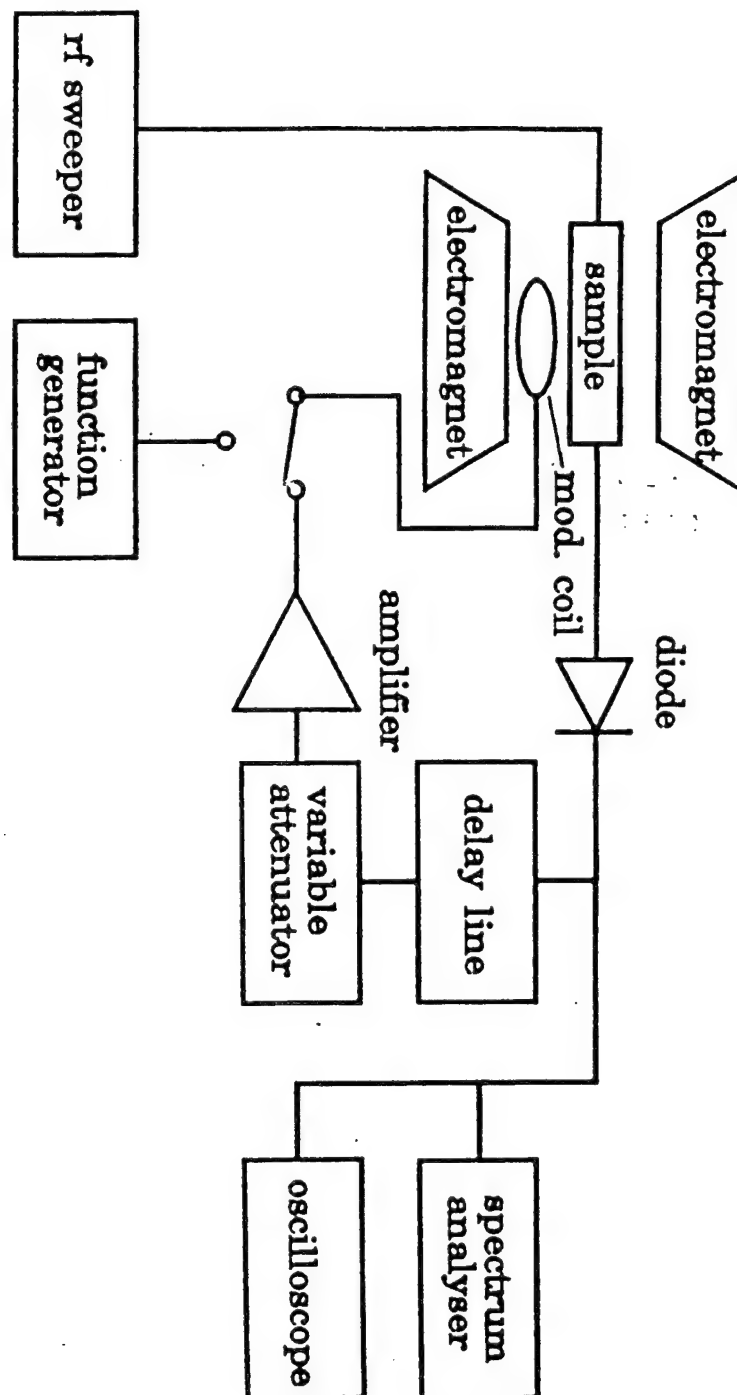
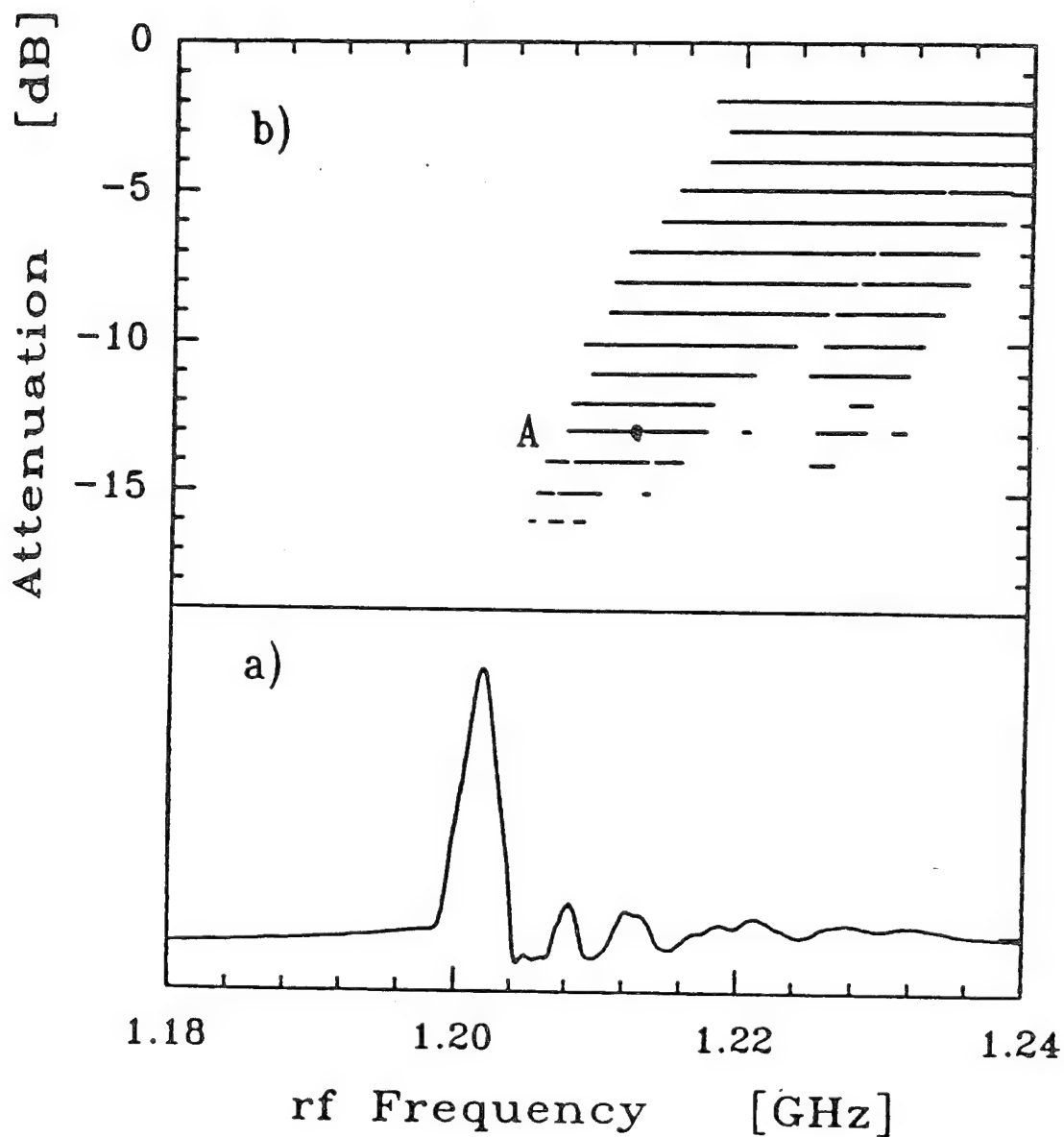
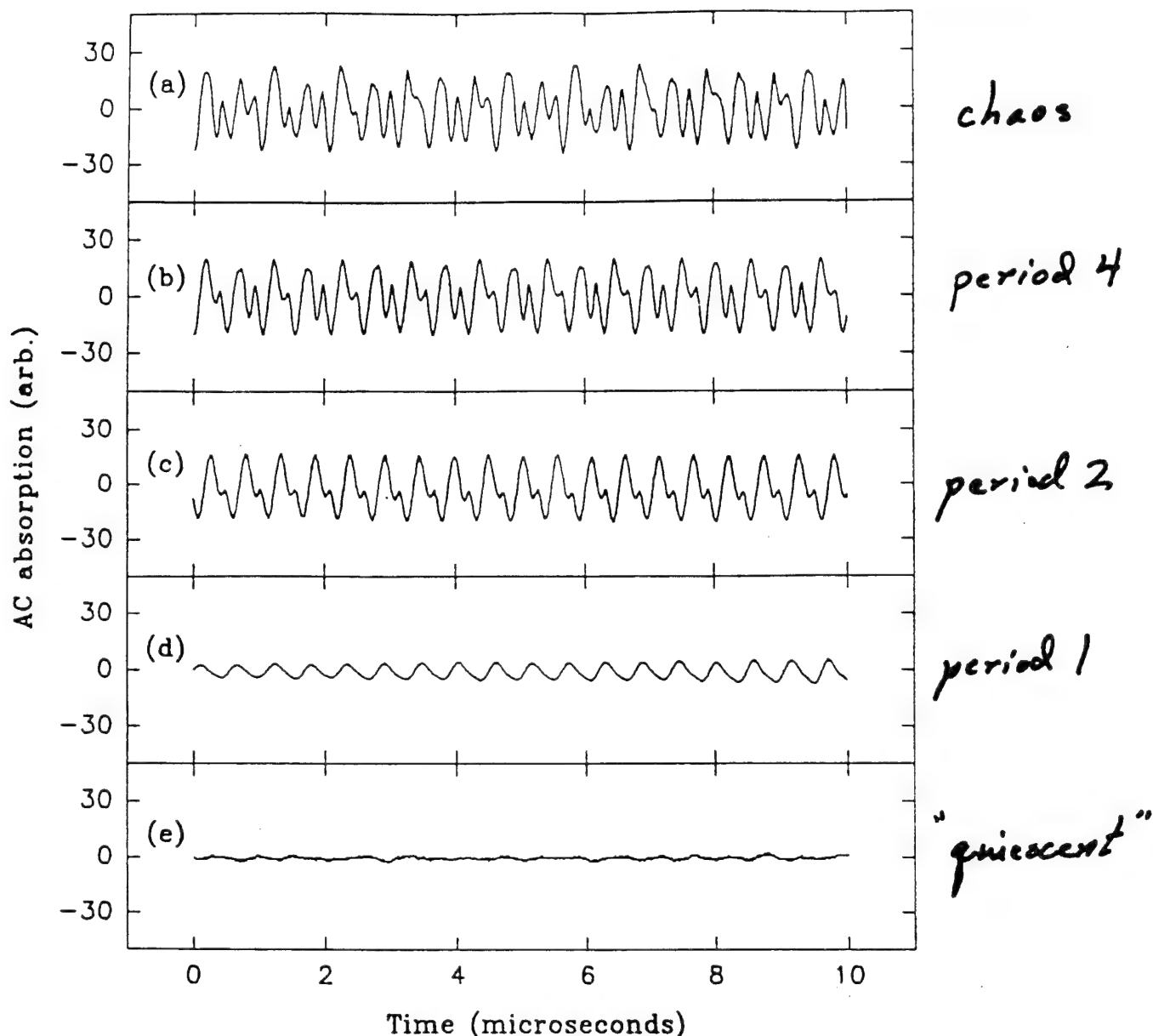


Diagram of FMR experiment for closed or open loop feedback. For open loop feedback, the function generator is engaged to perturb the sample, while in closed loop feedback, the delay line is employed.



a) Spectrum of low power FMR absorption of a thin circular YIG film as function of rf frequency; b) Regions of instability oscillation in the rf pumping power-rf frequency plane. The rf power and frequency used in the experiment of controlling chaos are denoted by point A.

$$\tau = 470 \text{ nsec}$$

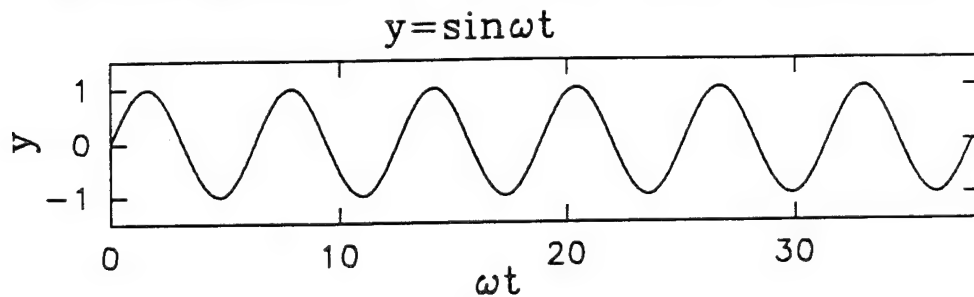


average background level decreases by
10 to 50%.

still a factor of 2 to 6 higher than
rt level at onset of auto-osc.

Experimental results of controlling chaos of FMR using the time delayed feedback method. a) Chaotic oscillation of FMR without perturbation converted to b) period 4 (gain=0.45 arbitrary unit), c) period 2 (gain=0.80 a.u.), d) period 1 (gain=0.50 a.u.), and e) the quiescent state (gain=6.50 a.u.), as the gain of the amplifier was increased.

Example of the conversion of a period one time signal to a cyclical plot in phase space

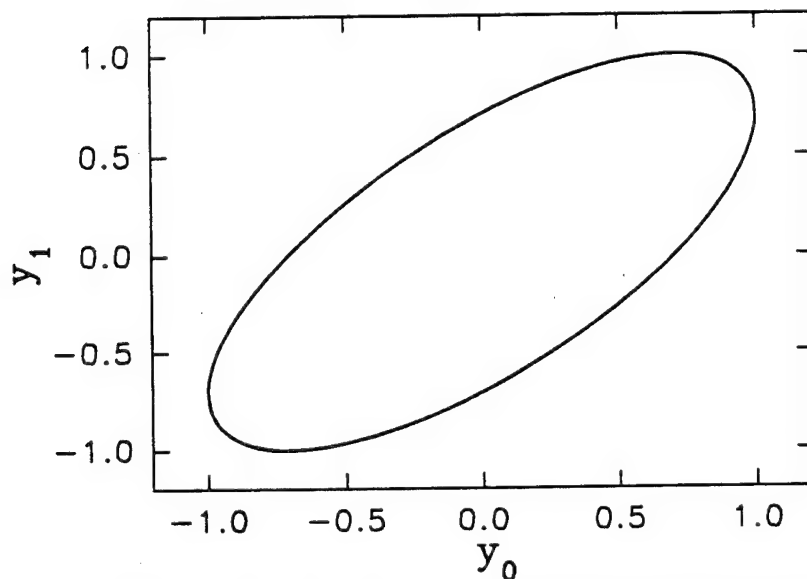


To convert the time series to a plot in N dimensional phase space:

$$y_n = \sin[\omega(t + n\tau)]$$

$$n = 0, 1, 2, \dots, N-1$$

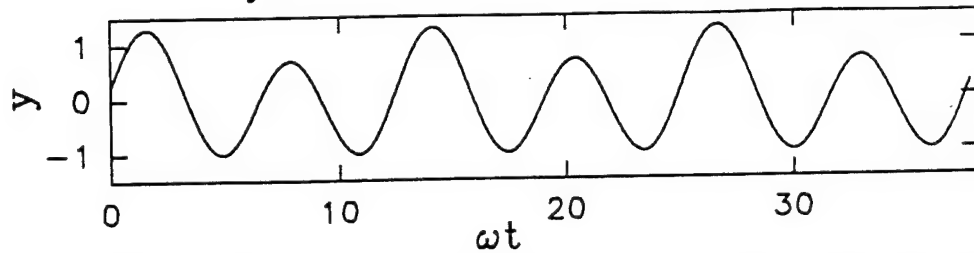
An example of a 2-D phase plot
with $\omega\tau = \pi/4$



The single loop represents a period one response (auto-oscillation)

Example of the conversion of a period two
time signal to a cyclical plot in phase space

$$y = \sin \omega t + 0.3 \sin[(\omega/2)t + \pi/4]$$

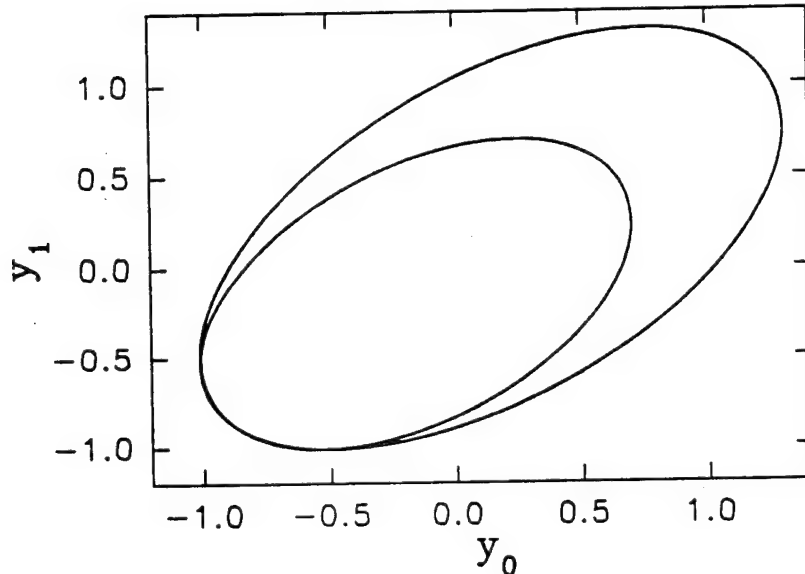


To convert the time series to a plot in
N dimensional phase space:

$$y_n = \sin[\omega(t+n\tau) + 0.3 \sin[\omega/2(t+n\tau) + \pi/4]]$$

$$n=0, 1, 2, \dots, N-1$$

An example of a 2-D phase plot
with $\omega\tau = \pi/3$



The double loop cycle represents a
period two response (bifurcation)

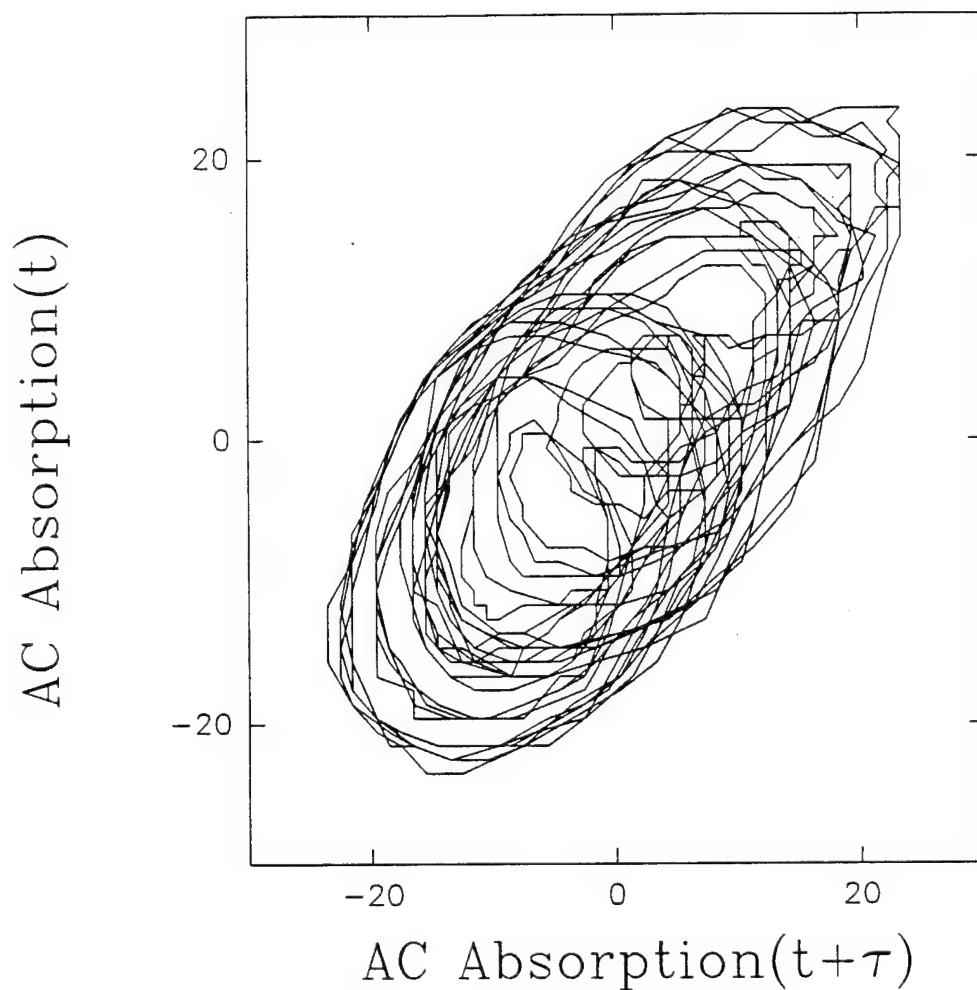
Computer Simulation of Controlling Chaos

The normal modes of FMR in circular disk are the magnetostatic modes with the space distributions of Bessel functions. In the computer model, the magnetization of YIG film is expanded as the superposition of these normal modes with the time dependent amplitudes, a_i . The equations of motion of a_i can be derived from the Hamiltonian of the system

$$\frac{da_i}{dt} = -i\gamma \left((H_0 - H_i^{res} - i\Gamma)a_i + \frac{h_p}{2} I_i^* + 2\pi M_s \sum_{jkl} A_{ijkl} a_j^* a_k a_l \right),$$

Here H_i^{res} is the low power resonance field of the i th mode, h_p is the rf pumping field. The coefficients A_{ijkl} introduce the nonlinear coupling between these modes. The nonlinear dynamics of high power FMR in thin circular YIG films can be simulated by this computer model.

Time Delay Plot of an Experimental Chaotic Signal



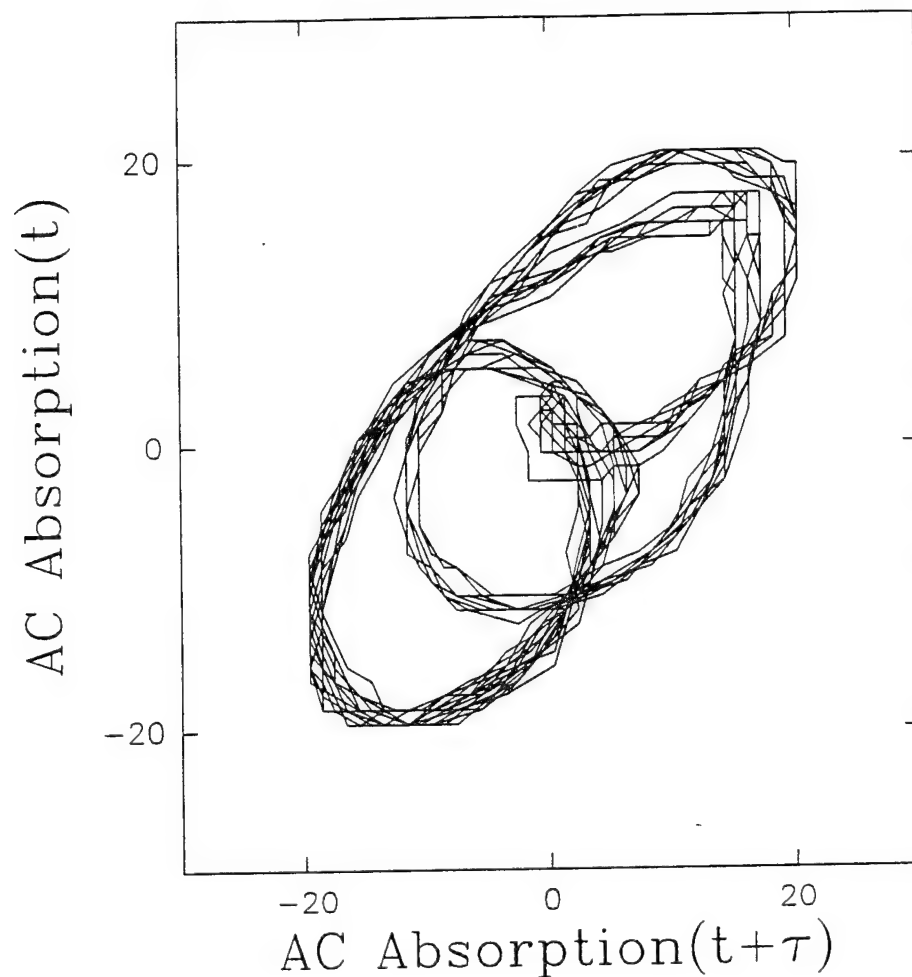
$\tau=50$ ns

Gain=0.0

Feedback Delay=470 ns

Arbitrary Absorption, Gain Units

Time Delay Plot of a Chaotic Experimental Signal Controlled to a Period-4 Signal



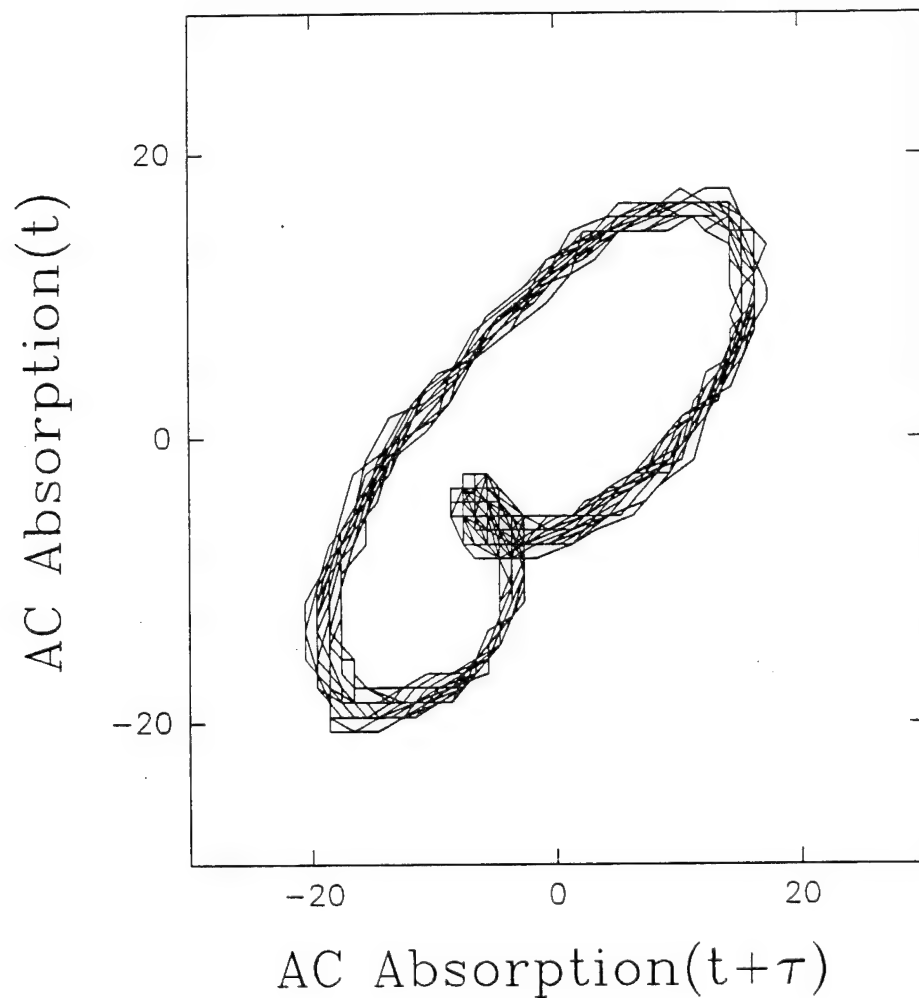
$\tau=50$ ns

Gain=0.4

Feedback Delay=470ns

Arbitrary Absorption, Gain Units

Time Delay Plot of a Chaotic
Experimental Signal Controlled to
a Period-2 Signal



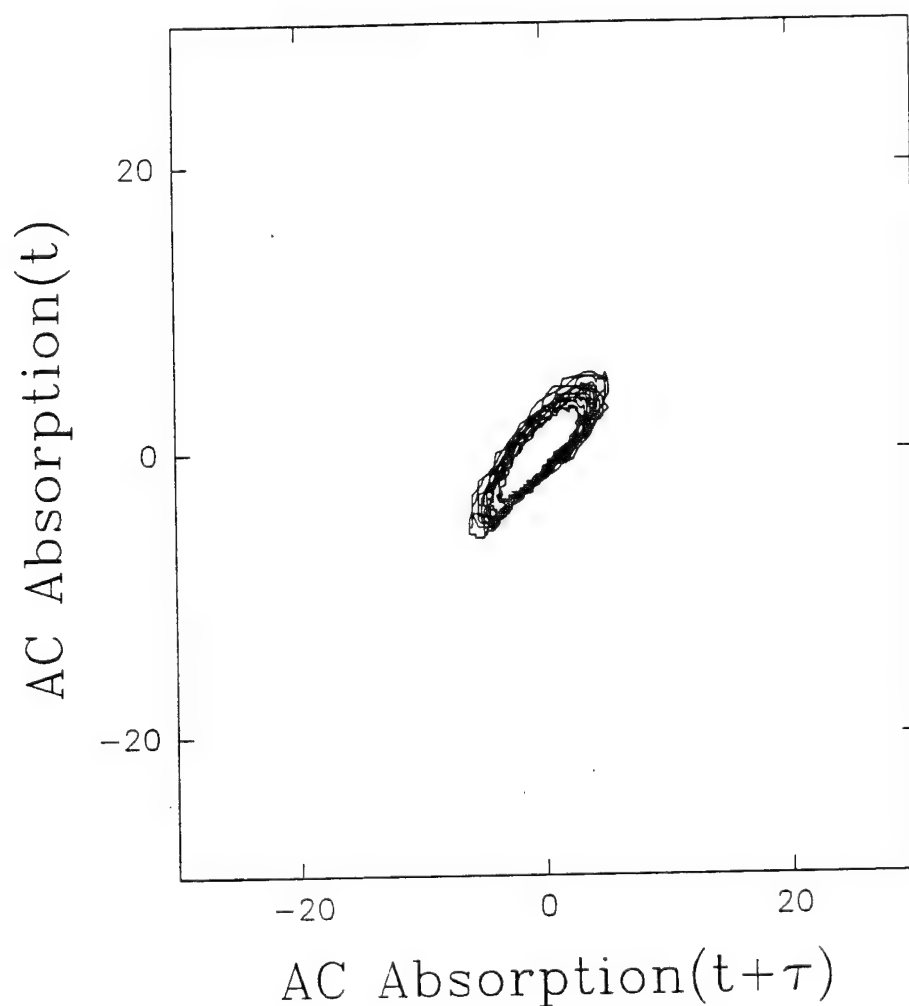
$\tau=50$ ns

Gain=0.8

Feedback Delay=470 ns

Arbitrary Absorption, Gain Units

Time Delay Plot of a Chaotic Experimental Signal Controlled to a Period-1 Signal



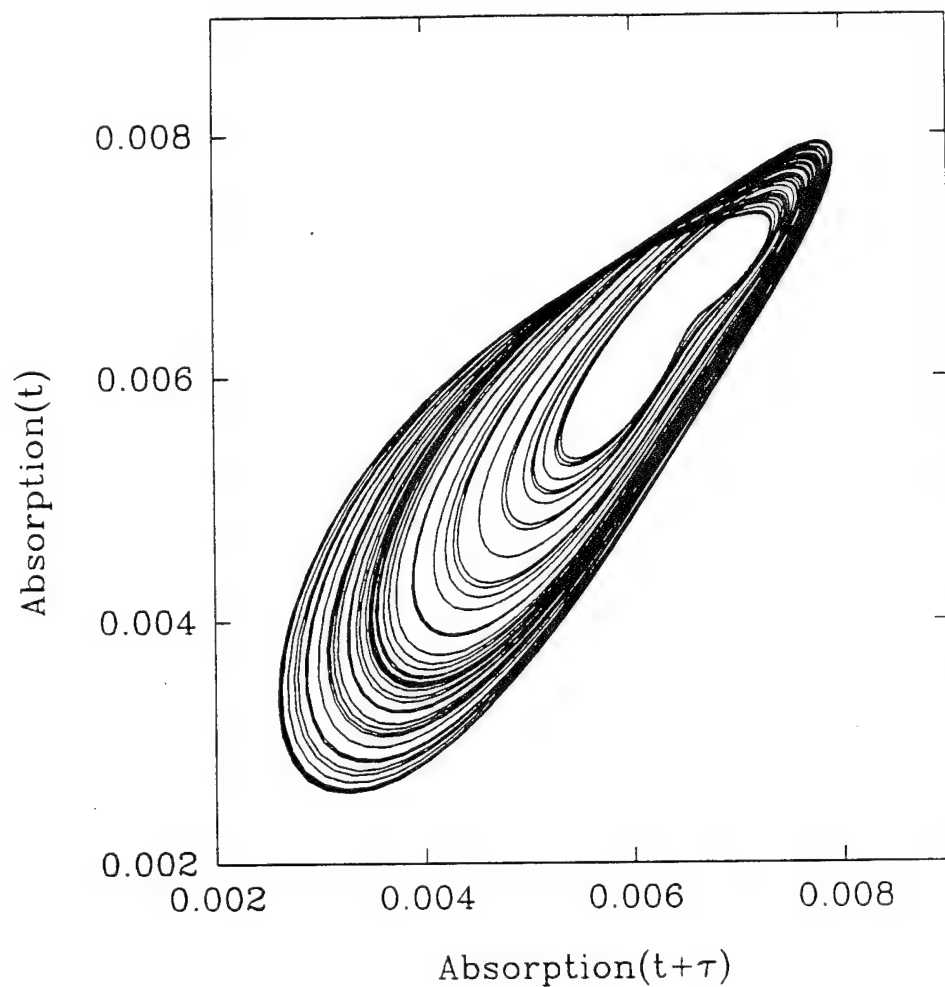
$\tau=50$ ns

Gain=5.5

Feedback Delay=470 ns

Arbitrary Absorption, Gain Units

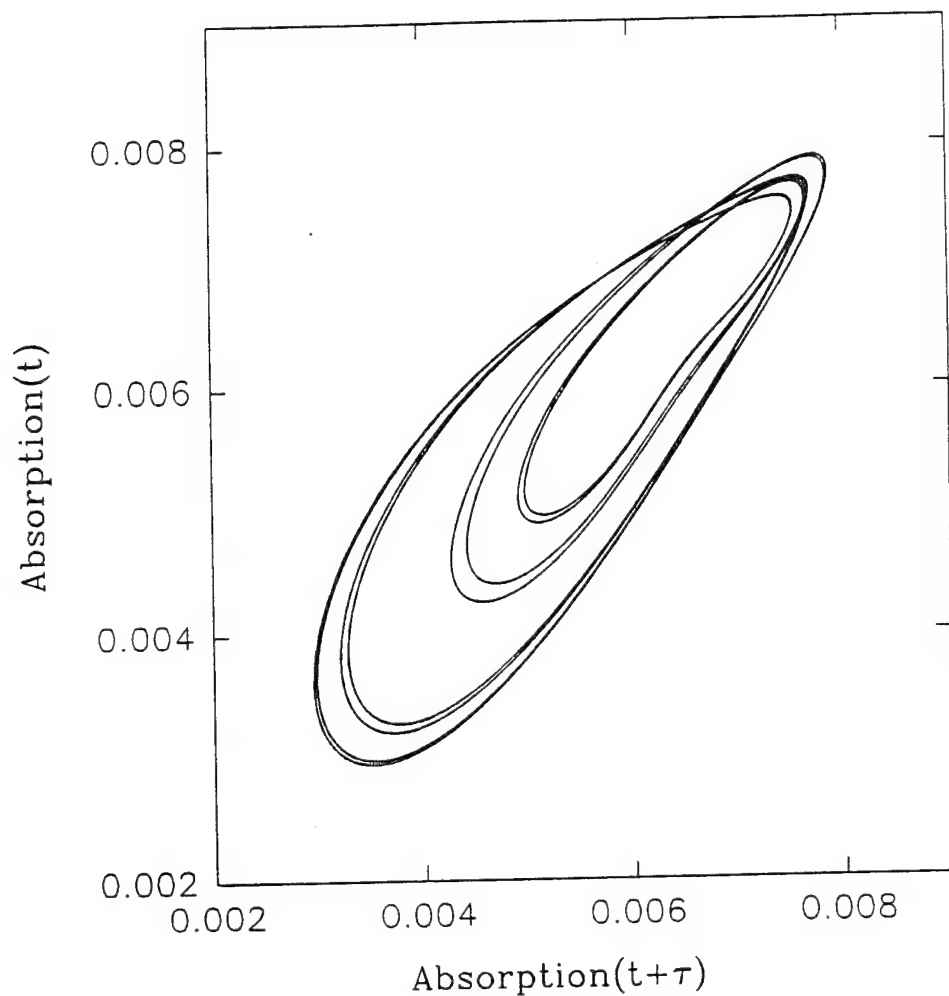
Time Delay Plot of a Chaotic Signal From the Model



Gain=0.00

Arbitrary Absorption, Gain Units

Time-Delay Plot of a Chaotic Signal Controlled to a Period-8 Signal in the Model



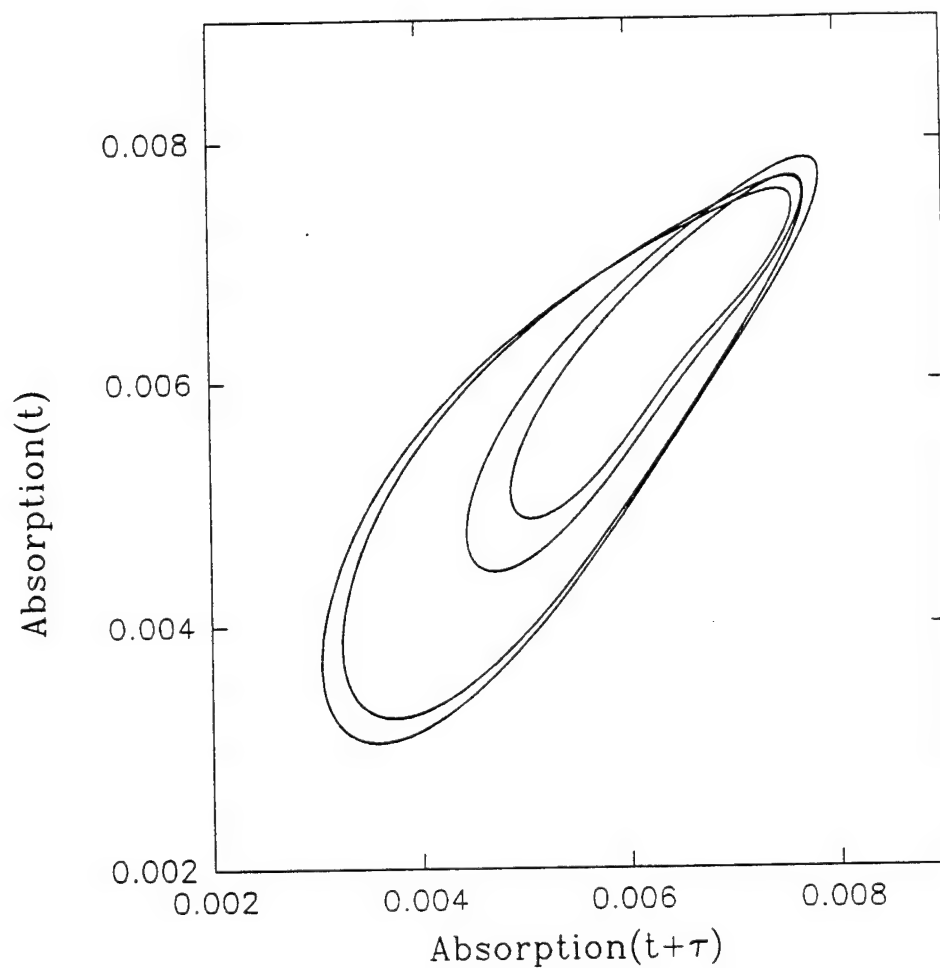
$\tau = 50$ ns

Gain=2.75

Feedback Delay=380 ns

Arbitrary Absorption, Gain Units

Time-Delay Plot of a Chaotic Signal Controlled to a Period-4 Signal in the Model



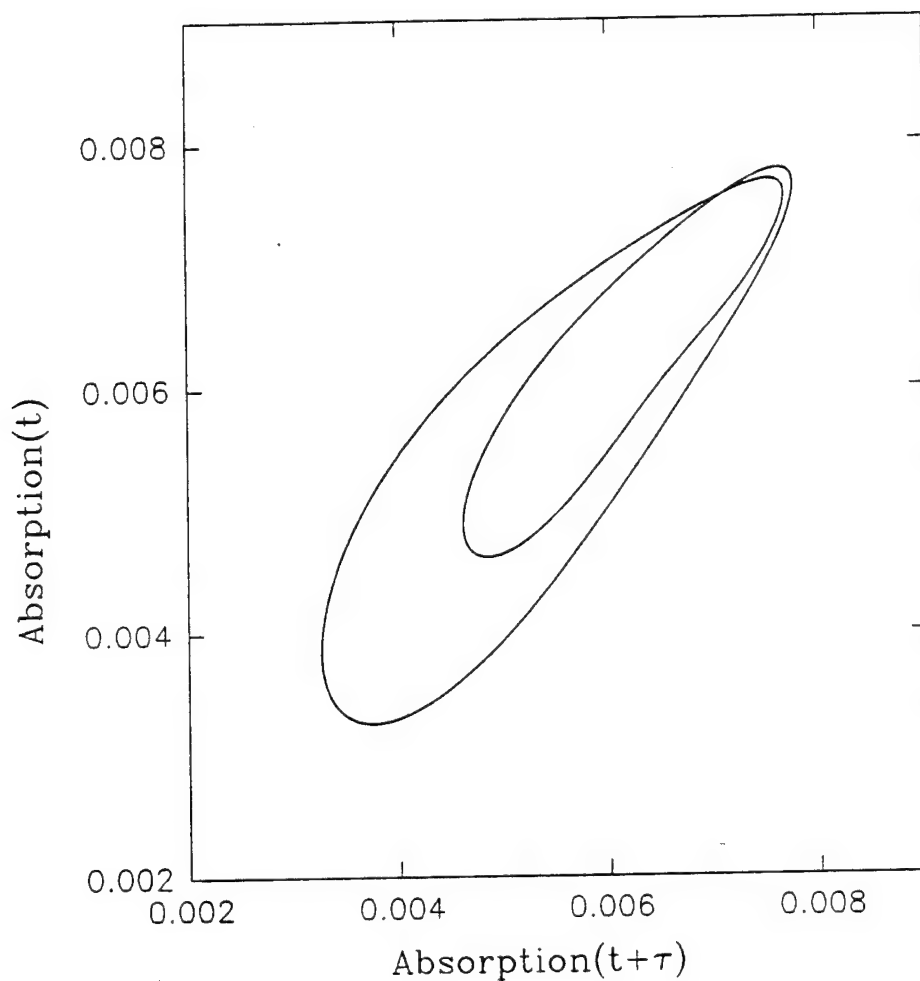
$\tau = 50$ ns

Gain=3.50

Feedback Delay=380 ns

Arbitrary Absorption, Gain Units

Time-Delay Plot of a Chaotic Signal Controlled to a Period-2 Signal in the Model



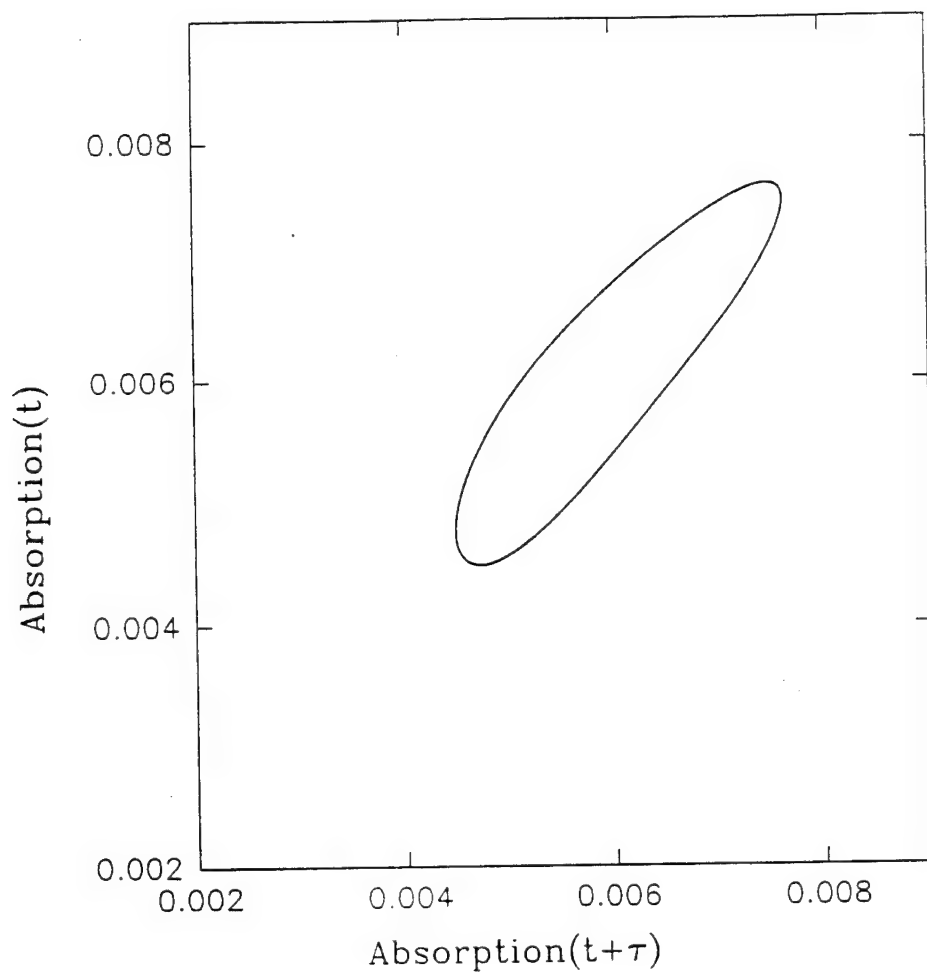
$\tau=50$ ns

Gain=5.00

Feedback Delay=380 ns

Arbitrary Absorption, Gain Units

Time-Delay Plot of a Chaotic Signal Controlled to a Period-1 Signal in the Model



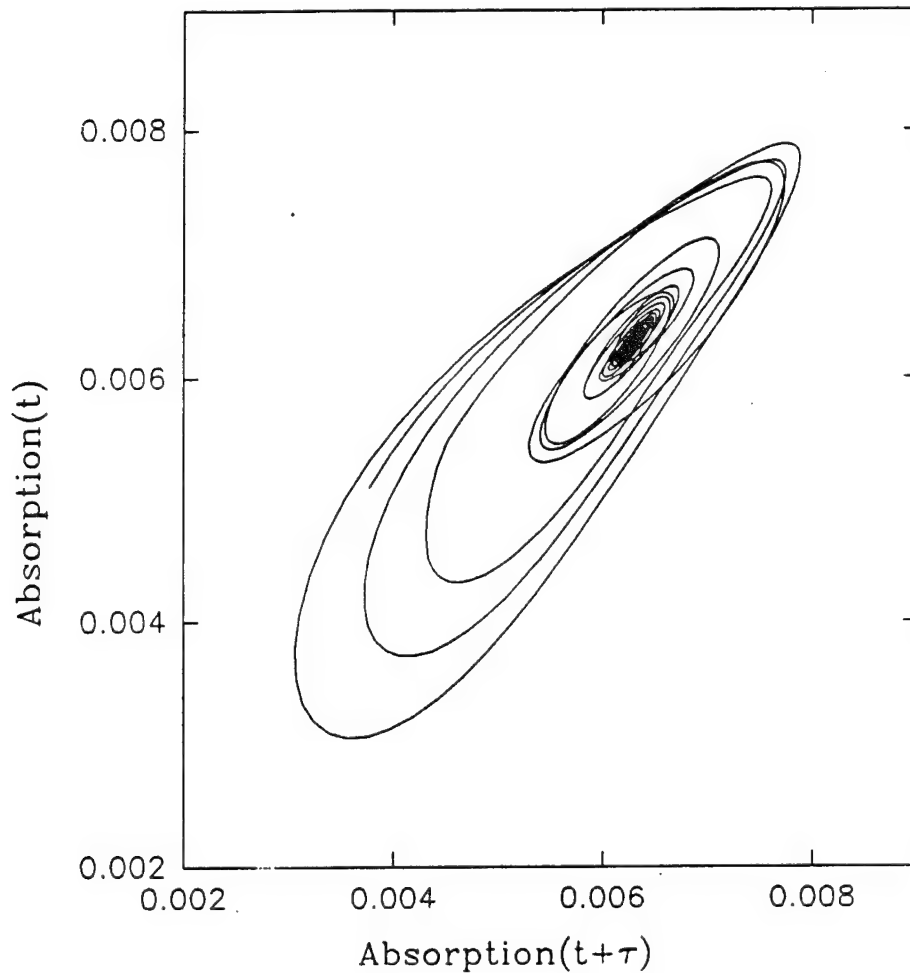
$\tau=50$ ns

Gain=15.0

Feedback Delay=380 ns

Arbitrary Absorption, Gain Units

Time Delay Plot of the Transient Response of the Controlled Chaotic Signal to the Quiescent State in the Model



$\tau = 50$ ns

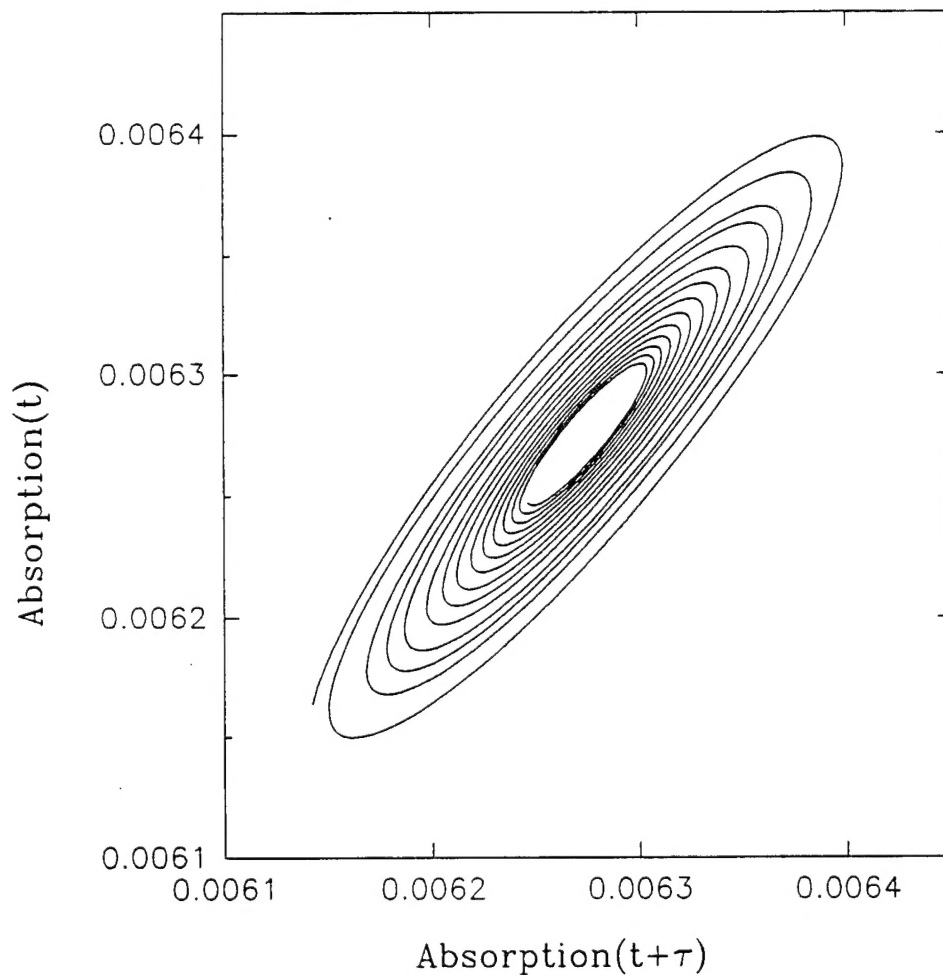
Gain=30.0

Feedback Delay=380 ns

Arbitrary Absorption, Gain Units

System evolves chaotically for 2 microseconds before the feedback is turned on, and after a transient period of about 5 microseconds, the system is controlled to the quiescent state..

Time Delay Plot of the Transient
Response of a Chaotic Signal
Showing the Spiral to the
Quiescence State in the Model

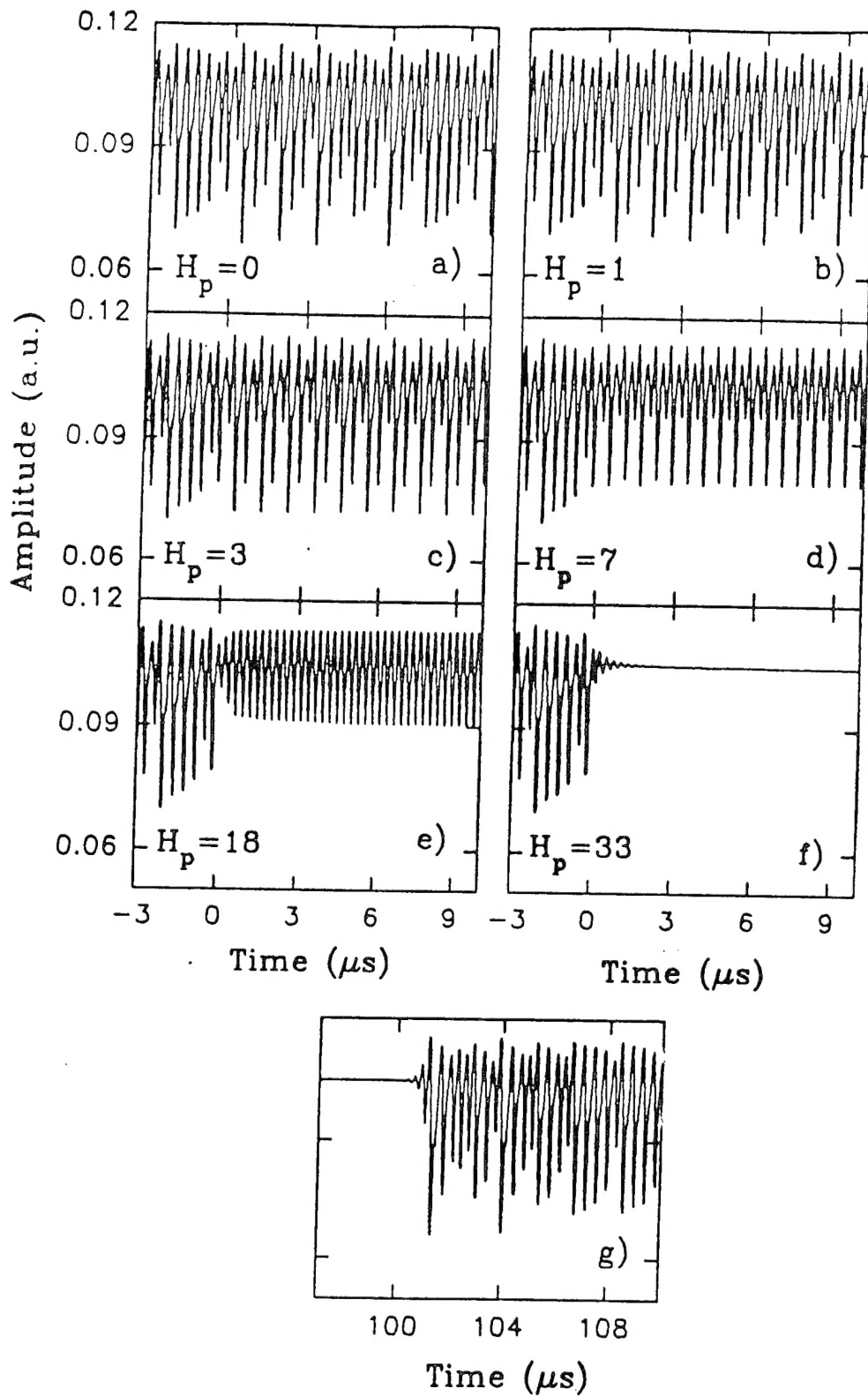


$\tau=50\text{ns}$

Gain=30.0

Feedback Delay=380 ns

Arbitrary Absorption, Gain Units

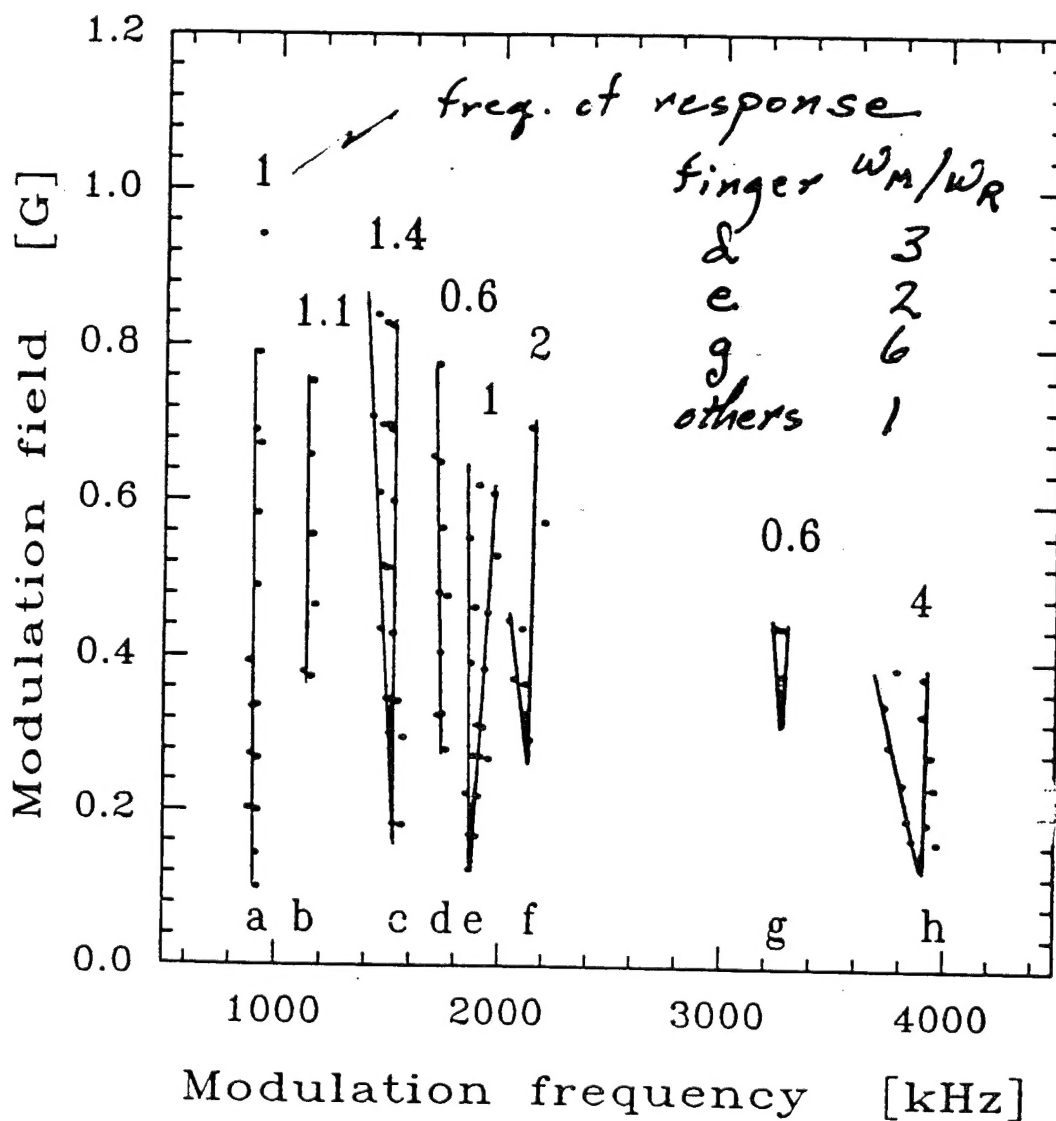


3 mode model (0,1) (0,2) (0,3)

Computer simulation results of controlling chaos of FMR using the time delayed feedback method. a) chaotic signal without perturbation. With increasing gain of the feedback loop H_p , chaos was converted to b) period 4 oscillation, c) period 3, d) period 2, e) period 1, f) quiescent state. The perturbation was turned on at $t=0$. g) The system returned to the chaotic state after turning off the perturbation at $t=100$ ns.

Open loop

$$\Delta H(t) = \Delta H \cos \omega t$$



Inside the triangular regions in the modulation field-frequency plane, the chaotic FMR signal was stabilized to periodic orbit by modulating the magnetic field with a sine-wave perturbation. The numbers denote the frequency (in MHz) of the periodic oscillation after stabilization.

CONCLUSIONS

Nonlinear dynamics in magnetic materials has been and continues to be an exciting and active field.

Numerical models of the equations of motion are readily available from the Hamiltonian.

Thin film geometrics limit the number of degenerate modes and truncation is not a serious limitation.

By appropriate perturbation techniques it is possible to return the system from a chaotic state to the quiescent state.

Chaos can be Controlled